Universality in Time-Crystalline Matter

Inaugural-Dissertation

zur

Erlangung des Doktorgrades

der Mathematisch-Naturwissenschaftlichen Fakultät

der Universität zu Köln

vorgelegt von

Carl Philipp Zelle
aus Bonn

Köln
September 2024

Berichterstatter:	Prof. Dr. Sebastian Diehl
	Prof. Dr. Joachim Krug
	Prof. Dr. Ryo Hanai
Tag der mündlichen Prüfung:	6.12.2024

Erklärung zur Dissertation

gemäß der Promotionsordnung vom 12. März 2020

Hiermit versichere ich an Eides statt, dass ich die vorliegende Dissertation selbstständig und ohne die Benutzung anderer als der angegebenen Hilfsmittel und Literatur angefertigt habe. Alle Stellen, die wörtlich oder sinngemäß aus veröffentlichten und nicht veröffentlichten Werken dem Wortlaut oder dem Sinn nach entnommen wurden, sind als solche kenntlich gemacht. Ich versichere an Eides statt, dass diese Dissertation noch keiner anderen Fakultät oder Universität zur Prüfung vorgelegen hat; dass sie - abgesehen von unten angegebenen Teilpublikationen und eingebundenen Artikeln und Manuskripten - noch nicht veröffentlicht worden ist sowie, dass ich eine Veröffentlichung der Dissertation vor Abschluss der Promotion nicht ohne Genehmigung des Promotionsausschusses vornehmen werde. Die Bestimmungen dieser Ordnung sind mir bekannt. Darüber hinaus erkläre ich hiermit, dass ich die Ordnung zur Sicherung guter wissenschaftlicher Praxis und zum Umgang mit wissenschaftlichem Fehlverhalten der Universität zu Köln gelesen und sie bei der Durchführung der Dissertation zugrundeliegenden Arbeiten und der schriftlich verfassten Dissertation beachtet habe und verpflichte mich hiermit, die dort genannten Vorgaben bei allen wissenschaftlichen Tätigkeiten zu beachten und umzusetzen. Ich versichere, dass die eingereichte elektronische Fassung der eingereichten Druckfassung vollständig entspricht.

Teilpublikationen

[1] Zelle, C., Daviet, R., Rosch, A., Diehl, S.: Universal Phenomenology at Critical Exceptional Points of Nonequilibrium $O(N)$ models, Phys. Rev. X 14, 021052 (2024)

[2] Daviet, R., Zelle, C., Rosch, A., Diehl, S.: Nonequilibrium Criticality at the Onset of Time-Crystalline Order, Phys. Rev. Lett. 132, 167102 (2024)

[3] Chiocchetta, A., Kiese, D., Zelle, C.P., Piazza,F., Diehl,S.: Cavity-induced quantum spin liquids. Nat Commun 12, 5901 (2021)[1]

Köln, 26.9.2024, Carl Philipp Zelle

[1] Diese Publikation entstand im ersten Jahr der Promotionsphase des Autors und ist nicht Teil dieser Dissertation.

Abstract

In this dissertation we explore universal structures associated to time translation symmetry breaking in nonequlibrium $O(N)$-models. We extend the paradigmatic model A dynamics of a nonconserved order parameter [1] to include nonconservative forces driving it manifestly out of equilibrium. These lead to temporal instabilities towards phases that break time translation symmetry. The ensuing time crystalline order marks a nonthermal phase of matter beyond the Landau paradigm in equilibrium. We identify two different time-crystalline patterns, an oscillating phase and a rotating phase. Both of them are distinguished by the symmetry generators they break.

By appropriate expansions of the underlying field theory, we analyse the critical phenomena associated to the instabilities towards time-crystalline order. This constitutes a generalization of the temporal instabilities defined in the classic work by Cross and Hohenberg [2] to include noise, the crucial step to determine universal scaling behavior. At the finite frequency instability marking the transition between fully symmetric phase and a dynamical many-body limit cycle, we find that the critical degrees of freedom are described by an $O(N) \times SO(2)$ model. The additional $SO(2)$ symmetry is an incarnation of time translations that are spontaneously broken along the transition. In a perturbative RG analysis in $d = 4 - \epsilon$ dimensions, we identify a novel, nonthermal universality class. Notably, even though the effective field theory could display an emergent thermal equilibrium, infinitesimal deviations from such an equilibrium suffice to push the system to the nonthermal fixed point on large scales. The transition between an ordered and the rotating phase is governed by a critical exceptional point, where a spectral nonanalyticity coincides with criticality. Such a point is impossible in equilibrium and leads to giant, superthermal fluctuations with nonanalytic dispersions. We show that these fluctuations can be controlled by a resummation of the perturbative series and establish that CEP fluctuations lead to a fluctuation induced first order transition.

The breaking of time translation symmetry in the time crystalline phases leads to a soft Goldstone mode even in the absence of any internal symmetries. This mode realises the KPZ universality class leading to subexponential decaying correlations in low dimensions. The interplay with internal Goldstone modes in the $O(N) \times SO(2)$ model leads to additional novel regimes described by strongly interacting weak scaling fixed points in the one-loop flow equations. This paves the way to a potential extension of the KPZ phenomenology in higher symmetry groups.

These phenomena can be realised in wide range of systems. We present a general approach to induce time-crystalline order by parametric pumps in systems that are

subject to model A type dynamics in equilibrium. We also show that the presented universal scaling laws also apply in dynamic phases of nonreciprocally coupled matter. Surprisingly, this phenomenology can also be realised by arbitrarily weak drives. We demonstrate this for a light irradiated ferrimagnet.

Contents

1

Introduction

The identification of quantitative, universal behaviors of macroscopic observables in phases and phase transitions is one of the most prominent endeavors in theoretical physics. It is usually impossible to track the motion of the 10^{23} and more microscopic particles that constitute the system at hand. Instead, one can build predictive effective field theories that do not require detailed knowledge of the microscopic particles, but only rely on a handful of phenomenological parameters that can be fixed experimentally. For example, the hydrodynamic Navier-Stokes equations accurately capture the dynamics of liquids without the need of any information about e.g. the molecules constituting water.

In more abstract words, this is an incarnation of scale separation. The dynamics at large scales should be determined by the state of the system at these large scales. The macroscopic degrees of freedom are then continuous, averaged densities $\phi(\mathbf{x}, t)$ of the microscopic degrees of freedom that vary over distances and times that are much larger then the respective microscopic scales. Then, an effective equation of motion, potential or free energy for these densities can be constructed as an expansion in these densities. The form of this effective field theory is constrained by the dimension of the system as well as the symmetries and conservation laws that it needs to respect. In turn, systems of very different microscopic ingredients, can result in effective models that are of the same shape on macroscopic scales, if they

share their symmetries. The quantitative values of the parameters of that effective theory, lifetimes of excitations, diffusion constants and their like, can however not be fixed by symmetry alone (even with a lot of hand waving) but do depend on the microscopic details. Their determination requires experiment or ab initio calculations based on the underlying microscopics.

There are however important exceptions, where the quantitative prediction of observable quantities by symmetry based effective field theories alone is possible. In the presence of a divergent correlation length, the system becomes scale invariant and observables such as correlation functions and susceptibilities of a system take an algebraic scaling form. The dimensionless exponents of this scaling form do not depend on any scales but typically only on symmetries and dimensionality. Scale invariance and universality are naturally of great interest in theoretical physics. It offers a way to understand complex systems by means of simple scaling laws and provides predictive power over wide ranges of systems sharing symmetry and dimensionality. But where can we expect to encounter universal scaling laws and how do we derive the respective universal exponents?

In thermal equilibrium, this is addressed within Landau's symmetry based classification of phases, transitions and critical phenomena. At the core of this idea is a symmetry based, phenomenological expansion of the free energy of the system in the spirit of effective field theories. The ground state of a phase is determined by the minimum of this free energy. Different phases can be classified according to the symmetries that are broken spontaneously by their ground state. Since the fact that a ground state has a certain symmetry or not is binary and cannot change continuously, transitions between different phases with different symmetries have to occur through either discontinuous first order transitions or through critical points at which the correlation length diverges. Such critical points then display scale invariance and the ensuing universal critical exponents constituting its *universality class* emerge in any system undergoing a transition characterized by the respective symmetries. The quantitative exponents of a universality class can be determined by the renormalisation group (RG). It describes how a system evolves under systematic coarse graining, by block spinning [3] in real space or integrating out fast modes in reciprocal space [4]. Over the past decades the powerful toolbox of fluctuating field theories and RG has been successfully employed to determine a plethora of respective universality classes [5], including relaxational dynamics around a thermal state [1].

Universal scaling is however not restricted to fine tuning a system to critical points. Goldstone theorem ensures, that in phases with spontaneously broken continuous symmetries, there is soft, gapless excitations leading to scale invariance without the

necessity of any fine tuning. Within field theories, the physics of Goldstone modes is determined by so called nonlinear sigma models [6].

So far, this discussion has been centered around universality in systems in thermal equilibrium. But what happens if we leave the realm of thermodynamic equilibrium? What are phases that cannot be described by an (emergent) thermal equilibrium, what is the fate of scale invariance and universality within these phases and at their transitions, and under which conditions can they emerge? The concept symmetry based effective phenomenological models is not tied to thermal equilibrium. Rather than modelling a free energy functional, we can directly construct effective equations of motion and identify phases with the stable late time solutions of these. Critical points can be identified via instabilities of these solutions [2]. This has been done successfully in a plethora of systems where the contraints of thermodynamic equilibrium are broken, ranging from light driven atomic gases and materials and growth phenomena, flocking transitions in biological systems over metamaterials and active matter to the dynamics of human populations [7, 8, 9, 10, 11, 12, 13, 14, 15, 16].

Universality can also emerge in these systems, the crucial technical step to describe it is the inclusion of noise fluctuations that 'wash out' any memory of initial conditions and fuel coarse graining. [1] In many cases, even though drives and dissipation may break equilibrium conditions (i.e. detailed balance), the system displays an emergent, effective thermal behavior at large scales and the universal exponents belong to known thermal universality classes [17, 18, 19]. This does however not always happen. Indeed, nonthermal universality classes have been identified e.g. in wetting transitions falling into the universality class of directed percolation [20, 21], self-organized criticality in e.g. avalanches [22, 23] or the famous KPZ equation [24, 7, 25], describing the roughening of surfaces. An overarching principle to classify nonthermal phases of matter and diagnose the respective scaling laws analogous to the Landau paradigm is not known. Identifying phases and universal structures far from equilibrium is a broad and active research field in physics.

A striking instance of a nonthermal phase of matter is a so called time crystal. Its order parameter is not static, as is usually the case, but continuously traces out a limit cycle even in the presence of dissipation. It thus breaks time translation symmetry. It cannot occur in thermal equilibrium [26, 27] as it would constitute a perpetuum mobile breaking the second law of thermodynamics. It can however occur as the nonequilibrium stable state of a driven system, where there is a constant energy influx. Such phases have caught a lot of attention recently in the context of

[1] Noise is generically present in a coarse grained system coupled to an external bath. Therefore, neglecting it is an approximation, not including it.

nonreciprocal matter [28, 29, 30, 31] but also theoretically as well as experimentally in driven-dissipative quantum gases [32, 33, 34, 35].

Phases and transitions breaking time translation symmetry have so far been uncharted territory from the stance of universality. In this thesis we set out to understand universal structures associated to time crystalline order. We extend the formalism of symmetry based effective field theories for real and vector valued order parameter fields beyond equilibrium and identify phases breaking time translation symmetry. At all ensuing transitions, as well as within the time crystalline phases, we identify the slow degrees of freedom that lead to scale invariant behavior. By systematic expansions the these degrees of freedom we derive the respective RG flows determining the universal scaling laws. At the critical points, we discover a novel, nonthermal universality class and fluctuation-induced first order transitions. Further, we identify nonequilibrium scaling laws within the time crystalline phases in low dimensions. For low symmetries, we find the paradigmatic KPZ universality. In more symmetric set ups, our analysis points at novel fixed points generalizing KPZ to $O(N) \times SO(2)$ symmetry groups. Since the effective model we use is minimal and only based on symmetries and dimension, it is expected to emerge for a large class of microscopic systems with the given symmetries on a coarse grained level, once driven suitably out of equilibrium. We present a general and one more explicit proposal, how to realize it in magnetic materials using simple driving schemes. We further connect to the existing proposal of nonreciprocally coupled matter.

2

The nonthermal O(N) model

We begin our analysis of universality in time-crystalline matter by giving an extended overview of the key mechanisms and results contained in this thesis. A more detailed derivation of these follows the ensuing chapters.

We start by introducing the Markovian, nonconservative $O(N)$ model, as the work horse of this thesis. In the spirit of effective field theories, we want to model the dynamics of an density $\boldsymbol{\phi}(\mathbf{x}, t)$ of system with an internal $O(N)$ symmetry in d spatial dimensions. $O(N)$ symmetric theories emerge in a broad range of systems from atomic gases over magnetic materials to the mesonic degrees of freedom in QCD. Since we are considering dynamics on length scales ξ much larger than the microscopic scales a (typically a lattice spacing), it is effectively continuous with rotational and translation symmetry. We start by considering the equilibrium case, where the system is coupled to a thermal bath that can exchange energy with the system and fixes its temperature T (we work in units with $k_B = 1$ throughout the entire thesis). This manifests in noise and dissipation. Further, we assume that the coupling to the bath breaks the conservation law associated to the $O(N)$ symmetry and therefore there are no gapless hydrodynamic modes. If the system is coupled to

a thermal bath, this culminates in model A of Hohenberg and Halperin [1]

$$2\gamma\partial_t\boldsymbol{\phi}(\mathbf{x},t) + \frac{\delta\mathcal{V}[\boldsymbol{\phi}]}{\delta\boldsymbol{\phi}(\mathbf{x},t)} + \boldsymbol{\xi}(\mathbf{x},t) = 0 \tag{2.1a}$$

$$\mathcal{V}[\boldsymbol{\phi}] = \int_{t,x} \frac{1}{2}\boldsymbol{\phi}(\mathbf{x},t)^T(r + \partial_t^2 + Z\nabla^2)\boldsymbol{\phi}(\mathbf{x},t) + \frac{\lambda}{4}\rho(\mathbf{x},t)^2 \tag{2.1b}$$

where ξ is a diagonal gaussian white noise $\langle\xi_i(\mathbf{x}',t')\xi_j(\mathbf{x},t)\rangle = 4\gamma T\delta_{ij}\delta(\mathbf{x}'-\mathbf{x})\delta(t'-t)$, $\rho(\mathbf{x},t) = \boldsymbol{\phi}(\mathbf{x},t)\cdot\boldsymbol{\phi}(\mathbf{x},t)$ is the $O(N)$ invariant field amplitude and $\mathcal{V}[\boldsymbol{\phi}]$ an effective $O(N)$ symmetric potential. This dynamics satisfies thermal equilibrium conditions at temperature T, the steady state probability distribution of the random variable $\boldsymbol{\phi}$ is $P[\boldsymbol{\phi}] \sim \exp(-\beta V[\boldsymbol{\phi}])$ [36]. The potential $\mathcal{V}[\boldsymbol{\phi}]$ is of the prototypical sombrero hat form, where r controls the ordering phase transition from symmetric to long ranged ordered phase.

We now want to leave the realm of thermodynamic equilibrium and its proximity and allow the system to relax to stable states that are not described by thermal distributions. To this end we consider systems where detailed balance conditions are broken on microscopic scales (in contrast to breaking it on the boundaries by e.g. bathes with different temperatures). This can for instance be achieved by drives with external nonthermal sources such as lasers or when the microscopic particles can themselves can burn energy, i.e. constitute active matter. At this point, we are not interested in understanding how exactly this happens microscopically, but want to understand the potential macroscopic impacts of breaking of detailed balance. Within our effective field theory approach, this means to add additional terms to (2.1) that are ruled out in equilibrium. The simplest (and most relevant) are non-conservative force terms beyond the simple dissipation, that do not derive from a potential. These are, to lowest order in field amplitudes and derivatives, nonconservative damping contributions $u\,\rho(\mathbf{x},t)\partial_t\boldsymbol{\phi}(\mathbf{x},t)$ and $u'\,\boldsymbol{\phi}(\mathbf{x},t)\partial_t\rho(\mathbf{x},t)$ and we finally arrive at the nonthermal $O(N)$ theory

$$\begin{aligned}\Big(&\partial_t^2 + (2\gamma - Z\nabla^2 + u\rho(\mathbf{x},t))\partial_t \\ &+ r + \lambda\rho(\mathbf{x},t) - v^2\nabla^2 + \frac{u'}{2}\partial_t\rho(\mathbf{x},t)\Big)\boldsymbol{\phi}(\mathbf{x},t) + \xi(\mathbf{x},t) = 0.\end{aligned} \tag{2.2}$$

While we have added the nonthermal terms on phenomenological basis here, we give examples how to realise the physics of this model in various set ups in chapter 7.

2.1 The mean field phase diagram

In a first step to understand the phase structure of the nonthermal $O(N)$ model, we perform a mean field analysis. This amounts to finding spatially homogeneous solutions $\boldsymbol{\phi}_0(t)$ to the noiseless equation of motion. The simple most solution is of course the trivial case, $\boldsymbol{\phi}_0(t) = 0$. It is however only stable against small fluctuations if $\gamma > 0, r > 0$.

Upon tuning r through zero while keeping a positive damping $\gamma > 0$, there is an instability towards a static, ordered phase with $\boldsymbol{\phi}_{0,s} = \sqrt{-r/\lambda}\hat{n}$ where $\hat{n}$ is a unit vector, whose direction is spontaneously chosen. This phase transition is the ordering transition induced by the equilibrium potential $\mathcal{V}$ taking the famous "sombrero hat" shape leading to spontaneous breaking of the $O(N)$ symmetry.

In equilibrium, tuning r through zero, is only meaningful is the presence of the $\boldsymbol{\phi}^4$ coupling (or a higher order nonlinearity), since else it would lead to an unbound, unphysical potential. Instead, it allows for a compensation of the negative potential curvature by means of a finite field expectation value $\rho_{0,s}$ such that $r + \lambda\rho_{0,s} = 0$.

Similarly, without the nonconservative nonlinearities u, u' a negative damping $\gamma < 0$ renders the system unstable and all solutions grow exponentially. This is remedied by the presence of e.g. the irreversible force $u\rho\partial_t\boldsymbol{\phi}$, allowing for a finite field expectation value $\rho_{0,d}$ that compensates for the negative damping, $2\gamma + u\rho_{0,d}$. In this case, however, the equilibrium force term stemming from the potential does not vanish and the remaining mean field equation of motion reads

$$\partial_t^2\boldsymbol{\phi}_0 + (r + \lambda\rho_d)\boldsymbol{\phi}_0 = 0 \tag{2.3}$$

$$(\boldsymbol{\phi}_0)^2 = \rho_d = -\frac{2\gamma}{u} \tag{2.4}$$

which leads to a perpetual rotation at angular velocity $E = \sqrt{r + \lambda\rho_d}$ at fixed amplitude ρ_d within a spontaneously picked plane, i.e.

$$\boldsymbol{\phi}_{0,d} = \sqrt{\rho_d}\left(\cos Et\,\hat{n}_1 + \sin Et\,\hat{n}_2\right). \tag{2.5}$$

Here $\hat{n}_1, \hat{n}_2$ are two spontaneously chosen mutually orthognal unit vectors that fix the plane of rotation.

The rotation is however not the only possible dynamical mean field solution that emerges when tuning the damping into an anitdamping. Instead of rotating, the field can also start to oscillate along a spontaneously picked axis, $\boldsymbol{\phi}_{0,\mathrm{VdP}} = \phi_{\mathrm{VdP}}(t)\hat{n}$. The amplitude oscillations are determined by the the paradigmatic Van der Pol

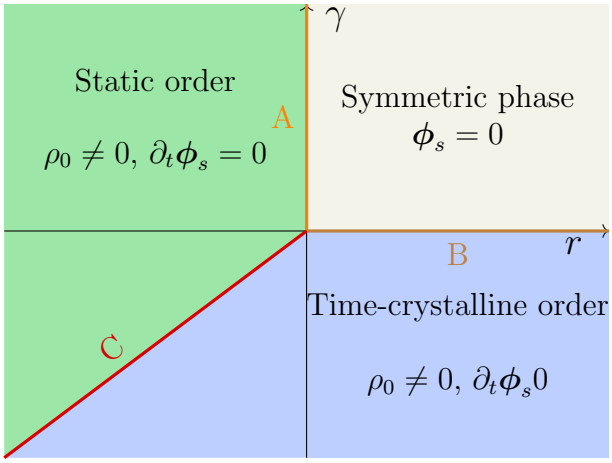

Figure 2.1: Mean field phase diagram of the nonthermal $O(N)$ model. Time-crystalline order emerges for negative values of the damping. Transition line A is the ordering transition of model A. Transition line B is the direct transition between no order and time-crystalline order. Its universality class is determined in chapter 4. Transition line C is the critical exceptional transition between ordered and time-crystalline phase and discussed in chapter 5. The universal scaling of Goldstone modes within the time-crystalline phase is adressed in chapter 6.

oscillator [37]

$$\left(\partial_t^2 + (2\gamma + (u+u')\phi_{\mathrm{VdP}}^2)\partial_t + r + \lambda\phi_{\mathrm{VdP}}^2\right)\phi_{\mathrm{VdP}} = 0 \tag{2.6}$$

which is well known to host perpertual oscillatory solutions at $\gamma < 0$ and has been a base model for both classical and quantum limit cycles [38, 39, 40, 41, 42]. These however contain higher harmonics and have no general closed analytic form. As we show in 4, whether the rotating or oscillatory state is realised depends on the relative strenght of u and u'. Clearly, in the special case of $N = 1$, the dynamics of a real valued field with $\mathbb{Z}_2$ symmetry, the oscillating phase is the only possible dynamic limit cycle.

This analysis reveals that, on mean field level, the nonthermal $O(N)$ model hosts phases where the order parameter traces out a limit cycle. It thus breaks the continuous time translation symmetry of the original model leading to time-crystalline order. The corresponding mean field phase diagram is depicted in Fig. 2.1.

The full model in d spatial dimensions including noise allows to determine the impact of fluctuations on the phase diagram. This is the crucial step to determine the universal scaling laws associated to time translation symmetry breaking in interplay with an internal $O(N)$ symmetry group. In chapter 3 we briefly introduce the field theoretic framework adapted throughout this thesis. The universality class of the

transition between the symmetric and the time-crystalline phase is determined in 4 and the transition between statically ordered phase and time-crystal in 5. Within the limit cycle phase, there is gapless Goldstone modes due to time translation symmetry breaking as well as the breaking of the internal $O(N)$ group leading to universal scaling behavior. We analyse the various symmetry breaking patterns and the ensuing scaling laws in chapter 6. Finally, we show how this universality class is realised in various physical set ups, ranging from nonreciprocal active matter over pumped magnets to driven dissipative spinor gases in chapter 7. Before delving into the details we present the main results in the remainder of this chapter.

2.2 Transition from symmetric phase

First, we consider the transition from the symmetric phase $\langle \boldsymbol{\phi} \rangle = 0$ into the limit cycle phases. The detailed analysis is given in chapter 4 which is based on [43]. The transition occurs, on mean field, when tuning the damping γ to zero while keeping a finite $r > 0$, i.e. transition line B in the mean field phase diagram Fig. 2.1 The first, important question regards the order of this transition. The finite value of r corresponds to a finite frequency scale at the transition. Indeed, the frequency at which the order parameter starts to rotate (or oscillate) does not go to zero close to the transition but jumps, a behavior usually associated to first order phase transitions.

$$E = \begin{cases} 0 & \text{for} \gamma > 0 \\ \sqrt{r - \frac{2\gamma\lambda}{u}} & \text{for} \gamma < 0 \end{cases} \tag{2.7}$$

for the rotating phase. On the other hand, the expectation value of the amplitude of the rotation does grow continuously at the transition

$$\phi_d = \begin{cases} 0 & \text{for} \gamma > 0 \\ \sqrt{-\frac{2\gamma}{u}} & \text{for} \gamma < 0 \end{cases} \tag{2.8}$$

indicating a second order phase transition. Both behaviors are also depicted in Fig 2.2. A stronger indication for a second order phase transition is the bare correlation function at the transition point

$$\mathcal{C}(t, \mathbf{q}) \propto q^{-2} e^{-q^2 t} \cos \sqrt{r} t. \tag{2.9}$$

Next to the oscillations at the finite frequency scale, it displays an algebraic infrared singularity, indicating a diverging correlation length – a clear signature of a second

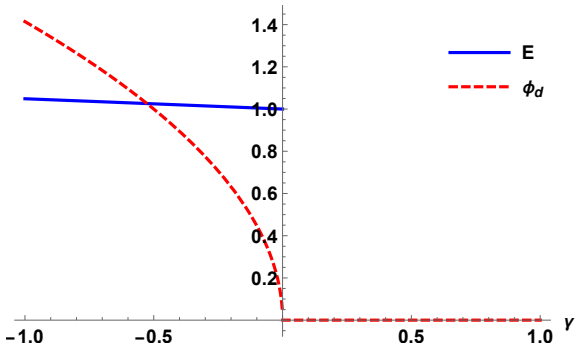

Figure 2.2: The mean field amplitude and angular velocity of the limit-cycle phase across the transition. While the amplitude grows continuously in with a square root behavior close to the transition, the angular velocity jumbs.

order phase transition.

Still, the finite frequency scale spoils a direct scaling ansatz for the correlations and responses and a straightforward RG analysis. As we show in chapter 4, this can be remedied by identifying the amplitudes of the oscillations as the relevant critical degrees of freedom. In that framework, time translation symmetry manifests as an internal $SO(2)$ symmetry and the transition is described by an $O(N) \times SO(2)$ symmetric field theory. This field theory can describe the instabilities to both the oscillating as well as the rotating phase, and we determine that the sign of $u - u'$ determines which phase is realised.

A perturbative renormalization group analysis of the $O(N) \times SO(2)$-model determines, that below the upper critical dimension $d_c = 4$, the transition is described by a nonequilibrium fixed point. Its nonthermal nature is most strikingly evident by different anomalous scaling exponents for dynamical correlation and response functions violating fluctuation dissipation relations. One can use the ratio of correlation and response to define an effective, scale dependent temperature. At the transition this temperature will however diverge with a universal exponent, a consequence of the nonthermal nature of the RG fixed point.

The Gaussian fixed point of this transition describes both the instability towards the rotating as well as the oscillating phase. Below the upper critical dimension, the interacting fixed point however only describes the transition into the rotating phase and there is no fixed point for the transition into the oscillating phase. This is a signature of a so called fluctuation induced first order phase transition, the transition into the oscillating phase is rendered discontinuous by interacting fluctuations. The phase diagram at fixed r for varying γ as well as $u - u'$ is depicted in Fig. 2.3.

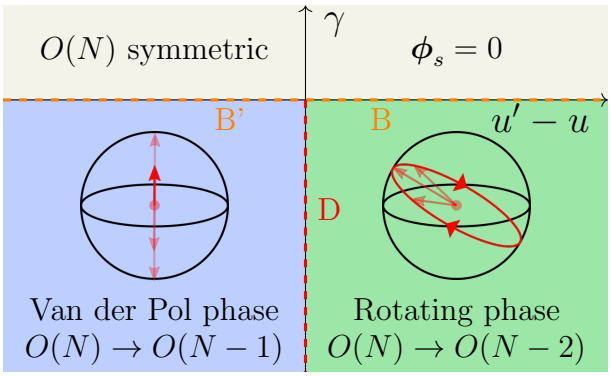

Figure 2.3: Phase transition line B between symmetric and time-crystalline order. There is an additional axis $u' - u$. For $u - u' > 0$ there is the transition B into the rotating phase, that falls into a nonthermal universality class. For $u' - u < 0$, there is the transition B' into the oscillating van der Pol phase. It occurs through a fluctuation induced first order transition. Within the time-crystalline regime the transition between the different symmetry breaking patterns D is of first order.

2.3 The CEP transition from the ordered phase

Next, we turn to the transition between the ordered phase, transition line B in Fig. 2.1 and the rotating phase in chapter 5, which is based on [44]. It has been argued, that such transitions are described by so called *critical exceptional point*s (CEPs) in the context of noreciprocal phase transitions [28] and on mean field, this is indeed the case in our model. Exceptional points have gained a lot of attention in recent years in the study of nonhermitian Hamiltonians arising in open systems [45, 46, 47, 48, 49, 50, 51, 52, 53, 54, 55, 56, 57]. They arise at points, where the Hamiltonian becomes nondiagonalizable due to its nonhermiticity and two or more eigenvectors coalesce. They typically separate purely dissipative, overdamped parts of the spectrum from underdamped regimes. The simple most example is of course the point separating over- from underdamped motion of the damped harmonic oscillator. Its dispersions are given by $\omega_{1,2} = -i\gamma \pm \sqrt{\omega_0^2 - \gamma^2}$ and the exceptional point sits at the branch cut of the square root at $\omega_0^2 = \gamma^2$, highlighting how exceptional points occur at spectral nonanalyticities.

Let us turn back to the phase transition at hand. The slow dynamics in the statically ordered phase are dominated by the gapless Goldstone modes, the phase fluctuations around the static order parameter. In chapter 5 analyse these fluctuations in the vicinity of the transition into the rotating phase. The transition is triggered by tuning the effective damping $\delta = 2\gamma + u\rho_s$ of the phase fluctuations to zero, while their mass vanishes due to their gapless nature. This amounts to indeed tuning an exceptional point to criticality, realising a CEP. We can thus address the fate of universal scaling

exponents in a fluctuating theory at a CEP within our field theoretic set up.
The universal theory is dominated by two key aspects of the CEP:
a) Spectral nonanalyticity Close to the CEP, the momentum dependent dispersion of the phase fluctuations are

$$\omega_{1,2}(\mathbf{q}) = -i(\delta + Z\mathbf{q}^2) \pm v|\mathbf{q}|. \tag{2.10}$$

Here, the scale Z amounts to diffusion while v is the velocity of the propagating exctiations. The damping δ marks the distance from the critical exceptional point (CEP). At the CEP, the coexistence of v and Z leads to an inhomogeneous scaling behavior in time, the real part of the dispersion scales linearly in momenta indicating a dynamical critical exponent $z = 1$, while the imaginary part scales quadratically corresponding to a $z = 2$ behavior. Furthermore, there is the nonanalyticity at $\mathbf{q} = 0$ typical for a CEP [50, 57].
b) Superthermal mode occupation At a finite noise level D, the statistical occupation of modes at a CEP is strongly enhanced as compared to thermal equilibrium [29]. It is measured by the equal time correlation function, which at the CEP scales as

$$\mathcal{C}_{\mathrm{CEP}}(t = 0, \mathbf{q}) \propto \frac{D}{\mathbf{q}^4}. \tag{2.11}$$

This strongly exceeds the thermal occupation of a gapless mode at low momenta $\mathcal{C} \sim \mathbf{q}^{-2}$.
Both effects strongly impact the transition below the upper critical dimension of four. The superthermal occupation (2.11) of fluctuations leads to an infrared divergence of fluctuations below four dimensions and thus destroys the ordered phase, pushing the system back into the symmetric phase, before one even reaches the transition.
On the other hand, if one starts deeply in the ordered phase, nonlinearities conspire with the nonanalytic spectrum to cause a fluctuation induced first order phase transition between static order and rotating time crystal. On the level of the loop corrections this is remiscent of the seminal work by Brazovskii [58], albeit in a physically very different setting. The nonanalytic structure of the spectrum leads to a suppression of two-loop topologies and allows for a controlled resummation of the entire perturbative series within the framework of Dyson-Schwinger equations revealing the first order transition.
There is a new interacting scale $\rho_0 g$, where ρ_0 is the strength of the static order and g of the interactions of the phase fluctuations, which determines wether the superthermal occupation destroys the preexisting order pushing the system in the symmetric phase, or if there is the fluctuation induced first order transition occuring first. The

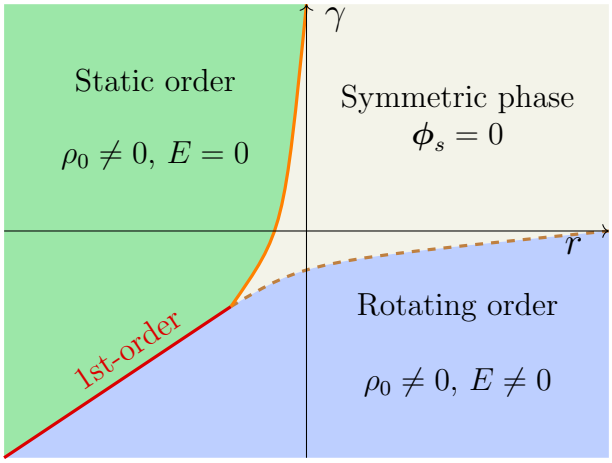

Figure 2.4: Schematic phase diagram beyond mean-field ($d < 4$). The CEP line is replaced by a first-order phase transition where the angular velocity E jumps from zero in the ordered phase to a finite value in the rotating phase. For initial values of δ and γ closer to zero, the enhanced fluctuations destroy the order parameter before reaching the CEP. The symmetric phase has thus an extended stability regime and the multicritical point moves.

corresponding schematic phase diagram is depicted in Fig 2.4.

2.4 Scaling within the time-crystalline order

The prior results establish the universal phenomoenology associated to critical points where time translation symmetry breaks spontaneously for a large class of systems, with any internal $O(N)$ group and no additional hydrodynamic modes. We turn to universal scaling laws within the time crystalline phases itself in chapter 6. Since these phases break continuous symmetries, first and foremost time translation symmetry, there is gapless Goldstone modes which in turn lead to universal scaling laws within the phases. These scalings are observable throughout the entire phase and do not require any fine tunings. We find that the scaling laws within the time crystalline phase can differ from the ones of thermal equilibrium realising the KPZ universality class and potentially generalizations thereof. Observation of these scaling laws is a signature of the time-crystalline orders described by the nonthermal $O(N)$ model.

2.4.1 No internal symmetry

In the case of $N = 1$, a simple real field, where there is no internal continuous symmetry, we show how the spontaneous breaking of time translation symmetry

leads to gapless fluctuations along the limit cycle. Since there is a distinct direction of growth along the limit cycle, these fluctuations are described by the paradigmatic KPZ equation, initially designed to describe roughening of growing surfaces. Further, since time translation symmetry is only broken to discrete translations by the limit cycle period, the broken symmetry group is $\mathbb{R}/\mathbb{Z} \cong SO(2)$. This means, that there is vortices in low dimensions which can unbind and destroy quasi-long range order through the BKT mechanism. The KPZ nonlinearity is marginally relevant in two dimensions and expected to unbind vortices, thus there is no true long quasi long range order in two-dimensional time crystals. In summary, in a situation with no continuous internal symmetries, the following scaling behavior is observable in time-crystalline matter:

One dimension – There is no long range order. However on length scales dominated by phase fluctuations, the decay of the correlation function $\mathcal{C}(t, \mathbf{x})$ is

$$\mathcal{C}(t, 0) \sim e^{-At^{2\beta}} \tag{2.12}$$

$$\mathcal{C}(0, r) \sim e^{-Br^{2\chi}}. \tag{2.13}$$

where χ is the roughness exponent, and $\beta = \chi/z$, where z is the dynamical critical exponents. For thermal diffusion in one dimension $z = 2$ and $\beta = 1/4$. In the KPZ phase, the exponents are known exactly in one dimension: $\beta = 1/3$, $\chi = 1/2$.

Two dimensions – There is nonuniversal length scales ξ_{KPZ} and ξ_{BKT} determining the onset of KPZ scaling and vertex unbinding respectively. If $\xi_{KPZ} \ll \xi_{BKT}$ this leads to the following scaling of the equal time correlation function

$$\mathcal{C}(0, r) \sim \begin{cases} e^{-r/\xi_{BKT}} & \text{for } r \gg \xi_{BKT} \\ e^{-Br^{2\chi}} & \text{for } \xi_{KPZ} \ll r \ll \xi_{BKT} \\ r^{-\alpha} & \text{for } r \ll \xi_{KPZ} \end{cases} \tag{2.14}$$

with the KPZ exponent $\chi \approx 0.78$ [59]. If $\xi_{BKT} \lesssim \xi_{KPZ}$, the KPZ scaling regime vanishes.

Three dimensions – In three spatial dimensions, the Gaussian fixed point of the phase fluctuations is stable. Therefore, there is a stable time-crystal order with

gapless diffusive behavior

$$\mathcal{C}(t,\mathbf{x}) = x^{2-d}\hat{\mathcal{C}}(x^2/t). \tag{2.15}$$

However, there is the KPZ roughening transition predicted in three dimensions at a finite strength of the nonlinearity. We therefore speculate, that the realisation of time-crystalline matter in three dimensions can provide a path towards a realization of this nonequilibrium transition in a physical system.

2.4.2 Time crystalline order in the $O(N)$ model

The situation becomes more cumbersome but also richer in the presence of an internal $O(N)$ symmetry group. Most strikingly, as we have seen for $N \geq 2$ there is not a single time-crystalline phase but two distinct ones, the oscillating and the rotating phase. Both of them spontaneously break not only the $SO(2)$ part of time translation but also the $O(N)$ group, but in different patterns. The oscillating phase breaks the $O(N) \times SO(2)$ group down to $O(N-1)$ while the rotating phase breaks it to $O(N-2) \times SO_d(2)$. There is a total of N broken symmetry generators ($N-1$ associated to the internal $O(N)$ group and one to time translations) and corresponding gapless modes in the oscillating phase. In the rotating phase this number grows to $2N-3$ broken generators and respective gapless excitations. How do these additional Goldstone modes impact the scaling behaviors identified above? Does scaling break down or is there new fixed points, differing from KPZ? To answer these questions, we develop an effective field theory for the Goldstone modes of the respective phases. Formally, the Goldstone modes live in the coset spaces of the respective symmetry breaking pattern $O(N) \times SO(2)/O(N-1)$ for the oscillating phase and $O(N) \times SO(2)/(O(N-2) \times SO_d(2))$ for the rotating phase. We systematically construct the actions for the modes within these symmetry spaces to leading order in field amplitudes and identify two additional nonlinearities that are marginal in two dimensions, such as the KPZ coupling, in the oscillating phase and three in the rotating phase. While the one-loop RG flow equations have been studied in the physically rather different set up of drifting polymers [60, 61], the ones of the rotating phase are entirely new to the knowledge of the author.

In a first analysis, we identify various fixed points governing the (sub)exponential decay of correlations in one dimensions. These scalings generalize the results presented for the case of the single Goldstone mode of time translation above. It turns out, that for many fixed points, there is only a weak scaling form, where the correlation functions of the Goldstone modes θ corresponding to the internal symmetry genera-

tors scale differently than the one of the Goldstone mode of time translations α. We thus distinguish between the respective exponents $z_\alpha, z_\theta, \chi_\alpha, \chi_\theta$. In the oscillating phase, for $N \leq 4$, there is a parameter regime where the system flows to a strongly coupled KPZ fixed point where $z_\alpha = z_\theta = 3/2$ and $\chi_\alpha = \chi_\theta = 1/2$. This fixed point exists however only for $N \leq 5$, and not at all in other parameter regimes, where the system displays weak scaling $z_\theta \neq z_\alpha$ with nontrivial scaling laws. In the rotating phase, we cannot identify a fixed point with strong scaling at all, at least on the one-loop level employed here. Instead, the system flows to weak scaling with $z_\theta = 2$ and $z_\alpha = 1/2$.
These results are restricted to one-loop approximations of the RG flow, but clearly identify a whole set of novel scaling regimes with nontrivial exponents in time-crystalline matter.

2.5 Realisations

In the last part of this thesis we present schemes to realise the phases and transitions described above in physical systems. The key ingredients are an $O(N)$ symmetry, no relevant conserved charges, and a nonequilibrium pumping contribution that triggers time translation symmetry. The many nonuniversal aspects of the transitions and phases, such as for instance the value of critical pump strengths or couplings etc, depend on the microscopic details of the respective systems and cannot be quantitatively predicted from effective field theory. The universal scaling exponents presented above and derived in detail in the main text of this thesis are however only relying on symmetry and should be observable in all presented systems.
In the following we will describe two generic ways to create time-crystalline phases in systems with an $O(N)$ (or $\mathbb{Z}_2$) symmetry. First, we consider parametric pumping at a high frequency of a system with a small damping. Then, we turn to nonreciprocally coupled order parameter fields. We finish by a concrete realisation scheme for a ferrimagnet driven by oscillating magnetic fields.

2.5.1 Parametrically pumped magnets

Based on symmetry, the question arises, how the time-crystalline phase can be induced in systems whose dynamics is described by an effective $O(N)$ potential theory in thermal equilibrium by suitable drives. A prime example of such a system are Heisenberg Antiferromagnet or Ferromagnets, whose long wavelength dynamics are captured by an $SO(3)$ symmetric theory. Typically, the total magnetization is not conserved by coupling to e.g. phononic bathes which leads to a Gilbert damping.

Can we induce a limit cycle phase in such a system by a realistic driving protocol? The key step to trigger the instability towards a dynamical limit cycle is, as discussed in the mean field analysis, to generate an antidamping from a pump. This can in principle be achieved by coupling a system to an inverted bath with a highly occupied reservoir at high frequencies. This is done for instance in driven-dissipative exciton polariton condensation [62, 63, 64]. By parametrically pumping an $O(N)$ order parameter density at a high frequency Ω, a high mode occupation is generated through parametric resonance at modes with momenta q_Ω such that their frequency is $\omega(\mathbf{q}_\Omega) = \Omega/2$. Such a pump can for instance be realised by oscillating electric fields [65]. These modes now scatter incoherently into the long wavelength regime. In a closed system this scattering is ultimately responsible for thermalization, we keep the long wavelength regime however at a finite temperature by coupling to a cold thermal bath. Under these circumstances, the parametrically excited modes at large momenta serve as the inverted reservoir and we derive analytically, that it yields the desired antidamping effect.
The crucial nonlinearities u and u' are generated, as well, however the reservoir also heats the system up. This will eventually overcome the antidamping contribution at very high reservoir occupations and the limit cycle phase can only be realised, if the equilibrium damping is not too large. We find the rotating phase also numerically in cubic systems subject to the parametric drive. The resulting schematic phase diagram is shown in 2.5.

2.5.2 Nonreciprocal Matter

Another general approach to realise time-crystalline phases in nonequilibrium systems is so-called nonreciprocal matter, a concept that has sparked considerable research activity recently [28, 29, 66, 67, 30, 68, 69, 31, 70, 71]. The basic idea is to couple to degrees of freedom A and B in a way that is ruled in equilibrium dynamics by the action-reaction principle through so called nonreciprocal interactions. This means that the way that A reacts to B is not mirrored by the way B reacts to A. A simple example in active matter is for instance flocking birds. Within a flock a bird only sees the bird in front of it and aligns with it but not the one behind it. The interaction between two individual birds is not reciprocal. This leads to models with so-called vision-cone interactions [72]. The more extreme case occurs when the reaction from A to B is attractive while the reaction from B to A is repulsive. If, for example, one considers two spins whose nonreciprocal interaction is such that A wants to align with B while B wants to antialign with A, there is a parameter regime where A and B start to perpetually rotate in a sort of "catch and run". This behavior

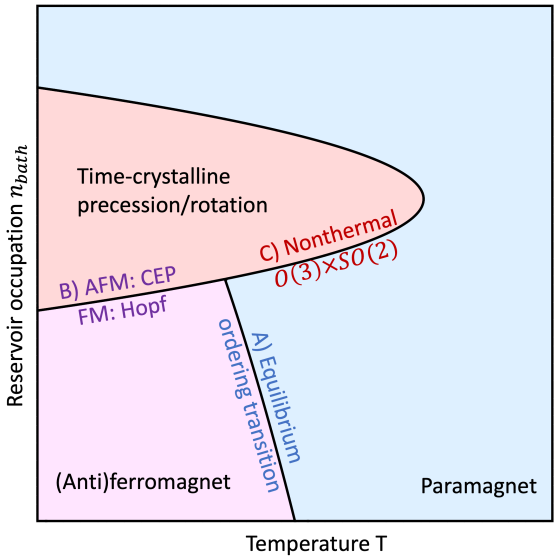

Figure 2.5: Schematic phase diagram of the parametrically pumped $SO(3)$ model. Heating competes with antidamping and time-crystalline order emerges in a finite range of pumping strengths. The universality classes of the transitions are determined in chapter 7.1.

extends to the case of nonreciprocally coupled fields in d spatial dimensions [28]. In 7.3, we show that the universal long wavelength dynamics of these dynamic phases and the 'nonreciprocal phase transition' into that phase are governed by the effective field theory developed in this thesis. This means that while there is a current effort to engineer spin systems, such that they interact nonreciprocally on the microscopic level and realise nonreciprocal phase transitions [30, 71], the macroscopic universal phenomena associated to time translation symmetry breaking can also be realised by the pumping scheme laid out above.

2.5.3 Rotating Ferrimagnet

The transition between the ordered and rotating phase can also be realised in principle by arbitrarily weak drives out of equilibrium in solid state systems. The gapless nature Goldstone mode makes it very easy to excite by drives. However, usually it is hard to generate a directed motion along the Goldstone mode, e.g. if it is a $O(2)$ phase φ induce a coherent rotation $\langle\varphi\rangle = \omega\, t$. Typically, there is at least a $\mathbb{Z}_2$ symmetry $\varphi \to -\varphi$ such that external drives induce a righthanded rotation equally often as a lefthanded one, and on average $\langle\varphi\rangle = 0$ and the system simply heats up. This is different, if there is low enough symmetry such that there is a preferred direction. Time reversal symmetry in thermal equilibrium still prevents a coherent

directed motion, the same arguments that rule out a continuous time crystal in equilibrium, but as soon as external drives break equilibrium conditions, directed motion is possible. This principle has been successfully demonstrated in systems where the translational symmetries of the microscopic lattice are broken by a large scale pattern, such as shown recently for large magnetic textures that are incomensurate with the microscopic lattice [73, 74, 75]. The breaking of spatial translation symmetry leads to a (quasi) gapless (quasi) Goldstone mode that moves the pattern. Since there is low enough symmetry such that there is a preferred direction, a very fast external drive can lead to a slow collective rotation of the structure.

In that spirit, we consider a ferrimagnetic system in 7.2. The closed system has no full $SO(3)$ spin rotation symmetry, but a $SO(2)$ symmetric xy plane and a $\mathbb{Z}_2$ symmetry flipping the orthogonal z component of the magnetic moments. Below a temperature T_N it develops an antiferromagnetic order within the xy plane, spontaneously breaking the $SO(2)$ symmetry. Upon cooling the system further, there is an Ising like transition at $T_c < T_N$ where the system develops ferromagnetic order along the z-axis. In this ferrimagnet (coexistence of antiferromagnetic and ferromagnetic orders), the Ising order parameter singles out a preferred direction of rotation. We show, that driving the system simply by a rapidly oscillating magnetic field, couples the xy Goldstone mode φ to the Ising order parameter m_z such that $\partial_t \varphi = \gamma_z m_z + ...$ and the staggered magnetization in the xy plane starts to rotate collectively in the xy-plane. Since γ_z is proportional to the driving power, this happens already at arbitrarily small drives. We show, that the transition between the ordered xy phase into the ferrimagnet at any finite drive strength is indeed governed by the nonthermal $O(N)$ model. We can thus predict the critical phenomena observable in the driven ferrimagnet – a fluctuation induced first order transition, the massive fluctuations close to the CEP, KPZ-scaling within the phase in low dimensions and a divergent effective 'temperature' at the transition between paramagnet and rotating ferrimagnet. The schematic phase diagram is shown in figure 2.6.

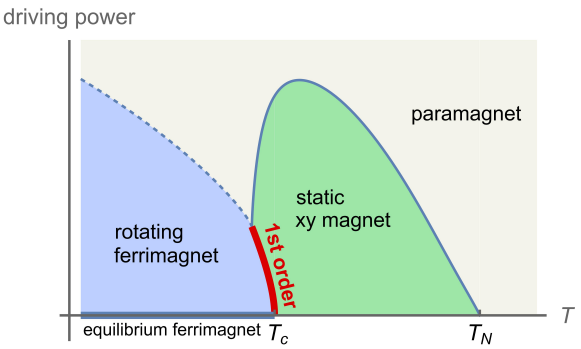

Figure 2.6: Schematic phase diagram of a driven ferrimagnet as function of temperature and the power of an external driving source, e.g., a laser or an oscillating magnetic field. We assume that in equilibrium the system displays antiferromagnetic xy order for $T < T_N$ and becomes a ferrimagnet for $T < T_c < T_N$ by developing an extra out-of-plane ferromagnetic component. Driving induces in the ferrimagnetic phase a rotation of the xy order parameter. The transition is governed by a critical exceptional point (CEP) with its characteristic first-order phase transition (red line). The enhancement of fluctuations close to the CEP bends the transition line between paramagnet and xy order down, culminating in a multicritical point where all transition lines meet. For larger driving strength also a direct transition from the paramagnetic into the rotating ferrimagnetic phase will occur. Thus, all phases and phase transitions of the effective model, Fig. 2.1, can be realized. Originally published in [44]

3

Field theory methods

Before turning to the detailed derivations of the results presented above, we briefly introduce the relevant methodology and notation in this chapter. This first three sections of this introduction are a modified version of the respective parts of [44].

3.1 MSRJD: From Langevin equations to path integrals

To systematically study how noise fluctuations in spatially extended systems in the presence of nonlinearities impact the critical behavior at transitions and within phases with spontaneously broken transitions, we turn to the powerful framework of path integrals and generating functionals for fluctuating field theories. For stochastic dynamics like (2.2), this is done via the Martin-Siggia-Rose-Janssen-DeDominicis (MSRJD) construction [76, 77, 78]. A Langevin equation

$$\mathcal{L}[\boldsymbol{\phi}]\boldsymbol{\phi}(t,\mathbf{x}) + \boldsymbol{\xi}(t,\mathbf{x}) = 0 \tag{3.1}$$

with Gaussian white noise

$$\langle \boldsymbol{\xi}_i(t,\mathbf{x})\boldsymbol{\xi}_j(t',\mathbf{x}')\rangle = 2D\delta(t-t')\delta(\mathbf{x}-\mathbf{x}')\delta_{ij}. \tag{3.2}$$

corresponds to a path integral

$$Z[\boldsymbol{\jmath}, \tilde{\boldsymbol{\jmath}}] = \int \mathcal{D}\boldsymbol{\phi}\mathcal{D}i\tilde{\boldsymbol{\phi}} e^{-S[\boldsymbol{\phi},\tilde{\boldsymbol{\phi}}]+\int_X \tilde{\boldsymbol{\jmath}}^T\boldsymbol{\phi}+\boldsymbol{\jmath}^T\tilde{\boldsymbol{\phi}}} \tag{3.3}$$

with the action

$$S[\tilde{\boldsymbol{\phi}}, \boldsymbol{\phi}] = \int_X \tilde{\boldsymbol{\phi}}^T(X)\mathcal{L}[\boldsymbol{\phi}]\boldsymbol{\phi}(X) - D\tilde{\boldsymbol{\phi}}^T(X)\tilde{\boldsymbol{\phi}}(X). \tag{3.4}$$

$\boldsymbol{\phi}$ is the N-component order parameter field also entering the Langevin equation, and we introduced $X = (\mathbf{x}, t)$ to streamline notation. $\tilde{\boldsymbol{\phi}}$ is an N-component auxiliary variable, associated to the noise, often referred to as response or quantum field. The MSRJD action of the nonthermal $O(N)$ model (2.2) is then

$$S[\boldsymbol{\phi}, \tilde{\boldsymbol{\phi}}] = S_0[\boldsymbol{\phi}, \tilde{\boldsymbol{\phi}}] + S_{\text{int}}[\boldsymbol{\phi}, \tilde{\boldsymbol{\phi}}], \tag{3.5a}$$

$$S_0[\boldsymbol{\phi}, \tilde{\boldsymbol{\phi}}] = \int_X \tilde{\boldsymbol{\phi}}(X)^T\Big(\partial_t^2 + (2\gamma - Z\nabla^2)\partial_t + r - v^2\nabla^2\Big)\boldsymbol{\phi}(X) - D\tilde{\boldsymbol{\phi}}(X)^T\tilde{\boldsymbol{\phi}}(X) \tag{3.5b}$$

$$S_{\text{int}}[\boldsymbol{\phi}, \tilde{\boldsymbol{\phi}}] = \int_X \lambda\tilde{\boldsymbol{\phi}}(X)^T\boldsymbol{\phi}(X)\rho(X) + u\tilde{\boldsymbol{\phi}}(X)^T\partial_t\boldsymbol{\phi}(X)\rho(X) + \frac{u'}{2}\tilde{\boldsymbol{\phi}}(X)^T\boldsymbol{\phi}(X)\partial_t\rho(X). \tag{3.5c}$$

The path integral $Z[\boldsymbol{\jmath}, \tilde{\boldsymbol{\jmath}}]$ generates the noise averaged correlation and response functions of the Langevin dynamics by taking derivatives with respect to the source fields $\boldsymbol{\jmath}$, $\tilde{\boldsymbol{\jmath}}$, and evaluating at vanishing sources. In particular, the (retarded) two-point response function and correlation function are, again using a shorthand notation $Q = (\mathbf{q}, \omega)$

$$\chi^R_{ij}(Q, Q') = \frac{\delta^2 \ln Z}{\delta\tilde{j}_i(Q)\delta j_j(Q')}\Big|_{\boldsymbol{\jmath}=\tilde{\boldsymbol{\jmath}}=0} \equiv G^R_{ij}(Q)\delta(Q + Q'), \tag{3.6}$$

$$\mathcal{C}_{ij}(Q, Q') = \frac{\delta^2 \ln Z}{\delta\tilde{j}_i(Q)\delta\tilde{j}_j(Q')}\Big|_{\boldsymbol{\jmath}=\tilde{\boldsymbol{\jmath}}=0} \equiv G^K_{ij}(Q)\delta(Q + Q'), \tag{3.7}$$

where we used time and space translation invariances. The rotating phase has a time-dependent stable state which generically breaks this structure, but we will see that in the proper comoving frame it is recovered.

These objects represent the *full* two-point Green functions of the theory, including all corrections due to nonlinearities and noise. Absent spontaneous symmetry breaking, they are $\propto \delta_{ij}$ by $O(N)$ symmetry. The full Green function in Fourier

space $\mathcal{G}(Q)$ is a 2×2 matrix in the Nambu space $\mathbf{\Phi}=(\boldsymbol{\phi},\tilde{\boldsymbol{\phi}})^T$ and has the form

$$\mathcal{G}(Q)=\begin{pmatrix} G^K(Q) & G^R(Q)\\ G^A(Q) & 0\end{pmatrix}. \tag{3.8}$$

We introduce here a notation borrowed from Keldysh field theory, with retarded (G^R), advanced ($G^A=(G^R)^\dagger$) and Keldysh (G^K) component for the Green function. It highlights the connection to the Keldysh formalism for quantum systems out of equilibrium, from which the MSRJD path integral emerges as a semiclassical limit, see e.g. [8] for a review.

3.2 The effective action

While the path integral for the dynamical partition function, Eq. (3.3), encodes all information of the problem, we transit here to another object – the effective action (see [79] for an in-depth discussion of this object, and [8, 36] for the nonequilibrium effective action). It encodes the same information but organizes it in a way that is beneficial for the analysis of the present problem, both conceptually and in terms of practical calculations. For example, it allows for a simple proof of Goldstone's theorem, and the construction of the associated soft modes including in the rotating phase. It will also enable us to develop a quantitative potential picture for the fluctuation induced first order transition.

The effective action functional is defined as the Legendre transform of the generating functional for connected correlation functions, $W[\boldsymbol{j},\tilde{\boldsymbol{j}}]=\ln Z[\boldsymbol{j},\tilde{\boldsymbol{j}}]$: $\Gamma[\boldsymbol{\varphi},\tilde{\boldsymbol{\varphi}}]=\sup_{j,\tilde{j}}[-W[\boldsymbol{j},\tilde{\boldsymbol{j}}]+\int_X \boldsymbol{j}\tilde{\boldsymbol{\varphi}}+\tilde{\boldsymbol{j}}\boldsymbol{\varphi}]$. Similarly to a classical action, the effective action induces an equation of motion. Its solution $\boldsymbol{\varphi}_s$ yields the physical field expectation value, with $\boldsymbol{\varphi}_s\neq 0$ signalling macroscopic occupation/condensation, while $\tilde{\boldsymbol{\varphi}}=0$ when evaluated at the physical point due to probability conservation [80]. The full equation of motion is given by

$$\frac{\delta\Gamma}{\delta\boldsymbol{\varphi}}\Big|_{\boldsymbol{\varphi}=\langle\boldsymbol{\phi}\rangle,\tilde{\boldsymbol{\varphi}}=\langle\tilde{\boldsymbol{\phi}}\rangle}=\frac{\delta\Gamma}{\delta\tilde{\boldsymbol{\varphi}}}\Big|_{\boldsymbol{\varphi}=\langle\boldsymbol{\phi}\rangle,\tilde{\boldsymbol{\varphi}}=\langle\tilde{\boldsymbol{\phi}}\rangle}=0. \tag{3.9}$$

The effective action has an intuitive path integral representation as

$$\Gamma[\boldsymbol{\varphi},\tilde{\boldsymbol{\varphi}}]=-\ln\int \mathcal{D}\boldsymbol{\phi}\mathcal{D}i\tilde{\boldsymbol{\phi}}e^{-S[\boldsymbol{\phi}+\boldsymbol{\varphi},\tilde{\boldsymbol{\phi}}+\tilde{\boldsymbol{\varphi}}]+\frac{\delta\Gamma}{\delta\tilde{\boldsymbol{\varphi}}}\tilde{\boldsymbol{\phi}}+\frac{\delta\Gamma}{\delta\boldsymbol{\varphi}}\boldsymbol{\phi}}, \tag{3.10}$$

with $\tilde{\boldsymbol{j}}=\frac{\delta\Gamma}{\delta\boldsymbol{\varphi}}$, $\boldsymbol{j}=\frac{\delta\Gamma}{\delta\tilde{\boldsymbol{\varphi}}}$. Eq. (3.10) states that the effective action obtains from the bare action by summing over all possible configurations of the Nambu field $\mathbf{\Phi}=(\boldsymbol{\phi},\tilde{\boldsymbol{\phi}})^T$.

Conversely, omitting fluctuations in a mean-field approximation reproduces the bare action, $\Gamma[\boldsymbol{\varphi}, \tilde{\boldsymbol{\varphi}}] = S[\boldsymbol{\varphi}, \tilde{\boldsymbol{\varphi}}]$. The representation makes it transparent that the effective action shares the symmetries of the bare one absent sources.

The second derivative with respect to the Nambu field $(\boldsymbol{\varphi}(Q), \tilde{\boldsymbol{\varphi}}(Q))^T$ around a time and space translation invariant solution of the equations of motion satisfies

$$\begin{aligned}\left(\Gamma^{(2)}(Q,Q')\right)^{-1} &= \begin{pmatrix} 0 & \Gamma^A(Q) \\ \Gamma^R(Q) & \Gamma^K(Q) \end{pmatrix}^{-1} \delta(Q+Q') \\ &= \begin{pmatrix} G^K(Q) & G^R(Q) \\ G^A(Q) & 0 \end{pmatrix} \delta(Q+Q'), \end{aligned} \tag{3.11}$$

and thus gives the full Green function of the theory in $\mathbf{q}, \omega$-space including the retarded and advanced responses $G^{R/A}(Q) = \left(\Gamma^{R/A}(Q)\right)^{-1}$ and the correlation function $G^K(Q) = -G^R(Q)\Gamma^K(Q)G^A(Q)$ [1].

Higher order field derivatives of Γ give the full one-particle irreducible (1PI), or amputated, correlators. To streamline equations in the remainder of the text, we introduce the following notation for field derivatives of the effective action evaluated on $\boldsymbol{\varphi} = \langle \boldsymbol{\phi} \rangle$:

$$\Gamma^{(m,n)}_{i_1 \ldots i_{n+m}}(X_1, \ldots, X_{n+m}) \equiv \frac{\delta^{m+n}\Gamma}{\delta\tilde{\varphi}_{i_1}(X_1)\ldots\delta\tilde{\varphi}_{i_m}(X_m)\delta\varphi_{i_{m+1}}(X_{m+1})\ldots\delta\varphi_{i_{n+m}}(X_{m+n})}. \tag{3.12}$$

Similarly, we can write the functional derivatives of the original MSRJD action $S^{(m,n)}$. In that sense, one can understand the vertices $\Gamma^{(m,n)}(X_1, \ldots, X_{m+n})$ as the fully renormalized, spacetime dependent analogs of the original couplings $S^{(m,n)}$. For instance, in the case of the nonthermal Ising or Van der Pol model, (3.5) but for $N = 1$, i.e. a single real field, we have

$$S^{(1,3)}(Q_1, Q_2, Q_3, Q_4)\Big|_{\tilde{\varphi}=\varphi=0} = (6\lambda - 2i(\omega_2 + \omega_3 + \omega_4)u)\ \delta\left(\sum Q_i\right). \tag{3.13}$$

And we can define the fully renormalised versions $\bar{\lambda}, \bar{u}$ of the couplings λ, u by projecting on the respective frequency structures of $\Gamma^{(1,3)}(Q_1, \ldots, Q_4)$.

[1] Note that a breaking of time translation invariance leads to Green functions that are not diagonal in frequency space.

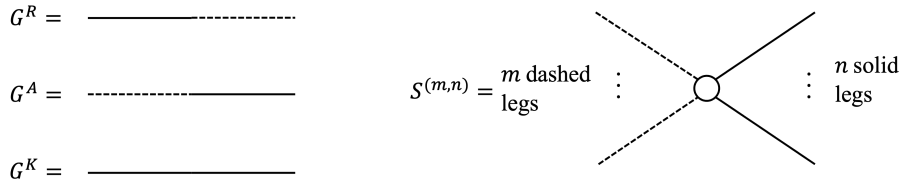

Figure 3.1: Basic diagrammatic rules adopted in this thesis.

3.2.1 Diagrammatics

Importantly, the vertices can be represented in a perturbative series in terms of the microscopic nonlinearities $S^{(m,n)}$ and the bare Green functions. The series can be represented diagramatically by the respective one-particle irreducible diagrams, see e.g. [36] or [80] for an introduction on dynamic perturbation theory and diagrammatic techinques for MSRJD or Schwinger-Keldysh path integrals. Here, we choose the convention, that straight lines correspond to fields $\boldsymbol{\varphi}$ while dashed lines correspond to response fields $\tilde{\boldsymbol{\varphi}}$. Thus, a bare Keldysh Green function is represented by a straight line, while a bare retarded Green function corresponds to a dashed line that turns into a full line (and vice versa for the advanced Green function). Vertices $S^{(m,n)}$ have m dashed and n full lines as sketched in Fig. 3.1

A full resummation of these diagrams yields the Dyson-Schwinger equations for the respective vertices [6]. For a real field theory whose microscopic action contains only contains terms up to quartic order in fields the lowest order Dyson-Schwinger equation (DSE) reads schematically

$$\Gamma^{(1)}_{I_1} = S^{(1)}_{I_1} + \frac{1}{2} S^{(3)}_{I_1} G - \frac{1}{6} S^{(4)}_{I_1} GGG\Gamma^{(3)}, \tag{3.14}$$

where the superscript (n) denotes the total number of field derivatives and I_1 denotes a super index containing all internal and external degrees of freedom characterising a field configuration (e.g. space, time and $\mathbb{R}^N$ vector index and an index distinguishing fields and response fields for a $O(N)$ symmetric MSRJD field theory). All internal indices that are traced over are supressed above. Importantly, (3.14) is valid for any field configuration. We can generate the higher order DSEs by taking functional derivatives with respect to the fields, using (3.11), i.e.

$$\frac{\delta}{\delta \boldsymbol{\phi}_{I_1}} G_{I_2 I_3} = -G_{I_2 I_4} \Gamma^{(3)}_{I_4 I_1 I_5} G_{I_5 I_3} \tag{3.15}$$

with traces over the superindices I_4, I_5 and only evaluated at the correct saddle point

(e.g. for an expansion in a symmetric phase $\boldsymbol{\varphi}, \tilde{\boldsymbol{\varphi}} = 0$) in the end. The resulting equations are exact self consistent equations for the fully renormalized, momentum and frequency dependent vertices of the theory. There is of course a conservation of difficulty, and they cannot be simply solved. E.g. iteratively solving the resulting tower of self consistent equations with the starting Ansatz $\Gamma = S$ reproduces the 1PI perturbative series. Still, the DSEs will come in handy in 5, where we can solve them in a controlled manner.

3.3 Thermal equilibrium via a symmetry

So far, we have not explained how exactly we diagnose an (emergent) thermal equilibrium in our system in practice. If the system is in thermal equilibrium, the full correlation and response functions obey a Fluctuation Dissipation Relation (FDR), which reads for the two-point functions ($k_\mathrm{B} = 1$)

$$G^K(Q) = \frac{2T}{i\omega}\Big(G^R(Q) - G^A(Q)\Big). \tag{3.16}$$

In thermal equilibrium with global detailed balance, fluctuation-dissipation relation (FDR)s have to hold not only for the full, renormalized two-point Green functions, but also for all higher n-point correlations and responses as well. This leads to an infinite tower of relations to be checked. This can however be elegantly avoided, as the FDR can be understood as a consequence of a symmetry of the MSRJD (or Schwinger-Keldysh) action and effective action [78, 81, 82, 83, 8, 84, 85, 86]. Rather than calculating all full n-point functions, it is sufficient to check if the MSRJD action has that symmetry to establish if the system is in thermal equilibrium or not. For $O(N)$ vector fields, this thermal symmetry is given by

$$\begin{aligned} &\boldsymbol{\varphi}(\mathbf{x}, t) \to \boldsymbol{\varphi}(\mathbf{x}, -t), \\ &\tilde{\boldsymbol{\varphi}}(\mathbf{x}, t) \to \tilde{\boldsymbol{\varphi}}(\mathbf{x}, -t) + \beta\partial_t \boldsymbol{\varphi}(\mathbf{x}, -t). \end{aligned} \tag{3.17}$$

There is one parameter in the transformation, which is associated to the temperature $\beta = \frac{1}{T}$, shared by all subsystems (all subsystems are in equilibrium with each other, sometimes referred to as detailed balance). Force terms $\sim \tilde{\boldsymbol{\phi}}(\mathbf{x}, t)F[\boldsymbol{\phi}]$ in the Lagrangian generate the following additional contribution under the symmetry

operation (3.17)

$$\int_t \tilde{\boldsymbol{\phi}}(\mathbf{x},t)F[\boldsymbol{\phi}] \to \int_t \tilde{\boldsymbol{\phi}}(\mathbf{x},t)F[\boldsymbol{\phi}] + \delta S, \tag{3.18}$$

$$\delta S = \int_t \beta\partial_t \boldsymbol{\phi}(\mathbf{x},t)F[\boldsymbol{\phi}]. \tag{3.19}$$

If now the force $F[\boldsymbol{\phi}]$ is conservative, i.e. $F[\boldsymbol{\phi}] = -\frac{\delta V}{\delta \boldsymbol{\phi}}$ we have

$$\delta S = \int_t \frac{dV[\boldsymbol{\phi}]}{dt} = 0. \tag{3.20}$$

Thus, any conservative term is invariant under (3.17). Non-conservative damping terms are allowed in equilibrium, however only if they come with associated noise terms with a strict relation for the coefficients, e.g. for the full momentum dependence of the damping

$$\sim \int_{\mathbf{q},t} \bar{\gamma}(\mathbf{q})\tilde{\varphi}_i(\partial_t\varphi_i - T\tilde{\varphi}_i), \tag{3.21}$$

$$\sim \int_{\mathbf{q},t} (2\bar{\gamma} + \bar{Z}\mathbf{q}^2 + \dots)\tilde{\varphi}_i(\partial_t\varphi_i - T\tilde{\varphi}_i), \tag{3.22}$$

so that the thermal symmetry is realised. The presence of the thermal symmetry is then equivalent to the existence of a fixed ratio between dissipative and fluctuating terms.

In other words, the quadratic part of the action (3.5a) is invariant under this transformation if the full renormalized damping $\bar{\gamma}(\mathbf{q})$ and the full renormalized noise level $\bar{D}(\mathbf{q})$ are proportional to each other with

$$T = \frac{\bar{D}(\mathbf{q})}{2\bar{\gamma}(\mathbf{q})}, \tag{3.23}$$

where in a state of true thermal equilibrium the temperature is independent of the momentum $\mathbf{q}$.

If the system is driven out of equilibrium on a more microscopic level, such a fine tuning of parameters is unnatural. However, thermal symmetry (i.e. equilibrium) can emerge under coarse graining at long wavelength, e.g. in the vicinity of phase transitions [17, 19, 87].

3.4 Universal scaling and critical phenomena

We now briefly introduce the concepts needed in this thesis to determine the universal critical exponents. For a more detailed introduction to renormalization group techniques, we refer to the literature, e.g. [6, 88]. Dynamic scaling and RG for MSRJD path integrals can be found for instance in [36] and [8].
At critical points, or more generally in the presence of gapless excitations, the correlation length of correlation as well as responses diverges. This leads to algebraic scaling behavior of physical observables. The exponents of this algebraic scaling are dimensionless numbers that do not depend on any scale, in fact at a critical point there is no inherent scale, and only have information about dimension and symmetries of the system. In the vicinity of a nonequilibrium critical point, we parametrize the dynamical correlation and response functions of a complex field as

$$\chi^R(\boldsymbol{q},t) \sim q^{-2+\eta'+z}\tilde{\chi}^R(tq^z, iq^{\eta-\eta_c}, qr^{-\nu}), \tag{3.24}$$

$$C(\boldsymbol{q},t) \sim q^{-2+\eta}\tilde{C}(tq^z, iq^{\eta-\eta_c}, qr^{-\nu}). \tag{3.25}$$

Here, r is the single parameter that is fine-tuned to zero to reach the critical point. The exponent ν describes how the correlation length diverges, as one tunes to criticality $\xi \sim r^{-\nu}$. The dynamical critical exponent z fixes how the life time of excitations τ diverges at the critical point with the correlation length $\tau \sim \xi^z$. The anomalous dimensions η and η' determine how interactions alter the singularities of correlation and response function from the ones of the bare, Gaussian theory. In thermal equilibrium they are tied to each other, $\eta = \eta'$ by the fluctuation dissipation theorem

$$\mathcal{C}(\omega,\mathbf{q}) = \frac{2T}{\omega}\chi^R(\omega,\mathbf{q}). \tag{3.26}$$

The static exponents ν and η fix the universality class in thermal equilibrium and are solely determined by symmetry and dimension. Relaxational dynamics towards the equilibrium additionally depends on the potential presence of conserved currents and require reversible mode coupling of critical and hydrodynamic modes determining the dynamical exponent z. For transitions breaking an $O(N)$ symmetry, this is the paradigmatic classification of Halperin and Hohenberg [1]. Far from thermal equilibrium fluctuation dissipation relations do not hold and the correlations and response can attain differing anomalous scaling dimensions. A subtle but important exponent is η_c, which has been identified in [89]. It is a subleading, anomalous scaling contribution that describes how an effective thermal equilibrium can emerge under coarse graining. It essentially captures how a violation of the thermal symmetry laid

out above can vanish under coarse graining. We will see this in more detail in 4. To determine these universal critical exponents, one thus needs to calculate the full inverse Green function $\Gamma^{(2)}(\omega, \mathbf{p})$ of the corresponding MSRJD field theory. This is of course easier said than done. An exact derivation of the full correlations and responses at any point in parameter space is usually impossible to begin with, but if the perturbative expansion in loop corrections may be convergent, so that one can get controlled, approximate results. At the critical point however, the simple perturbative loop corrections become singular and we need to something more. Fortunately, the scaling hypothesis comes to aid. We introduce a finite momentum type scale μ and evaluate at a point in parameter space where $r = \mu^2 \tilde{r}$ with $\tilde{r}$ the dimensionless distance from the critical point. Here, the perturbative corrections are still finite and we can derive how they gradually change when slowly decreasing μ. After one such small step, we can replace the bare vertices with the new, updated vertices and perform a small decrease of μ again. Doing this in infinitesimally small steps yields a set of coupled differential equations, the *dimensionfull* perturbative renormalization group β-functions.

$$\mu \partial_\mu g_i = \beta_i(\{g_i\}) \tag{3.27}$$

In the last step we introduce dimensionless versions of all coupling parameters g_i, $g_i = \mu^{\Delta_i} \tilde{g}_i$ such that $\beta_i(\{g_i\}) = \mu^{\Delta_i} \beta_i(\{\tilde{g}_i\})$. This then immediately gives rise to the *dimensionless* RG flow equations

$$\mu \partial_\mu \tilde{g}_i = -\Delta_i \tilde{g}_i + \beta_i(\{\tilde{g}_i\}). \tag{3.28}$$

If we now send $\mu \to 0$ to reach the critical point, we arrive at the fixed points of the dimensionless RG-equations. We remark that in this procedure we keep reinserting vertex corrections into the series. This corresponds to a resummation of an infinite set of perturbative diagrams and is sufficient to remedy the infrared singularity of bare perturbation theory. Since in the vicinity of the fixed point everything scales, we can infer the scaling exponents the scaling exponents scaling of the couplings and the corresponding self energy corrections with μ close to the fixed point. We will see this at work in 4. This procedure is laid out in more detail, for the equilibrium case in e.g. [88]. We note, that on the one-loop level rescaling with a momentum scale μ in the presence of a UV cutoff Λ leads to a UV cutoff Λ/μ for the dimensionless loop integral. This means that the cutoff dependence of the one-loop corrections reproduces the same β functions. Deriving RG equations from the dependence on the UV cutoff of one-loop diagrams corresponds to Wilsonian momentum shell RG

found in many textbooks.

4

Transition from no order to time crystal

We start our detailed discussion of the universal scaling laws in time-crystalline matter with an analysis the critical properties of the transition between the fully symmetric and both time crystalline phases, the rotating as well as the oscillating one. It is marked by a breaking of time translation symmetry. As discussed in chapter 2, time translation can be broken either into rotations or oscillations, both phases differ by their symmetry breaking pattern. The main results of the following field theoretic analysis are:

- The transitions are governed by an $O(N) \times SO(2)$ symmetric field theory
- While both transitions are of second order at mean field and above the upper critical dimension, fluctuations render one them first order below the critical dimension
- The other transition is governed by a nonthermal fix point at which no effective thermal equilibrium emerges. This manifests in critical exponents violating fluctuation dissipation relations and divergent effective scale dependent temperatures.

This chapter is based on [43] but rewritten and rearranged. The perturbative RG analysis adopts a slightly different scheme without multiplicative counter terms but

is equivalent at the leading order in perturbation theory considered here. All figures presented in this section were published in [43].

4.1 MF phases + Symmetry breaking pattern

At the transition between the fully disordered and the time-crystalline order, not only the internal $O(N)$ symmetry breaks spontaneously, but also time translation. Continuous time translation however does not break down fully, but only to discrete translations by the period of the order parameter limit cycle. Thus the part of time translation that is broken is $\mathbb{R}/\mathbb{Z} \cong SO(2)$ and the field theory describing the fixed point of the transition is characterised by an $O(N) \times SO(2)$ symmetry.
This can be derived explictly in the vicinity of the transition, i.e. at $\gamma \to 0$. The linearised equation of motion reads

$$\left(\partial_t^2 + (2\gamma - Z\nabla^2)\partial_t + r - v^2\nabla^2\right)\boldsymbol{\phi}(\mathbf{x},t) + \boldsymbol{\xi} = 0. \tag{4.1}$$

The corresponding bare correlation function reads

$$\langle \phi_i(\boldsymbol{q},t)\phi_i(-\boldsymbol{q},0)\rangle \sim D\frac{e^{-(\frac{Z}{2}q^2+\gamma)|t|}}{\frac{Z}{2}q^2+\gamma}\cos(\sqrt{r}t + \frac{v^2}{2\sqrt{r}}q^2 t), \tag{4.2}$$

displaying an algebraic divergence as $|\mathbf{q}| = q \to 0$ indicating a divergent correlation length $\xi \sim \gamma^{-\frac{1}{2}}$ implying a second order phase transition with mean field critical exponent $\nu = \frac{1}{2}$. There remains, however, a finite frequency scale $\omega_0 \sim \sqrt{r}$ that spoils full scale invariance. This hinders a straightforward RG analysis to incorporate the effect of interacting fluctuations.
We first have to absorb this scale to distill the correct critical degrees of freedom. To this end, let us first consider the solutions to the deterministic, linearised equations of motion for $\gamma \ll \sqrt{r}$:

$$\boldsymbol{\phi}(\mathbf{x},t) = \boldsymbol{\chi}_1(\mathbf{x},t)\cos\sqrt{r}t + \boldsymbol{\chi}_2(\mathbf{x},t)\sin\sqrt{r}t \tag{4.3}$$

The amplitude fields $\boldsymbol{\chi}_{1,2}(\mathbf{x},t) \in \mathbb{R}^N$ vary slowly in space $\xi \sim \gamma^{-\frac{1}{2}}$ and time $\tau \sim \gamma^{-1}$. Furthermore, it is the amplitudes $\boldsymbol{\chi}_{1,2}$ that develop a finite, static expectation value in the time-crystalline phase. If $\boldsymbol{\chi}_1 \perp \boldsymbol{\chi}_2$ the system is in the rotating phase while $\boldsymbol{\chi}_1 \parallel \boldsymbol{\chi}_2$ marks oscillations along an axis. The external $SO(2)$ time translation symmetry becomes internal in these degrees of freedom: A shift of the zero point of time $t \to t + \alpha$ according to the definition 4.3 corresponds to a rotation of $\boldsymbol{\chi}_1$ and

$\boldsymbol{\chi}_2$ into each other

$$\begin{pmatrix} \boldsymbol{\chi}_1 \\ \boldsymbol{\chi}_2 \end{pmatrix} \to R(\alpha) \begin{pmatrix} \boldsymbol{\chi}_1 \\ \boldsymbol{\chi}_2 \end{pmatrix}, \quad \text{where } R(\alpha) \in SO(2). \tag{4.4}$$

Thus, a theory in terms of these amplitudes will display an $O(N) \times SO(2)$ symmetry. It can be derived from the original equations of motion by the following procedure. First, it is useful to pass to a Hamiltonian formulation of the problem by introducing the conjugate fields $\boldsymbol{\Pi}(\mathbf{x}, t) = \frac{\phi(\mathbf{x},t)}{\sqrt{r}}$. We then insert the dynamic ansatz (4.3) into the coupled equations of motion, which now are first order in time. This produces sinodal terms oscillating at frequencies $\omega = n\sqrt{r}$, $n = 1, 2, 3$. Since these oscillations are much faster than the time scales of the amplitdue fields $\boldsymbol{\chi}_{1,2}$, $\sqrt{r} \gg \gamma$, we can average over them by means of a rotating wave approximation [90]. This removes all explicit time dependencies and the fast frequency scale $\sqrt{r}$ and we arrive at a fully $O(N) \times SO(2)$ symmetric dynamics for the amplitudes $\boldsymbol{\chi}_{1,2}$.

$$\begin{aligned} &\partial_t \boldsymbol{\chi}_a + \frac{\delta H_d}{\delta \boldsymbol{\chi}_a} + \epsilon_{ab} \frac{\delta H_c}{\delta \boldsymbol{\chi}_b} + \boldsymbol{\xi}_a = 0, \quad (a, b) \in \{1, 2\} \\ &H_l = \int d^d \boldsymbol{x} \frac{Z_l}{2} \left[(\boldsymbol{\nabla} \boldsymbol{\chi}_1)^2 + (\boldsymbol{\nabla} \boldsymbol{\chi}_2)^2 \right] + \frac{\gamma_l}{2} \rho + \frac{g_l}{8} \rho^2 + \frac{\kappa_l}{2} \tau, \end{aligned} \tag{4.5}$$

with $l \in \{c, d\}$, $\boldsymbol{\xi}_a$ two independent noises, and the two $O(N) \times SO(2)$ invariants: $\rho = \boldsymbol{\chi}_1^2 + \boldsymbol{\chi}_2^2$ and $\tau = \frac{1}{4} \left(\boldsymbol{\chi}_1^2 - \boldsymbol{\chi}_2^2 \right)^2 + (\boldsymbol{\chi}_1 \cdot \boldsymbol{\chi}_2)^2$. where the parameters of (4.5) in terms of the microscopic model (2.2) $\gamma_c = 0$, $\gamma_d = \gamma$, $Z_c = v^2/2\omega_0$, $Z_d = Z/2$, $g_d = u/2$, $\kappa_d = (u' - u)/4$, $g_c = \lambda/2\omega_0$ and $\kappa_c = \lambda/4\omega_0$. The equivalent MSRJD action is

$$S[\boldsymbol{\chi}, \tilde{\boldsymbol{\chi}}] = \int_{t,\mathbf{x}} \tilde{\boldsymbol{\chi}}_a(t, \mathbf{x}) \left(\partial_t \boldsymbol{\chi}_a(t, \mathbf{x}) + \frac{\delta H_d}{\delta \boldsymbol{\chi}_a(t, \mathbf{x})} + \epsilon_{ab} \frac{\delta H_c}{\delta \boldsymbol{\chi}_b(t, \mathbf{x})} \right) - D \tilde{\boldsymbol{\chi}}_a^2. \tag{4.6}$$

For $H_c = 0$ this model displays a full $O(N) \times O(2)$ symmetry with purely dissipative dynamics. This case is in fact well known as the effective field theory for some frustrated magnets in equilibrium [91]. There, the additional $O(2)$ symmetry stems from a pattern formation on very small scales in space rather than in time.

This $O(N) \times SO(2)$ symmetric model may break into to different patterns, resembling the two possible time crystalline orders. The instability of the symmetric phase above the upper critical dimension, i.e. where the Gaussian fixed point describes the transition, occurs at $\gamma_d = 0$. If now $\kappa_d > 0$, the system will condense to finite $\rho > 0$ but $\tau = 0$ which fixes $\boldsymbol{\chi}_1^2 = \boldsymbol{\chi}_2^2$ and $\boldsymbol{\chi}_1 \perp \boldsymbol{\chi}_2$, i.e. the system goes into the rotating phase. This phase breaks $O(N) \times SO(2)$ to $O(N-2) \times SO_d(2)$, where $SO(2)_d$

is a combination of an internal $O(N)$ rotation in the plane of the rotation and a time translation which compensates for this rotation and there is a total of $2N-3$ Goldstone modes corresponding to the broken generators. If however $\kappa_d < 0$, the relevant saddle point has $\tau > 0$ and since it has to be extremized it will have $\boldsymbol{\chi}_1 \parallel \boldsymbol{\chi}_2$ resembling the oscillating Van der Pol phase. This phase breaks the symmetry group to $O(N-1)$ and thus there is a total of N Goldstone modes. $N-1$ stem from the possible rotations of the oscillating axis. Modulations of the phase of the oscillations along the axis constitute an additional soft mode stemming from time translation symmetry breaking. In terms of the microscopic parameters of (2.2), $4\kappa_d = u' - u$ and thus for $u > u'$ there is oscillations, while for $u < u'$ there is rotations. We will elaborate on the nature of the soft modes deep within the time crystalline phases and their universal scaling behavior in chapter 6.

Before turning to the renormalization group analysis, we make a further connection to known models. We can represent the effective dynamics (4.5) by generalised complex Gross-Pitaevskii equations by introducing the complex vector valued field $\boldsymbol{\psi} = \boldsymbol{\chi}_1 + i\boldsymbol{\chi}_2 \in \mathbb{C}^N$. In terms of this field the dynamics becomes

$$(i\partial_t - Z\nabla^2 + i\gamma)\boldsymbol{\psi} + \frac{g}{2}(\boldsymbol{\psi}\cdot\boldsymbol{\psi}^*)\boldsymbol{\psi} + \frac{\kappa}{2}(\boldsymbol{\psi}\cdot\boldsymbol{\psi})\boldsymbol{\psi}^* + \boldsymbol{\xi} = 0, \tag{4.7}$$

with $Z = iZ_d + Z_c$, $g = ig_d + g_c$ and $\kappa = i\kappa_d + \kappa_c$. Eq. (4.7) is a generalized noisy Gross-Pitaevskii equation, where the imaginary parts encode the effect of drive and dissipation on top of the coherent Hamiltonian dynamics. This shows, that for $N = 1$, where $\boldsymbol{\psi}$ reduces to a complex scalar and (4.7) to the normal noisy Gross-Pitaevskii equation, the transition of the noisy Van der Pol equation in $d+1$ dimensions is identical with the one of driven dissipative Bose condensates [89, 92, 93] and the noisy Hopf bifurcation of classical oscillators [18, 94].

The RG fixed point of this transition displays emergent thermal equilibrium behavior and falls into the $O(2)$ model A universality class of Halperin and Hohenberg. The approach of this fixed point in the RG flow however features an additional exponent describing the emergence of equilibrium conditions under coarse graining, [89, 92, 36].

4.2 Field theoretic set up

We now turn to quantify the impact of interactions on the scaling behavior of the correlation and response functions at the critical point between symmetric and time crystalline phases for $N > 1$, where the action does not reduce to any known problem. For this sake we adopt the complex representation (4.7) cast into an MSRJD path

integral whose action reads

$$S[\tilde{\boldsymbol{\psi}},\boldsymbol{\psi}] = \int_{t,\mathbf{x}} \tilde{\boldsymbol{\psi}}^* \cdot (Z_t\partial_t - Z\nabla^2 + \gamma)\boldsymbol{\psi} + \frac{g}{2}(\tilde{\boldsymbol{\psi}}^* \cdot \boldsymbol{\psi})(\boldsymbol{\psi}^* \cdot \boldsymbol{\psi}) + \frac{\kappa}{2}(\tilde{\boldsymbol{\psi}}^* \cdot \boldsymbol{\psi}^*)(\boldsymbol{\psi} \cdot \boldsymbol{\psi}) + c.c. - 2D\tilde{\boldsymbol{\psi}}^* \cdot \boldsymbol{\psi}. \tag{4.8}$$

Here, all couplings $\lambda^i$are complex, i.e. $\lambda^i = \lambda^i_d + i\lambda^i_c$ with the exclusion of γ. Its imaginary part γ_c can always be absorbed by going into a rotating frame or introducing a chemical potential in the case of a Bose gas. We have also introduced Z_t since without rescaling, loop corrections can produce real as well as imaginary corrections to this term.

As we have introduced in chapter 3, we can diagnose the emergence of an (effective) thermal equilibrium on the level of the path integral via the thermal symmetry. Its presence is equivalent to thermal fluctuations dissipation relations for all n-point functions of the respective action. Recasting the symmetry operation (3.17) for complex fields yields [8]

$$\boldsymbol{\Psi}(\boldsymbol{x},t) \to \boldsymbol{\Psi}(\boldsymbol{x},-t)^*, \quad \tilde{\boldsymbol{\Psi}}(\boldsymbol{x},t) \to \tilde{\boldsymbol{\Psi}}(\boldsymbol{x},-t)^* + \frac{1}{2T}\partial_t\boldsymbol{\Psi}(\boldsymbol{x},-t)^*, \tag{4.9}$$

where T denotes the equilibrium temperature. Evidently, the thermal symmetry of the original fields is broken in the limit-cycle phases [44]. This propagates to the effective theory, and Eq. (4.9) is not a symmetry of the action (4.8) either. However, one can allow for a more general thermal symmetry in the presence of coherent and dissipative dynamics [92],

$$\begin{aligned} &\boldsymbol{\Psi}(\boldsymbol{x},t) \to \boldsymbol{\Psi}(\boldsymbol{x},-t)^*, \quad \tilde{\boldsymbol{\Psi}}_m(\boldsymbol{x},t) \to \tilde{\boldsymbol{\Psi}}_m(\boldsymbol{x},-t)^* + \frac{1}{2T}\partial_t\boldsymbol{\Psi}(\boldsymbol{x},-t)^*, \\ &\text{where} \quad \tilde{\boldsymbol{\Psi}}_m(\boldsymbol{x},t) = (1+ib)\tilde{\boldsymbol{\Psi}}(\boldsymbol{x},t), \end{aligned} \tag{4.10}$$

with b an additional parameter akin to a chemical potential of bosonic degrees of freedom. The action Eq. (4.8) is now symmetric under Eq. (4.10) if and only if $H_c = bH_d$ (which fixes the parameter b) with temperature $T = D/2$ in our units. This implies a fixed ratio between the real and imaginary parts of the couplings, $r_K = g_c/g_d = \kappa_c/\kappa_d$. There is no condition between the real and imaginary parts of $\gamma = i\gamma_d + \gamma_c$ because we can always shift the value of $\gamma_c \to \gamma_c + \Delta\omega$ via $\boldsymbol{\psi}(t) \to \exp(i\Delta\omega t)\boldsymbol{\psi}(t)$, i.e., a redefinition of the finite frequency parameter ω_0 as discussed above. (This means that the corresponding effective thermal behavior is found in a rotating frame.)

The presence of this symmetry can be rationalized by noting that, if $H_c = bH_d$,

we can rewrite the Langevin equation (4.7) as

$$\frac{\partial_t \boldsymbol{\psi}}{1-ib} + \frac{\delta H_d}{\delta \boldsymbol{\psi}^*} + \frac{\boldsymbol{\xi}}{1-ib} = 0, \tag{4.11}$$

and we in fact recover a purely conservative Hamiltonian dynamics that describe thermal equilibrium with a noise (i.e., $\tilde{\boldsymbol{\psi}}$) rescaled by $(1-ib)$, in agreement with Eq. (4.10).
On the bare, Gaussian level, the correlation function of this action is

$$C(\boldsymbol{q},t) = \langle \psi_i \psi_i^* \rangle(\boldsymbol{q},t) \propto \frac{D\ e^{-(Z_d q^2+\gamma-iZ_c q^2)|t|}}{Z_d q^2+\gamma} \tag{4.12}$$

which agrees with the original one, (4.2) up to the oscillating scale $\sqrt{r}$ which has been successfully absorbed by the change of frame. At the transition to the time cristalline phase $\gamma \to 0$, the correlation and response function obey a scaling form defining the universal critical exponents of the transition

$$\chi^R(\boldsymbol{q},t) \sim q^{-2+\eta'+z}\tilde{\chi}^R(tq^z, iq^{\eta-\eta_c}, q\gamma^{-\nu}), \tag{4.13}$$

$$C(\boldsymbol{q},t) \sim q^{-2+\eta}\tilde{C}(tq^z, iq^{\eta-\eta_c}, q\gamma^{-\nu}). \tag{4.14}$$

Here, the exponents ν, η and z defining an equilibrium fixed point are complemented by the nonthermal anomalous dimensions η' and η. Fluctuation dissipation theorem dictates that $\eta = \eta'$ in thermal equilibrium and thus a deviation marks a nonthermal fixed point violating FDR on the level of universal scalings. In the known case of driven-dissipative Bose condensation, $\eta = \eta'$ at the fixed point and there is an emergent equilibrium with purely dissipative dynamics, $r_K = 0$. However, the subleading exponent $\eta_c \neq \eta$ describes how coherent contributions stemming from the nonthermal microscopics slowly vanish equilibrium emerges upon coarse graining [89, 93].

4.3 RG analysis

4.3.1 Perturbative RG equations

We now want to derive the fluctuation corrections to the critical exponents below the upper critical dimension. To that end, we first rescale the response field as $\tilde{\boldsymbol{\psi}} \to Z_t^{-1}\tilde{\boldsymbol{\psi}}$ to get rid of the potentially complex prefactor of the time derivative

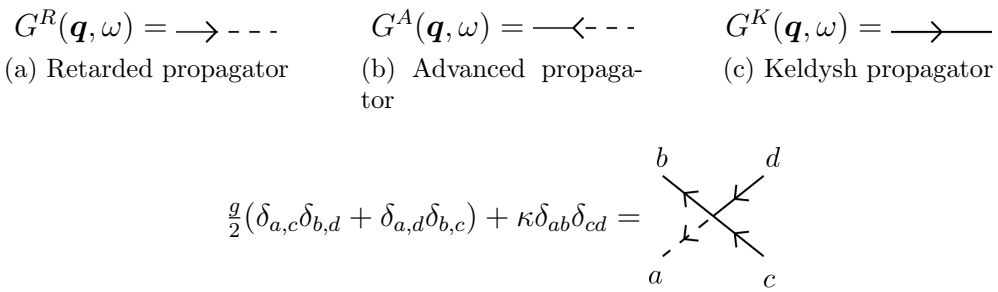

(a) Retarded propagator (b) Advanced propagator (c) Keldysh propagator

(d) Four-point vertex

Figure 4.1: Diagrammatic representation of the Feynman rules for the perturbation theory for the complex action (4.8).

which leads to

$$\bar{D} = DZ_t^{-2},\ K_d = \frac{Z_d \operatorname{Re} Z_t + Z_c \operatorname{Im} Z_t}{|Z_t|^2},\ K_c = \frac{Z_c \operatorname{Re} Z_t - Z_d \operatorname{Im} Z_t}{|Z_t|^2}. \tag{4.15}$$

We do another rescaling $\tilde{\boldsymbol{\psi}} \to \bar{D}^{-1/2} K_d^{\frac{1}{2}} \tilde{\boldsymbol{\psi}}$, $\boldsymbol{\psi} \to \bar{D}^{1/2} K_d^{-1/2}$ and $t \to t K_d^{-1}$. Further, we rescale all couplings with the respective constants to arrive at

$$\begin{aligned} S[\tilde{\boldsymbol{\psi}}, \boldsymbol{\psi}] = \int_{t,\mathbf{x}} \tilde{\boldsymbol{\psi}}^* \cdot (\partial_t - (1 + i r_K)\nabla^2 + \gamma)\boldsymbol{\psi} + \frac{g}{2}(\tilde{\boldsymbol{\psi}}^* \cdot \boldsymbol{\psi})(\boldsymbol{\psi}^* \cdot \boldsymbol{\psi}) \\ + \frac{\kappa}{2}(\tilde{\boldsymbol{\psi}}^* \cdot \boldsymbol{\psi}^*)(\boldsymbol{\psi} \cdot \boldsymbol{\psi}) + c.c. - \tilde{\boldsymbol{\psi}}^* \cdot \boldsymbol{\psi}. \end{aligned} \tag{4.16}$$

[1] Here, r_K describes the competition between coherent and dissipative dynamics and is an additional marginal parameter absent in equilibrium. In terms of the original bare action parameters it reads

$$r_K = \frac{K_c}{K_d} = \frac{Z_c \operatorname{Re} Z_t - Z_d \operatorname{Im} Z_t}{Z_d \operatorname{Re} Z_t + Z_c \operatorname{Im} Z_t}. \tag{4.17}$$

We now need to calculate the self energy corrections to scaling at the critical point. We turn to the perturbative expansion in terms of loop diagrams to leading order in the coupling κ, g, see Fig 4.1 for the definition of the diagrammatic rules. We work around the critical value of γ which to leading order in perturbation theory

[1] The rescaling of the couplings γ, g and κ with the wavefunction renormalisations pops up in a full RG treatment when connencting the vertex renormalizations back to the couplings. In the perturbative scheme we adopt here, this only leads to subleading contributions however, and we drop them right away for brevity.

is

$$\gamma_c = \left(g\frac{N+1}{2} + \kappa^R\right)\int_{\mathbf{q},\omega} G^K(\mathbf{q},\omega,\gamma=0) = \left(g\frac{N+1}{2} + \kappa\right)\int_{\mathbf{q}} \frac{1}{\mathbf{q}^2}. \tag{4.18}$$

and absorb this into a shift of γ, such that the critical point indeed occurs at $\gamma = 0 + O(g^2)$. We now look at the leading order loop corrections for γ as well as the renormalized vertices g^R and κ^R in the vicinity of the critical point. We are interested in the scaling of these as $\gamma \to 0$. For this we introduce a scaling variable μ such that $\gamma = \mu^2\hat{\gamma}, \mathbf{q} = \mu\hat{\mathbf{q}}$ within the loops and study how the corrections behave as we send $\mu \to 0$. The one-loop contributions are depicted in Fig 4.2. Importantly, the different contractions of the tensor structures of the $O(N)$ indices lead to factors of N everytime there is an unconstrained trace over an internal $O(N)$ index within the loops. All external frequencies and momenta are set to zero and the momentum as well as frequency integrations can be performed straight forwardly. We first note a few important points:

- In a perturbative expansion, for all couplings $\lambda_i = \gamma, g, \kappa$ we have $\lambda_i^R = \lambda_i + \mathcal{O}(g,\kappa)$ and we can thus interchange them
- The momentum rescaling sends any possibly existing cut off Λ to infinity as $\mu \to 0$
- All loops carry a UV divergence as $\epsilon \to 0$ which manifests as a simple pole. This is the leading order term in an ϵ-expansion
- Treating both g^R and κ^R as a perturbation is justified if at the RG fixed point $g^R, \kappa^R = \mathcal{O}(\epsilon)$ which we will verify a post.

Using all this information, to leading order in ϵ the loop contributions read

$$\gamma^R = \gamma - \left(g\frac{N+1}{2} + \kappa\right)\frac{\mu^{-\epsilon}\gamma}{(4\pi)^2\epsilon} + O(\kappa^2, g^2, \epsilon) \tag{4.19}$$

$$g^R = g - \frac{\mu^{-\epsilon}}{2(4\pi)^2\epsilon}\left(\frac{(N+3)g}{2}(g+g^*) + 2\kappa\kappa^* + 2g\kappa + g^*\kappa + g\kappa^* + \frac{1}{1+ir_K}gg\right) + \mathcal{O}\Big((g,\kappa)^3\Big) \tag{4.20}$$

$$\kappa^R = \kappa - \frac{\mu^{\epsilon}}{2(4\pi)^2\epsilon}\left(2g\kappa + g^*\kappa + g\kappa^* + \frac{1}{1+ir_K}(N\kappa\kappa + 2\kappa g)\right) + \mathcal{O}\Big((g,\kappa)^3\Big). \tag{4.21}$$

We now differentiate these corrections with respect to μ to arrive at the dimensionfull

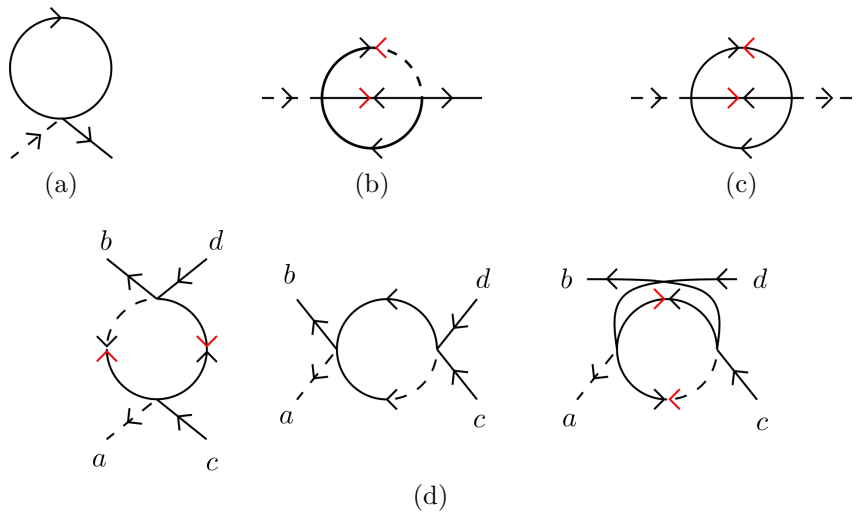

Figure 4.2: Loop diagrams considered in the text. The first three graphs renormalize the self-energies. (a) and (b) correct the retarded part of the action $\Gamma^{(2)}_{\tilde{\psi}_a^*\psi_a}$, while (c) corrects the noise part $\Gamma^{(2)}_{\tilde{\psi}_a^*\tilde{\psi}_a}$. The one-loop diagrams (d) renormalize the interaction. The red arrows indicate that diagrams with both arrow directions have to be considered.

β-functions

$$\mu\partial_\mu \gamma^R = \left(g\frac{N+1}{2} + \kappa\right)\frac{\mu^{-\epsilon}\gamma}{(4\pi)^2} \tag{4.22a}$$

$$\mu\partial_\mu g^R = \frac{\mu^{-\epsilon}}{(4\pi)^2}\left(\frac{(N+3)g}{2}(g+g^*) + 2\kappa\kappa^* + 2g\kappa + g^*\kappa + g\kappa^* + \frac{1}{1+ir_K}(g)^2\right) \tag{4.22b}$$

$$\mu\partial_\mu \kappa^R = \frac{\mu^{-\epsilon}}{(4\pi)^2}\left(2g\kappa + g^*\kappa + g\kappa^* + \frac{1}{1+ir_K}(N\kappa\kappa + 2\kappa g)\right). \tag{4.22c}$$

These flow equations can be rendered dimensionless by the scaling Ansatz $\gamma = \mu^2\hat{\gamma}$, $g = \mu^\epsilon\hat{g}$, $\kappa = \mu^\epsilon\hat{\kappa}$ and by identifying $\hat{\gamma}, \hat{g}, \hat{\kappa}$ with $\hat{\gamma}^R, \hat{g}^R, \hat{\kappa}^R$ at leading order in perturbation theory. This identification, is where the nontrivial difference between simple one-loop perturbation theory and perturbative RG flow equations arises. By integrating the flow only infenitesimally and reinserting the result into the perutrbative loop expansion, we effectively resum a whole class of diagrams [88]. We arrive

at the dimensionless one-loop RG beta functions

$$\beta_\gamma = \mu\partial_\mu\hat{\gamma} = -2\hat{\gamma} + \left(g\frac{N+1}{2} + \kappa^R\right)\frac{\hat{\gamma}}{(4\pi)^2} \tag{4.23}$$

$$\begin{aligned}\beta_g = \mu\partial_\mu\hat{g} &= -\epsilon\hat{g} \\ &+ \frac{1}{(4\pi)^2}\left(\frac{(N+3)\hat{g}}{2}(\hat{g}+\hat{g}^*) + 2\hat{\kappa}\hat{\kappa}^* + 2\hat{g}\hat{\kappa} + \hat{g}^*\hat{\kappa} + \hat{g}\hat{\kappa}^* + \frac{1}{1+ir_K}\hat{g}^2\right)\end{aligned} \tag{4.24}$$

$$\beta_\kappa = \mu\partial_\mu\hat{\kappa} = -\epsilon\hat{\kappa} + \frac{1}{(4\pi)^2}\left(2\hat{g}\hat{\kappa} + \hat{g}^*\hat{\kappa} + \hat{g}\hat{\kappa}^* + \frac{1}{1+ir_K}(N\hat{\kappa}^2 + 2\hat{\kappa}\hat{g})\right). \tag{4.25}$$

We are interested in the limit $\mu \to 0$ which is given by the fixed points $\beta_i = 0$ and the scaling close to the fixed points. The fixed point for $\hat{\gamma}$ will always be $\hat{\gamma}_* = 0$. We can already see, that the fixed point for the interactions $\hat{\kappa}$ and $\hat{g}$ will be of order ϵ justifying their perturbative treatment close to the upper critical dimension. However, at one loop level we cannot fix r_K and thus we need to including leading two-loop corrections to determine its own beta function.
To that end, we consider the corrections to the marginal action parameters Z_t, Z_d, Z_c, D, which we all rescaled at the level of the bare action. After loop corrections, they thus read

$$Z_t = 1 + i\partial_\omega\Sigma^R(\omega = 0, \mathbf{q} = 0) \tag{4.26}$$

$$Z_d = 1 - \mathrm{Re}\,\partial_{\mathbf{q}^2}\Sigma^R(\omega = 0, \mathbf{q} = 0) \tag{4.27}$$

$$Z_c = r_K - \mathrm{Im}\,\partial_{\mathbf{q}^2}\Sigma^R(\omega = 0, \mathbf{q} = 0) \tag{4.28}$$

$$D = 1 - \Sigma^K(\omega = 0, \mathbf{q} = 0) \tag{4.29}$$

where Σ^R denotes the retarded part of the self energy and Σ^K the noise part. To this end we need to calculate the sunset loop integrals depicted in Fig. 4.2. The corresponding frequency and momentum dependent contributions to the retarded inverse propagator read

$$\begin{aligned}\Delta\Gamma^{(1,1)}(\omega, \mathbf{p}) = &-(g^2\frac{N+1}{2} + N\kappa^2 + 2g\kappa)I_1(\omega, \mathbf{p}) \\ &-\frac{1}{2}(gg^*\frac{N+1}{2} + \kappa\kappa^* + g\kappa^* + g^*\kappa)I_2(\omega, \mathbf{p})\end{aligned} \tag{4.30}$$

with

$$I_1(\omega,\mathbf{p}) = \int_{Q_1,Q_2} G^R(-Q_1-Q_2+P)G^K(Q_1)G^K(-Q_2) \tag{4.31}$$

$$I_2(\omega,\mathbf{p}) = \int_{Q_1,Q_2} G^R(Q_1+Q_2-P)G^K(Q_1)G^K(Q_2). \tag{4.32}$$

where we used the shorthand notation $Q_i = (\omega_i, \mathbf{q}_i)$. Similarly, the sunset diagram renormalizing the

$$\Delta\Gamma^{(2,0)}(0,0) = \left(\tilde{g}\tilde{g}^*\frac{(N+1)}{2} + \tilde{\kappa}\tilde{\kappa}^* N + \tilde{g}\tilde{\kappa}^* + \tilde{\kappa}g^*\right)\times$$
$$\int_{Q_1,Q_2}\left(G^K(-Q_1-Q_2)G^K(Q_1)G^K(-Q_2) + G^K(Q_1+Q_2)G^K(Q_1)G^K(Q_2)\right) \tag{4.33}$$

The frequency and momentum integration itself coincides with the ones done in [94, 93] and we refer for there for the detailed calculation. To leading order in ϵ we thus arrive at

$$\partial_{\mathbf{q}^2}\Sigma^R = \frac{\mu^{-2\epsilon}}{2\epsilon(4\pi)^4}\Big[(g^2\frac{N+1}{2} + N\kappa^2 + 2g\kappa)\frac{2-ir_K}{4(3-ir_K)}$$
$$-\frac{1}{2}(gg^*\frac{N+1}{2} + \kappa\kappa^* + g\kappa^* + g^*\kappa)\frac{1-ir_K}{6-2ir_K}\Big], \tag{4.34}$$

$$i\partial_\omega\Sigma^R = \frac{\mu^{-2\epsilon}}{(4\pi)^4 2\epsilon}\Big[\frac{\log\left(\frac{4}{(3-ir_K)(1+ir_K)}\right)\left(\kappa g^* + g\kappa^* + \frac{1}{2}|g|^2(N+1) + N|\kappa|^2\right)}{2(1-ir_K)^2}$$
$$-\frac{\log\left(\frac{4}{3-ir_K}\right)\left(\frac{1}{2}g^2(N+1) + 2g\kappa + \kappa^2 N\right)}{(1+ir_K)^2}\Big] \tag{4.35}$$

for the spectral parts and

$$\Sigma^K = \frac{\mu^{-2\epsilon}\left(\frac{1}{2}\tilde{g}\tilde{g}^*(N+1) + \tilde{\kappa}\tilde{\kappa}^* N + \tilde{g}\tilde{\kappa}^* + \tilde{\kappa}g^*\right)}{8\epsilon(4\pi)^4\left(1+r_K^2\right)}\Big[3\log\left(\frac{16}{(9+r_K^2)(1+r_K^2)}\right)$$
$$+2r_K\left(\arctan(r_K) + \arctan\left(\frac{r_K}{3}\right)\right)\Big] \tag{4.36}$$

for the noise level. We note that the spectral parts are only dimensionless if rescaling the external momenta and frequencies with their canonical dimension, i.e. $\mathbf{p} = \mu\tilde{\mathbf{p}}, \omega = \mu^2\tilde{\omega}$. The respective dimensionless RG-flow derivatives $\mu\partial_\mu Z_t$, $\mu\partial_\mu(Z_d + iZ_c)$ and $\mu\partial_\mu D$ can now straightforwardly obtained by first taking μ derivatives of the self-energy contributions and then plugging in the dimensionless couplings, as before.

We are left to find the RG β-function for r_K. To that end, we need to rescale the full effective action as we did in the beginning with the bare action and use (4.17) to find at leading order in perturbation theory, that

$$\beta_{r_K} \equiv \mu\partial_\mu r_K = \mu\partial_\mu Z_c - r_K \mu\partial_\mu Z_d - (1+r_K^2)\mu\partial_\mu \operatorname{Im} Z_t. \tag{4.37}$$

Summing all the respective β- functions is straightforward but however yields a very long expression whose exact form does not give any insight to the reader but can be handled easily with the computer algebra tool of choice.

4.3.2 Fixed point structure

We are now finally in a position to derive the RG-fixed points describing the transition between the disordered phase $\langle\boldsymbol{\phi}\rangle = 0$ and the time-crystalline phases with rotating or oscillating long range order. To that end we need to solve for the zeroes of the RG flow equations (4.22) and (4.37) . While the fixed point of β_γ is always $\gamma_* = 0$, the remaining system of coupled equations cannot be solved analytically but only numerically.

First, we consider the equilibrium fixed point as a limiting case. As shown above, an emergent equilibrium emerges, if at the fixed point there is an effective thermal symmetry, which is the case if

$$r_K = \frac{g_{c*}}{g_{d*}} = \frac{\kappa_{c*}}{\kappa_{d*}}. \tag{4.38}$$

Restricting oneself to that plane in parameter space, i.e. fixing $g_c = r_K g_d$ and $\kappa_c = r_K \kappa_d$, then solving the one-loop flow equations β_g, β_κ for r_K dependent fixed points g_{d*} and κ_{d*} and plugging this into $\beta_{r_K} = 0$ yields

$$\beta^*(r_K) = \frac{1}{2}\left(4\tilde{g}_d^*\tilde{\kappa}_d^* + (N+1)\tilde{g}_d^{*2} + 2N\tilde{\kappa}_d^{*2}\right) f(r_K), \tag{4.39}$$

$$\begin{aligned} f(r_K) = &\Bigg(r_K \log\left(\frac{16}{(r_K^2+1)(r_K^2+9)}\right) \\ &+ \left(r_K^2-1\right)\arctan\left(r_K\right) + \left(r_K^2+3\right)\arctan\left(\frac{r_K}{3}\right)\Bigg). \end{aligned} \tag{4.40}$$

If we set $N = 1$, where we expect to recover the case of the noisy, complex Gross Pitaevskii equation or Hopf-bifurcation, we indeed do [93]. Since $f(r_K)$ is monotonically increasing and crosses zero at $r_K = 0$, all stable equilibrium fixed points have $r_{K*} = g_{c*} = \kappa_{c*} = 0$, which entails they display an emergent $O(N) \times O(2)$ symmetry

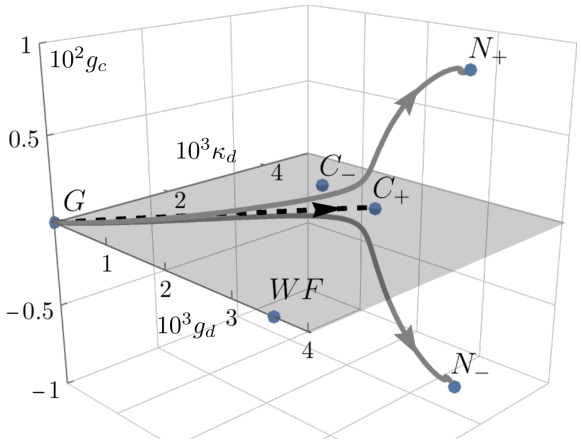

Figure 4.3: RG flow diagram of the $O(N) \times SO(2)$ model. In the equilibrium plane there is the Guassian fixed point G, the $O(2N)$ symmetric Wilson-Fisher fixed point WF at $g_c = \kappa_c = \kappa_d = 0$ and the two $O(N) \times O(2)$ equilibrium fixed points $C_\pm$. The equilibrium plane is shaded in grey. Infinitesimal deviations out of the equilibrium plane from the Gaussian fixed point are however enough to drive the flow to the stable, complex conjugated nonthermal fixed points $N_\pm$. Figure was originally published in [43]

rather than $O(N) \times SO(2)$. The universality class of $O(N) \times O(2)$ also describes transitions in some frustrated magnetic systems, and we recover the leading order in ϵ flow equations in the $r_K = 0$, equilibrium plane [95].
These equilibrium fixed points are however not stable if one allows for deviations from equilibrium. The full stable fixed point comes in a pair of complex conjugated fixed points which have the same critical exponents and importantly do not obey the thermal constraint (4.38). Thus, the $O(N) \times SO(2)$ theory is one of the rare cases, where deviations from equilibrium constitute a relevant perturbation out of the equilibrium plane, and coarse graining will enhance nonequilibrium effects rather than washing them out.
At the fixed point, we have $\kappa_d^* > 0$ for all $N > N_c \approx 1.6$ and it therefore describes the transition between the symmetric phase and the rotating phase. There is no fixed point left, that describes the transition between symmetric and oscillating phase, a signature of a fluctuation induced first order phase transition [79].

At the fixed point, we can now derive the critical exponents from the RG flow equations straightforwardly. The rescalings used above together with the scaling ansatz (4.13) imply

$$\begin{aligned} \nu^{-1} &= -\mu\partial_\mu \ln(\hat{\gamma}), \quad \eta = \mu\partial_\mu \ln Z_\psi, \quad z = 2 - \mu\partial_\mu \ln K_d^{-1}, \\ \eta' &= \mu\partial_\mu \ln(Z_t) + \mu\partial_\mu \ln K_d^{-1}, \quad \eta_c = \eta - \mu\partial_\mu \ln(r_K). \end{aligned} \tag{4.41}$$

N	Phase	$\nu^{-1}-2$	η	$z-2$	η'	η_c
22, eq.	Rot.	$-27/50\epsilon$	$0.0207\epsilon^2$	$0.0207c\epsilon^2$	η	$-0.0207c'\epsilon^2$
22, neq.	Rot.	-0.942ϵ	$-0.142\epsilon^2$	$0.0055\epsilon^2$	$(0.00030+0.018i)\epsilon^2$	η
3, eq.	None	X	X	X	X	X
3, neq.	Rot.	-1.27ϵ	$-1.49\epsilon^2$	$-0.017\epsilon^2$	$(-0.035+0.067i)\epsilon^2$	η
2, eq.	vdP	$-\epsilon/2$	$\epsilon^2/48$	$c\epsilon^2/48$	η	$-c'\epsilon^2/48$
2, neq.	Rot.	-0.853ϵ	$-0.353\epsilon^2$	$0.0072\epsilon^2$	$(0.010+0.0070i)\epsilon^2$	η

Table 4.1: Critical exponents for different values of N in- and out-of-equilibrium to lowest nontrivial order in ϵ. The equilibrium static results are reproduced, see [95]. The column "Phase" indicates the transition into which phase (rotating or Van der Pol (vdP)) is second order, while the other one is fluctuations induced first-order. For the $N=3$ equilibrium case, no attractive fixed point exists, and both phase transitions are first-order. We use $c=(6\log(4/3)-1)$ and $c'=(4\log(4/3)-1)$. This table was originally published in [43]

where all the μ derivatives are evaluated at the fixed point and to leading order, i.e. we always use that $Z_d=\mathrm{Re}\,Z_t=\bar{D}=1+\mathcal{O}(\epsilon^2)$, $Z_c=r_K+\mathcal{O}(\epsilon^2)$ and $\mathrm{Im}(Z_t)=\mathcal{O}(\epsilon^2)$ and then plug in the one-loop β function for ν and the two-loop corrections for all the anomalous exponents. Since the fixed point values at leading order are only available numerically, the same holds for the critical exponents. The results are summarised in table 4.1.

Note, that at the stable fixed points $\mathrm{Im}\,\eta'\neq 0$. This indicates of oscillatory behavior of the RG flow towards the fixed point. Remarkably, $\eta\neq\mathrm{Re}\,\eta'$, i.e. the anomalous scaling corrections to dynamical correlations and responses differ. This is in violation of fluctuation dissipation relations. If one in turn uses FDR to define an effective scale dependent temperature

$$T_{eff}=\frac{\omega\mathcal{C}(\omega,\mathbf{q})}{\mathrm{Im}\,\chi^R(\omega,\mathbf{q})} \tag{4.42}$$

it would diverge as $T_{eff}\sim q^{\mathrm{Re}\,\eta'-\eta}$ at the phase transition between symmetric and rotating phase. Such an effective temperature can in principle be measured by probes for the frequency dependence of the mode occupation, for instance comparing Stokes- and Anti-Stokes-peaks in Raman spectroscopy. In this way the nonthermal nature of the phase transition is directly observable experimentally. Altogether, this leads to the phase diagram depicted in the introduction Fig. 2.3.

5

Critical Exceptional Points

After determining the universality class of the transition between the symmetric and the limit cycle phase, we turn to the transition between statically ordered and rotating phase in this chapter. To that end we focus on the case of $N \geq 2$ components and the transition into the rotating phase. As outlined in the introduction, this transition occurs through a so called critical exceptional point. This puts us in the position to determine the universal behavior associated to a CEP. The main results are

- Critical exceptional points lead to superthermal occupation of long wavelength modes and nonanalytic spectra.
- The superthermal mode occupation melts down any order before reaching the CEP below for dimensions.
- Interactions and the nonanalytic spectrum can lead to a fluctuation induced first order phase transition before the meltdown of order.
- The competition of meltdown and first order transition is determined by an emerging interaction scale

The contents and figures of this chapter have been published in a modified version of sections IV-VI of [44].

5.1 EPs and CEPs

Before delving into the analysis of loop contributions of critical fluctuations at the transition, that we have claimed to be a critical exceptional point in the introduction, let us define what we exactly mean by that word in this context and how it fits into the discussion of exceptional points in nonhermitian systems.

5.1.1 Modes, dispersions and critical points

First, we briefly fix some further basic conventions and nomenclature for the remainder of this work. We can access the *mode spectrum* around a given stable state $\boldsymbol{\varphi}_s$ by linearizing the coarse grained equation of motion around its solution

$$\sum_j \Gamma^R_{ij}(\mathbf{q},t)\Big|_{\boldsymbol{\varphi}=\boldsymbol{\varphi}_s} \delta\varphi_j(\mathbf{q},t) = 0, \tag{5.1}$$

where we have assumed that the equation of motion is Markovian, i.e. depends only on one time variable, as it is the case for this work. The set of linearly independent solutions $\left(\boldsymbol{\delta\varphi}_\alpha(\mathbf{q},t)\right)_{\alpha=1,..}$ are the excitation modes. Put differently, the modes span the kernel of the inverse Green function in time and momentum space $\Gamma^R(\mathbf{q},t)$. If $\Gamma^R(\mathbf{q},t)$ is not explicitly time dependent but only contains time derivative operators, the modes usually take the $\boldsymbol{\delta\varphi}_\alpha(\mathbf{q},t) = e^{-i\omega_\alpha(\mathbf{q})t}\boldsymbol{\delta\varphi}_\alpha(\mathbf{q},0)$, where $\omega_\alpha(\mathbf{q})$ are the mode dispersions. The dispersions are also the roots of $\det\Gamma^R(\omega,\mathbf{q}) = 0$ and equivalently the poles of the retarded Green function in frequency space. The real part of a dispersion gives the *frequency* or inverse *period* at which the corresponding mode oscillates, while the imaginary part yields how fast the mode dissipates, i.e. its inverse *life time*. See also Fig. 5.1 for an illustration.

For the solution $\boldsymbol{\varphi}_s$ to be stable, no dispersion can have a positive imaginary part since this corresponds to an exponentially growing fluctuation. Therefore, an instability towards a new phase occurs if one tunes some parameter such that a dispersion is at the verge of moving into the upper complex half plane, i.e. when the imaginary part of the dispersion goes to zero. The system reaches a *critical point* and a continuous phase transition takes place, indicated by a divergence of e.g. the two-point correlation function at equal-time $G^K(q, t = 0)$. Typically, continuous transitions occur for a vanishing dispersion $\omega(\mathbf{q}) = 0$ but an instability at finite frequency can however occur, too. This corresponds, for example, to the cases $\mathbf{I}_0$ ($\mathbf{q}_c = 0$) and $\mathbf{III}_0$ ($\mathbf{q}_c \neq 0$) in the classification of instabilities in noiseless systems by Cross and Hohenberg [2].

In the simplest case of a single scalar field variable, the linearized renormalized

equation of motion at low frequencies reduces to the damped harmonic oscillator

$$\left(\partial_t^2 + 2\bar{\gamma}(\mathbf{q})\partial_t + \bar{r}(\mathbf{q})\right)\boldsymbol{\delta\varphi}(\mathbf{q},t) = 0 \tag{5.2}$$

or, equivalently

$$\Gamma^R(\mathbf{q},\omega) = (-\omega^2 - 2\bar{\gamma}(\mathbf{q})\omega + \bar{r}(\mathbf{q})). \tag{5.3}$$

The modes are

$$\delta\varphi_{1,2}(\mathbf{q},t) = e^{-i\omega_{1,2}(\mathbf{q})t} \tag{5.4}$$

with dispersions

$$\omega_{1,2}(\mathbf{q}) = -i\bar{\gamma}(\mathbf{q}) \pm \sqrt{\bar{r}(\mathbf{q}) - \bar{\gamma}(\mathbf{q})^2}, \tag{5.5}$$

As an example at the mean-field level, we have $r(\mathbf{q}) = v^2\mathbf{q}^2 + r$ and $\gamma(\mathbf{q}) = \gamma + \frac{Z}{2}\mathbf{q}^2$ using (2.2).

Stability, i.e. a finite lifetime for both modes, demands that $r > 0$, $\gamma > 0$. If one tunes the *mass term* r to zero, one dispersion becomes gapless $\omega_1 = 0$ while the other remains decaying $\omega_2 = -2i\bar{\gamma}(\mathbf{q})$. The first becomes unstable upon tuning the mass r negative. In our case, we reach the critical point describing the phase boundary A of the phase diagram Fig. 2.1. Tuning the damping γ negative also induces an instability. However, it does not proceed through a point where the dispersions vanish in the complex plane, but both dispersions maintain a finite real part $\omega_{1,2} = \pm\sqrt{r}$ at $\gamma = 0$. It corresponds to the phase transition B in Fig. 2.1, as discussed in chapter 4.

5.1.2 (Critical) exceptional point

We first consider the case of a single damped oscillator, $N = 1$. A special point occurs when there is a wavevector $\mathbf{q}^*$ at which $\bar{\gamma}^2(\mathbf{q}^*) = \bar{r}(\mathbf{q}^*)$ and both formerly independent modes coalesce. At this point a new linearly independent solution emerges: $\boldsymbol{\delta\varphi}_{EP}(\mathbf{q}^*,t) = te^{-i\omega(\mathbf{q}^*)t}\boldsymbol{\delta\varphi}_{EP}(\mathbf{q}^*,0)$. This marks an *exceptional point*. The damped harmonic oscillator's EP separates a purely dissipative, overdamped regime, where both dispersions are imaginary without a real part, and an underdamped regime where excitations oscillate due to a finite real part of their dispersions. Clearly, at an EP the square root appearing in (5.5) vanishes and therefore the EP occurs at a nonanalyticity of the dispersion relations.

Equivalently, it is also possible to rewrite Eq. (5.2) as a first-order linear differential equation of the form $\partial_t \delta\boldsymbol{\varphi} = M\delta\boldsymbol{\varphi}$. An exceptional point, i.e. a coalescence of modes, is then defined as a point in parameter space where the 2×2 matrix M is not diagonalizable in internal indices, making contact with the more usual definition of EP [46, 50, 57].

We say that there is a *critical exceptional point*, if the dispersion at which the EP occurs is gapless, i.e. when $\bar{\gamma}(\mathbf{q}^*) = \bar{r}(\mathbf{q}^*) = 0$. For $\mathbf{q}^* = 0$, we then have, at the CEP,

$$\Gamma^R(\mathbf{q}^* = 0, \omega) = -\omega^2, \tag{5.6}$$

underlying the necessity to keep the second order time derivative. We emphasize again that a CEP is hence a property of the full renormalized inverse retarded Green function.

We now generalize the notion of a CEP to the dynamics of N component fields. A full retarded Green function that can be diagonalized in field space,

$$\Gamma^R_{ij}(Q) = \Gamma^R_i(Q)\delta_{ij}, \tag{5.7}$$

where Γ^R_i are of the form (5.3) therefore displays a CEP if and only if the full diagonalized inverse Green function has at least one element Γ^R_i which verifies (5.6). We show later that the case of a CEP occurring through a nondiagonalizable Green function can always be mapped to this case in the vicinity of the CEP. Since the dynamics is diagonal and thus decoupled, we now drop the index i and concentrate on the pair of modes becoming critical and exceptional simultaneously. In our case at mean-field, the inverse Green function is diagonal and all its elements take the form

$$\Gamma^R(\mathbf{q}, \omega) = -\omega^2 - Zi\omega\mathbf{q}^2 + v^2\mathbf{q}^2, \tag{5.8}$$

and the dispersions at the CEP are

$$\omega_{1,2}(\mathbf{q}) = -i\frac{Z}{2}\mathbf{q}^2 \pm v|\mathbf{q}|. \tag{5.9}$$

Reaching a CEP generically requires two fine tunings, both $\bar{\gamma}(\mathbf{q} = 0)$ and $\bar{r}(\mathbf{q} = 0)$ have to be tuned to zero. We will show however in Sec. 5.2 that the transition between the static and the rotating phase constitutes a CEP. There is only one fine tuning necessary as the vanishing of $\bar{r}(\mathbf{q} = 0)$ for phase fluctuations in the static ordered phase is guaranteed by Goldstone's theorem. The idea to generate CEPs with only

one fine-tuning by considering systems with a Goldstone mode was first put forward in [66, 28].

5.1.3 Superthermal mode occupation

The discussion of (critical) exceptional points above makes it clear that these are spectral properties, related to the retarded Green function. Now, we study the consequences of such points for the statistical properties, i.e. mode occupation numbers. These are encoded in the full equal-time correlation function or Keldysh Green function. The CEP is signalled by a vanishing of two coalescing modes $\omega_{1,2}(\mathbf{q})$ as $\mathbf{q} \to 0$. Near the CEP, the Keldysh Green function associated to the coalescing critical modes takes the form

$$G^K(Q) = \frac{2\bar{D}(Q)}{|\omega - \omega_1(\mathbf{q})|^2 |\omega - \omega_2(\mathbf{q})|^2}, \tag{5.10}$$

where $\bar{D}(Q) \equiv \Gamma^K(Q)$ is a generic frequency and momentum dependent noise kernel of the respective field direction.

To determine the physics at low frequencies and momenta, we can restrict the discussion to $\bar{D}(Q \to 0) \equiv \bar{D}$, which absent fine tuning is larger than zero, corresponding to a generic Markovian noise level [1].

This general property of a CEP reproduces the structure pointed out in [66]. There are two poles at $\omega = 0$ that multiply, causing a significantly enhanced infrared divergence of the correlation function, irrespective of the precise forms of the dispersions. This can be easily seen by inspecting the equal-time Keldysh Green-function obtained from (5.10),

$$G^K(\mathbf{q}, t = 0) \sim \frac{\bar{D}}{\bar{\gamma}(\mathbf{q})\bar{r}(\mathbf{q})}, \tag{5.11}$$

since both γ and r go to zero precisely at the CEP.

With the mean-field dispersions (5.9), the equal-time correlation function is given

[1] The constant noise level also distinguishes the CEP from the Goldstone fixed point of models with conserved currents such as in the Hohenberg-Halperin E, F and G [1, 36], where the spectrum of the Goldstone excitations in the ordered phase coincide with that of a CEP. However, their noise kernel has to vanish as $D(\mathbf{q}) \sim \mathbf{q}^2$ due to conservation laws and thus there is no enhanced fluctuations as at a CEP transition. These scaling regimes do not describe transitions but the fixed points of symmetry broken phases itself.

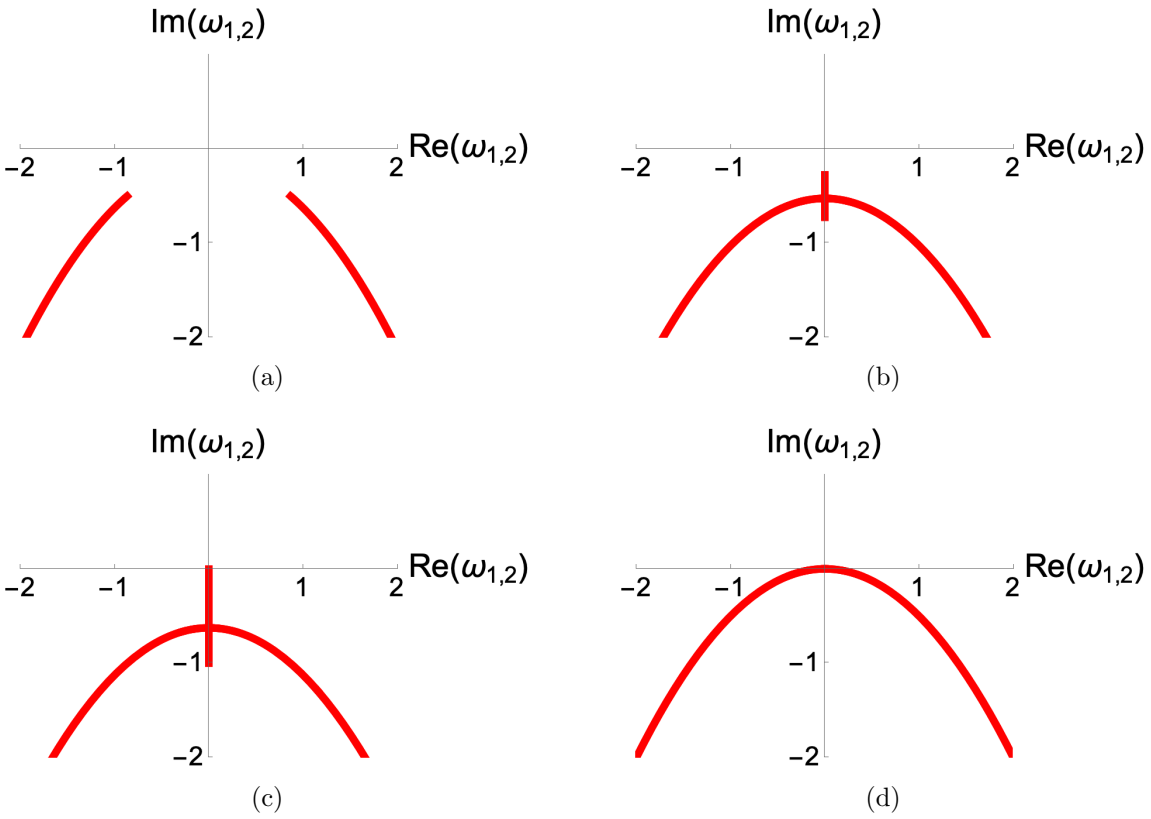

Figure 5.1: Position of the poles of the retarded response of a scalar field in the complex plane. The dispersions are parametrized as $\omega_{1,2} = -\frac{i}{2}(2\gamma + Z\mathbf{q}^2) \pm \sqrt{r + v^2\mathbf{q}^2 - (2\gamma + Z\mathbf{q}^2)^2/2}$, with $v = Z = 1$. a) Purely underdamped motion $r = 2\gamma$, all poles have a finite distance from the real and imaginary axis. b) Underdamped excitations exist, constituting a line of poles on the imaginary axis. The gap between real axis and the pole spectrum remains finite $r = 0.4\gamma$. At large enough wavevectors, there is an EP separating the underdamped from the overdamped regime. It can be clearly detected by the pole lines with finite real part terminating nonanalytically in the line of overdamped excitations. c) Gapless (critical) excitation spectrum, $2\gamma > 0, r = 0$. The line of underdamped poles touches the zero in the complex plane. At finite damping, a gapless spectrum always has an underdamped regime at low momenta. d) CEP spectrum, $2\gamma = r = 0$. The EP, where the underdamped motion terminates sits at the zero in the complex plane. At finite momenta, all excitations are underdamped. Real and imaginary parts of the dispersions scale differently with momentum.

by

$$G^K(\mathbf{q}, t = 0) \sim \frac{D}{\mathbf{q}^4}, \tag{5.12}$$

which has a significantly stronger infrared divergence as in the vicinity of a usual (Gaussian) critical point where $G^K(\mathbf{q}, t = 0) \sim \mathbf{q}^{-2}$ e.g. at the phase boundary A and B of the phase diagram Fig. 2.1, where respectively r and γ are fine-tuned to 0. In particular, it is superthermal: the fluctuation-dissipation relation (see next subsection) implies generally that $G^K(\mathbf{q}, t = 0) \sim \mathbf{q}^{-2}$. This is a hint that a CEP is a genuine non-equilibrium feature.

5.1.4 Critical Exceptional Points of N-component fields

We now elaborate on how any CEP occurring in noisy Markovian dynamics of a vector valued field can be mapped to the damped harmonic oscillator case discussed above.

We first note that we can always map a system of N differential equations of second order in time derivatives into a set of $2N$ first order differential equations by introducing $\boldsymbol{\pi} = \partial_t \boldsymbol{\phi}$ as an independent variable. In physics terminology we pass from a Lagrangian to a Hamiltonian representation. Using this, the (diagonal) linearized equation of motion or inverse Green function $\Gamma^R(\mathbf{q}, t)$ of the N-component damped harmonic oscillator discussed in 5.1.2, can always be written as

$$(\partial_t \mathbb{1} + M(\mathbf{q}))\delta\boldsymbol{\Phi} = 0 \tag{5.13}$$

where $\boldsymbol{\Phi}$ is a $2N$ component vector and $\mathbb{1}$ and $M(\mathbf{q})$ are $2N \times 2N$ matrices. The eigenvalues of $M(\mathbf{q})$ are the dispersions $i\omega_\alpha(\mathbf{q})$ and the corresponding eigenvectors the $2N$ linearly independent modes. In this representation an exceptional point (EP), where two modes coalesce, occurs if and only if $M(\mathbf{q})$ is not diagonalizable at $\mathbf{q}^*$, and therefore has at least one 2×2 Jordan block

$$M(\mathbf{q}^*) = \begin{pmatrix} i\omega_{EP} & 1 \\ 0 & i\omega_{EP} \end{pmatrix}. \tag{5.14}$$

The dynamics of excitations close to a CEP at $\mathbf{q}^* = 0$ is governed by an inverse Green function that is block diagonal with blocks that are at most of size 2×2 and

with at least one block taking the form

$$\Big(\partial_t \mathbb{1}_2 + \begin{pmatrix} i\omega_1(\mathbf{q}) & 1 \\ 0 & \omega_2(\mathbf{q}) \end{pmatrix}\Big)\delta\mathbf{\Phi}_{CEP} = 0 \tag{5.15}$$

where $\delta\mathbf{\Phi}_{CEP}$ are the fluctuations contributing to the CEP and $\omega_1(\mathbf{q}=0) = \omega_2(\mathbf{q}=0) = 0$. This structure also implies the superthermal mode occupation in the presence of generic Markovian noise as shown in [66].

Reciprocally, by reverting this procedure, any system that has a CEP arising from the structure (5.15) can generically be brought back to the form of a damped harmonic oscillator with a diagonalizable inverse Green-function even in presence of noise. This done explicitly in the discussion of nonreciprocal field theories in 7.3.

5.1.5 CEP exists only out-of-equilibrium

Here we show that indeed a CEP cannot occur at thermal equilibrium. In that circumstance, the full correlation and response functions obey a FDR, which reads for the two-point functions ($k_\mathrm{B} = 1$)

$$G^K(Q) = \frac{2T}{i\omega}\Big(G^R(Q) - G^A(Q)\Big). \tag{5.16}$$

In thermal equilibrium with global detailed balance, FDRs have to hold not only for the full, renormalized two-point Green functions, but also for all higher n-point correlations and responses as well. As we have discussed in chapter 3.3, this is equivalent to a symmetry of the MSRJD action. Requiring thermal equilibrium at a temperature T of the quadratic sector thus amounts to

$$T = \frac{\bar{D}(\mathbf{q})}{2\bar{\gamma}(\mathbf{q})} \tag{5.17}$$

where $\bar{\gamma}(\mathbf{q})$ is the renormalized momentum dependent damping

$$\bar{\gamma}(\mathbf{q}) \equiv \partial_{-i\omega}\Gamma^R(\omega = 0, \mathbf{q}) \tag{5.18}$$

and $\bar{D}(\mathbf{q})$ the renormalized noise level

$$\bar{D}(\mathbf{q}) \equiv \Gamma^K(\omega = 0, \mathbf{q}). \tag{5.19}$$

We have argued in chapter 3.3, that typically, this defines an effective temperature at low scales, where both $\bar{\gamma}$ and $\bar{D}$ are some finite constants.

This reasoning however breaks down as a matter of principle as one tunes γ through zero entering the rotating phase. Intuitively, this phase is clearly nonthermal, as it has a time dependent stable state and such a *perpetuum mobile* cannot occur in equilibrium. This behavior should extend to phase boundaries of the rotating phase, and therefore in particular at a CEP.

More formally, for the damped harmonic oscillator (5.3) with $\bar{\gamma}(\mathbf{q} = 0) \neq 0$, it is always possible to realize the thermal symmetry (3.17) with a temperature $T = \frac{D(\mathbf{q})}{2\gamma(\mathbf{q})}$. But, by definition of a CEP where the full renormalized damping at zero momentum is tuned to zero, $\bar{\gamma}(\mathbf{q} \to 0) \sim |\mathbf{q}|^\alpha$ with $\alpha > 0$, in the presence of a finite noise level $\bar{D}(\mathbf{q} \to 0) \sim \bar{D}$, the dynamics has to break thermal equilibrium conditions. Indeed, (5.17) does not hold and the quadratic action does not respect thermal symmetry at a CEP.

5.2 Gaussian Theory and Symmetry restoration

Spectra

After these general considerations about modes EPs and CEPs, we now turn back to the transition from ordered to rotating phase. To that end, we analyse the linearised spectra close to the transition. We write the action of fluctuations around their respective mean-field solutions $\boldsymbol{\varphi}_s$ which also serve as a low frequency, long wavelength description of the phases. That is, we expand the action to quadratic order

$$S[\boldsymbol{\phi}_s + \Delta\boldsymbol{\phi}, \tilde{\boldsymbol{\phi}}] \approx \int_{\mathbf{x},t} (\Delta\boldsymbol{\phi}(\mathbf{x},t), \tilde{\boldsymbol{\phi}}(\mathbf{x},t)) \mathcal{G}_0^{-1} \begin{pmatrix} \Delta\boldsymbol{\phi}(\mathbf{x},t) \\ \tilde{\boldsymbol{\phi}}(\mathbf{x},t) \end{pmatrix}. \tag{5.20}$$

We note that, by reversing the MSRJD construction, this corresponds to expanding the Langevin equation to linear order around a respective mean-field solution. This allows us to access the spectrum of dispersions $\omega_i(\mathbf{q})$, to derive the inverse bare Green function $\mathcal{G}_0^{-1}$ of fluctuations in the various phases, and to identify the CEPs and their properties. In the static phase, we pass to a phase-amplitude representation

$$\begin{aligned} \boldsymbol{\phi} &= \sqrt{\rho_0 + \delta\rho}\, \exp(\sum_{i=2}^{N} \theta_i T_{1,i}) \hat{e}_1, \\ \tilde{\boldsymbol{\phi}} &= \sqrt{\rho_0}\, \exp(\sum_{i=2}^{N} \theta_i T_{1,i}) \tilde{\chi}, \end{aligned} \tag{5.21}$$

where $\tilde{\chi} \in \mathbb{R}^N$ is parametrized as $\tilde{\chi} = (\tilde{\delta\rho}, \tilde{\theta}_2, \ldots, \tilde{\theta}_N)$, and expand to quadratic order. The amplitude sector is

$$\begin{aligned} S^0_\rho = \rho_0 \int_{\mathbf{x},t} \tilde{\rho}(\partial_t^2 + (\delta + u'\rho_0 - Z\nabla^2)\partial_t \\ + 2\lambda\rho_0 - v^2\nabla^2)\rho - D\tilde{\rho}^2, \end{aligned} \tag{5.22}$$

with the relative amplitude fluctuation $\rho = \frac{\delta\rho}{2\rho_0}$ while the Gaussian fluctuations of the phases $\theta_2, ..., \theta_N$ are described by

$$S^0_\theta = \rho_0 \int_{\mathbf{x},t} \tilde{\theta}_i(\partial_t^2 + (\delta - Z\nabla^2)\partial_t - v^2\nabla^2)\theta_i - D\tilde{\theta}_i^2. \tag{5.23}$$

This action also serves as a starting point for an effective long wavelength theory describing the transitions out of the statically ordered phase.
Using the phase-amplitude description of the broken phases, we can approach the transition from the static into the rotating phase. It occurs upon tuning the effective damping

$$\delta = 2\gamma - \frac{ur}{\lambda} \tag{5.24}$$

through zero. This marks it as a CEP as defined in Sec. 5.1.1, since the modes becoming critical have no mass-like contribution to begin with due to their Goldstone nature.

Furthermore, the amplitude fluctuations remain gapped and damped for any $u' > 0$

$$\omega_\rho(\mathbf{q} = 0) = -i\frac{\delta + u'\rho_0}{2} \pm \frac{(8\lambda\rho_0 - (\delta + u'\rho_0)^2)^{1/2}}{2}. \tag{5.25}$$

They can thus be discarded from an effective long wavelength description. See App. 8.3 for a discussion of the transition into the oscillating phase at $u' < 0$. At the phase transition, there is a 'condensation' of $\partial_t\theta_i = E$ (i.e., the angular velocity picks up a finite value), while the choice which mode θ_i starts to rotate is made spontaneously. The equal-time correlator of the phase fluctuations

$$\mathcal{C}_\theta(t = 0, \mathbf{q}) = \frac{D}{\rho_0 v^2 \mathbf{q}^2 (Z\mathbf{q}^2 + \delta)} \tag{5.26}$$

displays an enhanced divergence $\sim \mathbf{q}^{-4}$ at $\delta = 0$, as expected in the vicinity of a CEP.

This CEP transition does not fall into any known universality class a priori. We thus first discuss the scaling behavior of the linear fluctuations in the vicinity of the CEP in more detail. This discussion is exact above the upper critical dimension of the transition, which we determine also to be $d_c = 4$ in Sec. 5.3. There, we will also analyze the problem beyond Gaussian fluctuations.

In the following, v sets the highest momenta, i.e. we work at $q \lesssim v$, where our effective field theory at low momenta is valid. We are also close to the CEP i.e. we work with $\delta^{1/2} \lesssim v, Z$. In this regime for finite damping $\delta > 0$, the dispersions of the phase fluctuations are

$$\omega_{1,2}(\mathbf{q}) = -\frac{i}{2}(\delta + Z\mathbf{q}^2) \pm \sqrt{v^2\mathbf{q}^2 - \frac{\delta^2}{4}}. \tag{5.27}$$

There is thus a non-critical EP at a finite momentum scale $q_{\mathrm{EP}} = \frac{\delta}{2v^2}$. It only affects the dynamics, separating overdamped, purely dissipative modes from underdamped, propagating modes. This translates to a length scale

$$\xi_{\mathrm{EP}} \sim v/\delta, \tag{5.28}$$

separating both regimes. In contrast to a critical length scale, it does not signal the divergence of a correlation function. The correlation function displays an enhanced divergence $\sim \mathbf{q}^{-4}$ as expected for a CEP. The additional divergence as the damping gap δ is tuned to zero generates is indeed not controlled by ξ_{EP}, but by a divergent length scale

$$\xi_c = \delta^{-1/2}, \tag{5.29}$$

indicating a critical exponent

$$\nu = \frac{1}{2} \tag{5.30}$$

for the mean-field transition.

This critical length scale diverges less quickly than the exceptional length scale ξ_{EP} close to the transition, so that in the critical regime $x \ll \xi_c$ fluctuations are underdamped. The critical regime is therefore found for momenta satisfying

$$q \gg \delta^{\frac{1}{2}} \gg q_{\mathrm{EP}}. \tag{5.31}$$

At the CEP $\delta = 0$ however, the coexistence of dissipation and propagation persists

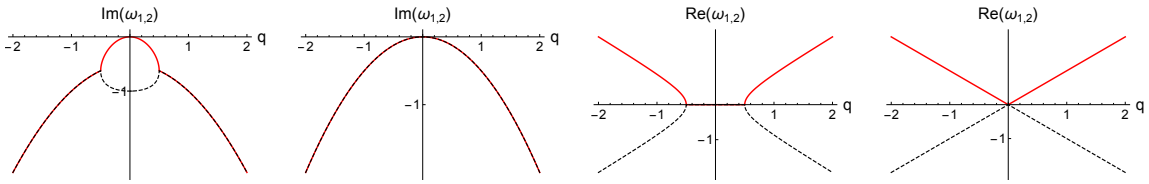

Figure 5.2: The dispersions of the phase fluctuations close to the critical exceptional point. a) and c) show the imaginary (dissipative) and real (propagating) part of the dispersion at a finite damping with $\delta/v^2 = 1$. The exceptional point separating purely dissipative dynamics from underdamped motion is clearly visible. At vanishing momenta one mode becomes gapless marking its Goldstone nature, whereas the other mode maintains a gap δ. As one approaches the CEP $\delta = 0$ shown in b) and d), the egg-shaped structure in the dissipative part shrinks to zero, both modes dissipate as $\sim \mathbf{q}^2$ and display a linear scaling in their real parts, indicating propagation at a constant velocity in real space.

down to vanishing momentum, where

$$\omega_{1,2} = -\frac{i}{2} Z\mathbf{q}^2 \pm v|\mathbf{q}|, \tag{5.32}$$

see Fig. 5.2. The linear scaling of the real part of the dispersion in momentum space will manifest as spherical propagation of excitations at constant velocity v, whereas the dissipative part will lead to diffusive decay in real space around the mean position $|\mathbf{x}| = vt$. This is also seen by inspecting the correlation function in $(\mathbf{q}, t)$ space

$$G^K(\mathbf{q}, t) \propto \frac{D}{v^2 Z\mathbf{q}^4} \exp^{-\frac{1}{2}Z\mathbf{q}^2 t} \cos(|v\mathbf{q}t|). \tag{5.33}$$

Hence, there is no unique dynamical z exponent: the lifetime of a critical fluctuation scales as $\tau_d \sim q^{-2}$ at the CEP, and its oscillation period in momentum space as $\tau_c \sim q^{-1}$. These two scaling behaviors coexist, controlling different properties of the dynamics of excitations, and inhibit the existence of a homogeneous scaling solution of the action and a true scale invariance of correlation functions even at the Gaussian fixed point [2].

[2] One may then be tempted to keep only the lowest order power in momenta in the dispersion (5.32) arriving at a dynamical exponent $z = 1$. This would amount to neglecting the damping term Z in Eq. (5.23). This is non-physical, because the system would only receive energy from the noise without any dissipation. More formally, Eq. (5.33) would be infinite for $Z \to 0$. We are thus forced to keep the lowest power in momenta for both imaginary and real part of the dispersions. This has to be contrasted with the quantum case, where there is no dissipation but where also the noise vanishes as $|\omega| \to 0$.

5.2.1 Symmetry Restoration

We now provide a simple argument stating that the enhancement of fluctuations in the vicinity of a CEP renders it impossible to reach below four dimensions if interactions are not taken into account. We will see that the fluctuations either restore the full symmetry before the CEP is reached, or render the transition between statically ordered and rotating phase first order. We use the phase-amplitude decomposition (5.21). As we have seen, the phase fluctuations become critically exceptional at the transition, and the static correlation function is

$$\langle \theta_i(\mathbf{q}, t_0)\theta_j(-\mathbf{q}, t_0)\rangle = G^K_{0,ij}(\mathbf{q}, t = 0) \sim \frac{D\delta_{ij}}{\rho_0 v^2 \mathbf{q}^2 (Z\mathbf{q}^2 + \delta)}. \tag{5.34}$$

The CEP is reached as the damping $\delta \to 0$. This implies in the Gaussian approximation

$$G^K_{\theta,ii}(\mathbf{q}, t = 0) \xrightarrow{\delta\to 0} \frac{1}{\mathbf{q}^4}. \tag{5.35}$$

Thus, the Gaussian correlation function $G^K_{0,ii}(\mathbf{x} = 0, t = 0)$ develops an infrared divergence in $d < 4$ spatial dimensions in the vicinity of the CEP, which is regularized by the damping:

$$\langle \theta_i(\mathbf{x}_0, t_0)\theta_i(\mathbf{x}_0, t_0)\rangle = G^K_{0,ii}(\mathbf{x} = 0, t = 0) = C\frac{\delta^{\frac{d-4}{2}}}{\rho_0}. \tag{5.36}$$

Here $C > 0$ is a non-singular constant that depends on the dimension and the ultraviolet cutoff of the theory. Its exact value is not important for our argument, we only rely on the fact that it is positive and finite. We see that when the damping vanishes, the Gaussian fluctuations of the Goldstone modes diverge and would destroy any order. Indeed, neglecting amplitude fluctuations,

$$\begin{aligned}
\langle \boldsymbol{\varphi}(\mathbf{x}_0, t_0)\rangle &= \sqrt{\rho_0}\langle \exp\Big(\sum_{i=2}^{N} \theta_i(\mathbf{x}_0, t_0)T_{1,i}\Big)\rangle \hat{e}_1 \\
&= \sqrt{\rho_0}\exp\Big(2\mathrm{tr}\langle \theta_i(\mathbf{x}_0, t_0)\theta_j(\mathbf{x}_0, t_0)\rangle T_{1,i}T_{1,j}\Big)\hat{e}_1 \\
&= \sqrt{\rho_0}\exp\Big(\frac{-2(N-1)C\delta^{\frac{d-4}{2}}}{\rho_0}\Big)\hat{e}_1 \xrightarrow{\delta\to 0} 0,
\end{aligned} \tag{5.37}$$

and the enhanced Gaussian fluctuations due to the CEP alone destroy the order parameter before one can reach the CEP at $\delta = 0$ below four dimensions. The order parameter is suppressed when the argument of the exponential in Eq. (5.37) is of

order one, i.e. at a symmetry restoring scale

$$\frac{\delta_{\rm sym}}{Z} \sim \left(\frac{v^2 Z}{D}\rho_0\right)^{\frac{2}{d-4}}, \tag{5.38}$$

restoring all parameters previously absorbed in C. This argument is reminiscent of the Mermin-Wagner theorem, which prevents the existence of symmetry breaking in and below two dimensions in the usual case. However, it applies only to the critical point here, not to the entire phase. On the other hand, the rotating phase exists and is not destroyed by fluctuations above two dimensions.

This leaves three scenarios for the transition upon including the effect of fluctuations and interactions :
(i) There is no direct transition between static and rotating phases, but a fully symmetric, disordered regime in between. This is the expectation solely based on the exceptional Gaussian fluctuations.
(ii) There is a (weakly) first order transition, induced by interactions. A non-trivial scaling regime close to the transition may still emerge in principle.
(iii) The phase transition is second order. This is only possible, if nonlinear effects reduce fluctuations by generating a sufficiently large anomalous dimension. In equilibrium this happens, for example, for the 2d Ising model, where the anomalous dimension shift the naive lower critical dimension from two to one.

The third scenario will be ruled out by our analysis. We will show, that indeed a first order transition occurs for sufficiently large ρ_0. For smaller ρ_0 the interaction effects do not have room to build, and as one approaches the CEP the enhanced fluctuations push the system back in the symmetric phase through the model A transition.

The same mechanism has to arise while approaching the CEP line from the rotating phase and the symmetry restoring nature of the enhanced fluctuations will therefore strongly move the phase boundaries as sketched in Fig. 2.4.

5.3 Fluctuation induced first order

We now show how a first order phase transition into the rotating phase at finite δ can occur.

As we have seen in Sec. 5.2, the amplitude fluctuations around the stable state in the broken phase remain damped and gapped in the vicinity of the CEP at $\delta = 0$, and can be integrated out. For $N = 2$, this yields the effective Gaussian action for

the phase field (5.23),

$$S_0 = \int_{t,\mathbf{x}} \tilde{\theta}(\partial_t^2 + (\delta - Z\nabla^2)\partial_t - v^2\nabla^2)\theta - D\tilde{\theta}^2. \tag{5.39}$$

We rescaled the fields $\theta \to \theta/\sqrt{\rho_0}$ and $\tilde{\theta} \to \tilde{\theta}/\sqrt{\rho_0}$.

The symmetry $O(2) \cong SO(2) \ltimes \mathbb{Z}_2$ acts on the phase field as

$$SO(2): \ \theta \to \theta + \alpha, \quad \mathbb{Z}_2: \ (\theta, \tilde{\theta}) \to -(\theta, \tilde{\theta}). \tag{5.40}$$

This approach assumes that the fluctuations of the amplitude modes are small $\delta\rho \ll \rho_0$ and thus breaks down once the renormalized amplitude becomes small. Approaching the CEP below four dimensions, this will be the case if we reach the scale $\delta \sim \rho_0^{(d-4)/2}$, signalling that we instead reach a regime where the symmetry gets restored as we have shown above. In the following we work in a regime with sufficiently large ρ_0, assuming that the scale at which the symmetry gets restored is not reached. This yields a criterion, whether symmetry restoration occurs or the scenario laid out below is realized.

We first discuss in greater detail how the transition is explained from this action above the upper critical dimension, and develop an effective potential picture which will turn out to be useful in the following. When crossing the phase transition by tuning δ through zero, the order parameter starts to rotate at a finite angular velocity and the $\mathbb{Z}_2$ symmetry is spontaneously broken. In terms of the phase variable, it corresponds to the 'condensation' of $\Pi = \partial_t\theta$, which evolves in an effective Ising like potential

$$V_{\text{eff}}(\Pi) = \frac{\delta}{2}\Pi^2 + \frac{g_1}{4!}\Pi^4, \tag{5.41}$$

where the fourth order term has been added to make the mean-field theory well-defined in the rotating phase ($\delta < 0$). In that phase, we obtain $\Pi = \sqrt{\rho_0}E = \sqrt{-6\delta/g_1}$ and recover the square root behavior of the angular velocity encountered in mean field in chapter 2. Therefore, this potential picture works despite the out-of-equilibrium nature of the problem. Beyond mean-field, we will get an effective equation of motion for the dressed order parameter using the effective action formalism (see Eq. (3.9)). The potential picture will in turn remain applicable.

Since a $\mathbb{Z}_2$ is broken spontaneously along the transition, it is natural to compare it to the Ising universality class. Indeed, on the mean-field level, the phase transition is reminiscent to some extent to the usual Ising transition, where the role of the Ising field is played by $\partial_t\theta$. This can be rationalized by noting that the Ising model is recovered when $v = 0$. However, recall from the shape of the correlation function

(5.33), that setting v to zero would destabilize the entire theory and our model and transition differs from the Ising field theory.

5.3.1 Beyond Gaussian Fluctuations

We now determine how interactions lead to a fluctuation induced first order scenario below the upper critical dimension for sufficiently large ρ_0. To this end, we approach the CEP from the statically ordered phase. The broken $SO(2)$ symmetry, Eq. (5.40), ensures that the field θ can only appear with derivatives, while invariance under $\mathbb{Z}_2$ excludes cubic – or higher odd powers – interactions; in particular, it rules out the Kardar-Parisi-Zhang nonlinearity $\tilde{\theta}(\nabla\theta)^2$ and the cubic nonlinearity $\tilde{\theta}(\partial_t\theta)^2$. The lowest order local interaction terms that one can add to the quadratic action within these bounds are

$$S_{\rm int} = \frac{g_1}{6}\int_{\mathbf{x},t}\tilde{\theta}(\partial_t\theta)^3 + \frac{g_2}{2}\int_{\mathbf{x},t}\tilde{\theta}\partial_t\theta(\nabla\theta)^2. \tag{5.42}$$

These are the most relevant allowed couplings in an renomalization group (RG) sense. The existence of two time scalings in the Gaussian Green functions, as discussed in Sec. 5.2, renders a simple power counting analysis at the Gaussian fixed point impossible. Therefore, we will instead calculate the diagrams renormalizing the various couplings, and infer their scaling dimensions from the associated infrared divergences. These two time scalings also suggest that, for non-static quantities, not only δ but also the quantity δ/v^2 shall control the form of correlation functions. We will see that this scale indeed explicitly appears in the renormalization corrections beyond mean-field.

Perturbative corrections

The diagrammatic rules associated to the four-point vertices (5.42) and the perturbative corrections to two-point functions (self-energies) up to two loop-order are presented in Fig. 5.3. One-loop corrections to the four-point functions are given in Fig. 5.4.

Interactions – We now discuss how the parameters of the effective action are renormalized perturbatively, and how they are impacted by the presence of the non-analyticity of the CEP in the spectrum. For this sake we first take a look at the one-loop diagrams renormalizing the four point vertices displayed in Fig. 5.4, but the phenomenology will go beyond this particular example. First, we consider the

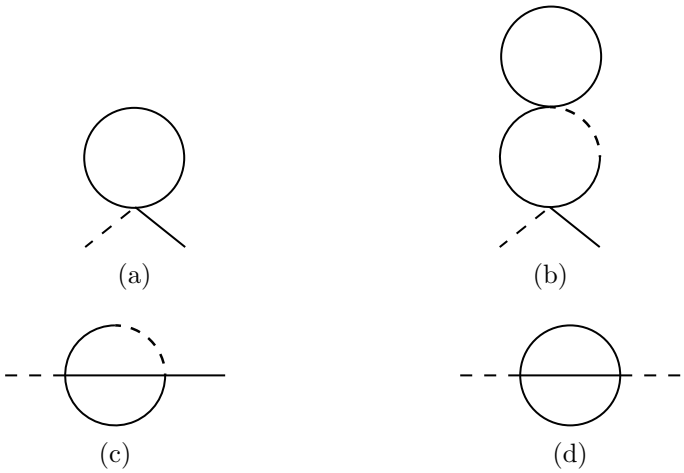

Figure 5.3: Self-energies up to two loop-order. The first three graphs correct the retarded part of the action $\Gamma^{(11)}$, and the last one the noise term $\Gamma^{(20)}$. The solid line denotes the bare Keldysh Green function G^K, and the solid-to-dashed line the retarded Green function G^R. The four-point vertices can be either g_1 or g_2 defined in (5.42).

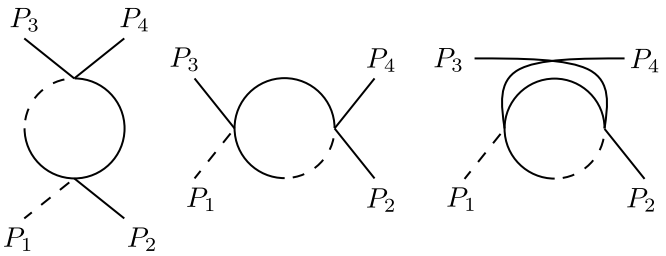

Figure 5.4: One-loop corrections to $\Gamma^{(13)}$ renormalizing the interactions, $P_i = (\mathbf{p}_i, \omega_i)$.

case where g_1 is renormalizing itself. The first diagram in Fig. 5.4 with g_1 as vertices is equal to $\omega_2\omega_3\omega_4\, I_{1l,I}$ with

$$I_{1l,I}(\mathbf{p},\omega_p) = \int_{\mathbf{q},\omega} i(\omega+\omega_p)\omega^2 G^R(\mathbf{q}+\mathbf{p},\omega+\omega_p)G^K(\mathbf{q},\omega), \tag{5.43}$$

where $\mathbf{p} = \mathbf{p}_1 + \mathbf{p}_2$, $\omega_p = \omega_1 + \omega_2$ and $\int_{\mathbf{q},\omega} \equiv \int d\mathbf{q}d\omega/(2\pi)^{(d+1)}$. The two other diagrams are obtained by permutation of momenta. We now are interested in the infrared behavior of this loop as one tunes $\delta \to 0$, i.e. approaches the CEP. When δ/v^2 becomes small, we find that it diverges as

$$I_{1l,I}(\mathbf{p},\omega_p) \sim \delta^{\frac{d-4}{2}}, \tag{5.44}$$

for small dimensionless momenta $\tilde{p} = \frac{p}{\sqrt{\delta}} \ll \sqrt{\delta}/v$, but that this IR divergence is smaller for finite dimensionless momenta

$$I_{1l,I}(\mathbf{p},\omega_p) \sim \delta^{\frac{d-4}{2}}(\frac{\delta}{v^2})^{\frac{d-1}{4}} h(\mathbf{p},\omega_p), \tag{5.45}$$

with h some nonsingular scaling function, and therefore become subleading. This implies a very sharp non-analytic behavior as shown in Fig. 5.5. This is due to the peculiar form of the dispersions at the CEP which induces a resonance condition in the integral to get the highest divergence, as discussed below and in App. 8.4 where Eqs. (5.44) and (5.45) are also proven.

Similar scaling shapes hold for all combinations of the vertices $g_{1,2}$. From (5.44), we can infer that the upper critical dimension is $d_c = 4$. Above it, all interactions are irrelevant and the Gaussian theory is exact asymptotically at long wavelengths. (5.45) implies, that only loops with transfer momentum $\tilde{p} \ll \frac{\sqrt{\delta}}{v} \xrightarrow{\delta\to 0} 0$ contribute to the renormalization of the vertices as we approach the CEP. We can thus regard all finite transfer momenta to lead to subleading contributions.

This means, that divergences of vertex corrections depend on the momentum configuration of the respective vertex in a highly non-analytic way and a derivative expansion around $p = 0$ is not possible. In particular, we find that the two limits $\tilde{\mathbf{p}} \to 0$ and $\delta \to 0$ cannot be exchanged, see Fig. 5.5. This non-analytic structure can be related to the nonanalyticity of the exceptional point. Intuitively, this is indicated by the EP momentum scale $q_{EP} = \frac{\delta}{v}$ already seen in the linear spectrum in Sec. 5.2 above which dimensionful transfer momenta $\mathbf{p}$ are cut off (since the critical regime is described by $q/\sqrt{\delta} \sim 1$, we are generally interested in momenta $q \gg q_{EP}$).

We now illuminate the origin of these different scalings, which result from a resonance condition on the external momentum. In a nutshell, after frequency inte-

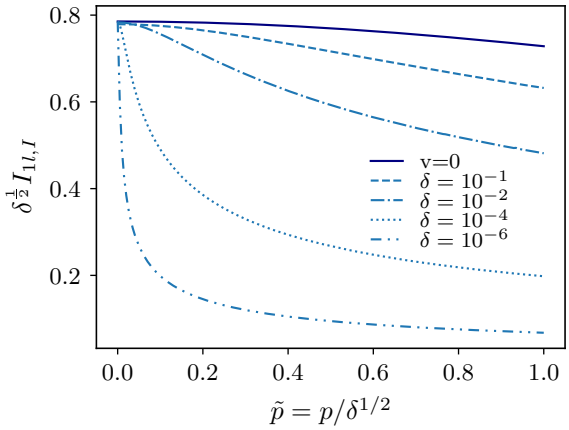

Figure 5.5: $I_{1l,I}(\tilde{p} = p/\delta^{1/2}, \omega_p = 0)$ defined by Eq. (5.43) in $d = 3$ for $v = 0$ (solid line) for $v = 1$ and different values of δ (dashed/dotted lines). For $v = 0$, the rescaled integral is independent of δ and diverges as $\delta^{-1/2}$. For $v \neq 0$, this divergence is found only for smaller and smaller $\tilde{p} \lesssim \delta^{1/2}/v$ as $\delta \to 0$, and the integral is more and more peaked around zero. For $\delta \to 0$, $I_{1l,I}$ therefore becomes non-analytic and is non negligible only at $\tilde{p} = 0$.

gration, rescaling of momenta by introducing $\tilde{\mathbf{q}} = \mathbf{q}/\delta^{1/2}$, and for small values of δ, the diagram 5.3c at zero external frequency reduces to

$$I_{1l,I} = \frac{\delta^{\frac{d-4}{2}}}{2} \int_{\tilde{\mathbf{q}}} \frac{f_1(\tilde{\mathbf{q}}, \tilde{\mathbf{p}}) + O(\delta)}{\frac{v^2}{\delta} \left(\tilde{\mathbf{p}}^2 + 2\tilde{\mathbf{p}} \cdot \tilde{\mathbf{q}}\right)^2 \Delta\left(\tilde{\mathbf{q}}^2\right) + f_1(\tilde{\mathbf{p}}, \tilde{\mathbf{q}}) \Delta\left(\tilde{\mathbf{q}}^2\right) \left(\Delta\left(\tilde{\mathbf{q}}^2\right) + \Delta\left((\tilde{\mathbf{p}} + \tilde{\mathbf{q}})^2\right)\right) + O(\delta)}. \tag{5.46}$$

In this expression, we use $\Delta(y) = y+1$, and $f_1(\tilde{\mathbf{q}}, \tilde{\mathbf{p}}) = (\tilde{\mathbf{p}}+\tilde{\mathbf{q}})^2\Delta(\tilde{\mathbf{q}}^2)+\tilde{\mathbf{q}}^2\Delta((\tilde{\mathbf{p}}+\tilde{\mathbf{q}})^2)$. In the denominator, we keep a higher order in terms of δ since it becomes the dominant term in the expansion as soon as $v^2\left(\mathbf{p}^2 + 2\mathbf{p} \cdot \mathbf{q}\right)$ is small. This is always true for $\mathbf{p} = 0$, but only occurs for special configuration of momenta when $\mathbf{p} \neq 0$. When this is fulfilled the integrand behaves as $\delta^{d/2-2}$ and only as $\delta^{d/2-1}$ when it is not: there is a resonance condition to get the highest divergence. Mathematically, the integrand in (5.46) becomes non-analytic and behaves as a Dirac distribution in the $\delta/v^2 \to 0$ limit to still give the stronger divergence. This behavior can in turn be used to compute the integrals, see App. 8.4.

This is in sharp contrast with more standard renormalization corrections, where the leading momentum dependent term scales accordingly to the momentum independent part, and where higher order terms in momentum are negligible in the infrared in the spirit of a gradient expansion. This expansion in momentum cannot be used here because of the non-analytic structure. Indeed, we show in App. 8.6 that

such an expansion generates spurious divergences with arbitrarily high power in δ. This also illustrates why standard power counting does not work: the presence of the additional scale v^2/δ allows for a more complex scaling of integrals, which breaks the generic scaling behavior.

Self-energies – This structure also strongly impacts the perturbative corrections at higher loop orders. We now discuss that matter for the two-point vertex $\Gamma^{(2)}$. We will see that it makes sunset diagrams 5.3c and 5.3d less divergent than the tadpoles one 5.3a and 5.3b. We begin the analysis with the tadpole diagrams. They are linear in the external frequency, and momentum independent. They therefore only renormalize the momentum independent damping coefficient δ. The one-loop tadpole gives

$$I_{1l} = \frac{K_d}{2}(g_1 + g_2)\int dq \frac{q^{d-1}}{q^2+\delta}, \tag{5.47}$$

where $K_d = S_d/(2\pi^d)$ with S_d the surface of the d-dimensional sphere. In these expressions, new dimensionless quantities have been introduced via the following rescaling: $\delta \to \delta Z$, $g_1 \to g_1 Z^2/D$ and $g_2 \to g_2 Z^2 v^2/D$. Performing the integral over momentum gives

$$\overline{\delta} = \delta' - K'_d \frac{g_1+g_2}{2}\delta^{\frac{d-2}{2}}, \tag{5.48}$$

with $K'_d = -K_d\pi/(2\sin(\pi d/2)) > 0$, and $\delta' = \delta + (g_1+g_2)K_d/2\int_0^\Lambda dq/q^2$. Here, Λ denotes the UV cutoff used to regularize the loops. This is consistent with $d_c = 4$, since the perturbative corrections in (5.48) to the damping become non-negligible below four dimensions. The contribution of the two-loop tadpole diagram 5.3a is simply given by the square of Eq. (5.47) and behaves as δ^{d-3}.

We now turn our attention to the loop integrals of the sunset diagrams Fig. 5.3c (for two g_1 vertices going into the loop, the same however holds for all vertex combinations) at vanishing external momenta. It can be written as

$$I_{2l} = g_1^2 \int_{\mathbf{q},\omega'} \omega'^2 G^K(\mathbf{q}) I_{1l,I}(\mathbf{q},\omega). \tag{5.49}$$

I.e. the bubble diagram analysed earlier reappears as a subgraph of the sunset diagrams and their transfer momentum is integrated over. Since the point of vanishing transfer momentum at which the resonance occurs is a zero measure set, only the subleading scaling of $I_{1l}(\mathbf{q},\omega)$ contributes to the sunset diagram. Thus the whole sunset diagram, even at finite momentum or frequency, is subleading when compared to the other terms in the renormalized two-point function at small damping. Indeed,

while I_{2l} scales as δ^{d-3} for $\delta/v^2 \gg 1$ (like the tadpole diagram 5.3b), it is suppressed in the critical regime $\delta/v^2 \ll 1$ where

$$I_{2l} \sim \delta^{d-3}\left(\frac{\delta}{v^2}\right)^{\frac{d-1}{4}} \ll \delta^{d-3}. \tag{5.50}$$

Eq. (5.50) is proven in App. 8.4, and a similar result is found for diagram 5.3d with δ^{d-3} replaced by δ^{d-4}. At finite external momentum, the sunsets are even less divergent since they display the same non-analytic structure in their p dependencies than the one found for the one-loop diagrams (see Fig. 5.5). More details can be found in App. 8.4.

This shows that the presence of the EP leads, for $d > 1$ and in particular for the dimensions of interest $d \geq 2$, to smaller infrared divergences in two-loop sunset diagrams, which in turn indicates that they will contribute only subdominantly in the critical regime and can be neglected. Only one-loop contributions without transfer momentum survive and the corrections to v, K, and D associated to anomalous dimensions and z exponents all vanish.

Formally, this is a valid assumption if $I_{2l}(p)$ remains very small compared to all terms in Eq. (5.48) i.e. to the renormalized damping $\bar{\delta}$. Because I_{2l} diverges when the damping becomes small, this necessarily implies a condition on the prefactor of the loop i.e. on the interactions $g_1 + g_2$, which have to be sufficiently small. This condition can only be self-consistently checked once we have computed $\bar{\delta}$, and we therefore defer its discussion to Sec. 5.3.2.

In principle, one has to check that higher loop terms for the self-energies and for interactions follow a similar pattern and are also negligible. The discussed pattern however extends to all diagrams in the perturbative series that contain loops with more than one momenta. Thus, only graphs with a one-loop structure i.e. graphs that are products of one-loop graphs, and without momentum transfer survive when δ/v^2 becomes small. Alternatively, this is elegantly recovered in the DSE framework since the full effective action can be computed solely from (dressed) tadpole and sunset diagrams, see App. 8.5.

Self-consistent equations and first-order phase-transition

Because of the emergent one-loop structure, with negligible higher loop effects, it is possible to resum the entire perturbation series, or equivalently to solve the corresponding DSE, see Fig. 5.6 for a diagrammatic representation.

For the reason laid out above, we neglect the sunset topology of the DSE. Then the DSE for the for the damping of the retarded two-point function (i.e. the renormalized

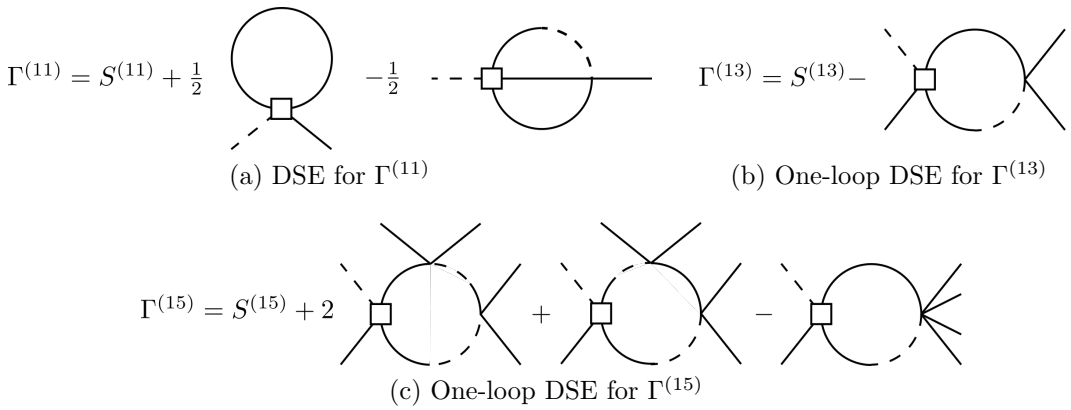

(a) DSE for $\Gamma^{(11)}$

(b) One-loop DSE for $\Gamma^{(13)}$

(c) One-loop DSE for $\Gamma^{(15)}$

Figure 5.6: Diagrammatic representation of the DSE. The solid and solid-to-dashed lines correspond respectively to the *full* Keldysh and retarded Green functions. The vertices correspond also to the *full* vertices $\Gamma^{(13)}$ and $\Gamma^{(15)}$, except for those that are represented with a square box, which correspond to the bare vertices $S^{(13)}$. Diagrams obtained by permutation of external legs attached to θ fields (solid line legs) are not shown.

control parameter of the transition $\bar{\delta}$) reads

$$\overline{\delta} = \delta' - K'_d \frac{g_1 + g_2}{2} \overline{\delta}^{\frac{d-2}{2}}. \tag{5.51}$$

We have to do a little more work and consider some momentum dependency of the fully renormalized vertices $\bar{g}_{1,2}(\mathbf{p}_1, \mathbf{p}_2, \mathbf{p}_3)$. First, we write out the diagrammatic DSE for the four-point vertex in terms of the vertices of the full effective action Γ and the bare action S and the Green's function $\mathcal{G}$:

$$\begin{aligned}\Gamma^{(13)}(P_4, P_1, P_2, P_3) &= S^{(13)}(P_4, P_1, P_2, P_3)\times \\ &\left(1 - \int_Q G^K(Q) G^R(Q + P_1 + P_2) \Gamma^{(13)}(-(Q + P_1 + P_2), Q, P_1, P_2)\right) + \text{perm.},\end{aligned} \tag{5.52}$$

where $P_4 = -(P_1 + P_2 + P_3)$ and where the permutations apply on the set P_1, P_2 and P_3. We know from our previous analysis, that only the constellations where there is no momentum transfer through loop contribute close to the transition and thus on the right hand site only the vertex $\Gamma^{(13)}(P_1, -P_1, P_2, -P_2)$ enters the self consistency equation. We thus make the Ansatz, that only the following momentum constellations or "hot spots" contribute to the flow. We parametrize them as

$$g_{1,a} \equiv \bar{g}_1(-\mathbf{p}, \mathbf{q}, -\mathbf{q}, \mathbf{p}),\ \mathbf{p}, \mathbf{q} \neq 0, \mathbf{p} \neq \mathbf{q} \tag{5.53}$$

for which only one of the momentum permutation in 5.4 contributes,

$$g_{1,b} \equiv \bar{g}_1(-\mathbf{p}, \mathbf{p}, -\mathbf{p}, \mathbf{p}),\ \mathbf{p} \neq 0 \tag{5.54}$$

for which two permutations contribute and

$$g_{1,c} \equiv \bar{g}_1(0, 0, 0, 0) \tag{5.55}$$

for which all three diagrams contribute. Carrying out the frequency integration leads to the self consistency equations for the full macroscopic couplings,

$$g_{1,a} = g_1 - \frac{g_1 + g_2}{2} g_{1,a} \int_{\mathbf{q}} \frac{1}{(q^2 + \overline{\delta})^2}, \tag{5.56a}$$

$$g_{1,b} = g_1 - 2\frac{g_1 + g_2}{2} g_{1,a} \int_{\mathbf{q}} \frac{1}{(q^2 + \overline{\delta})^2}, \tag{5.56b}$$

$$g_{1,c} = g_1 - 3\frac{g_1 + g_2}{2} g_{1,a} \int_{\mathbf{q}} \frac{1}{(q^2 + \overline{\delta})^2}. \tag{5.56c}$$

The integral that appears in Eqs. (5.56) can be calculated and the equations can be inverted to give

$$g_{1,a} = \frac{g_1}{1 + \alpha_2 \overline{\delta}^{\frac{d-4}{2}}}, \tag{5.57a}$$

$$g_{1,b} = g_1 \frac{1 - \alpha_2 \overline{\delta}^{\frac{d-4}{2}}}{1 + \alpha_2 \overline{\delta}^{\frac{d-4}{2}}}, \tag{5.57b}$$

$$g_{1,c} = g_1 \frac{1 - 2\alpha_2 \overline{\delta}^{\frac{d-4}{2}}}{1 + \alpha_2 \overline{\delta}^{\frac{d-4}{2}}}, \tag{5.57c}$$

with $\alpha_2 = (g_1 + g_2) K'_d (d-2)/2 > 0$. We see that, while the coupling $g_{1,a}$ at finite momenta is always positive, the couplings $g_{1,c}$ with zero incoming momenta can be negative for sufficiently small $\overline{\delta}$. This therefore opens the route to a fluctuation induced first-order phase transition since a potential with a negative quartic term typically displays a first-order transition [79]. The fourth-order is now momentum dependent, and one has to specify which quartic couplings should enter the effective potential Eq. (5.41) for the order parameter $E = \partial_t \theta / \sqrt{\rho_0}$ and check if it is negative. The condensation mechanism occurs at zero momenta, and E is given by minimizing the effective equation of motion $\Gamma^{(10)}$ with a constant order parameter $\partial_t \theta(x,t) = E$.

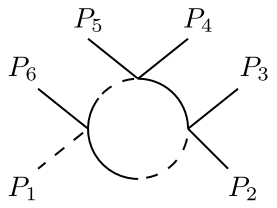

Figure 5.7: One-loop contribution to the six-point function $\Gamma^{(15)}$. The diagrams obtained by permutation of external and internal lines are not shown.

It translates, in momentum space, to

$$\partial_t \theta(\mathbf{p}, \omega) = E\Pi(\mathbf{p}, \omega) = \sqrt{\rho_0} E \delta(\mathbf{p})\delta(\omega). \tag{5.58}$$

In the effective equation of motion for E, the fourth order term is proportional to $\overline{g}_1(0,0,0)\partial_t\theta(\mathbf{p}=0,\omega=0)^3 = g_{1,c}(\sqrt{\rho_0}E)^3$. The coupling that fixes the limit cycle rotation frequency E is therefore $g_{1,c}$ which can indeed turn negative because of Eq. (5.57c). This will drive the first-order phase transition. The coupling $g_{1,b}$ can also turn negative (see Eq. (5.57b)) which could indicate some instability at finite momentum close to the transition. However, it is larger than $g_{1,c}$ and turns negative for even smaller damping, for which the first-order transition we discussed has already taken place. It therefore does not alter the first-order scenario we describe. Since the renormalized coupling $\bar{g}_2$ does not enter its flow, but only its bare version, we do not give its analog self consistent solution here but refer to the appendix 8.5. We note the structural similarity of these slef consistent equations to the mechanism of fluctuation induced first order transitions for systems with pattern formation [58, 96].

Now, to have a well defined potential, we need to add a sextic term in the potential, i.e. $u_1\tilde{\theta}(\partial_t\theta)^5/5!$ in the action. Exactly as for the quartic couplings, there are several hotspot configurations of momenta for which only one-loop diagrams contribute. One has to consider different couplings associated to each of these hotspot regions. To describe the effective potential, we however only need the value of this coupling at zero external momenta,

$$u_{1,e} = \overline{u}_1(0,0,0,0,0). \tag{5.59}$$

Being an irrelevant coupling, its value is entirely set by the quartic couplings at small $\bar{\delta}$. Its renormalization is then given by the one-loop diagram displayed in Fig. 5.7. The resummed expression is obtained by using dressed propagators and interactions.

This leads to

$$u_{1,e} = 15 g_1^2 \frac{\alpha_3 \bar{\delta}^{\frac{d-6}{2}}}{(1+\alpha_2 \bar{\delta}^{\frac{d-4}{2}})^3}, \tag{5.60}$$

where $\alpha_3 = (g_1+g_2)K'_d(d-2)(4-d)/8$.

We are now in the position to solve the resulting equations, and discuss in greater details how the first-order transition takes place.

5.3.2 Solution of self-consistent equations

The resulting system of equations constituted by Eqs. (5.51), (5.57) and (5.60) is solved by extracting the damping $\bar{\delta}$ from the first equation, and inserting it into the others.

Asymptotically, the system does not reach any fixed-point, ruling out the second-order phase transition scenario (iii) of Sec. 5.1.2. We find that the $(\partial_t\theta)^4$ coupling becomes negative and the effective potential describes a first-order transition for sufficiently small δ as shown in Fig. 5.9: new minima appear for a finite $\partial_t\theta = E$, and the order parameter jumps from zero to a finite value. From Eq. (5.57c), the phase transition happens approximately when the quartic term becomes negative, i.e. at a first order transition scale

$$(g_1+g_2)\bar{\delta}_{\rm fo}^{(d-4)/2} \sim 1, \tag{5.61}$$

giving

$$\bar{\delta}_{\rm fo} \sim (g_1+g_2)^{2/(4-d)}. \tag{5.62}$$

We are left to compare this scale for the onset of a first order transition to our previous result on the symmetry restoration $\delta_{\rm sym}$ via the suppression of ρ_0. The system displays a new scale (in terms of the original non rescaled variables)

$$\frac{\delta_{\rm fo}}{\delta_{\rm sym}} = \rho_0 \frac{Z(g_1+v^2 g_2)}{v^2} \equiv \rho_0 g, \tag{5.63}$$

which sets whether there is symmetry restoration ($\rho_0 g \ll 1$) or a fluctuation induced first order transition ($\rho_0 g \gg 1$) separated by the multicritical point ($\rho_0 g \sim 1$) where both transition lines meet. The resulting qualitative phase diagram is shown in Fig. 2.4. Furthermore we remark, that the first order transition scale $\delta_{\rm fo}$ coincides with the Ginzburg criterion where non-Gaussian fluctuations are expected to play a role. (The Ginzburg criterion can be simply derived by comparing one-loop contributions to the order parameter fluctuations to the bare one). This means that in

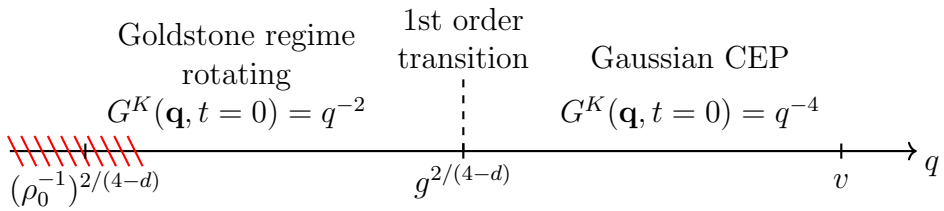

(a) First-order scenario

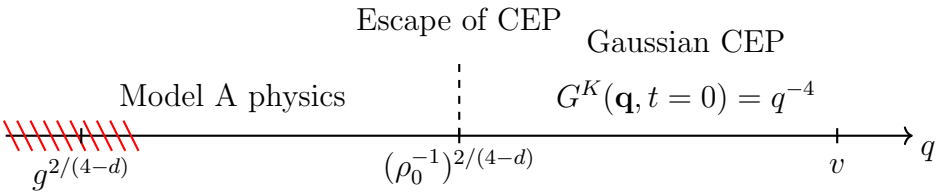

(b) Symmetry restoration scenario

Figure 5.8: Summary of scales for the two different scenarios obtained while approaching the CEP. (a) The first-order scenario occurs before reaching the point where the symmetry get restored since $\rho_0^{-1} \gg g$, and the system ends up in the rotating phase. (b) The symmetry gets restored at large distances, and the system is in the disordered phase. In both cases the red dashed area indicates the scale which is never reached because the other scenario takes place first.

a situation close to the weakly first-order situation, i.e. $1 \gg \delta > \delta_{\rm sym}, \delta_{\rm fo}$, one can observe the Gaussian scaling behavior described in Sec. 5.2 on length scales $\xi < \sqrt{\frac{Z}{\delta}}$ but there is no intermediate regime where one can observe interaction corrections to that scaling, including anomalous dimensions, before reaching the regime of either symmetry restoration or first order transition. This is different from e.g. driven-dissipative condensates below the lower critical dimension, where one can observe KPZ scaling at finite length scales smaller than the length scales at which order breaks down [8, 97]. The different possible scenarios are summarized on Fig. 5.8.

To get a complete picture describing all regimes, one needs a method that can describe both the broken phase within which the first-order transition occurs and the regime in which the amplitude goes to zero. One possible route would be to use the functional RG (FRG) which is known to describe both the phase transition and the broken phase in equilibrium [98].

Validity – Let us finally assess the validity of the assumptions made, and discuss quantitatively under which conditions the subleading corrections are negligible. The sunset contribution Eq. (5.50) (using the renormalized damping in the loop) to $\bar{\delta}$ can be neglected when it is small compared to all terms in Eq. (5.51). The most

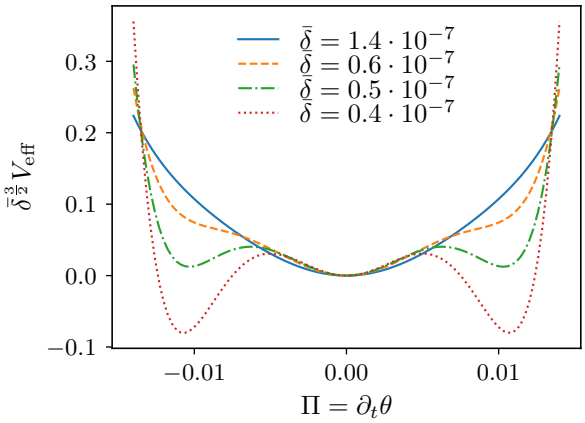

Figure 5.9: The effective potential as a function of $\Pi = \partial_t \theta$ obtained by solving Eqs. (5.51), (5.57) and (5.60) becomes characteristic of a first-order phase transition at a finite renormalized damping $\bar{\delta}$. The results are presented for $d = 3$, $g_1 = g_2 = 10^{-1}$ and $v = 1$.

stringent condition is obtained by demanding it to be negligible with respect to the zero-order term $\bar{\delta}$. It gives the following condition,

$$(g_1 + g_2)^2 \bar{\delta}^{d-4} \bar{\delta}^{(d-1)/4} \ll 1. \tag{5.64}$$

The one-loop diagrams with momentum transfer can be neglected when (5.45) is way smaller than $g_1 + g_2$, and the sunset 5.3d when it is way smaller than D, which both lead to the very same condition. Equivalently, the condition (5.64) is recovered nonperturbatively using DSE as discussed in App. 8.5.

The condition (5.64) becomes, using Eq. (5.62), $(g_1 + g_2)^{(d-1)(4-d)/8} \ll 1$, which is satisfied in $2 < d < 4$ for sufficiently small values of the bare coupling constants, i.e. for a microscopic theory not too far away from the Gaussian fixed-point. In that case, $\bar{\delta}$ is generically small close to the transition because of Eq. (5.51). The transition is then weakly-first order and the condition $\bar{\delta}/v^2 \ll 1$ is in turn also not violated, and our calculation is fully justified in this regime.

One can formally still try to solve the equations for even smaller values of $\bar{\delta}$ i.e deep in the ordered phase where the true damping is instead defined at the nonzero minima. This always gives a solution with $\bar{\delta} > 0$, and the minimum at $\partial_t \theta = 0$ does not disappear. Note that this issue also arises in Brazovskii's phase-transitions scenario [96]. However, the condition (5.64) is not satisfied in this regime, and the solution does not apply anymore. We are however interested in the critical regime here. We analyse the nature of the phase fluctuations deep in the phase in chapter 6.

5.3.3 $\mathbb{Z}_2$ symmetry breaking and $SO(2) \simeq U(1)$ case

Explicit $\mathbb{Z}_2$ breaking – We now discuss the case where the symmetry is $SO(2)$ or $U(1)$ instead of the $O(2)$ symmetry discussed so far. In that case the $\mathbb{Z}_2$ symmetry is explicitly broken, and a linear term $\partial_t\theta = \mu_0 + ...$ is allowed in (5.39), together with the cubic non-linearity $\tilde{\theta}(\partial_t\theta)^2$ and the Kardar–Parisi–Zhang (KPZ) non-linearity $\tilde{\theta}\nabla\theta\cdot\nabla\theta$. This induces an explicit rotation of the order parameter, and thus no static phase. Since there is no unbroken internal symmetry left that could be spontaneously broken, no second-order phase transition can occur at the mean-field level, and no CEP is found. This is equivalent to adding a magnetic field μ_0 in the Ising case: the effective potential for $\partial_t\theta$ generically does not display spontaneous symmetry breaking anymore, but rather describes a first-order phase transition at the mean-field level already between phases with different rotation speeds. There is thus no divergent correlation length occurring, and there is no way to get the enhancement of the fluctuations found at the CEP.

The CEP transition can still be reached by tuning only one additional parameter: μ_0 can be chosen such that there is an emergent additional $\mathbb{Z}_2$ symmetry at the critical point, where our model is then recovered. There is thus a first-order phase transition line whose end point is exactly the CEP described in this work. This is the transition discussed in [66]. However, their study of fluctuations include the cubic and KPZ non-linearity, while their values are zero at the CEP because of the additional fine-tuning. It therefore does not describe the CEP transition of interest here. All of this is analogous to the second order transition found at the endpoint of the liquid-gas transition that falls in the Ising universality class with upper critical dimension $d_c = 4$. It has an emergent $\mathbb{Z}_2$ symmetry at the transition, and one does not consider the cubic non-linearities.

5.3.4 $O(N > 2)$ case

We now turn to the generic $O(N)$ case. We first discuss the corresponding action and the additional interactions that arise between Goldstone modes for $N > 2$ that add some complexity. We then explain how we can generalize the previous results for the first-order scenario even in the presence of these new interactions.

The model one obtains after phase-amplitude decomposition and integration of the amplitude mode, defines what is often referred to as non-linear σ model (NLσM). The Gaussian part of the action in the static phase is given by

$$S_0 = \int_{\mathbf{x},t} \tilde{\boldsymbol{\pi}} \cdot (\partial_t^2 + (-K\Delta + \delta)\partial_t - v^2\Delta)\boldsymbol{\pi} - D\tilde{\boldsymbol{\pi}} \cdot \tilde{\boldsymbol{\pi}}, \tag{5.65}$$

where $\boldsymbol{\pi} = (\theta_2, \dots, \theta_N)$. Beyond mean-field, we need to consider the generalization of (5.42),

$$S_{\text{int}} = \frac{g_1}{6} \int_{\mathbf{x},t} \tilde{\boldsymbol{\pi}} \cdot \partial_t \boldsymbol{\pi} (\partial_t \boldsymbol{\pi})^2 + \frac{g_2}{2} \tilde{\boldsymbol{\pi}} \cdot \partial_t \boldsymbol{\pi} (\nabla \boldsymbol{\pi})^2. \tag{5.66}$$

However, contrary to the $O(2)$ case, there are higher order terms that do not only involve derivative terms for $N > 2$ as usual for NLσM [6]. This is due to the fact that the $O(N)$ symmetry does not act anymore as a shift symmetry for the Goldstone modes when $N > 2$ [99]. For example, the term $\tilde{\boldsymbol{\phi}}^T \partial_t \boldsymbol{\phi}$ leads, following the procedure explained in Sec. 5.2, to

$$\tilde{\boldsymbol{\phi}}^T \partial_t \boldsymbol{\phi} = \tilde{\boldsymbol{\pi}} \cdot \partial_t \boldsymbol{\pi} + \frac{\rho_0^{-1}}{6} ((\boldsymbol{\pi} \cdot \boldsymbol{\pi}) \tilde{\boldsymbol{\pi}} - (\tilde{\boldsymbol{\pi}} \cdot \boldsymbol{\pi}) \boldsymbol{\pi}) \cdot \partial_t \boldsymbol{\pi} + \dots, \tag{5.67}$$

where the neglected terms are irrelevant. A similar pattern arises for every operator present in (5.65) and (5.66). The coefficients of these new operators are not independent from the one in (5.65) and (5.66) because they are generated by the same operator. This originates from the underlying $O(N)$ symmetry of the model and therefore remains true even beyond mean-field. It is then common to refer to ρ_0^{-1} as a coupling constant in the NLσM. The new operators then lead to a non-trivial (self-)renormalization of the amplitude which is absent in the $O(2)$ case. Within the statically ordered phase, the renormalized amplitude is finite, and at sufficiently small scale, the higher order terms can be neglected and the action reduces to its Gaussian part. Indeed, for large ρ_0, only fluctuations with $|\boldsymbol{\pi}| \lesssim 1$ contribute to the functional integral and higher order terms become negligible since they come with powers of ρ_0^{-1} [6] [3].

We are now ready to discuss the situation when approaching the CEP. From previous subsections, we expect g_1 and g_2 but also ρ_0^{-1} to have dimension $4-d$. This can be checked diagrammatically. Mean-field results can then be used above four dimension sufficiently deep in the ordered phase [4] and we start by discussing it since it will be useful below. It turns out that we can generalize the potential picture developed for the $O(2)$ case. Omitting the addtional terms coming from (5.67), we

[3] This argument can be made quantitative by the RG. The coupling ρ_0^{-1} goes to zero in dimensionless units at the Goldstone fixed point associated to the ordered phase [6] and the action reduces to its Gaussian part at low-energy.

[4] The irrelevance of ρ_0^{-1} does not preclude the existence of non-trivial corrections above four dimensions (by analogy with the usual equilibrium NLσM above two dimensions).

again have a potential of the form

$$V_{N,\text{eff}}(\rho_{\boldsymbol{\pi}} = (\partial_t \boldsymbol{\pi})^2) = \frac{\delta}{2}\rho_{\boldsymbol{\pi}} + \frac{g_1}{4!}\rho_{\boldsymbol{\pi}}^2. \tag{5.68}$$

This potential is simply the generalization of Eq. (5.41). It would display the typical spontaneous symmetry breaking of $O(N-1)$ down to $O(N-2)$. Here, we have additional terms of the form (5.67) that prevent our model from reducing to the equilibrium $O(N)$ case for $\partial_t \boldsymbol{\pi}$ even when $v = 0$. However, they are present to ensure that the $O(N)$ symmetry is intact, and they fix the value of the amplitude. We can therefore expect that they do not play any role when it comes to the rotational angular velocity. Again, extremising this potential yields the mean field expextation for the angular velocity $E \sim \sqrt{\delta}$. In addition, one can also study the fluctuations around the rotating order by writing the field as $\boldsymbol{\pi} = (\sqrt{\rho_0}Et + \theta_\parallel, \boldsymbol{\theta}_\perp)$, with $\theta_\parallel$ the longitudinal mode and $\boldsymbol{\theta}_\perp \in \mathbb{R}^{N-2}$ the transverse modes of the broken $O(N-1)$ symmetry. Their respective action matches (8.9) and (8.7) obtained directly from the expansion around the rotating phase in appendix 8.3.1. This fully justifies our assertion that the potential picture works also in the $O(N)$ case. We therefore again rely on it also beyond mean-field as we discuss now.

Below four dimensions, g_1, g_2 and also ρ_0^{-1} become relevant. They have the same dimension around the Gaussian fixed-point and therefore grow at the same rate next to it. We can use the same strategy as in the $O(2)$ case: We expect the g_1 and g_2 couplings to again favour the first-order phase transition. Sufficiently deep in the ordered phase at the bare scale, we can therefore neglect the restoring effect linked to ρ_0^{-1} since its contribution to loops will become non-negligible only at larger scale. In that case, we get the generalizations to $O(N-1)$ field of the different diagrams discussed in Sec. 5.3.1. This only adds N dependent prefactors in front of the loop integrals but leaves the integrals involved unchanged, and therefore their momentum structures and divergences.

The self-consistent equations are therefore similar to the $O(2)$ case. The same mechanism for first-order transition apply again because the structure pointed out for the quartic couplings $g_{1,c}$ which led to this scenario in the $O(2)$ also arises. Explicitly, we find (see App. 8.5) that

$$g_{1,c} = g_1 \frac{(9 - 4\alpha_2 \bar{\delta}^{\frac{d-4}{2}}(\alpha_2 \bar{\delta}^{\frac{d-4}{2}}(N'+2)+3))}{(2\alpha_2+3)(\alpha_2 \bar{\delta}^{\frac{d-4}{2}}\ (N'+2)+3)}, \tag{5.69}$$

with $N' = N - 1$. We can conclude that $g_{1,c}$ turns negative when

$$\bar{\delta} = \left(\frac{2\alpha_2 2(N'+2)}{3(\sqrt{3+N'}-1)} \right)^{\frac{2}{4-d}}, \tag{5.70}$$

i.e. at the same scale we have in the $O(2)$ case, given by (5.62), up to a N-dependent factor.

In the opposite limit, the ρ_0^{-1} coupling grows first and we approach the point where the symmetry gets restored first. In a generic situation, the NLσM will break down again. We reach the same conclusion as for the $O(2)$ case, and also obtain the qualitative phase diagram Fig. 2.4.

5.4 Summary

Let us briefly summarize this long, and technical chapter. We have considered the transition between the ordered and the rotating time-crystalline phase. It is purely dominated by the fluctuations of the gapless phase fluctuations and on the Gaussian level occurs through a *critical exceptional point*. The ensuing diagrammtic analysis thus also constitutes a general study of fluctuations at such a CEP. The CEP induces nonanalytic momentum dependencies of loop corrections. And while complicates matters in the first step it turns out to be a very useful feature, suppressing a large class of diagrams. This allowed us to determine in a controlled resummation of the diagrammatics, that the strongly enhance fluctuations at a CEP do not always destroy preexisting order and make a direct transition between static order and rotation impossible. Instead, there occurs a fluctuation induced first order transition, if preexisitng order is strong enough.
This finishes our discussion of criticality at the onset of time crystalline order.

6

Time-crystalline matter

In this chapter we focus on the universal scaling laws emerging within phases with time translation symmetry breaking. Scaling at the transitions into the limit cycle phases emerges due to the finetuning to criticality exactly at the transition. Within the phases, the spontaneous breaking of time translation symmetry ensures the existence of gapless modes through the mechanism of Goldstone theorem leading to universal scaling behavior throughout the entire phase without requiring any fine tuning. In the case of an additionally broken $O(N)$ symmetry with $N \geq 2$, there is additional Goldstone modes that couple to the one arising from time translations. Below, we first formally show how a soft mode indeed arises around a time dependent stable state of time translation invariant dynamics. We then argue and show for concrete examples that this soft mode is subject to a KPZ nonlinearity, which will impact its scaling in low dimensions

The results presented in this section are unpublished so far. They are results of discussions of Romain Daviet, Sebastian Diehl and Carl Zelle. The derivations have been carried out in collaboration by Romain Daviet and Carl Zelle. The numerical simulations presented in 6.2.3 where performed by Armin Asadohalli for his Bachelor thesis under supervision of Romain Daviet, Sebastian Diehl and Carl Zelle.

6.1 Time translation symmetry breaking

First we consider the case where there is no continuous internal symmetry present and thus soft modes solely arise due to the breaking of time translation symmetry and thus have no equilibrium counter part. This establishes how critical scaling can emerge in an entire phase far from equilibrium without breaking any internal symmetries. Let us first define, in what sense we consider a system to display continuous time translation symmetry and how it may be spontaneously broken. We consider MSRJD generating functionals of the form

$$Z[j,\tilde{j}] = \int \mathcal{D}\phi\mathcal{D}i\tilde{\phi}e^{-S[\phi,\tilde{\phi}]+\int_{t,x}\tilde{j}\cdot\phi+j\cdot\tilde{\phi}} \tag{6.1}$$

$$S[\phi,\tilde{\phi}] = \int_{t,x} \tilde{\phi}(t,x)\cdot F[\ddot{\phi}(t,x),\dot{\phi}(t,x),\nabla^{\alpha}\phi(t,x),\phi(t,x)] + 2\tilde{\phi}(t,x)\cdot D[\phi,\partial_{\mu}]\cdot\tilde{\phi}(t,x) \tag{6.2}$$

The dependence of the deterministic part F on spatial gradients is not restricted to any power in derivatives. The noise kernel D may also depend on ϕ, i.e. contain multiplicative noises, as well include derivative operators, i.e. colored (time derivatives) or conserved (gradients) noise. We are interested in the dynamics of fluctuations in a *stable state* where all information on initial condition is lost. In that case the time integration runs over the whole time domain $t \in (-\infty,\infty)$ and there is no boundary contribution to the integral. This dynamics is time translation invariant, if both deterministic as well as noise kernel do not depend on time explicitly, i.e. $\partial_t F = 0$, and only implicitly through the time depends of the field(s). Then, shifting time $t \to t + t_0 \equiv \tau$ leaves the action invariant, as such a simple shift of variables has no Jacobian and $\partial_t\phi = \partial_\tau\phi$ and boundary terms do not contribute. The latter would not be true in a case with information on initial conditions singling out a time frame. Since the path integral measure is also time translation invariant, invariance of the action implies invariance of the effective action $\Gamma[\tilde{\phi},\phi]$, the Legendre transform of the logarithm of the MSRJD path integral. As shown in 3.1, its second derivatives w.r.t. the fields yields the full Green Functions of the theory, i.e. correlator as well as retarded and advanced response while its first derivative gives access to the fully noise averaged order parameter ϕ_{EoM} through a generalized equation of motion.

$$\left.\frac{\delta\Gamma[\tilde{\phi},\phi]}{\delta\tilde{\phi}(t)}\right|_{\tilde{\phi}=0,\phi=\phi_{EoM}(t)} = 0. \tag{6.3}$$

A system is in a phase with time translation symmetry breaking, if the noise averaged expectation value of the field is time dependent

$$\partial_t \varphi(t) = \partial_t \langle \phi(t) \rangle_\xi \neq 0. \tag{6.4}$$

or, in terms of the effective action, if the solution generalized equation of motion (6.3) is time dependent. Since we identify phases with stable states of noisy, dissipative dynamics and all information on initial states is lost, time translation invariance of the effective action itself implies that if $\varphi(t)$ is a solution to (6.3), so is $\varphi(t+\alpha)$. We thus have a continuous set of equivalent stable states, fluctuations between which are soft Nambu-Goldstone modes. We now translate this in more concrete technical terms. First, recap the shorthand notation

$$\begin{aligned}&\Gamma^{(mn)}(t_1, x_1; t_2, x_2; ...; t_{m+n}, x_{m+n}) \\ &\equiv \frac{\delta^m}{\delta\tilde{\phi}(t_1, x_1)...\delta\tilde{\phi}(t_m, x_n)} \frac{\delta^n}{\delta\phi(t_{m+1}, x_{m+1})...\delta\phi(t_{m+n}, x_{m+n})} \Gamma[\tilde{\phi}, \phi].\end{aligned} \tag{6.5}$$

For small time shifts we have $\phi(t+\epsilon) = \phi(t) + \epsilon\partial_t\phi(t)$ and equivalently for the response field. Since time translation is a symmetry, we have:

$$\begin{aligned}0 &= \Gamma[\tilde{\phi}, \phi] - \Gamma[\tilde{\phi} + \epsilon\partial_t\tilde{\phi}, \phi + \epsilon\partial_t\phi] \\ &= \epsilon \left(\Gamma^{(01)}[\tilde{\phi}, \phi; t, \mathbf{x}]\partial_t\phi(t, \mathbf{x}) + \Gamma^{(10)}[\tilde{\phi}, \phi; t, \mathbf{x}]\partial_t\tilde{\phi}(t, \mathbf{x}) \right)\end{aligned} \tag{6.6}$$

Evaluating this on the physical saddle point in field space, $\varphi(t)$, this does not yield any information, since there the first functional derivatives of Γ vanish by definition. We can however take another derivative, before evaluating on the saddle point. We immediately drop all terms that vanish trivially on the saddle point and arrive at

$$\epsilon \int_{t', \mathbf{x}'} \Gamma^{(11)}(t', \mathbf{x}'; t, \mathbf{x}) \partial_t \phi_{EoM}(t) = 0 \tag{6.7}$$

where $\Gamma^{(11)}$ is now also evaluated on the saddle point, i.e. it constitutes the physical spectral part of the fully renormalized inverse Green function. Note that this is only a nontrivial statement if we are indeed in a phase with time translation symmetry breaking, i.e. if $\partial_t\phi_{EoM} \neq 0$. In that case, given in tact translational symmetry in space and using the fact that ϵ is arbitrary we have

$$\int_{t', \mathbf{x}'} \Gamma^{(11)}(t', t; \mathbf{x}' - \mathbf{x}) \partial_t \phi_{EoM}(t) = \int_{t'} \Gamma^{(11)}(t', t; \mathbf{q} = 0) \partial_t \phi_{EoM}(t) = 0. \tag{6.8}$$

This formally shows, that the full, nonperturbative Green function has indeed a pole corresponding to a nondecaying mode at vanishing momenta in a phase with spontaneously broken time translation symmetry. If we can go into a frame that is comoving with the limit cycle where $\partial_t \phi_{EoM}(t) = v\hat{e}_{\parallel}$, we have

$$\Gamma^{(11)}_{\parallel}(\omega = 0, \mathbf{q} = 0) = 0, \tag{6.9}$$

the standard Goldstone mode as a pole of the full Green function at vanishing frequency and momenta. This extends the paradigm of soft Nambu-Goldstone modes arising in phases with broken spontaneous symmetries to nonthermal time crystalline phases even absent internal symmetries.

6.2 Time translation symmetry breaking - KPZ and BKT

We now consider the case of a limit cycle or time crystalline order without any further continuous internal symmetries in more detail. We are interested in the fluctuations of the Goldstone mode along the limit cycle at very long time scales, much larger than the period of the limit cycle itself. We can thus average over the limit cycle period to eliminate explicit time dependencies in a phase expansion and arrive in the case of (6.9).

6.2.1 Scaling predictions from EFT

Before carrying this procedure out explicitly, we develop an effective field theory solely based on symmetry and dimension predicting the respective scaling behaviors. This has also been done in [100] but without the crucial step to analyse the impact of nonlinearities on the scaling behavior of the Goldstone mode. As already shown in chapter 4, spontaneous time translation symmetry breaking through a limit cycle order parameter is described by an $SO(2)$ symmetry breaking. Thus, all terms of the equilibrium theory of an $SO(2) \cong U(1)$ Goldstone mode θ are present in an effective field theory for phase fluctuations along the limit cycle. On top of that, the only possibly relevant nonlinearity, that is not compatible with equilibrium conditions is the KPZ coupling $\sim \lambda_{KPZ}\tilde{\theta}(\nabla\theta)^2$. The KPZ nonlinearity breaks equilibrium conditions, as it does not derive from a potential, and is furthermore disallowed if there is a $\mathbb{Z}_2$ symmetry $(\theta, \tilde{\theta}) \to -(\theta, \tilde{\theta})$. Thermal equilibrium conditions are

necessarily broken to generate time dependent ground state behaviors to begin with. Because there is a notion of directionality – the phase θ grows continuously in one direction – there is also no $\mathbb{Z}_2$ symmetry and the KPZ coupling will be generated. Putting all of this together, the action of the Goldstone mode of time translation in a comoving frame takes the form

$$S = \int_{\mathbf{x},t} \tilde{\theta} \left(X[\theta]\partial_t\theta(\mathbf{x},t) - Z[\theta]\nabla^2\theta(\mathbf{x},t) + \frac{\lambda}{2}(\nabla\theta(\mathbf{x},t))^2 \right) - D[\theta]\tilde{\theta}^2. \tag{6.10}$$

Here, $X[\theta_c], Z[\theta_c]$ are the equilibrium couplings of the $SO(2)$ Goldstone action. Their functional shape is fixed by the nonlinear realisation of the symmetry. We still need to discuss the noise kernel $D[\theta_c]$. Since there is no conservation law or other symmetry restriction, the leading order contribution to it will be simply a constant, corresponding to a Gaussian white noise. Since all other contributions come with higher order derivatives, due to the shift symmetry and are thus less relevant, we ignore them.

We now briefly recapitulate the power counting of this action at the Gaussian fixed point. The dynamical exponent of time at the Gaussian fixed point is $z = 2$. Demanding that the noise kernel is marginal for stability and dimensionlessness of the action yields

$$[\tilde{\theta}] = \frac{d+2}{2}, \quad [\theta] = \frac{d-2}{2}. \tag{6.11}$$

This leads to

$$[\lambda] = \frac{2-d}{2}. \tag{6.12}$$

In three dimensions and higher, the KPZ nonlinearity λ is power counting irrelevant at the Gaussian fixed point. Since this is also true for all equilibrium nonlinearities captured in $X[\theta]$ and $Z[\theta]$, the Gaussian fixed point captures the universal scaling behavior of phase fluctuations of a limit cycle. This predicts universal algebraic scaling of correlations and responses in time crystalline phases at large time and length scales in three dimensions

$$\mathcal{C}(\omega,\mathbf{q}) = q^{-2}\hat{\mathcal{C}}\left(\frac{\omega}{\mathbf{q}^2}\right) \tag{6.13}$$

$$\chi(\omega,\mathbf{q}) = \hat{\chi}\left(\frac{\omega}{\mathbf{q}^2}\right). \tag{6.14}$$

In one dimension, long range order is washed out by the massive fluctuations of the gapless Goldstone modes, as expected from Mermin-Wagner theorem. The correlation function can however still be dominated by the phase fluctuations. For the field itself, these fluctuations show up as

$$\mathcal{C}(\mathbf{x},t) = \langle \phi(\mathbf{x},t)\phi(0,0)\rangle \sim e^{-\frac{1}{2}\langle(\theta(\mathbf{x},t)-\theta(0,0))^2\rangle}. \tag{6.15}$$

[1] The dominance of the phase fluctuations is true for intermediate scales until the gapped amplitude fluctuations are activated as well. Since the KPZ nonlinearity is relevant in $1D$, the correlation function of θ is expected to obey the exactly known KPZ scaling exponents in one dimension

$$\mathcal{C}(0,t) \sim e^{-At^{2\beta}} \tag{6.16}$$

$$\mathcal{C}(r,0) \sim e^{-Br^{2\chi}}. \tag{6.17}$$

where χ is the roughness exponent, and $\beta = z\chi$, where z is the dynamical critical exponents. In the KPZ phase, the exponents are known exactly in one dimension: $\beta = 1/3$, $\chi = 1/2$. In regimes where thermal diffusion dominates, i.e. when the initial KPZ coupling is so small that at intermediate scales the Gaussian fixed point dominates the θ correlation function, or if the correlation is already dominated by the gapped amplitude fluctuations, we have $\chi = 1/2$ and $\beta = 1/4$.
In two spatial dimensions the phenomenology is somewhat richer. Restricting to the equilibrium case, there is a quasi long range ordered phase with algebraic equal time correlation function

$$\mathcal{C}(r,0) \sim r^{-\alpha} \tag{6.18}$$

with a noise dependent exponent

$$\alpha \sim D. \tag{6.19}$$

Upon increasing the noise level topological defects, the vortices, unbind through the BKT transtion and disorder the system leading to exponentially decaying correlations.
The KPZ coupling in two dimensions is marginally relevant. Thus, starting from the QLRO phase, it grows slowly under RG and ultimately destroys the QLRO above

[1] This form can be shown explicitly for sinodal limit cycles. It follows from the rational of acting with $e^{\theta(t,\mathbf{x})\mathcal{T}}$, with $\mathcal{T}$ the symmetry generator, on the ground state and using that envelope of the very long time dynamics is governed by the phase fluctuations.

a length scale ξ_{KPZ} leading to subexponentially decaying correlation functions with $\beta \approx 0.24$ and $\chi \approx 0.78$ for $r \ll \xi_{\mathrm{KPZ}}$ and $t \ll \xi_{\mathrm{KPZ}}^{\beta/\chi}$ [101]. From one-loop beta functions, one can estimate

$$\xi_{\mathrm{KPZ}} \propto e^{-8\pi/\lambda_0} \tag{6.20}$$

where λ_0 is the bare KPZ coupling. Further, the KPZ nonlinearity is expected to 'activate' vortices leading to defect unbinding and ultimately the full breakdown of QLRO and exponentially decaying correlations [102]. In summary, for limit cycle order in two spatial dimensions, we expect no QLRO at very long distances. If however the microscopic KPZ nonlinearity is small, such that ξ_{KPZ} is large, there is algebraically decaying correlation functions for distances $r \ll \lambda_{\mathrm{KPZ}}$. If on the other hand ξ_{KPZ} is small, but the noise level is also small, such that the length scale ξ_{BKT} at which vortices unbind and lead to exponential correlations, one can observe the scaling exponents of two-dimensional KPZ for distances $\xi_{\mathrm{KPZ}} \ll r \ll \xi_{\mathrm{BKT}}$. On the one hand this scaling behavior is a testable prediction of effective field theory for any system with time crystalline order and no other broken continuous symmetries. On the other, it also points at new experimental platforms that realize two-dimensional KPZ scaling, e.g. large arrays of synchronized and noisy oscillators conceivable for instance in electrical circuits or the 'magnon condensates' introduced in chapter 7. In three dimensional systems, there is true long range order and topological defects are not expected to play a similarly important role as in two dimensions. This may give a new angle to realise the strong coupling roughening transition of the three-dimensional KPZ equation, a task so far elusive in experiment.

6.2.2 $N = 1$ as an explicit example

We now turn from the general, symmetry based arguments and predictions from above to a more concrete expample. We consider the $\mathbb{Z}_2$ version of the nonthermal $O(N)$ model (2.2) for a real field $\phi(t, \mathbf{x}) \in \mathbb{R}$

$$\left(\partial_t^2 + (2\gamma + u\phi^2 - Z_1\nabla^2)\partial_t + \omega_0^2 + \lambda\phi^2 - Z_2\nabla^2\right)\phi + \xi = 0, \tag{6.21}$$

which is a generalisation of the paradigmatic van der Pol oscillator to spatially extended fields. In chapter 4, we have shown, that it captures the transition of driven dissipative Bose condensation described by a noisy, complex Gross-Pitaevskii equation. Just below the transition $\gamma < 0$, $|\gamma| \ll \omega_0$, its mean field solutions are

approximately sinudal

$$\phi_0(t) = A\cos\omega_D t \tag{6.22}$$

with $A = \sqrt{-4\gamma/u}$ and $\omega_D^2 = \omega_0^2 - 2\lambda\gamma/u$. To derive this solution, one has to average over the oscillation period, to wit

$$\cos^2\omega_D t \approx \frac{\omega_D}{2\pi}\int_0^{2\pi/\omega_D}\cos^2(\omega_D t)\mathrm{d}t = \frac{1}{2}. \tag{6.23}$$

This is justified, as $\omega_D^{-1} \gg -\gamma^{-1}$ is a very fast scale by assumption.
We parametrize fluctuations around the mean field as

$$\phi(t,\mathbf{x}) = (A + a(t,\mathbf{x}))\cos(\omega_D t + \theta(t,\mathbf{x})). \tag{6.24}$$

Here, $\theta(t,\mathbf{x})$ is assumed to by a slow fluctuation, such that $\partial_t^2\theta \approx 0$ and we anticipate that the amplitude fluctuations $a(t,\mathbf{x})$ are overdamped, as well $\partial_t a \approx 0$. Plugging this Ansatz into the equation of motion and using (6.23) yields

$$\left(-\omega_D\dot{a} - 2uA^2\omega_D a - Z_1 A\omega_D(\nabla\theta)^2 + Z_2 A\nabla^2\theta\right)\sin(\omega_D t+\theta) + \xi = 0 \tag{6.25}$$

$$\left(-2\omega_D A\dot{\theta} + Z_2 A(\nabla\theta)^2 - Z_2\nabla^2 a + 2\lambda A a\right)\cos(\omega_D t+\theta) + \xi = 0. \tag{6.26}$$

Here we have also restricted to the linear level in $a(t,\mathbf{x})$. We can now project these equations on the sin and cos contribution respectively and thus generating to independent noises with equal noise level. Furthermore, we see that the amplitude fluctuations decay exponentially for long wavelengths and will follow the phase fluctuations adiabatically. We can then use the first equation to adiabatically eliminate a (i.e. $\partial_\mu a = 0$ and solve for $a(\partial_\mu\theta)$) and plug into the second equation to arrive at an effective noisy equation of motion

$$\partial_t\theta - Z\nabla^2\theta + g(\nabla\theta)^2 + \xi_\theta = 0. \tag{6.27}$$

We have explicitly derived the KPZ equation for the phase fluctuations of the van der Pol limit cycle with

$$Z = \frac{\lambda Z_2}{2u\omega_D^2 A}, \quad g = \frac{1}{2\omega_D}\left(\frac{\lambda Z_1}{2uA} - Z_2\right) \tag{6.28}$$

and $\xi_\theta(t,\mathbf{x})$ is again delta correlated white noise with noise level $D_\theta = (2\omega_D A)^{-1}D$, where D is the noise level of the original microscopic noise.

In the above derivation, we have relied on the van der Pol limit cycle having an approximately sinodal form. This is not true deep within the oscillating phase. The derivation can however be generalized to generic limit cycles. To that end we switch again to a Hamiltonian or phase space representation $\Phi = (\phi, \Pi)^T$. In the case of a generic limit cycle, we have $\Phi_0(t) = (f(t), f'(t))$. We now introduce a generalized comoving frame given by the tangent vector of the limit cycle in phase space $\vec{T}(t)$ and its normal $\vec{N}(t)$

$$\vec{T}(t) = (f'(t), f''(t))^T, \quad \vec{N}(t) = (-f''(t), f'(t))^T. \tag{6.29}$$

We then parametrize fluctuations around the mean field as

$$\Phi(t, \mathbf{x}) = \begin{pmatrix} \phi(t, \mathbf{x}) \\ \Pi(t, \mathbf{x}) \end{pmatrix} = \begin{pmatrix} f(t + \theta(t, \mathbf{x})) \\ f'(t + \theta(t, \mathbf{x})) \end{pmatrix} + a(t, \mathbf{x})\vec{N}(t + \theta(t, \mathbf{x})). \tag{6.30}$$

Since $\phi = f(t + \theta)$ solves the equation of motion, the gaplessness of the phase fluctuations θ is ensured. The general procedure is now the following. First, one plugs this parametrization into the equation of motion and then projects on $\vec{T}(t + \theta(t, \mathbf{x}))$ and $\vec{N}(t, \mathbf{x})$. Since ∇^2 operators will generate terms $\sim (\nabla\theta)^2$ when they hit f or f' KPZ couplings are already seeded. There will however remain explicit time dependencies through f and f'. Since deep in the phase the fluctuations of θ persist on time scales much larger than the limit cycle period τ of $f(t)$, one can use the method of averaging over the period τ [90] to eliminate these time dependencies.

6.2.3 Numerics

Above, we have argued on a formal level as well as derived within controlled approximations, that in phases where time translation symmetry is broken by a limit cycle there are universal scaling regimes governed by the KPZ equation for a compact variable without relying on any continuous internal symmetries. In this section we aim to confirm this by numerical simulation of the van der Pol equation (6.21) on one- and tow-dimensional lattices. We then compute the correlation function $\mathcal{C}(t, \mathbf{x})$ on these lattices and test the predicted scaling behavior from section 6.2.1.
These simulations have been carried out by Armin Asadollahi for his Bachelor thesis under the supervision of Romain Daviet and the author of this thesis. We indeed find subexponential decay of the autocorrelation function in one dimension with a dynamical critical exponent $1/z = 0.62$ for a chain of length $L = 128$, close to the exact value $1/z = 2/3$, see left panel of Fig. 6.1. We note that in the similar case of KPZ in a Bose condensate, the numerically found value for $1/z$ from the auto-

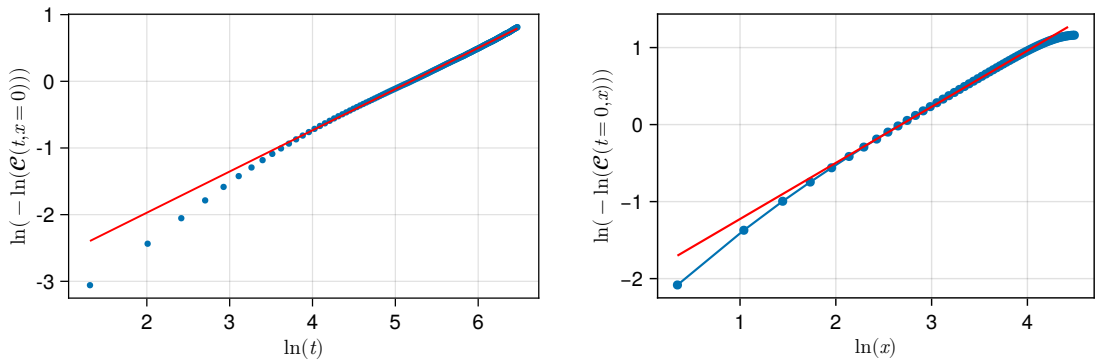

Figure 6.1: KPZ scaling of the of the correlation function of a one-dimensional noisy Van der Pol oscillator arrays. Left panel: Envelope of the autocorrelation function of a $1d$ oscillator chain with $L = 128$ sites (blue points). We clearly see subexponential decay as described by (6.16) and find $1/z \approx 0.62$, red line. Right panel: analogeous analysis of the equal time correlation function of a square lattice with 128×128 sites. We find $2\chi \approx 0.73$
.

correlation function is also smaller than the exact result , $1/z_{BC} \approx 0.614$ [103]. In two dimensions, we find algebraically decaying correlations with a noise dependent exponent, with a crossover to a exponentially decaying regime, a clear signature of a BKT crossover at finite system sizes, as predicted above in (6.18) and (6.19), see Fig. 6.2. For a different set of initial parameters, increasing the value of the bare KPZ nonlinearity, we find subexponential decay in the equal time correlation function with an exponent $2\chi \approx 0.73$ which is again in good agreement with numerical simulations of the KPZ equation $2\chi_{\mathrm{KPZ}} \approx 0.78$ [101], see right panel of Fig. 6.1. A similar analysis has been performed for the complex Gross-Pitaevskii equation for driven dissipative exciton-polariton condensation [104] where one can exactly eliminate the limit cycle frequency. They observe a regime where vortices do not destroy order and find KPZ scaling in two dimensions, analogeously to the results presented here. Their numerical result $2\chi \approx 0.72$ agrees very well with the one we identify for the Van der Pol oscillator.

6.3 Goldstone modes of the $O(N) \times SO(2)$ model

While we have shown that the Goldstone mode of time translation symmetry realizes the known, nonthermal universality class of the KPZ equation, entirely new scaling laws are seem possible if the Goldstone mode of time translation couples to Goldstone

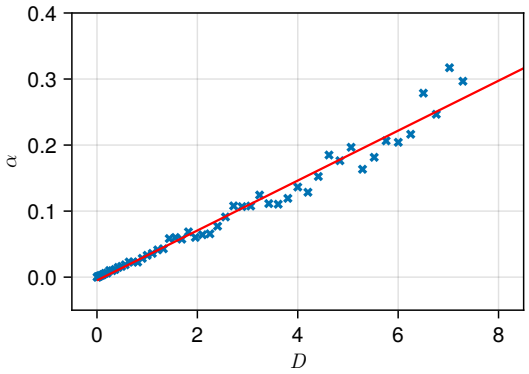

Figure 6.2: Noise dependence of the exponent α of the correlation function $\mathcal{C}(t = 0, x) \sim x^{-\alpha}$ in the QLRO regime of the Van der Pol square lattice ($L \times L = 128 \times 128$). We observe the linear noise dependence of the scaling exponent and breakdown of algebraic scaling at high noise strength, as expected.

modes from other internal symmetries. I.e. in the time crystalline phases of the nonthermal $O(N)$-model. In this section we systematically develop the Goldstone actions for these phases.

6.3.1 Effective actions

Before delving into the RG analysis we systematically construct the effective long wavelength field theories for the Goldstone modes of the oscillating and the rotating phase respectively. To that end, we analyse the symmetry breaking pattern to determine the number of modes and how the unbroken part of the symmetry group restricts their interactions

Oscillating Phase The oscillating phase is characterised by an order parameter field that oscillates along a spontaneously picked direction in field space. WLOG we choose this to be the 1-axis and write

$$\langle \boldsymbol{\phi} \rangle = \phi_0(t)(1, 0, ..., 0)^T. \tag{6.31}$$

In the amplitude bases that absorbs the explicit time dependence introduced in chapter 4, this corresponds to

$$\langle \boldsymbol{\chi}_1 \rangle = \phi_0(1, 0, ..., 0)^T, \ \langle \boldsymbol{\chi}_2 \rangle = 0. \tag{6.32}$$

As already argued in 4, this phase breaks the $SO(2)$ part of time translation symmetry and also breaks the internal $O(N)$ symmetry down to the unbroken subgroup

$O(N-1)$. We thus have a total of N broken symmetry generators giving rise to gapless Goldstone mode. Their equation of motion is constraint by the nonlinear realisation of the broken symmetry generators as well as by the way these modes transform under the unbroken subgroup $O(N-1)$. Formally speaking they live in the coset

$$O(N) \times SO(2)/O(N-1). \tag{6.33}$$

First, we consider the Goldstone mode from time translation which we call $\alpha(t, \mathbf{x})$. Time translation acting on $\langle \boldsymbol{\phi} \rangle$ as defined in (6.31) only acts nontrivially on the first component of $\langle \boldsymbol{\phi} \rangle$. The elements of the unbroken subgroup rotate the 2^{nd} through N^{th} component of $\langle \boldsymbol{\phi} \rangle$ into each other and thus time translation and the unbroken subgroup commute. Therefore, $\alpha(t, \mathbf{x})$ transforms as a scalar under $O(N-1)$.
The broken $O(N)$ generators are the ones that rotate the first component of $\langle \boldsymbol{\phi} \rangle$ into the remaining $N-1$ components. Clearly, the unbroken $O(N-1)$ group rotates the broken $O(N)$ generators into each other. Thus, the $N-1$ corresponding Goldstone modes transform as a vector under $O(N-1)$ and we can write them as $\boldsymbol{\theta}(t, \mathbf{x}) = (\theta_1(t, \mathbf{x}), ..., \theta_{N-1}(t, \mathbf{x}))^T \in \mathbb{R}^{N-1}$. We can now construct an effective equation of motion by the following rules The rules to construct the effective field theory are:

- α is a scalar without a $\mathbb{Z}_2$ symmetry.
- $\boldsymbol{\theta} \to R\boldsymbol{\theta}$, with $R \in O(N-1)$.
- To implement the nonlinear symmetry to lowest order, all the Goldstone modes have a shift symmetry, and only derivative interactions are allowed.

The resulting equations of motion are given by

$$\partial_t \alpha - Z_\alpha \nabla^2 \alpha + \lambda_\alpha (\nabla \alpha)^2 + \lambda_\theta (\nabla \boldsymbol{\theta})^2 + \xi_\alpha = 0, \tag{6.34}$$
$$\partial_t \boldsymbol{\theta} - Z_\theta \nabla^2 \boldsymbol{\theta} + g \nabla \alpha \nabla \boldsymbol{\theta} + \boldsymbol{\xi}_\theta = 0. \tag{6.35}$$

or an equivalent MSRJD action

$$\begin{aligned} S_{osc} = \int_{t,\mathbf{x}} & \tilde{\alpha} \left(\alpha - Z_\alpha \nabla^2 \alpha + \lambda_\alpha (\nabla \alpha)^2 + \lambda_\theta (\nabla \boldsymbol{\theta})^2 - \gamma_\alpha \tilde{\alpha} \right) \\ & + \tilde{\boldsymbol{\theta}} \cdot \left(\partial_t \boldsymbol{\theta} - Z_\theta \nabla^2 \boldsymbol{\theta} + g \nabla \alpha \nabla \boldsymbol{\theta} - \gamma_\theta \tilde{\boldsymbol{\theta}} \right). \end{aligned} \tag{6.36}$$

Notably, this model has been studied within perturbative RG in [60, 61] in the

physically very different context of drifting polymers. We will refer to the respective results in our RG analysis.

Rotating phase We perform the same analysis for the rotating phase, where WLOG we choose the $1-2$ plane as the plane of rotation

$$\langle \boldsymbol{\phi} \rangle = \phi_0(\cos Et, \sin Et, ..., 0)^T. \tag{6.37}$$

or in the language of the $O(N) \times SO(2)$ field theory

$$\langle \boldsymbol{\chi}_1 \rangle = \phi_0(1, 0, ..., 0)^T, \, \langle \boldsymbol{\chi}_2 \rangle = \phi_0(0, 1, 0, ..., 0)^T. \tag{6.38}$$

This phase breaks the $O(N) \times SO(2)$ symmetry to the unbroken subgroup $H = O(N-2) \times SO(2)_d$. The $O(N-2)$ part of H rotates the $N-2$ vanishing components of $\langle \boldsymbol{\phi} \rangle$ into each other. The $SO(2)_d$ is a combination of time translation symmetry, which rotates the mean field along the circle in the $1-2$ combined with an internal $O(N)$ rotation in the $1-2$ plane that exactly compensates for this rotation. Thus, there is one broken $SO(2)$ generator corresponding to rotations along the limit cycle, leading to one Goldstone that we again call $\alpha(t, \mathbf{x})$. We note that a rotation in the $1-2$ plane generated by α, commutes with $SO(2)_d$ and also with the rotations of the 3^{rd} to N^{th} component of $\langle \boldsymbol{\phi} \rangle$ that constitute $O(N-2)$. Thus $\alpha(t, \mathbf{x})$ again transforms as a scalar under the unbroken group H.
The remaining $2(N-2)$ broken generators are the $N-2$ generators that rotate the first component into the 3^{rd} to N^{th} component and we call the ensuing modes $\theta_{+,1,...,N-2}$ and the $N-2$ generators that rotate the second component into the 3^{rd} to N^{th} component correspinding to modes $\theta_{-,1,...,N-2}$. As the unbroken $O(N-2)$ group only acts on the 3^{rd} to N^{th} component, it rotates the θ_+ modes into each other and the θ_- modes respectively, it does however not mix the two sets. Thus, the two sets $\boldsymbol{\theta}_\pm = (\theta_{\pm,1}, ..., \theta_{\pm,N-2})^T \in \mathbb{R}^{N-2}$ transform as vectors under $O(N-2)$. On the other hand, since $SO(2)_d$ rotates the first and second component and thus mixes $\theta_{+,i}$ with $\theta_{-,i}$ and thus the $\sigma = \pm$ component transforms as a vector under $SO(2)_d$. We arrive at the following rules to construct the EFT for the $2N-3$ Goldstone modes $\boldsymbol{\theta}_\pm, \alpha$

- α is a scalar without a $\mathbb{Z}_2$ symmetry.
- $\boldsymbol{\theta}_\pm \to R\boldsymbol{\theta}_\pm$, with $R \in O(N-2)$. The only allowed tensor to contract the $O(N-2)$ indices of $\theta_{\sigma,i}$ is δ_{ij}.
- The allowed tensors to contract the $SO(2)$ $\sigma = \pm$ indices are $\delta_{\sigma,\sigma'}$ and $\epsilon_{\sigma,\sigma'}$.

- Only derivative terms are allowed, and we only keep the possibly relevant ones.

The equations of motion read as

$$\partial_t \alpha - Z_\alpha \nabla^2 \alpha + \lambda_\alpha (\nabla\alpha)^2 + \lambda_\theta \left((\nabla \boldsymbol{\theta}_+)^2 + (\nabla \boldsymbol{\theta}_-)^2 \right) \Big) + \xi_\alpha = 0, \tag{6.39}$$

$$\partial_t \boldsymbol{\theta}_\sigma - (Z_\theta \delta_{\sigma\sigma'} + Z_c \epsilon_{\sigma\sigma'}) \nabla^2 \boldsymbol{\theta}_{\sigma'} + (g_d \delta_{\sigma\sigma'} + g_c \epsilon_{\sigma\sigma'}) \nabla\alpha \nabla \boldsymbol{\theta}_{\sigma'} \Big) + \boldsymbol{\xi}_{\boldsymbol{\theta}_\sigma} = 0. \tag{6.40}$$

Here, g_c constitutes a genuinely new cubic nonequilibrium coupling impacting the scaling behavior.

6.3.2 One-loop RG analysis

We now analyse how the scaling of the Goldstone modes in limit cycle phases is impacted by the cubic nonlinearities in a perturbative one-loop expansion. Since we restrict ourselves to one-loop, we can do a simple momentum shell RG, where we consecutively integrate out small momentum shells. To that end, we first calculate the self energy corrections to the Goldstone modes at vanishing frequencies with a UV cutoff Λ for the loop integrals. There is an intimate connection between the diagrammatics of the rotating and the oscillating phase, which becomes clearer by again introducing a complexfield $\boldsymbol{\theta} = \boldsymbol{\theta}_+ + i\boldsymbol{\theta}_- \in \mathbb{C}^{N-2}$ where the MSRJD action of the soft modes of the rotating phase takes the form

$$S_{rot} = \int_{t,\mathbf{x}} \tilde{\alpha} \left(\alpha - Z_\alpha \nabla^2 \alpha + \lambda_\alpha (\nabla\alpha)^2 + \lambda_\theta |\nabla\boldsymbol{\theta}|^2 - \gamma_\alpha \tilde{\alpha} \right) \tag{6.41}$$

$$+ \tilde{\boldsymbol{\theta}}^* \cdot \Big(\partial_t \boldsymbol{\theta} - (Z_d + iZ_c) \nabla^2 \boldsymbol{\theta} + (g_d + ig_c) \nabla\alpha \nabla\boldsymbol{\theta} - \gamma_\theta \tilde{\boldsymbol{\theta}} \Big) . \tag{6.42}$$

We thus have a generalization of the oscillating case to a complex vector field $\boldsymbol{\theta}$ with $N-2$ complex components. Note that α remains a real field and thus $Z_\alpha, \lambda_\alpha, \lambda_\theta$ remain real couplings. Thus, we can treat oscillating and rotating phase to some extent on the same level diagrammatically. When computing the diagrams, we have to be careful about dealing with real parameters or complex ones. The corresponding one loop diagrams are depicted in Figures 6.4 and 6.3.

Scaling solutions in the oscillating phase

β-functions We start by discussing the derivation of the flow equations in the oscillating phase. In the oscillating phase, the diagrams for the spectral part read

$$\begin{aligned}\Sigma^R_\alpha(\omega=0,\mathbf{p}) = 4\lambda_\alpha^2 \int_{\mathbf{q},\omega} &(\mathbf{q}\cdot(\mathbf{q}-\mathbf{p}))(\mathbf{p}\cdot(\mathbf{q}-\mathbf{p}))G^R_\alpha(\omega,\mathbf{q})G^K_\alpha(\omega,\mathbf{q}-\mathbf{p})\\ &(\mathbf{q}\cdot(\mathbf{p}-\mathbf{q}))(\mathbf{q}\cdot\mathbf{p})G^R_\alpha(\omega,\mathbf{q}-\mathbf{p})G^K_\alpha(\omega,\mathbf{q})\\ +2(N-1)\lambda_\theta g \int_{\mathbf{q},\omega} &(\mathbf{q}\cdot(\mathbf{q}-\mathbf{p}))(\mathbf{p}\cdot(\mathbf{q}-\mathbf{p}))G^R_\theta(\omega,\mathbf{q})G^K_\theta(\omega,\mathbf{q}-\mathbf{p})\\ &(\mathbf{q}\cdot(\mathbf{p}-\mathbf{q}))(\mathbf{q}\cdot\mathbf{p})G^R_\theta(\omega,\mathbf{q}-\mathbf{p})G^K_\theta(\omega,\mathbf{q})\end{aligned} \tag{6.43}$$

and

$$\begin{aligned}\Sigma^R_\theta(\omega=0,\mathbf{p}) = g^2 \int_{\mathbf{q},\omega} &(\mathbf{q}\cdot(\mathbf{q}-\mathbf{p}))(\mathbf{p}\cdot(\mathbf{q}-\mathbf{p}))G^R_\theta(\omega,\mathbf{q})G^K_\alpha(\omega,\mathbf{q}-\mathbf{p})\\ &(\mathbf{q}\cdot(\mathbf{p}-\mathbf{q}))(\mathbf{q}\cdot\mathbf{p})G^R_\theta(\omega,\mathbf{q}-\mathbf{p})G^K_\alpha(\omega,\mathbf{q})\\ +2\lambda_\theta g \int_{\mathbf{q},\omega} &(\mathbf{q}\cdot(\mathbf{q}-\mathbf{p}))(\mathbf{p}\cdot(\mathbf{q}-\mathbf{p}))G^R_\alpha(\omega,\mathbf{q})G^K_\theta(\omega,\mathbf{q}-\mathbf{p})\\ &(\mathbf{q}\cdot(\mathbf{p}-\mathbf{q}))(\mathbf{q}\cdot\mathbf{p})G^R_\alpha(\omega,\mathbf{q}-\mathbf{p})G^K_\theta(\omega,\mathbf{q}).\end{aligned} \tag{6.44}$$

The noise contributions read

$$\Sigma^K_\alpha(0,0) = 2\lambda_\alpha^2 \int_{\mathbf{q},\omega} \mathbf{q}^4 G^K_\alpha(\omega,\mathbf{q})^2 + 2\lambda_\theta^2(N-1)\int_{\mathbf{q},\omega}\mathbf{q}^4 G^K_\theta(\omega,\mathbf{q})^2 \tag{6.45}$$

$$\Sigma^K_\theta(0,0) = g^2 \int_{\mathbf{q},\omega} \mathbf{q}^4 G^K_\alpha(\omega,\mathbf{q})G^K_\theta(\omega,\mathbf{q}). \tag{6.46}$$

where the Green's functions are

$$G^R_{\theta,\alpha}(\omega,\mathbf{q}) = \frac{1}{-i\omega + Z_{\theta,\alpha}\mathbf{q}^2} \tag{6.47}$$

$$G^K_{\theta,\alpha}(\omega,\mathbf{q}) = \frac{2\gamma_{\theta,\alpha}}{\omega^2 + Z^2_{\theta,\alpha}\mathbf{q}^4}. \tag{6.48}$$

We can perform the frequency integrations analytically and project the momentum

dependence of the spectral self energy and arrive at

$$\partial_{\mathbf{p}^2}\Sigma^R_\alpha(0,0) = \left(2\lambda_\alpha^2\frac{\gamma_\alpha}{Z_\alpha^2} + 2(N-1)\lambda_\theta g\frac{\gamma_\theta}{Z_\theta^2}\right)\frac{2-d}{2d}\Omega_d\int_0^\Lambda \mathrm{d}q q^{d-3} \tag{6.49}$$

$$\begin{aligned}\partial_{\mathbf{p}^2}\Sigma^R_\theta(0,0) =& -\frac{g\Omega_d}{(Z_\theta+Z_\alpha)^2} \\ &\left(g\frac{\gamma_\alpha((d-1)Z_\alpha+dZ_\theta)}{dZ_\alpha} + 2\lambda_\theta\frac{\gamma_\theta((d-1)Z_\theta+dZ_\alpha)}{dZ_\theta}\right)\int_0^\Lambda \mathrm{d}q q^{d-3}\end{aligned} \tag{6.50}$$

$$\Sigma^K_\alpha(0,0) = \left(\lambda_\alpha^2\frac{\gamma_\alpha^2}{Z_\alpha^3} + \lambda_\theta^2(N-1)\frac{\gamma_\theta^2}{Z_\theta^3}\right)\Omega_d\int_0^\Lambda \mathrm{d}q q^{d-3} \tag{6.51}$$

$$\Sigma^K_\theta(0,0) = \frac{g^2\gamma_\alpha\gamma_\theta}{Z_\alpha Z_\theta(Z_\theta+Z_\alpha)}\Omega_d\int_0^\Lambda \mathrm{d}q q^{d-3} \tag{6.52}$$

where Ω_d is the area of the sphere in d-dimensions divided by $(2\pi)^d$. For the spectral contribution, one needs to take care to also include the p dependence stemming from the propagators and also use $\int \mathrm{d}^d q(\mathbf{q}\cdot\mathbf{p})^2 f(\mathbf{q}^2) = (p/d)^2\int \mathrm{d}^d q\mathbf{q}^2 f(\mathbf{q}^2)$. These self energies are the one-loop corrections of $Z_{\theta,\alpha}, 2\gamma_{\theta,\alpha}$. From this, we can derive the *dimensionfull* β-functions by simply taking a cutoff derivative [2]:

$$\Lambda\partial_\Lambda Z_\alpha = \left(2\lambda_\alpha^2\frac{\gamma_\alpha}{Z_\alpha^2} + (N-1)\lambda_\theta g\frac{\gamma_\theta}{Z_\theta^2}\right)\frac{d-2}{2d}\Omega_d\Lambda^{d-2} \tag{6.53}$$

$$\Lambda\partial_\Lambda Z_\theta = \frac{g\Omega_d}{(Z_\theta+Z_\alpha)^2}\left(g\frac{\gamma_\alpha((d-4)Z_\alpha+dZ_\theta)}{dZ_\alpha} + \lambda_\theta\frac{2\gamma_\theta((d-4)Z_\theta+dZ_\alpha)}{dZ_\theta}\right)\Lambda^{d-2} \tag{6.54}$$

$$\Lambda\partial_\Lambda\gamma_\alpha = -\left(\lambda_\alpha^2\frac{\gamma_\alpha^2}{Z_\alpha^3} + \lambda_\theta^2(N-1)\frac{\gamma_\theta^2}{Z_\theta^3}\right)\Omega_d\Lambda^{d-2} \tag{6.55}$$

$$\Lambda\partial_\Lambda\gamma_\theta = -\frac{g^2\gamma_\alpha\gamma_\theta\Omega_d}{Z_\alpha Z_\theta(Z_\theta+Z_\alpha)}\Lambda^{d-2} \tag{6.56}$$

We are left to calculate the vertex corrections to get the flow equations for the couplings. Importantly, if all three internal propagator lines belong to the same field, these diagrams cancel out. In the pure KPZ case, this is due to the Galilean invariance of the KPZ equation and holds also at strong coupling. Following the

[2] This is equivalent to a Wilsonian momentum shell RG with sharp cutoffs, which only works at the one-loop level.

same steps as above, we arrive at the following *dimensionfull* flow equations

$$\Lambda\partial_\Lambda\lambda_\alpha = 0 \tag{6.57}$$

$$\Lambda\partial_\Lambda\lambda_\theta = 2\lambda_\theta\Omega_d\Lambda^{d-2}\frac{(Z_\alpha g - 2Z_\theta\lambda_\alpha)(2\gamma_\theta Z_\alpha\lambda_\theta - \gamma_\alpha Z_\theta g)}{dZ_\alpha^2 Z_\theta^2(Z_\alpha + Z_\theta)} \tag{6.58}$$

$$\Lambda\partial_\Lambda g = g\Omega_d\Lambda^{d-2}\frac{(g - 2\lambda_\alpha)(\gamma_\alpha Z_\theta g - 2\gamma_\theta Z_\alpha\lambda_\theta)}{dZ_\alpha Z_\theta(Z_\alpha + Z_\theta)^2} \tag{6.59}$$

We now introduce dimensionless couplings to find scaling fixed points and connect to the scaling exponents:

$$\tilde{\lambda}_\alpha = \sqrt{\frac{\Omega_d\gamma_\alpha}{Z_\alpha^3\Lambda^{2-d}}}\lambda_\alpha, \quad \tilde{\lambda}_\theta = \sqrt{\frac{\Omega_d\gamma_\theta^2}{\Omega_d\gamma_\alpha Z_\theta^3\Lambda^{2-d}}}\lambda_\theta, \quad \tilde{g} = \sqrt{\frac{\Omega_d\gamma_\alpha}{Z_\alpha^2 Z_{\theta,d}k^{2-d}}}g, \quad r = \frac{Z_\theta}{Z_\alpha}. \tag{6.60}$$

With these, we arrive at the dimensionless flow equations

$$\nu_\alpha = -\frac{\Lambda\partial_\Lambda Z_\alpha}{Z_\alpha} = \frac{2-d}{2d}\left(\tilde{\lambda}_\theta\tilde{g}(N-1) + 2\tilde{\lambda}_\alpha^2\right) \tag{6.61}$$

$$\nu_\theta = -\frac{\Lambda\partial_\Lambda Z_\theta}{Z_\theta} = -\tilde{g}\frac{2\tilde{\lambda}_\theta(d + r(d-4)) + \tilde{g}(d(1+r) - 4)}{2d(1+r)^2} \tag{6.62}$$

$$\eta_\alpha = -\frac{\Lambda\partial_\Lambda\gamma_\alpha}{\gamma_\alpha} = \tilde{\lambda}_\alpha^2 + (N-1)\lambda_\theta^2 \tag{6.63}$$

$$\eta_\theta = -\frac{\Lambda\partial_\Lambda\gamma_\theta}{\gamma_\theta} = \frac{\tilde{g}^2}{1+r} \tag{6.64}$$

$$\beta_{\tilde{\lambda}_\alpha} = \frac{1}{2}(d - 2 - \eta_\alpha + 3\nu_\alpha)\tilde{\lambda}_\alpha \tag{6.65}$$

$$\beta_{\tilde{\lambda}_\theta} = \frac{1}{2}\tilde{\lambda}_\theta\left(d - 2 - 2\eta_\theta + \eta_\alpha + 3\nu_\theta - \frac{(\tilde{g} - 2\tilde{\lambda}_\theta)(\tilde{g} - 2\sqrt{r}\lambda_\alpha)}{d(1+r)}\right) \tag{6.66}$$

$$\beta_{\tilde{g}} = \frac{1}{2}\tilde{g}\left(d - 2 + 2\nu_\alpha + \nu_\theta - \eta_\alpha - \frac{\sqrt{r}(\tilde{g} - 2\tilde{\lambda}_\theta)(\tilde{g}\sqrt{r} - 2\tilde{\lambda}_\alpha)}{d(1+r)^2}\right) \tag{6.67}$$

$$\beta_r = r(\nu_\theta - \nu_\alpha) \tag{6.68}$$

We note, that we have reproduced the one-loop flow equations from [60, 61], where the focus was put on the one-dimensional case. In the limit $N = 1$, where there is no additional Goldstone mode next to the one from trime translation α, we recover the one-loop KPZ flow equations and are back in the scenario 6.2.

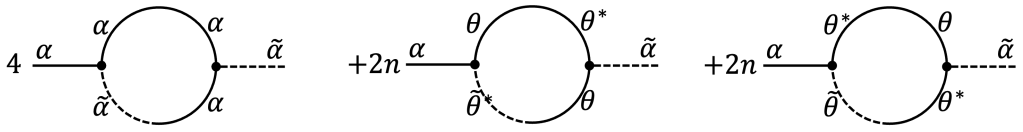

(a) Retarded self energy contributions to α

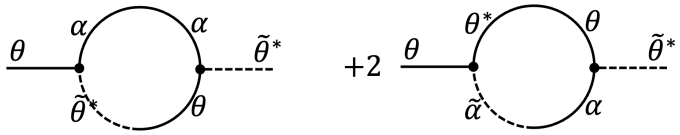

(b) Retarded self energy contributions to θ

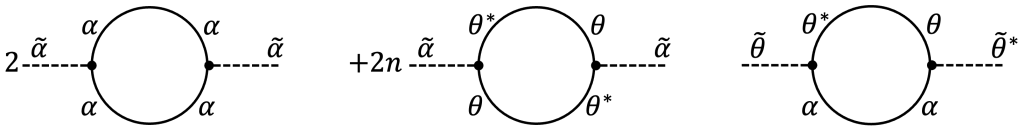

(c) Noise contributions to γ_α

(d) Noise contributions to γ_θ

Figure 6.3: Diagrammatic one-loop contributions to the couplings of the Goldstone modes within the rotating phase

Fixed points and scaling exponents We now turn to the fixed point solutions of the large N flow equations and the ensuing scaling exponents. In analogy to the scaling form of the KPZ mode arising in the case without internal symmetries discussed in 6.2, we define the scaling exponents of the fields via the asymptotic scaling of their correlation function as follows

$$\mathcal{C}_\alpha(t,\mathbf{x}) \sim |\mathbf{x}|^{2\chi_\alpha}\hat{\mathcal{C}}_\alpha(|\mathbf{x}|^{z_\alpha}/t) \tag{6.69}$$

$$\mathcal{C}_\theta(t,\mathbf{x}) \sim |\mathbf{x}|^{2\chi_\theta}\hat{\mathcal{C}}_\theta(|\mathbf{x}|^{z_\theta}/t). \tag{6.70}$$

Here we allow for a *weak scaling* where there is no unique scaling of time if $z_\alpha \neq z_\theta$. From the definitions above, it is straightforward to identify

$$z_{\alpha,\theta} = 2 - \nu_{\alpha,\theta} \tag{6.71}$$

$$2\chi_{\alpha,\theta} = 2 - d - \nu_{\alpha,\theta} + \eta_{\alpha,\theta}. \tag{6.72}$$

In the flow equations, at a strong scaling fixed point r takes finite values, which fixes $\nu_\theta = \nu_\alpha$, while it either grows to 0 or infinity at a fixed point with weak scaling.
The scaling in inferred from the $d = 1$ fixed point determines the exponential decay of the correlations of the oscillating fields itself, equivalently to the Van der Pol oscillator field discussed previously in 6.2.
Following [60, 61] for the flow equations of the oscillating phase in $d = 1$, we note that the one-loop flow equations, the couplings do not change their sign. WLOG

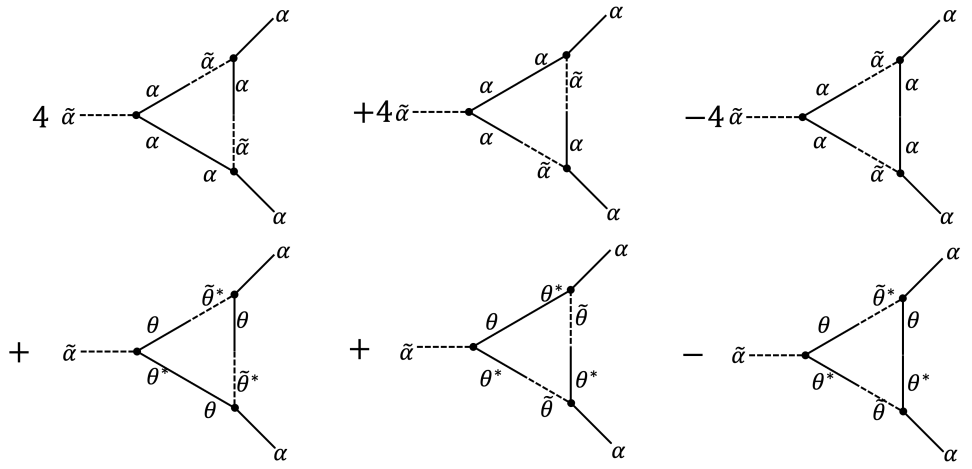

(a) Contributions to λ_α

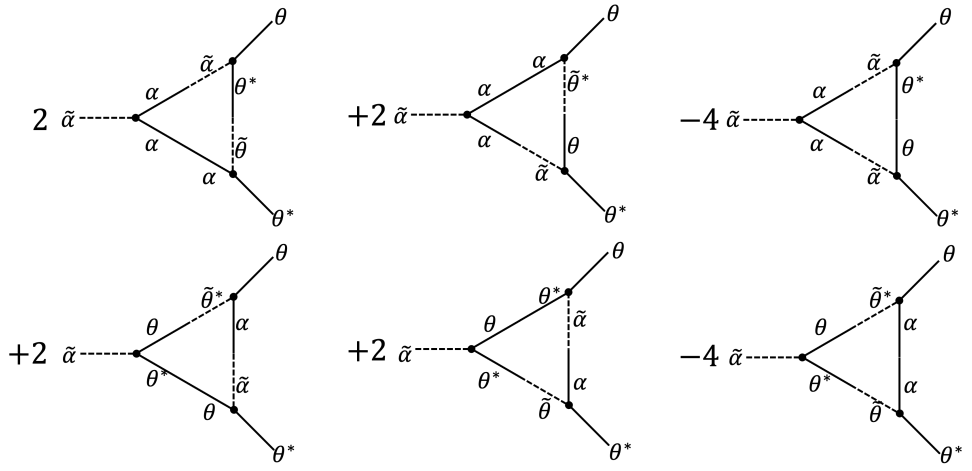

(b) Contributions to λ_θ

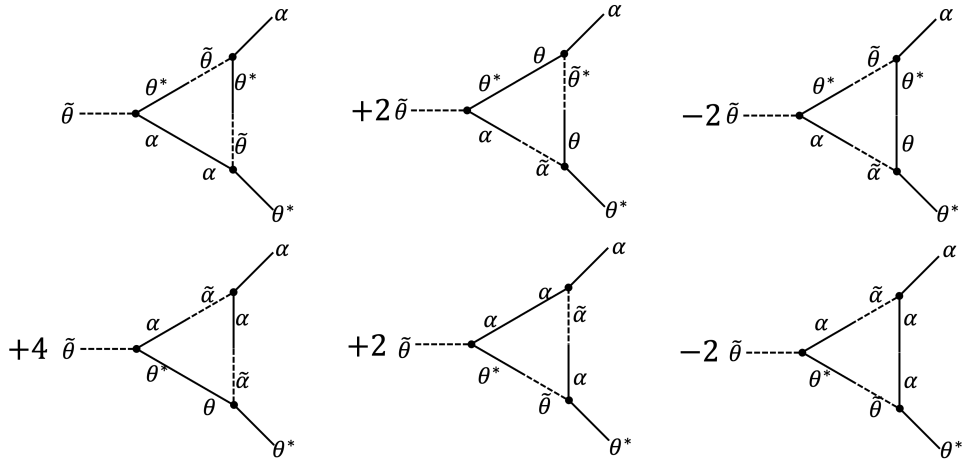

(c) Contributions to $g_d - ig_c$

Figure 6.4: Diagrammatic one-loop contributions to the couplings of the Goldstone modes within the rotating phase

we can set $\lambda_\alpha \geq 0$. Then, the phase diagrams can be separated into four quadrants determined by the sign of λ_θ and g. In the case $\lambda_\theta > 0, g > 0$, there is a KPZ fixed point where $\tilde{g} = 2\tilde{\lambda}_\theta$ and $\nu_\theta = \nu_\alpha = \eta_\theta = \eta_\alpha = 1/2$ and thus

$$z_{\alpha,\theta} = \frac{3}{2}, \quad \chi_{\alpha,\theta} = \frac{1}{2}. \tag{6.73}$$

This fixed point however only exists, if $N \leq 5$, as also found by numerical simulations of the original equations of motion [60, 61]. A glance at the flow equations shows, that indeed as long as $\tilde{g} = 2\tilde{\lambda}_\theta$, $\nu_\alpha = 1/2$ requires that $\tilde{g}^2$ has to decrease as $(N-1)^{-1}$ for growing N while $\nu_\theta = 1/2$ bounds it from below. We see that for too large N, we expect $\nu_\alpha \geq \nu_\theta$ and thus weak scaling with $r \to 0$. Therefore, the flow equation for $\tilde{g}$ at $r = 0$ demands

$$-1 + 2\nu_\alpha + \nu_\theta - \eta_\alpha = 0. \tag{6.74}$$

Since $\nu_\alpha \geq \nu_\theta$, this means that

$$-1 + 2\nu_\alpha + \nu_\theta - \eta_\alpha \geq 0 \tag{6.75}$$

and we see from β_{λ_α}that $\lambda_\alpha = 0$ is stable at this fixed point. The fixed point still has $\tilde{g} = 2\tilde{\lambda}_\theta$ and therefore from $\beta_{\lambda_\theta} = 0$ follows

$$-1 + \eta_\alpha - 2\eta_\theta + 3\nu_\theta = 0. \tag{6.76}$$

and we find

$$(\nu_\alpha - \eta_\alpha) = (\nu_\theta - \eta_\theta). \tag{6.77}$$

With $\tilde{\lambda}_\alpha = 0$ and $\tilde{g} = 2\tilde{\lambda}_\theta$, the flow equations for ν_α and η_α imply $\nu_\alpha = \eta_\alpha$ and thus $\nu_\theta = \eta_\theta$. Using all this, from the flow equations of η_θ and ν_α, we can immediately deduce $\nu_\alpha = (N-1)/4\eta_\theta$. Now plugging everything together, we have

$$\nu_\alpha = \eta_\alpha = \frac{N-1}{N+3}, \quad \nu_\theta = \eta_\theta = \frac{4}{N+3} \tag{6.78}$$

We have assumed $\nu_\alpha \geq \nu_\theta$ which holds for $N \geq 5$. For $N \leq 5$ the KPZ fixed point remains stable. At $N = 5$ both coincide and may only be distinghuished beyond the one-loop level. We thus have arrived at a new scaling form, for large N, where there

is only weak scaling and with exponents

$$z_\alpha = 2 - \frac{N-1}{N+3}, \quad z_\theta = 2 - \frac{4}{N+3}, \quad \chi_\alpha = \chi_\theta = \frac{1}{2}. \tag{6.79}$$

In a similar fashion, we turn to the case $\tilde{g} < 0, \tilde{\lambda}_\theta > 0$ and identify a weak scaling fixed point with $\nu_\alpha > \nu_\theta$ and thus $r = 0$. In this case, there remains a loop correction to the flow of $\tilde{\lambda}_\theta$ while the one to $\tilde{g}$ vanishes again due to $r = 0$. The resulting fixed point equations can be solved analytically and yield the following scaling exponents for any value of N:

$$z_\alpha = z_\theta = 2 - \frac{3N-1}{5N-3}, \quad \chi_\alpha = \frac{3N-1}{5N-3}, \quad \chi_\theta = \frac{2N-2}{5N-3} \tag{6.80}$$

We do not find a stable fixed point for $\tilde{g} > 0, \lambda_\theta < 0$. The weak scaling behaviors we identified here have been observed numerically in [60].

Scaling solutions in the rotating phase

In an analogous way, we calculate the dimensionfull β-functions for the rotating phase. In their full glory, they are lengthy and we refer to appendix 8.7 for their full form. Any finite value of g_c has an important qualitative impact on the RG flows. The loops contributing to the flow of the KPZ coupling λ_α do not cancel entirely anymore. Using the same rescaled couplings as above, we arrive at the dimensionless β-function for λ_α:

$$\beta_{\lambda_\alpha} = \frac{1}{2}\tilde{\lambda}_\alpha \left(2 - d - \eta_\alpha + 3\nu_\alpha\right) + \frac{4 g_c^2 \lambda_\theta (N-2)}{\sqrt{r}}. \tag{6.81}$$

We can already anticipate the impacts of this. The strong scaling fixed point where both α and θ fields display KPZ behavior destabilized by any finite g_c and indeed we do not find such a fixed point anymore. Further, at weak scaling $r \to 0$, the rescaled couplings 6.60 are not leading to well behaved flows anymore as the novel contribution becomes singular at $r \to 0$. This can however be remedied, by using a different ansatz for the rescaled couplings introducing $\hat{\lambda_\theta}, \hat{g}_c, \hat{g}_d$ via

$$\tilde{\lambda}_\theta = r^{1/6}\hat{\lambda}_\theta, \quad \tilde{g}_{c,d} = r^{1/6}\hat{g}_{c,d}. \tag{6.82}$$

Within these variables, we can safely go to a weak scaling fixed point $r \to 0$, where the flow equations take the form

$$\nu_d \equiv -\Lambda\partial\Lambda Z_d = 0 \tag{6.83}$$

$$\nu_c \equiv -\Lambda\partial\Lambda Z_c = 0 \tag{6.84}$$

$$\eta_\theta = 0 \tag{6.85}$$

$$\nu_\alpha = \eta_\alpha = \tilde{\lambda}_\alpha^2 \tag{6.86}$$

$$\beta_{\tilde{\lambda}_\alpha} = \frac{1}{2}\left(d - 2 - \eta_\alpha + \nu_\alpha\right)\tilde{\lambda}_\alpha + 4(N-2)\hat{\lambda}_\theta \hat{g}_c^2 \tag{6.87}$$

$$\beta_{\hat{\lambda}_\theta} = \frac{1}{2}\left(d - 2 + \eta_\alpha - 2\eta_\theta + 8/3\nu_d + 1/3\nu_\alpha\right)\hat{\lambda}_\theta \tag{6.88}$$

$$\beta_{\hat{g}_{c,d}} = \frac{1}{2}\left(d - 2 - \eta_\alpha + 7/3\nu_\alpha + 2/3\nu_d\right)\hat{g}_{c,d} \tag{6.89}$$

If now λ_α and λ_θ have the same sign, we can identify a fixed point where all couplings are finite. We clearly have

$$\nu_\alpha = \eta_\alpha = \frac{3}{2} \tag{6.90}$$

implying the scaling exponents

$$z_\alpha = \frac{1}{2}, \quad z_\theta = 2 \quad \chi_\alpha = \chi_\theta = \frac{1}{2}. \tag{6.91}$$

We thus have identified yet another scaling regime with weak scaling and a field with the somewhat exotic dynamical critical exponent $z = 1/2$.

6.4 Summary

This concludes our discussion of the scaling behavior in time-crystalline phases. We have seen, that time translation symmetry breaking leads to the presence of soft Goldstone modes and thereby algberaic scaling behavior of this mode. It is generically described by a KPZ equation but may additionally lead to topological defects and a BKT transition in $d = 2$. In low dimensions, where no true long range order, and no true long range time crystal, is expected, the decay of the correlation and response functions can still be governed by this KPZ mode, as demonstrated analytically as well as numerically.

This scaling behavior is impacted by the presence of additional Goldstone modes due to the breaking of an additional $O(N)$ group. We have developed an effective field theory governing these fluctuations. The one-loop RG analysis revealed

that there is novel fixed points with weak scaling altering the behavior identified for time-crystalline order with no internal symmetries. This analysis will be extended to higher dimensions with true long range order in future work. We also remark, that the identified fixed points are strongly interacting and the perturbative loop expansion thereby not controlled. Other than in the case of the KPZ equation there is no additional symmetries fixing the scaling laws. A quantitatively reliable prediction requires the use of more sophisticated nonperturbative methods, like the functional renormalisation group, and numerical simulation of the underlying dynamics.

7

Realisations

In the prior chapters we derived the universal scaling laws emerging in nonequilibrium systems with $O(N)$ symmetries when they break time translation symmetry and develop a dynamical long range order. We now turn to the question what physical systems can realize such phases. The key ingredient is $\mathbb{Z}_2$ or $O(N)$ symmetry and a sufficient drive out of equilibrium. Since this is very basic, we anticipate that this physics can be realized in a broad range of set ups, underscoring the universality of the mechanism.

A prominent route to realize dynamical limit cycle phases that has drawn a lot of attention recently is utilizing nonreciprocity [28, 68, 29, 30, 31, 71] . While in equilibrium Newton's laws dictate that interactions between different classical degrees of freedom has to be symmetric under exchange – every action causes an equal opposite reaction – this reciprocity can be broken in active matter. As a plastic example one can consider birds that flock – while a bird will align with the bird in front, the individual in front is not affected by what happens behind it. Such nonreciprocity can occur in plethora of active systems and metamaterials. It is easily imaginable, that if it is strong enough, one can engineer phases where a subgroup tries to align with the other while the other tries to antialign and a stable, dynamical catch and run phase emerges. While various set ups to realize such phases have been proposed, we show in 7.3 that on the universal level it is indeed captured by the field theory

analysed above.
Engineering microscopic interactions to be suitably nonreciprocal is however not the only way to generate time crystalline order. The field theory suggests, that if one pumps the system in such a way, that pump exceeds dissipation into the environment and one effectively tunes a damping into an antidamping, the dynamical order emerges. A single particle pump that exceeds loss is the origin of driven-dissipative Bose condensation where the – unobservable – phase of the condensate rotates [62]. We have already encountered a close connection to driven-dissipative condensates on the level of the universal effective field theory in 4. In 7.1, we propose a similar driving scheme for magnets, or other systems described by an $O(N)$ symmetric density. Using parametric resonance at high frequencies, we generate a highly occupied, inverted bath that serves as an effective pump for the long wavelength degrees of freedom. We show analytically, as well as through numerical simulations, how this indeed triggers a slow rotation of the overall magnetization. The driving protocol may be viewed as a generalization of driven dissipative Bose condensation to systems with a higher symmetry group.
In a more specific set up, we show how oscillating magnetic fields, can induce moving order in ferrimagnets with an $O(2)$ symmetry 7.2. We then elaborate on the connection to nonreciprocal field theories in more detail and finish with a quantum mechanical description using Lindbladian dynamics for pumped bosonic spinors.

7.1 Pumped Magnets

The contents of this section are prepared for publication by Carl Zelle, Romain Daviet, Andrew J. Millis and Sebastian Diehl in parallel to completion of this thesis.

In this section we present a quite general scheme to induce a limit cycle order. The idea is to use parametric drives that do not break any internal symmetry to create an inverted bath. While the laid out theory works for $O(N)$ models at arbitrairy N we focus on $N = 3$ as it describes the universal long wavelength dynamics in magnetic systems with full spin symmetry, for instance fully spin symmetric Heisenberg models.
Below we first briefly introduce the equilibrium models for $SO(3)$ symmetric (anti) ferromagnets. We show explicitly, how the inverted bath created by parametric resonance leads to an antidamping contribution by integrating out the bath and computing the leading order self energy contributions. It does however also increase the overall noise level of the system, heating it up and eventually destroying any or-

der. Therefore, a fine tuning is necessary to truly induce the time crystalline phase, too strong drives will simply lead to a hot, fully symmetric paramagnet.

There is an important difference between ferro- and antiferromagnet: While the effective field theory for the AFM is $O(3)$ symmetric, the ferromagnet only has a $SO(3)$ symmetry allowing for an additional cubic coupling term. This leads to a different mean-field picture of the dynamical phases. While the staggered magnetization of the antiferromagnet rotates as discussed above, the magnetisation of the ferromagnet precesses around a spontaneously picked axes. The $SO(3)$ cubic nonlinearity also impacts the loop analyses carried out throughout this section and alters the universality class of the transition between ferromagnet and limit cycle.

Equilibrium Dynamics We consider the effective dynamics of a (staggered) magnetization density $\boldsymbol{\phi}(t, \mathbf{x})$ of an (anti)ferromagnet with full $SO(3)$-spin symmetry. If the system is solely coupled to a thermal bath, it follows model A type dynamics

$$\alpha \partial_t \boldsymbol{\phi}(t, \mathbf{x}) + \kappa \boldsymbol{\phi}(t, \mathbf{x}) \times \partial_t \boldsymbol{\phi}(t, \mathbf{x}) + \frac{\delta \mathcal{V}[\boldsymbol{\phi}]}{\delta \boldsymbol{\phi}(t, \mathbf{x})} + \boldsymbol{\xi}(t, \mathbf{x}) = 0 \tag{7.1}$$

where, as usual, the temperature is set by noise strength and dissipation α. $\mathcal{V}[\phi]$ is an $O(3)$ symmetric effective potential which can be expanded in field amplitudes as

$$\mathcal{V}[\phi] = \int_{t,\mathbf{x}} \frac{1}{2} \boldsymbol{\phi}(t, \mathbf{x})^T \left(\partial_t^2 + r - Z \nabla^2 \right) \boldsymbol{\phi}(t, \mathbf{x}) + \frac{\lambda}{4} \left(\boldsymbol{\phi}(t, \mathbf{x}) \cdot \boldsymbol{\phi}(t, \mathbf{x}) \right)^2 . \tag{7.2}$$

Such a dynamics can for instance be derived by coarse graining a noisy LLG equation for Heisenberg spins and is also the expected low energy effective field theory based on symmetries. The equilibrium transition from para- to ordered (anti)ferromagnet is controlled by the reduced temperature $r = \frac{T - T_c}{T_c}$. Since the staggered magnetization has an direction but no orientation, i.e. $\boldsymbol{\phi}$ and $-\boldsymbol{\phi}$ describe the same state, $\kappa = 0$ for the AFM and there is full $O(3)$ symmetry.

Pumping Scheme We now drive this system symmetrically. The simplest way is a parametric drive at large frequencies $r \to r(t) = r_0 + r_D \cos 2\Omega t$. Following the theory of parametric resonance, after averaging over fast drive oscillations, this will lead to a large occupation of fluctuations at momenta $\mathbf{q}_\Omega$ where the frequency of the excitations equals half the drive frequency $\omega(\mathbf{q}_\Omega) = \Omega$. Let's briefly recapitulate the theory of parametric resonance. To that end, focus on a single underdamped

harmonic oscillator subject to a parametric drive

$$\partial_t^2\phi + 2\gamma\partial_t\phi + (\omega_0^2 + r_D\cos\Omega t) = 0. \tag{7.3}$$

Standard analysis reveals, that if the driving frequency is close to twice the oscillators eigenfrequency $\omega_d^2 = \omega_0^2 - \gamma^2$, $\Omega^2 \approx \omega_d^2$, the damping of the solutions of (7.3) is reduced to

$$\bar{\gamma} = \gamma - \frac{r_D\Omega}{4} + O(\Delta\omega) \tag{7.4}$$

where $\Delta\omega = \omega - \Omega/2$ is the detuning from resonance [105]. At this level, for $\bar{\gamma} > 0$, the system either decays to $\phi = 0$ or blows up exponentially. Above the threshold of the driving amplitude, the unbound growth of the resonant oscillator is remedied by nonlinearities, that are generically present in a physical system. In the deterministic case, there is still a threshold behavior, below a critical pumping strength the drive has no effect on the time averaged occupation. This changes as one includes noise fluctuations, which constantly kick the system out of its equilibrium. The life time of these excitations is now decreased by the drive to $\tau^{-1} = \bar{\gamma}$ which leads to an increasing occupation with drive amplitude also below threshhold in the presence of noise, see Fig. 7.1.

This leads to the following picture visualized in Fig. 7.2: The low frequency excitations are occupied thermally while there is a high, sharply peaked occupation at frequencies Ω. These occupations can now scatter into the low frequency regime, effectively acting as a pumping reservoir. We aim to show that this manifests in a negative shift of the damping (i.e. an antidamping) of the low frequency excitations. If this overcomes the bare damping due to dissipation of the low frequency modes, the instability discussed in the previous chapters is triggered. This is in spirit very similar to the pumping protocols put forward for driven dissipative Bose condensation of exciton polaritons [64, 62, 89, 106, 102] which has been experimentally realised [97]. In fact, also the nonthermal nonlinearities u and u' of the nonthermal $O(N)$ model (2.2) are generated.

We now want to derive this effect. To this end we split the modes into the low frequency modes $\boldsymbol{\phi}^<$ and the large frequency modes that are highly occupied $\boldsymbol{\phi}^>$. Since the occupation of the fast modes is strongly peaked at a momentum shell $\mathbf{q}_\Omega$ with width δq, we can write the Keldysh Green function of the fast modes as

$$G_>^K(\omega,\mathbf{q}) = P\delta(q - q_\Omega)\delta q\, G^R(\omega,\mathbf{q})\cdot G^A(\omega,\mathbf{q}) \tag{7.5}$$

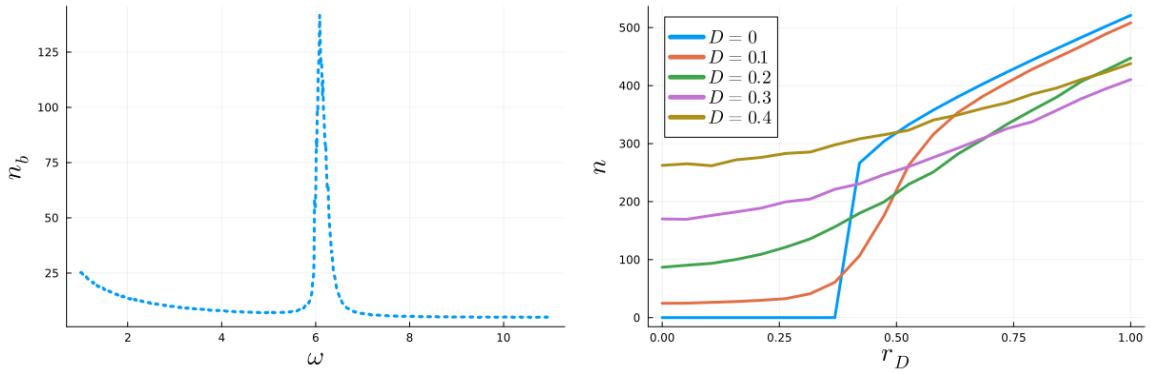

(a) (b)

Figure 7.1: Parametric pump of a single damped, noisy oscillator subject to parametric driving and a nonlinear force term $\sim \phi^3$. Left: occupation of the oscillator at constant drive frequency as a function of the oscillator's eigenfrequency. Clearly, on top of a thermal distribution there is a sharply peaked occupation at high frequencies due to the drive. Right: Occupation at resonance as a function of drive amplitude for increasing noise levels. At vanishing noise, there is a clear threshold behavior, as explained in the text. As expected, the occupation increase due to pumping is smooth in the presence of noise.

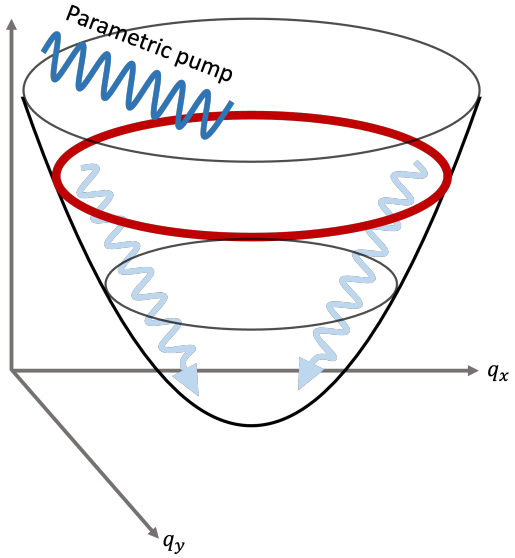

Figure 7.2: Schematic pumping scheme. The parametric drive leads to a sharply peaked, high occupation at all momenta $|\mathbf{q}| = q_\Omega$ (red band). This reservoir then pumps the slow degrees of freedom through incoherent scattering processes.

where we fix P by demanding that only integrating over frequencies yields the occupation of a single pumped resonator $\int_\omega G^K(\omega,\mathbf{q}) = n_{\rm bath}\,\delta q\delta(q-q_\Omega)$. We assume for the spectral Green function, that

$$G^R = \frac{-1}{(\omega + i(\gamma + Z_1\mathbf{q}^2))^2 - Z_2^2\mathbf{q}^4} \tag{7.6}$$

i.e. that the frequency at zero momentum can be neglected at the relevant momenta $\omega \ll \Omega$. We stress that the exact momentum dependence of the Green functions is not of crucial importance for our mechanism. It has to be adapted for a concrete material to get the correct fully nonuniversal numbers.

7.1.1 Self-energy contributions

The antidamping impact on $\boldsymbol{\phi}^<$ modes is given by the self energy contributions stemming Σ_p stemming from integrating out $\boldsymbol{\phi}^>$, i.e. all internal loop propagators are associated to the fast fields $\boldsymbol{\phi}^>$. The Green function of the slow modes $\boldsymbol{\phi}^<$ including the Keldsyh structure then is $\mathcal{G}_<^{-1}(\omega,\mathbf{q}) = \mathcal{G}_0^{-1}(\omega,\mathbf{q}) - \Sigma_p(\omega,\mathbf{q})$. We are interested in the shift of the damping caused by Σ_p, i.e. $\partial_\omega\Sigma_p^R(\omega=0,\mathbf{q}=0)$.

Antiferromagnet In the case of an antiferromagnet, where $\kappa = 0$, we have the usual model A type $O(N)$ theory to start with. The leading order contribution to the frequency dependence of the self energy is the sunset diagram stemming from the $\lambda\phi^4$ coupling. The loop integral reads

$$\begin{aligned} I_{sunset}(\omega,\mathbf{q}=0) = (2\pi)^{-2d-2}\int_{\mathbf{q}_1,\mathbf{q}_2,\mathbf{q}_3}\int_{\omega_1,\omega_2,\omega_3}&\delta(\omega_1+\omega_2+\omega_3+\omega)\delta(\mathbf{q}_1+\mathbf{q}_2+\mathbf{q}_3)\\ &G_>^K(\omega_1,\mathbf{q}_1)G_>^K(\omega_2,\mathbf{q}_2)G^R(\omega_3,\mathbf{q}_3)\end{aligned} \tag{7.7}$$

Using a Fourier representation of the δ distributions, we rewrite

$$I_{sunset}(\omega,0) = (2\pi)^{-3d-3}\int_{\boldsymbol{s},t} e^{it\omega}\left(\int_{\mathbf{q}_1,\omega_1} e^{i\boldsymbol{s}\cdot\mathbf{q}_1+it\omega_1}G_>^K(\omega_1,\mathbf{q}_1)\right) \tag{7.8}$$

$$\left(\int_{\mathbf{q}_2,\omega_2} e^{i\boldsymbol{s}\cdot\mathbf{q}_2+it\omega_2}G_>^K(\omega_2,\mathbf{q}_2)\right)\left(\int_{\mathbf{q}_3,\omega_3} e^{i\boldsymbol{s}\cdot\mathbf{q}_3+it\omega_3}G^R(\omega_3,\mathbf{q}_3)\right). \tag{7.9}$$

Now we use rotational invariance of the Greens functions, i.e. that they only depend on $q \equiv |\mathbf{q}|$ and restrict ourselves to $d = 3$ to perform the angular momentum

integrations. To this end we use

$$\int \mathrm{d}^3\mathbf{q}\, e^{i\boldsymbol{s}\cdot\mathbf{q}} F(q) = 2\pi \int_{-\infty}^{\infty} q^2 \mathrm{d}q \frac{\sin qs}{qs} F(q) \tag{7.10}$$

where $s = |\boldsymbol{s}|$. We can now straightforwardly perform the integration over $\boldsymbol{s}$ by $\int \mathrm{d}^3\boldsymbol{s} s^{-3} \sin^3(sq_\Omega) = \pi^2$. We now compute the subintegrals $I_1 = \int \mathrm{d}\omega \int q\mathrm{d}q e^{it\omega} G^R(\omega, q)$ and $I_2 = \int \mathrm{d}\omega \int q\mathrm{d}q e^{it\omega} G^K_>(\omega, q)$. Since G^R has only poles in the lower complex half plane, I_1 is proportional to $\theta(-t)$. Performing the frequency as well as momentum integration yields

$$I_1 = \frac{4e^{\gamma t}\pi^2 \arctan Z_2/Z_1}{Z_2}\theta(-t) \tag{7.11}$$

For I_2 we can use the momentum shell constraint of 7.5 to wit, for $t < 0$

$$\begin{aligned} I_2 &= 4\pi q_\Omega \delta q n_{\mathrm{bath}} \int_\omega e^{it\omega} \frac{2i\gamma_\Omega}{(\gamma_\Omega^2 + (\omega - \Omega)^2)(\gamma_\Omega^2 + (\omega + \Omega)^2)} \\ &= -\frac{4\pi q_\Omega \delta q n_{\mathrm{bath}} e^{\gamma_\Omega t}(\gamma_\Omega \sin \Omega t - \Omega \cos \Omega t)}{\Omega}. \end{aligned} \tag{7.12}$$

where γ_Ω is the decay rate into the bath of excitations at q_Ω. In three dimensions, we thus arrive at

$$I_{sunset}(\omega, 0) = 2^{-6}\pi^{-3} \int_{-\infty}^{\infty} \mathrm{d}t e^{i\omega t} I_1 I_2^2. \tag{7.13}$$

We are only interested in the frequency derivative at $\omega = 0$:

$$\partial_\omega I_{\mathrm{sunset}}(\omega = 0, \mathbf{q} = 0) = 2^{-6}\pi^{-3} \int_{-\infty}^{\infty} \mathrm{d}t\, it e^{i\omega t} I_1 I_2^2 \tag{7.14}$$

This integral can be performed analytically. For $\Omega \gg \gamma_\Omega \gg \gamma$ it yields

$$\partial_\omega I_{\mathrm{sunset}}(\omega = 0, \mathbf{q} = 0) \approx -i \frac{(q_\Omega \delta q\, n_{\mathrm{bath}})^2 \arctan Z_2/Z_1}{256 Z_2 \gamma_\Omega^2} \tag{7.15}$$

The full self energy contains additional factors of $(\lambda/4)^2$, the bare scattering of the original theory, a combinatorial factor of $2 \cdot 3$ and a factor N from the traces over the internal $O(N)$ indices and thus

$$\partial_\omega \Sigma_p^R(\omega = 0, \mathbf{q} = 0) = \frac{3N\lambda^2}{8} \partial_\omega I_{\mathrm{sunset}}(\omega = 0, \mathbf{q} = 0) \tag{7.16}$$

The shift of the damping is, by definition for the AFM ($N = 3$)

$$\delta\gamma = \mathrm{Im}\,\partial_\omega \Sigma_p^R(\omega = 0, \mathbf{q} = 0) \approx -\mathcal{N}_\gamma \frac{(q_\Omega \delta q\, n_{\mathrm{bath}})^2}{\gamma_\Omega^2} < 0 \tag{7.17}$$

proving that the pumping effectively leads to an antidamping contribution. Here $\mathcal{N}_\gamma = \frac{\arctan Z2/Z1}{256 Z_2}$.

Equivalently, the pumped bath will also lead to a noise increase ΔD in the low energy modes that will counteract ordering instabilities. This also manifests in a self energy contribution stemming from a sunset diagram with three internal Keldysh Green functions,

$$\Delta D = N\lambda^2 2^{-5}\pi^{-3} \int_{-\infty}^{0} \mathrm{d}t I_2^3 \approx \frac{5(q_\Omega \delta q\, n_{\mathrm{bath}})^3}{32\Omega^2} \tag{7.18}$$

where we symmetrised the t integration which initially runs from $-\infty$ to ∞ and again used $\gamma_\Omega \ll \Omega$.

Ferromagnet In the case of a ferromagnet, there is an interaction $\kappa\epsilon_{ijk}\tilde{\boldsymbol{\phi}}_i \partial_t \boldsymbol{\phi}_j \boldsymbol{\phi}_k$ and thus the leading contribution to $\partial_\omega \Sigma_p^R$ stems from a one loop integral. We however have to be careful with contracting the antisymmetric vertices. The configuration, where the time derivative of the vertex hits an external leg leads to a contribution to the damping

$$\kappa^2 \epsilon_{ijk} \frac{1}{(2\pi)^4}(\epsilon_{jik} + \epsilon_{kij}) \int_{\omega,\mathbf{q}} (-i\omega) G^R(\mathbf{q},\omega) G_>^K(\mathbf{q},\omega) = 0. \tag{7.19}$$

The remaining contributions are

$$\begin{aligned}
\partial_\omega \Sigma_p^R =& \frac{\kappa^2}{(2\pi)^4} \partial_\omega \Big|_{\omega=0} \epsilon_{ijk} \Big(\epsilon_{kji} \int_{\nu,\mathbf{q}} (-i(\nu-\omega))^2 G_>^K(\nu-\omega,\mathbf{q}) G^R(\nu,\mathbf{q}) \\
&+ \epsilon_{jki}(-i(\nu-\omega)) G_>^K(\nu-\omega,\mathbf{q})(-i\nu) G^R(\nu,\mathbf{q}) \Big) \\
=& -\kappa^2 \int_{\nu,\mathbf{q}} \nu G_>^K(\nu,\mathbf{q}) G^R(\nu,\mathbf{q}) = -i \frac{n_{\mathrm{bath}} q_\Omega^2 \delta q}{4\pi^3 \gamma_\Omega}.
\end{aligned} \tag{7.20}$$

As above, we have established, that the slow spin waves experience an effective antidamping contribution due to the reservoir modes.
Similarly to the case of the antiferromagnet, there is also a self energy contribution to the noise, which reads

$$\Delta D = 2\kappa^2 \int_{\omega,\mathbf{q}} G^K_>(\omega\mathbf{q})^2 \approx \frac{(n_{\text{bath}} q_\Omega^2 \delta q)^2}{2\pi\gamma_\Omega}. \tag{7.21}$$

7.1.2 Nonlinear dampings

As elaborated in the discussion of the phase diagram of the nonthermal $O(N)$ model in 2, the nonlinear damping contributions to the MSRJD Lagrangian $u(\tilde{\boldsymbol{\phi}}\cdot\partial_t\boldsymbol{\phi})(\boldsymbol{\phi}\cdot\boldsymbol{\phi})$ and $u'/2(\tilde{\boldsymbol{\phi}}\cdot\boldsymbol{\phi})\partial_t(\boldsymbol{\phi}\cdot\boldsymbol{\phi})$ are crucial to stabilize the limit cycle phases. Since they are RG relevant in the vicinity of the transition into the rotating and oscillating phases below four dimensions, as the prior analysis showed, we expect them to be generated as soon as symmetries allow them upon coarse graining close to the antidamping instability. Here we show explicitly how they are generated on the one-loop level as above.

To that end we first look at the full frequency dependence, at vanishing external momenta, of the vertex in leading order perturbation theory

$$\begin{aligned}\Gamma^{(13)}(\omega_1,\omega_2,\omega_3) =& \frac{\delta^4\Gamma}{\delta\tilde{\boldsymbol{\phi}}_a(-\sum\omega_i)\boldsymbol{\phi}_a(\omega_1)\boldsymbol{\phi}_b(\omega_2)\boldsymbol{\phi}_b(\omega_3)} \\ =& \lambda - \lambda^2(2\pi)^{-d-1}\int_{\mathbf{q},\omega}\Big(N^2 G^K_>(\omega-\omega_2-\omega_3)G^R_>(\omega) \\ &+ G^K_>(\omega-\omega_1-\omega_3)G^R_>(\omega) + G^K_>(\omega-\omega_1-\omega_2)G^R_>(\omega)\Big) + \mathcal{O}(\lambda^3)\end{aligned} \tag{7.22}$$

Now, we identify

$$u = i\partial_{\omega_1}\Gamma^{(13)}(\omega_1,\omega_2,\omega_3)\Big|_{\omega_i=0} \tag{7.23}$$

$$u' = \frac{i}{2}\left(\partial_{\omega_2}+\partial_{\omega_2}\right)\Gamma^{(13)}(\omega_1,\omega_2,\omega_3)\Big|_{\omega_i=0} \tag{7.24}$$

to find that

$$u = i\frac{2\lambda^2}{(2\pi)^{d+1}}\int_{\mathbf{q},\omega}\left(\partial_\omega G^K_>(\omega)\right)G^R_>(\omega) + \mathcal{O}(\lambda^3) \tag{7.25}$$

$$u' = i\frac{(N^2+1)\lambda^2}{(2\pi)^{d+1}}\int_{\mathbf{q},\omega}\left(\partial_\omega G^K_>(\omega)\right)G^R_>(\omega) + \mathcal{O}(\lambda^3). \tag{7.26}$$

The loop integral over the reservoir Green's functions can be performed straightforwardly, in the same manner as in the self energy contributions and we find

$$u = \frac{\lambda^2(\Omega^2 + 5\gamma_\Omega^2)q_\Omega^2 n_{\text{bath}}\delta q}{4\gamma_\Omega(\Omega^2+\gamma_\Omega^2)^2(2\pi)^3} > 0 \tag{7.27}$$

$$u' = \frac{N^2+1}{2}u \tag{7.28}$$

We thus have established, that the nonlinearities stabilizing the limit cycle phases are genereted with the correct signs by integrating out the pumping reservoir. Furthermore, $u' > u$ at leading order perturbation theory and the system will go into the rotating phase rather than show amplitude oscillations.

7.1.3 The fate of $SO(3)$

We have shown how the effective field theory described and analysed in the chapters 2, 4, 5, 6 emerges in magnets that are pumped parametrically at high frequencies. There is however one key difference in the ferromagnetic case; the coupling force term $\kappa\partial_t\boldsymbol{\phi}\times\boldsymbol{\phi}$ is not fully $O(3)$ but only $SO(3)$ symmetric and therefore absent in the $O(N)$ theories above. This alters the mean field phase itself: rather than rotating aroung a grand circle of the sphere, the magnetization precesses around a spontaneously picked axis (here the z-axis)

$$\langle\boldsymbol{\phi}(t)\rangle = \phi_0\left(\sin\Omega\cos\omega_0 t, \sin\Omega\sin\omega_0 t, \cos\Omega\right)^T \tag{7.29}$$

with field amplitude $\phi_0^2 = -\frac{2\gamma}{u}$, angular velocity, $\omega_0^2 = r + (\lambda+\kappa^2)\rho_0$ and tilt angle $\tan\Omega = \sqrt{\frac{r+\lambda\rho_0}{\kappa\rho_0}}$, see figure 7.3 for a visualization of the different patterns. The precession still breaks all three generators of $SO(3)$ and the generator of broken time translations coincides with the generator of rotations along the precession axis, as in the case of the rotating phase of $O(3)$. We now discuss the impact of $\kappa \neq 0$ on the universal exponents.

$SO(3)$ paramagnet to limit cycle We now consider the transtion between paramagnet and time crystal, characterised by $SO(3)\times SO(2)$ symmetry breaking. The field theory describing $O(3)\times SO(2)$ symmetry breaking into a time crystalline phase was discussed in Chapter 4 and [43]. We thus have to check if the terms distinguishing $SO(3)\times SO(2)$ from $O(3)\times SO(2)$ are contributing to the perturbative RG flow. The relevant degrees of freedom are the ampitude vectors $\vec{\chi}_{1,2}$. In index notation

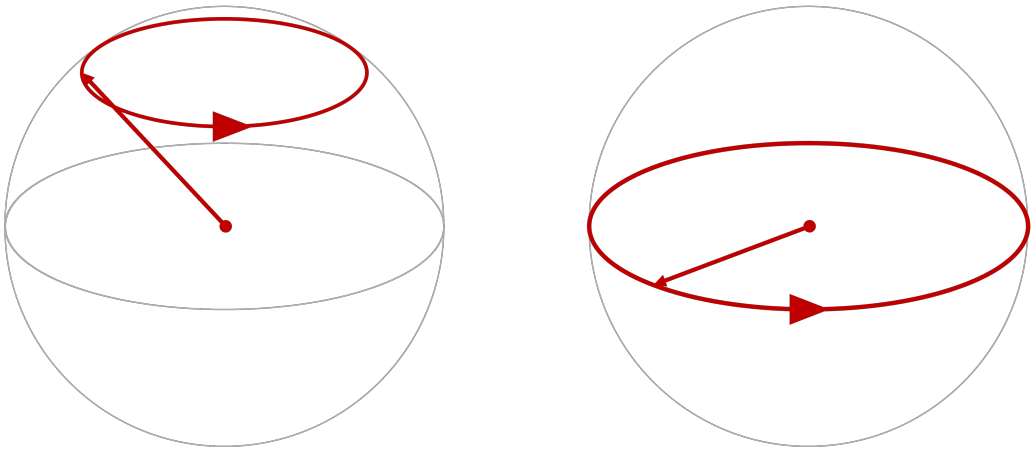

Figure 7.3: Limit cycle orders in driven magnets. Left: precession of a ferromagnet. Right: rotation of an antiferromagnet. The planes of rotation and precession are chosen spontaneously. There are two soft modes associated to tilting them. There is one soft mode associated to spatial modulations of the phase along the precession and rotation respectively

we write χ^i_α where upper Roman indices $i = 1, 2, 3$ are the $SO(3)$ indices while the lower Greek indices $\alpha = 1, 2$ are the $SO(2)$ ones. The simplemost $SO(3) \times SO(2)$ invariants that are *not* also invariant under $O(3) \times SO(2)$ are of the form

$$\left(\epsilon_{ijk}\tilde{\chi}^\alpha_i \delta^{\alpha\beta}\chi^\beta_j\chi^\gamma_k\right)\delta^{\gamma\gamma'}\left(\epsilon_{mno}\left(\nabla^2\chi^{\alpha'}_m\right)\delta^{\alpha'\beta'}\chi^{\beta'}_m\chi^{\gamma'}_n\right) \tag{7.30}$$

and permutations thereof. These are thus of second order in derivatives and sextic order in fields and therefore highly irrelevant. Hence, they will not impact the universal exponents in a perturbative expansion and the universal exponents coincide with those of $O(3) \times SO(2)$.

Ferromagnet to limit cycle WLOG, we assume the magnetic order to lay in the z axis and expand fluctuations around the mean field solution $\phi = (m_1, m_2, \sigma + \sigma_0)$. The longitudinal fluctuations σ_0 are gapped and we restrict ourselves to the dynamics of the Goldstone modes $m_{1,2}$. At linear level, we have

$$\partial_t^2 m_i + (\delta - Z_1\nabla^2)\partial_t m_i + \sigma_0\kappa\epsilon_{ij}\partial_t m_j - Z_2\nabla^2 m_i + \xi = 0. \tag{7.31}$$

Here, $\delta = 2\gamma + u\sigma_0^2$ is the tuning parameter which triggers the transition between static ($\delta > 0$) and rotating ($\delta < 0$) phase and ϵ_{ij} is the totally antisymmetric tensor. The gapless nature of the Goldstone modes implies that m can only appear with derivatives acting on it, while the unbroken subgroup $U(1)$ has to be linearly realised,

restricting the mixing of $m_{1,2}$. To study the transition, it turns out to be useful to switch to a "Hamiltonian" description of the dynamics, introducing a conjugate field momentum π to wit

$$\partial_t \pi_i + (\delta - K\nabla^2)\pi_i + \sigma_0 \kappa \epsilon_{ij} \pi_j - Z\nabla^2 m_i + \xi = 0 \tag{7.32}$$

$$\partial_t m_i = \pi_i. \tag{7.33}$$

We now write the real, two component fields $(\pi_1, \pi_2)^T, (m_1, m_2)^T$ as complex numbers $\pi = \pi_1 + i\pi_2 \in \mathbb{C}$, $m = m_1 + im_2 \in \mathbb{C}$. The equation of motion becomes

$$\partial_t \pi + (\delta + i\sigma_0 \kappa - Z\nabla^2)\pi - Z\nabla^2 m + \xi = 0 \tag{7.34}$$

$$\partial_t m = \pi. \tag{7.35}$$

This reveals that the universal fluctuations are captured by a noisy Hopf bifurcation or complex Gross-Pitaevskii equation coupled to a Goldstone mode. Recasting the Langevin dynamics presented in the main text, (7.34), into an MSRJD action reads

$$\begin{aligned} S_0 = \int_{t,\mathbf{x}} \tilde{\pi}^*(t,\mathbf{x}) \Big(\partial_t \pi(t,\mathbf{x}) + (\delta + i\sigma_0\kappa - Z_1\nabla^2)\pi(t,\mathbf{x}) - Z_2\nabla^2 m(t,\mathbf{x}) \Big) + c.c. \\ - 2D\tilde{\pi}^*\tilde{\pi} + \tilde{m}^*(t,\mathbf{x}) \left(\partial_t m(t,\mathbf{x}) - \pi(t,\mathbf{x}) \right) + c.c. \end{aligned} \tag{7.36}$$

The critical point is reached upon tuning $\delta = 0$. The finite imaginary part $\sigma_0\kappa$ is absorbed by going to a rotating frame, as usual for complex GPEs and can thus be set to zero. This however spoils a straightforward canonical power counting from the second line in the action. This breakdown of canonical power counting is frequently occuring at time translation symmetry breaking transitions as we have seen in chapters 4 and 5 of this thesis. First, we take a look at the pole structure of the Gaussian action in momentum and frequency space. To that end, we collect the coherent and dissipative couplings into complex ones $\mu = \delta + i\sigma_0\kappa$, $K_1 = Z_1$ $K_2 = Z_2$ where $K_{1,2}$ may also pick up imaginary parts under RG. The frequency poles are

$$\omega_{1,2}(\mathbf{q}) = \frac{i(\mu + K_1\mathbf{q}^2)}{2} \pm \sqrt{\frac{-(\mu + K_1\mathbf{q}^2)^2}{4} + K_2\mathbf{q}^2}. \tag{7.37}$$

At the Hopf bifurcation, $\mu \sim k^2$ is relevant while $K_1 \sim k^0$ is marginal (where k is a momentum scale). Evidently, full scale invariance is only maintained if K_2 was relevant as well, turning the point multicritical. At dynamical transitions, there may not be a single dynamical exponent z [44] and we may fix K_2 to be marginal and expand the frequencies to leading order in momentum scales, bearing in mind that

the imaginary part of μ stays finite at the transition due to $\kappa \neq 0$ to wit

$$\omega_{Hopf}(\mathbf{q}) = -i(\delta - i\sigma_0\kappa) - i(Z_1 - iZ_2)\mathbf{q}^2 \tag{7.38}$$

$$\omega_{GM}(\mathbf{q}) = -i(Z_1 - iZ_2)\mathbf{q}^2. \tag{7.39}$$

We thus have the poles of a diffusive Goldstone mode together with a Hopf bifurcation at finite frequency as δ is tuned to criticality. We now want to check to which extend the coupling to the gapless field m changes the universal behavior of the Hopf bifurcating π. To that end, we consider the lowest order coupling between both degrees of freedom, which is the following interaction in the MSRJD Lagrangian

$$\lambda_m(\tilde{\pi}^*\pi)\nabla m^* \cdot \nabla m \tag{7.40}$$

Since canonical power counting does not work, we consider the one loop corrections to λ_m generated λ_m itself. This leads to a dimensionfull RG β function

$$k\partial_k\lambda_m = \lambda_m^2 I_\lambda \tag{7.41}$$

where I_λ contains all the loop integrals. Here k denotes an momentum shell, a regularization of frequency integrals is not necessary. Clearly, this flow is becoming dimensionless, if $\lambda_m \sim k^{\Delta_\lambda}$ and $I_\lambda \sim k^{-\Delta_\lambda}$, i.e. the RG-scaling of λ_m can be read of the momentum scaling of the loop integral. For this, one has to use the scaling of the Gaussian action parameters discussed above and perform the frequency integral analytically via residue theorem.
Inverting the Gaussian part of the action to get the free Green functions and the performing the frequency integrals of the respective loops, is straightforward following e.g. [36] and using (7.38) but lengthy and with no important information. Importantly, all contributions to I_λ diverge as

$$I_\lambda \sim k^{d-2} + O(k^{d-1}) \tag{7.42}$$

and thus the scaling dimension of λ_m is $2 - d$ and it is irrelevant for dimensions $d \geq 2$. We can thus treat m on the Gaussian level. As usual for a criticality at a single finite frequency, we go into a rotating frame, $\pi \to e^{iEt}\pi$, $m \to e^{iEt}m$ with $E = \sigma_0\kappa$. This gives a mass like contribution to the mode m and it can be integrated out adiabatically. This exactly reproduces the action of a noisy complex

Gross Pitaevskii equation for π in the rotating frame

$$S_0^{eff}[\tilde{\pi},\pi] = \int_{t,\mathbf{x}} \tilde{\pi}^* \left(\partial_t \pi + \delta\pi + (Z_1 - iZ_2/E)\nabla^2\pi\right) + h.c. + 2D\tilde{\pi}^*\pi \tag{7.43}$$

where canonical power counting is possible again and the standard RG machinery can be employed and consequently the universal critical exponents in $d = 4-\epsilon$ remain those of the Hopf bifurcation. This shows that the universal exponents of transition between ferromagnet and time-crystal is described by the Hopf universality class [18, 89, 93]
This is consistent mean field picture of a precession, at the transition we see a finite frequency condensation of the conjugate spin wave momentum

$$\vec{\pi} = \pi_0(\cos\sqrt{\sigma_0\kappa}t, \sin\sqrt{\sigma_0\kappa}t, 0)^T. \tag{7.44}$$

Plugging this back into $\vec{\phi} = (m_1, m_2, \sigma + \sigma_0)$, $\partial_t\vec{\phi} = \vec{\pi}$ yields exactly the precessing phase from 7.29. This RG fix-point is known [18, 89, 93], in fact we have encountered it in chapter 4, it has an effective emergent temperature, i.e. $\eta = \eta'$. However, the subleading exponent η_c describing the emergence of equilibrium conditions under coarse graining distinguishes it from the Model A dynamical universality class in the classification of Hohenberg and Halperin [1].

7.1.4 Phase Diagram

We now collect all analyses carried out above into a phase diagram of the pumped ferro- and antiferromagnet. The physical tuning parameter that we use for the pump strength is the occupation of the reservoir. At small pumping strengths, i.e. positive effective dampings $\gamma > 0$, there is the usual (anti)ferromagnetically ordered phase at low bath temperatures, corresponding to the symmetric phase of the nonthermal $O(N)$ model, see 2.1. Upon increasing the bath temperature through the critical temperature, magnetic order is destroyed, the critical point is described by model A [1]. As we have shown above, the pumping reservoir leads to a shift of the effective damping, $\gamma = \alpha - \delta\gamma$. If $\delta\gamma$ surpasses the Gilbert damping α, there is an effective antidamping triggering an instability towards a phase with periodically moving average (staggered) magnetization $\langle\vec{\phi}(t)\rangle$. As we have shown, the heating contribution of the pumping reservoir always exceeds the antidamping at large reservoir occupations, $\delta\gamma/\Delta D \sim n_{\text{bath}}$. Therefore, at too large pumping strengths, noise fluctuations destroy any order pushing the system back into a thermal paramagnet. If the Gilbert damping is too large, the required driving strength to overcome it is too large and

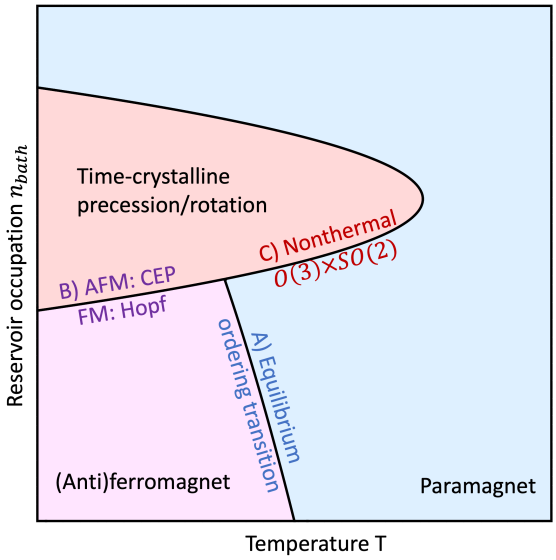

Figure 7.4: At small drives there are the two static phases, paramagnet and antiferro- or ferromagnet for positive or negative Heisenberg J respectively. At suitably strong drives and low noise levels, time crystalline order emerges. Too strong drives push the system back in a thermal paramagnetic state.

the limit cycle phase cannot be reached. The resulting schematic phase diagram is depicted in figure 7.4.

The transition between paramagnet and the rotational limit cycle of the order parameter falls into the universality class of the $O(3) \times SO(2)$ model discussed above and is thus marked by the respective nonthermal exponents. As shown above, the transition between antiferromagnet and time-crystal is governed by the CEP phenomenology established in 5. There is giant fluctuations, melting antiferromagnetic order close to the transition, and for low bath temperatures a first order transition. The transition between ferromagnet and limit cycle is captured by the universality class of the complex noisy Gross-Pitaevskii equation [89, 93].

7.1.5 Numerics

The field theoretical prediction of an emergent limit cycle behavior is confirmed by numerical simulations of the original model (7.1) with parametrically driven potential as described above. Simulations of a 3-dimensional cubic model of size $L = 32$ show, that indeed initially a sufficient drive induces a high occupation of modes at momenta q_Ω. This however quickly scatter into the low momentum regime and lead to a macroscopic occupation at $\mathbf{q} = 0$, and at a finite frequency. There is a coherent, long range ordered rotation of the order parameter, as predicted and visualized in

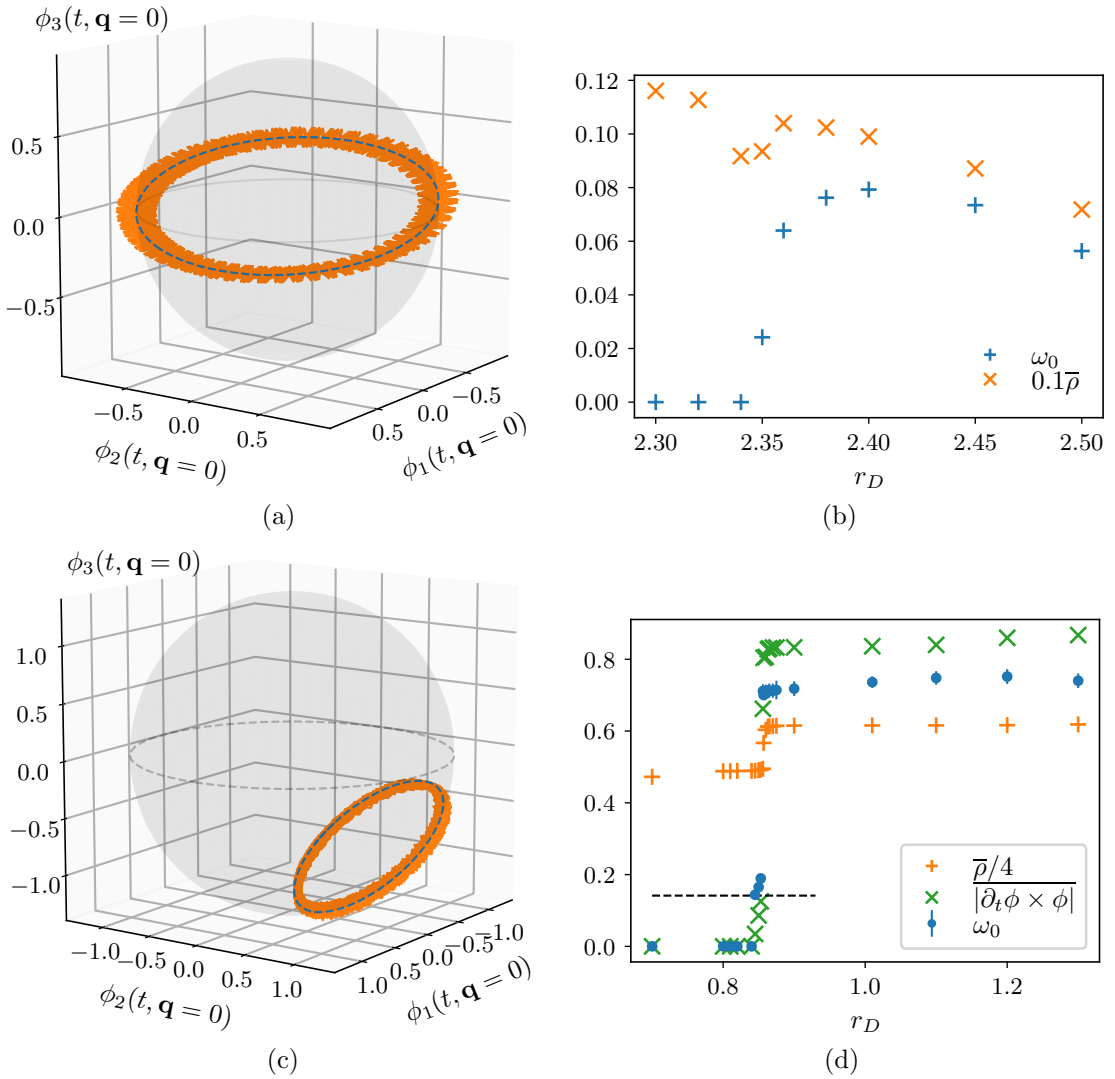

Figure 7.5: Numerical simulations of Eq. (7.1) with $r = -1, \lambda = 0.5, 2\gamma = 10^{-3}$ and $\kappa = 0$ (antiferromagnetic case). The driving frequency $\Omega = 2.15$ is chosen to have a parametric resonance of the longitudinal mode around momentum $q_\Omega \sim \pi/2$. (a) Large time solutions with $r_D = 2.4$ is given by the orange solid line. The blue dashed line shows the same trajectories averaged over the fast amplitude oscillations (with frequency Ω). The order parameter indeed traces out a circle. (b) Frequency of the limit cycle ω_0 and its averaged amplitude over the fast oscillations $\overline{\rho}$ as a function of the driving power r_D. c) and d) show the same for the ferromagnetic case $\kappa = 1$.

Fig 7.5. Along the transition between antiferromagnet and time crystalline order, the mapping to the critical exceptional point of driven $O(N)$ models predicts a decrease of the amplitude at the transition due to the exceptionally enhanced fluctuations and a square root behavior of the angular velocity going deeper into the rotating phase from the transition. Both is confirmed by the numerical simulations as shown in panel b) of Fig 7.5.

7.2 Ferrimagnet

In the parametric pumping scheme developed above, we have essentially created an antidamping overcoming the intrinsic damping of the system. Most solid state systems show however fas relaxation rates mainly due to coupling to thermal phonon reservoirs, and thus one needs strong pumps which can in turn heat the system up too quickly and destroy any order. In contrast, in the following, we will show that it is possible to create the rotating time-crystalline phase in a ferrimagnetic system with arbitrarily weak drives. A modified version of the following section including figures has been published in Sec VII of [44]. The driving protocol was designed by Achim Rosch.

7.2.1 Rotating order and CEP transition in the driven ferrimagnet

We consider an equilibrium spin system on a cubic lattice. The system is assumed to have an anisotropy breaking the $SO(3)$ spin symmetry down to $U(1)$ rotations within an easy xy plane and a $\mathbb{Z}_2$ reflection symmetry along the z-axis. We assume the system spontaneously orders in the easy plane for equilibrium temperatures $T < T_N$ constituting an xy (anti)ferromagnet. Furthermore it can undergo a ferrimagnetic Ising like transition below a temperature $T_c < T_N$ where an out of plane magnetization along the z-axis develops. Instances of systems showing such type of phase transitions are, for example, found in Refs. [107, 108, 109]. In the vicinity of this phase transition the slow, long wavelength dynamics is captured by the $U(1)$ Goldstone mode of the order in the xy plane, θ, and an Ising variable m_z describing the ferrimagnetic order parameter. We thus construct the effective dynamics for these degrees of freedom. Since there is no additional conserved charge, there is no hydrodynamic modes that need to be considered on top of them. The symmetries act

as

$$\begin{aligned} U(1): &\quad \theta \to \theta + \alpha, \\ \mathbb{Z}_2: &\quad \theta \to -\theta,\ m_z \to -m_z. \end{aligned} \tag{7.45}$$

Since the reflection and $U(1)$ rotation do not commute the symmetry group of this system is $U(1) \ltimes \mathbb{Z}_2 \cong O(2)$. We now drive the system out of thermal equilibrium by applying a rapidly oscillating magnetic field with amplitude B_0. Since the drive is very fast, the effective dynamics of θ and m_z is still Markovian and the drive effectively couples the Ising and the Goldstone mode. The $O(2)$ symmetry of the system, the absence of conserved currents and the markovianity of the long time dynamics indicate, that its coarse grained dynamics will be described the $O(N=2)$ model discussed above. We derive the effective dynamics of the spatially averaged collective Goldstone and Ising modes $\langle\theta\rangle$, $\langle m\rangle$ explicitly from a microscopic model in Sec. 7.2.1. Since the correlation length ξ is orders of magnitude larger than the microscopic lattice spacing, $\xi \gg a$, the spatial fluctuations of the dynamics can be treated in a continuum limit with emergent rotational symmetry in space, as usual for the effective dynamics close to a critical point. We thus model the spatial fluctuations beyond the effective single mode with phenomenological constants K_θ, K_0, K_m at order ∇^2. This procedure yields the following effective dynamics

$$\begin{aligned} \alpha_\theta \partial_t \theta =& \alpha_\theta \gamma_z m_z + K_\theta \nabla^2 \theta - \partial_t m_z + \xi_\theta, \\ \alpha_m \partial_t m_z =& -\frac{\delta V}{\delta m_z} + \partial_t \theta + K_0 \nabla^2 \theta + \xi_m, \end{aligned} \tag{7.46}$$

where α_{θ,m_z} stem from the Gilbert damping of the original spin system. ξ_θ, ξ_m are respective Gaussian white noises which close to equilibrium are set by temperature and α_{θ,m_z}. V is an Ising potential for the ferrimagnetic order parameter, which can be parametrised as

$$V = \int_{\mathbf{x},t} \frac{1}{2}\left(r m_z^2 + K_m (\nabla m_z)^2\right) + \frac{\lambda}{4!} m_z^4 \tag{7.47}$$

with $r = T - T_c$ the distance from the equilibrium ferrimagnetic transition. The effect of the drive are nonvanishing values of K_0 and $|\gamma| \propto B_0^2$ which do not exist in equilibrium. We give a microscopic derivation of these dynamics below. Evidently, the presence of a finite γ indicates that a build up of ferrimagnetic order $\langle m_z\rangle \neq 0$ immediately induces a finite angular velocity for the xy order causing it to rotate in the easy plane. For time and length scales above $(\alpha_\theta \gamma)^{-1}$ the effect of ξ_θ in the first equation get suppressed, and we can use this first equation of motion to eliminate

m_z and plug it into the second to indeed reproduce the nonlinear σ model for the $N = 2$ CEP discussed in Sec. 5.3,

$$\left(\partial_t^2 + (\delta - Z\nabla^2)\partial_t - v^2\nabla^2\right)\theta + \frac{g}{6}\left(\partial_t\theta\right)^3 + \xi = 0. \tag{7.48}$$

Since the spin damping coefficients $\alpha_{m,\theta}$ are typically very small, we can restrict ourselves to leading order contributions in these. We then have $\delta = \frac{\gamma_z\alpha_\theta(r-\gamma_z)}{r}$, and thus there is a transition into a rotating phase occuring at $r = \gamma_z$ rendered first order by CEP fluctuations as discussed above for all finite drivings γ_z. In the vicinity of the transition, $r \approx \gamma_z$, the remaining parameters are $Z = \frac{K_\theta}{\alpha_\theta}$, $v^2 = K_\theta\gamma_z + K_0\alpha_\theta\gamma_z \approx K_\theta\gamma_z$, $g = \frac{\alpha_\theta\lambda}{\gamma_z^2}$, $\xi = \frac{\gamma_z}{\alpha_\theta}\xi_m$. In these units, we have $\rho_0 = 1$ and thereby, by the criterion found in the field theoretic analysis (5.63), there is a first order phase transition between xy order and rotating ferrimagnet if

$$\frac{\lambda\alpha_\theta^2}{\gamma_z} \gg 1, \tag{7.49}$$

and the xy order is destroyed in the opposite limit.

Finally we remark on the connection to the equilibrium case $\gamma_z, K_0 \to 0$, where there is an Ising transition into a static ferrimagnet. At the Ising fixed point however, the nonequilibrium coupling γ_z is relevant, so that once it is allowed via the breaking of equilibrium conditions in terms of the drive, it will flow to a value of $\mathcal{O}(1)$ under the RG for sufficiently large system sizes. In that sense the equilibrium transition constitutes a multicritical point which will not impact the transition phenomenology once one drives the system out of equilibrium.

Our results are summarized in the phase diagram sketched in Fig. 7.6, which explores the phases as function of temperature T and driving power P_D. Here T is the equilibrium temperature of the undriven system which in experiments is set by phonon or electron baths and their coupling to a cryostat. The phase diagram is based on the assumption, that in equilibrium, $P_D = 0$, the system undergoes a sequence of two phase transitions upon lowering T, first into an xy ordered phase and then into the ferrimagnetic phase as discussed above. Driving the system has, first, the effect that the effective temperature and thus the fluctuations grow linearly in the driving power P_D for small P_D. Importantly, the coupling γ_z linear in P_D emerges in the effective field theory, Eq. (7.46), which is highly relevant in the renormalization group sense. Due to γ_z, the static ferrimagnetic order is transformed into a rotating ferrimagnet for arbitarily small P_D as discussed above. Arbitrarily small, but finite driving also destabilizes the second-order phase transition and one obtains instead a weak fluctuation-induced first order transition characteristic of the CEP as for

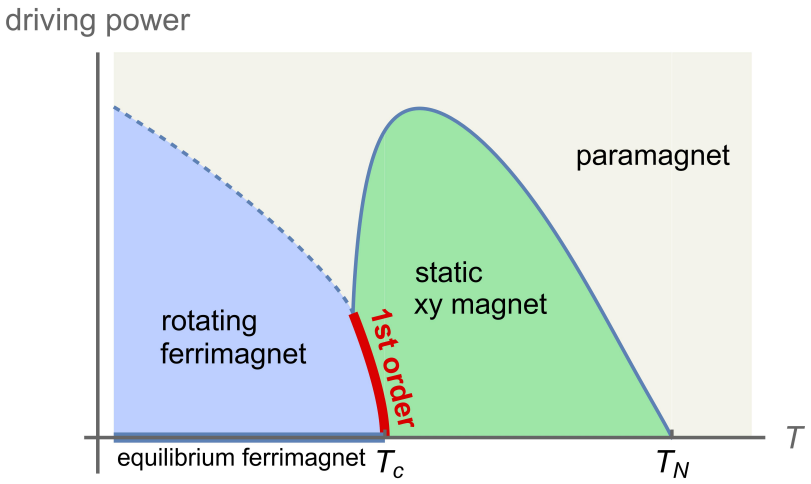

Figure 7.6: Schematic phase diagram of a driven ferrimagnet as function of temperature and the power of an external driving source, e.g., a laser or an oscillating magnetic field. We assume that in equilibrium the system displays antiferromagnetic xy order for $T < T_N$ and becomes a ferrimagnet for $T < T_c < T_N$ by developing an extra out-of-plane ferromagnetic component. Driving induces in the ferrimagnetic phase a rotation of the xy order parameter. The transition is governed by a critical exceptional point (CEP) with its characteristic first-order phase transition (red line). The enhancement of fluctuations close to the CEP bends the transition line between paramagnet and xy order down, culminating in a multicritical point where all transition lines meet. For larger driving strength also a direct transition from the paramagnetic into the rotating ferrimagnetic phase will occur. Thus, all phases and phase transitions of the effective model, Fig. 2.1, can be realized. This figure is also shown in chapter 6.

small γ_z, the condition of Eq. (7.49) is always obeyed. At larger driving, $\gamma_z \sim \alpha_\theta^2 \lambda$, the line of first-order transition ends when the xy order is destroyed by the strong fluctuations arising from the superthermal mode occupation in the vicinity of the CEP. We therefore expect, as sketched in Fig. 7.6, that the long-ranged xy-order melts most easily just above the transition temperature T_c. In the figure, we also took into account that a finite P_D always leads to a net heating of the system proportional to P_D, thus all transition lines bend to the left in Fig. 7.6.

Let us finally compare the symmetry $U(1) \ltimes \mathbb{Z}_2$, Eq. (7.45), to the symmetry $U(1) \times \mathbb{Z}_2$, realized by replacing the second line of that equation by $m_z \to -m_z$, while leaving θ invariant. In this case, on the right hand side of the first line of (7.46), a field-independent constant (as well as a KPZ non-linearity) is also symmetry allowed, and will be generically non-vanishing once the drive is switched on. The system is thus always in a rotating phase for finite drive, and no phase transition of the above type would be realized. In other words, time translation invariance is broken explicitly, as opposed to spontaneously as in our case.

Microscopic derivation

In the following, we provide a microscopic theory to show how a rotation of Goldstone modes is induced at a ferrimagnetic transition if the system is driven out of thermal equilibrium by an oscillating magnetic field $B_z(t)$. We consider classical spins $\mathbf{S}_i$, $|\mathbf{S}_i| = 1$, on a three-dimensional cubic lattice with

$$\begin{aligned} H =& J \sum_{\langle i,j \rangle} S_i^x S_j^x + S_i^y S_j^y - \Delta S_i^z S_j^z \\ &+ \sum_i \delta_2 S_i^{z2} + \delta_4 S_i^{z4} - g_i B_z(t) S_i^z . \end{aligned} \tag{7.50}$$

The model is invariant under global spin rotations around the z axis and we assume $J, \Delta, \delta_4 > 0$. The sign in front of Δ is chosen to obtain a ferrimagnet. At $T = 0$, $B_z = 0$, the system orders antiferromagnetically in the xy-plane for $\delta_2 > zJ(\Delta - 1)$ ($z = 6$ is the number of nearest neighbors) but the spins tilt out of the plane for $\delta_2 < zJ(\Delta - 1)$ developing a uniform out-of-plane magnetization. By tuning δ_2, one can thus describe the transition from an xy antiferromagnet to a ferrimagnet.

The dynamics of the system is obtained from the Langevin (or, equivalently, Landau-Lifshitz-Gilbert) equation

$$\partial_t \mathbf{S}_i = -\mathbf{S}_i \times \left(\frac{\partial H}{\partial \mathbf{S}_i} + \alpha \partial_t \mathbf{S}_i + \boldsymbol{\xi}_i(t) \right), \tag{7.51}$$

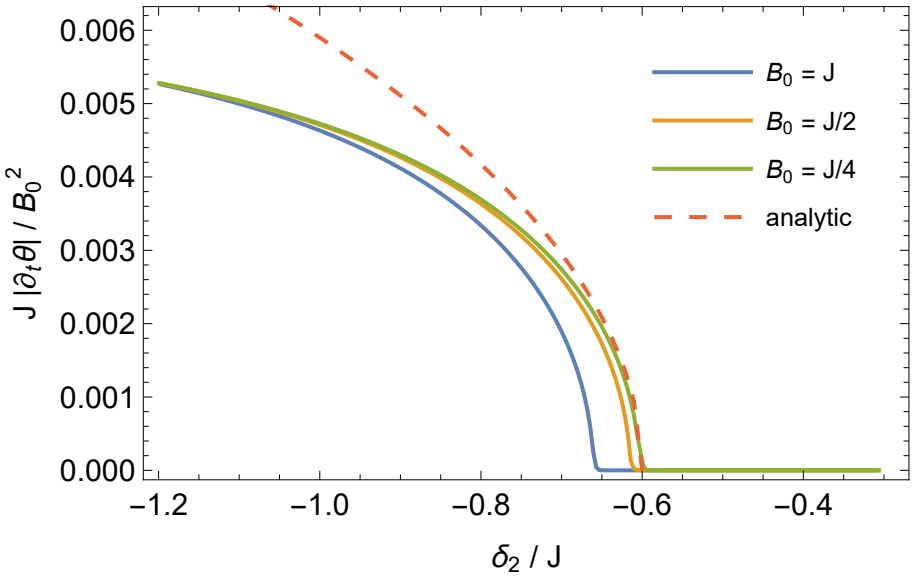

Figure 7.7: Average precession rate $\partial_t\theta$ as function of the anisotropy δ_2 for the model defined in Eqs. (7.50) and (7.51). For sufficiently large δ, the magnet develops an out-of-plane magnetization and, simultaneously, the spins start to rotate. Solid lines: mean-field numerics (i.e., for a noiseless model) for three different amplitudes B_0 of the oscillating field, dashed line: analytical result valid close to the phase transition for small B_0 using Eq. (7.46), Eq. (7.55) and the mean-field order parameter $|m_z| = \sqrt{\frac{-\delta_2 - zJ(1-\Delta)}{\delta_4}}$. The parameters are $B_z(t) = B_0 \cos(\omega t)$, $\omega = 7.2\,J$, $\alpha = 0.2$, $g_A = 1$, $g_B = 2$, $\Delta = 0.9$, $\delta_4 = 6\,J$.

where the Gilbert damping α allows for a relaxation of the magnetization.

To obtain an equation for the time-dependence of the angle θ parametrizing the Goldstone mode, Eq. (7.46), and thus for γ_z, it is most convenient [75] to compute first the time-dependence of the relevant conservation laws, i.e., of the total magnetization $M_z = \sum_i S_i^z$. Due to the damping terms, the magnetization M_z is not conserved and one obtains

$$\frac{\partial M_z}{\partial t} = -\alpha \sum_i \left(\mathbf{S}_i \times \partial_t \mathbf{S}_i\right)_z = -\alpha \sum_i \left(1 - S_i^{z2}\right) \partial_t \theta_i, \tag{7.52}$$

where θ_i is the angle describing the in-plane orientation of $\mathbf{S}_i$ and we ignored contributions from $\boldsymbol{\xi}_i(t)$ which at low temperature will only give rise to small corrections to the value of γ_z. Next, we average Eq. (7.52) over time in the presence of an oscillating magnetic field $B_z(t)$. The time average of $\partial_t M_z$ vanishes, $\overline{\partial_t M_z} = 0$, as it is a total derivative of a bounded quantity. In contrast, $\overline{\partial_t \theta_i}$ can be finite, as the angle is not bounded and can have a net growth in each oscillation period T, $\overline{\partial_t \theta_i} = (\theta_i(t+T) - \theta_i(t))/T$. Thus, we obtain a remarkably simple equation for the

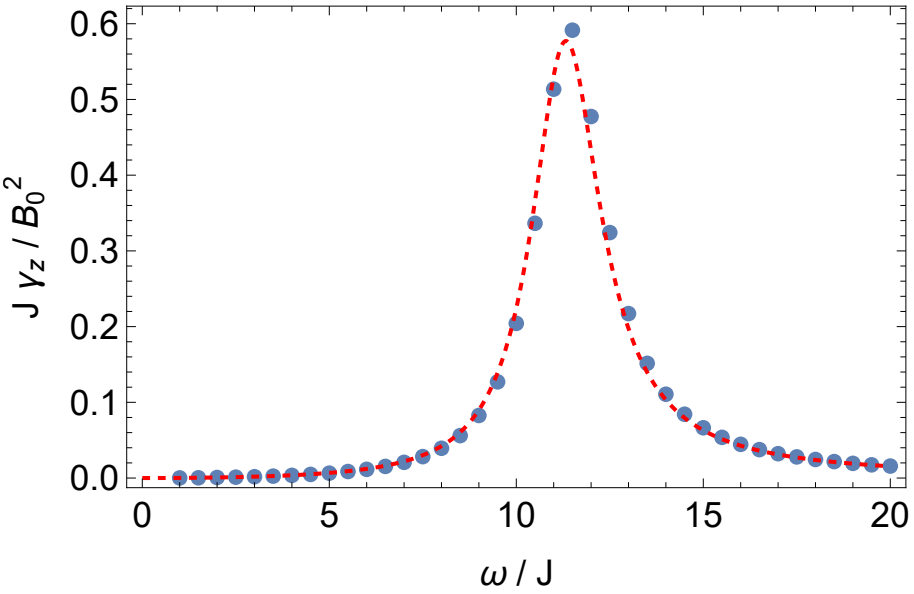

Figure 7.8: Coupling γ_z defined in Eq. (7.46) as function of the driving frequency ω (points: numerics for $B_0 = 0.25\,J$, line: analytical result, Eq. (7.55)). The parameters are $\alpha = 0.2$, $g_A = 1$, $g_B = 2$, $\Delta = 0.9$, $\delta_2 = -0.66\,J$, $\delta_4 = 6\,J$.

average angle $\theta = \overline{\langle\theta_i\rangle} = \frac{1}{N}\sum_i \overline{\theta_i}$ which is *independent* of the friction constant α

$$\partial_t\theta = \overline{\langle S_i^{z\,2}\partial_t\theta_i\rangle}, \tag{7.53}$$

where $\langle\dots\rangle$ denotes the average over different sites i. Assuming that our system is weakly driven out of thermal equilibrium by a small, time-dependent field $B_z(t)$, we evaluate Eq. (7.53) in second-order perturbation theory and *linear* in the uniform magnetization $m_z = \overline{\langle S_i^z\rangle}$. Comparing to Eq. (7.46), we find

$$\gamma_z = 2\overline{\langle S_i^z\partial_t\theta_i\rangle}_c, \tag{7.54}$$

where we omitted corrections from $\overline{\langle S_i^{z\,2}\rangle}\,\overline{\partial_t\langle\theta_i\rangle}$ as they are of higher order in either m_z or B_z. Eq. (7.54) should be evaluated at the critical point, i.e., for $\delta_2 = zJ(\Delta-1)$. The contribution to second order in $B_z(t)$ can be obtained by evaluating both S_i^z and $\partial_t\theta_i$ to first order and we find for an oscillating field of the form $B_z(t) = B_0\cos(\omega t)$

$$\gamma_z \approx \frac{B_0^2(g_A-g_B)^2 zJ\omega^2}{2\left(\omega^2(1+\alpha^2) - 4(zJ)^2\Delta\right)^2 + \alpha^2 8(zJ)^2\omega^2(\Delta+1)^2}, \tag{7.55}$$

where g_A, g_B are the g factors on the two sublattices.

In Fig. 7.7 the precession rate $\partial_t\theta$ obtained from a noiseless solution, $\boldsymbol{\xi}_i(t) = 0$, of the equation of motions, Eq. (7.51), is shown in comparison to the analytical results.

In the noiseless case (or, equivalently, in a $T = 0$ mean-field theory) one can use translational symmetry and simulate only the equation of motion of two spins, one on each sublattice of the antiferromagnet. Close to the phase transition and for small amplitudes of the oscillating fields, excellent agreement of numerics and analytics is obtained. The frequency dependence of γ_z is shown in Fig. 7.8. The analytical result fits the numerical result for all frequencies. For $\omega \approx 2zJ\sqrt{\Delta}$ the oscillating field resonantly couples to a magnon mode, giving rise to a pronounced peak in γ_z as a function of ω.

Our analytical and numerical results confirm that a rotation of the Goldstone mode (and thus also a critical exceptional point) can be induced by driving the system only weakly away from thermal equilibrium. In our specific (noiseless) model, we used an oscillating magnetic field and different g factors on the two sublattices to induce a non-equilibrium state. General symmetry arguments suggest, however, that the coupling γ_z defined in Eq. (7.46) is always finite when the system is not in thermal equililbrium. For example, one could instead use a laser tuned to an electronic resonance. In this case an absorbed photon will trigger a complex cascade of electronic, spin and phonon excitations which are difficult to describe quantitatively. We expect, however, that their net effect can be absorbed in an effective parameter γ_z which describes that the spins will start to precess in the ferrimagnetic phase.

7.3 Nonreciprocal matter

Recently much attention has been devoted to systems with nonreciprocal interactions on the microscopic level [28, 31, 69, 29, 30, 71, 68]. Nonreciprocity in that context means, that there are at least to degrees of freedom ϕ_A and ϕ_B whose coupling is not symmetric under switching $A \leftrightarrow B$. These interactions have been shown to give rise to dynamical limit cycle and oscillating phases [28, 68] and inspired varios proposals to realise this for instance in spin systems [30, 71]. The basic intuition is that if ϕ_A wants to align with ϕ_B while ϕ_B wants to antialign with ϕ_A, there is a "dynamic frustration" that can lead to a continuous motion of ϕ_A and ϕ_B around each other like a dog hunting its own tail.

All the above cases consider nonreciprocity on the level of the linearised dynamics for two fields $\boldsymbol{\phi}_a \in \mathbb{R}^N$, $a = A, B$

$$\partial_t \boldsymbol{\phi}_a = K_{ab}\boldsymbol{\phi}_b + \boldsymbol{\xi}_a \tag{7.56}$$

with noise $\boldsymbol{\xi}_a$. This dynamics is nonreciprocal if $K_{ab} \neq K_{ba}$. One should think of this dynamics as an expansion around a stable solution of some more complicated dynamics. Then, stability demands that the eigenvalues λ_i of the matrix K have negative real values

$$\operatorname{Re}\lambda_i < 0 \,\forall \lambda_i \in \operatorname{spec} K. \tag{7.57}$$

An instability towards a new phase then occurs, if the real part of at least one of these eigenvalues is tuned through zero. Importantly, there is an instability towards a dynamical phase, if the imaginary part of the respective eigenvalue remains finite. This is indeed what happens at the finite frequency critical point discussed in 4. In that sense it is a generalisation of Type III_0 instabilities of Cross and Hohenbergs classification [2] to include noise.
Let us look at a simple two-component nonreciprocal model with

$$K = \begin{pmatrix} -m_1 & g_1 \\ g_2 & -m_2 \end{pmatrix} \tag{7.58}$$

where nonreciprocity implies that $g_1 \neq g_2$. The eigenvalues of K are

$$\lambda_{1,2} = -\frac{m_1 + m_2}{2} \pm \sqrt{\frac{(m_1 - m_2)^2}{4} + g_1 g_2}. \tag{7.59}$$

Clearly, to induce an instability towards a dynamical phase, i.e. tune the real part of the eigenvalues through zero while maintaining a finite imaginary part , g_1 and g_2 have to have opposite signs. In other words, there has to be a strong nonreciprocity in the sense of competing aligning and antialigning forces. The instabiliy mirrors the behavior of the gap at the finite frequency criticality of the nonthermal $O(N)$ model. At the instabilities, there is a pair of critical eigenvalues with complex conjugated imaginary value $\lambda^c_{1,2} = \pm i\sqrt{-g_1 g_2}$. The connection can be made more explicitly by using that if either g_1 or $g_2 \neq 0$ (WLOG we choose $g_1 \neq 0$) and solve the equation of motion of ϕ_A for ϕ_B:

$$\phi_B = \frac{(m_1 + \partial_t)\phi_A + \xi_A}{g_1} \tag{7.60}$$

This can then in turn be plugged into the second equation of motion to wit

$$\partial_t^2 \phi + 2\gamma \partial_t \phi + r\phi + \xi = 0 \tag{7.61}$$

with

$$2\gamma = m_1 + m_2,\ r = m_1 m_2 - g_1 g_2,\ \xi = g_1 \xi_B + (\partial_t - g_2 m_2)\xi_A. \tag{7.62}$$

If the noises $\xi_{A,B}$ are now white and Gaussian to begin with (which generically is the case) and we consider long times, where the frequency dependence stemming from $\partial_t \xi_A$ is negligible, we have exactly reproduced the linear part of the nonthermal $O(N)$ model.
This can be generalized to the case of spatially extended and potentially vector valued order parameter fields $\boldsymbol{\phi}_{A,B}(t, \mathbf{x}) \in \mathbb{R}^N$ with a common $O(N)$ symmetry $\boldsymbol{\phi}_{A,B} \to R \cdot \boldsymbol{\phi}_{A,B}$ with $R \in O(N)$ moving in $O(N)$ symmetric ϕ^4 potentials that are nonreciprocally coupled:

$$\partial_t \boldsymbol{\phi}_A + (m_1 - K_1 \nabla^2)\boldsymbol{\phi}_A + \lambda_A (\boldsymbol{\phi}_A)^2 \boldsymbol{\phi}_A - g_1 \boldsymbol{\phi}_B + \xi_A = 0 \tag{7.63}$$

$$\partial_t \boldsymbol{\phi}_B + (m_2 - K_2 \nabla^2)\boldsymbol{\phi}_B + \lambda_B (\boldsymbol{\phi}_B)^2 \boldsymbol{\phi}_B - g_2 \boldsymbol{\phi}_A + \xi_B = 0 \tag{7.64}$$

Following the same procedure as before, we eliminate $\boldsymbol{\phi}_B$ utilizing $g_1 \neq 0$ in the first equation and arrive at the nonthermal $O(N)$ model (2.2) after neglecting higher order terms in field amplitudes and derivatives, which are irrelevant in an RG sense. We remark that one could also include nonreciprocal nonlinearities. This may make the solution of the first equation of motion cumbersome, but assuming analyticity one the microscopic level one can expand everything in derivatives and field amplitudes and arrive again at the form of (2.2).
Nonreciprocal models of the type (7.63) have been studied numerically in two spatial dimensions with $N = 2$ in [28]. While after eliminating ϕ_B the static aligned and antialigned phases cannot be distinguished anymore, all other phases can be identified with the ones presented in this thesis. The 'chiral' phase, where ϕ_A and ϕ_B circle around each other at a constant angle, maps to the rotating phase. The van der Pol or oscillating phase corresponds to the 'swap phase' of [28].

This clearly shows, that the field theory analysis above does apply to nonreciprocal phase transitions and vice versa engineering nonreciprocal matter is a route to realise the phenomena laid out above. From the perspective of the effective field theory paradigm of Landau and Halperin and Hohenberg, this does not come all to surprising. After all both models share the same symmetry group $O(N)$, break thermal equilibrium conditions and have no conserved currents that lead to additional hydrodynamic modes.

7.4 Driven Open Quantum Matter

This subsection has been published as section VII.B. of [44]. The model (2.2) can also emerge as a semiclassical limit of driven dissipative bosons subject to Lindbladian time evolution. We consider the dynamics of N spatially extended bosonic fields with creation operators $a_i^\dagger(\mathbf{x},t)$ which is symmetric under $O(N)$ rotations of the bosonic fields. Based on symmetry, it is to be expected that the universal phenomenology of the vector valued expectation value of these bosons after coarse graining is captured by the model (2.2). We now give an explicit example for Lindblad jump operators together with an $O(N)$ symmetric Hamiltonian time evolution, where the coarse graining procedure to obtain (2.2) can be done analytically. This has to be understood as a proof of principle, that given the right symmetries (2.2) emerges as an effective theory and is expected to happen for different microscopic setups where the coarse graining is not straightforward, as well. To generate the nonlinear dampings, two-body or higher order loss terms are necessary while the negative damping or pumping required for the rotating phase can be obtained by an effective single particle pump.
We consider a Lindbladian time evolution for the density matrix $\hat{\rho}$

$$\begin{aligned}\partial_t\hat{\rho} =& -i[\hat{H},\hat{\rho}] \\ &+\sum_\alpha \gamma_\alpha\Big(\int_{\mathbf{x}} \hat{L}_\alpha(\mathbf{x})\hat{\rho}\hat{L}_\alpha^\dagger(\mathbf{x}) - \frac{1}{2}\{\hat{L}_\alpha^\dagger(\mathbf{x})\hat{L}_\alpha(\mathbf{x}),\hat{\rho}\}\Big).\end{aligned} \tag{7.65}$$

The Hamiltonian is split into a quadratic and an interacting part $\hat{H} = \hat{H}_0 + \hat{H}_{\text{int}}$ with

$$\hat{H}_0 = \sum_{i=1}^{N}\int_{\mathbf{q}} r_c(\mathbf{q})\hat{a}_i^\dagger(\mathbf{q})\hat{a}_i(\mathbf{q}), \tag{7.66}$$

and we add a generic $O(N)$ symmetric ϕ^4 interaction

$$\hat{H}_{\text{int}} = \lambda_c\sum_{ij}\int_{\mathbf{x}} \hat{\phi}_i(\mathbf{x})^2\hat{\phi}_j(\mathbf{x})^2 \tag{7.67}$$

with canonical field variable $\hat{\phi}_j = \frac{i}{\sqrt{2}}(\hat{a}_j - \hat{a}_j^\dagger)$. We consider local single particle pump and loss $\hat{L}_1(\mathbf{x}) = \hat{a}_i^\dagger(\mathbf{x})$ and $\hat{L}_2(\mathbf{x}) = \hat{a}_i(\mathbf{x})$ with respective rates $\gamma_1 \equiv \gamma_{in}$, $\gamma_2 \equiv \gamma_{out}$, where the identical rates forall $i = 1,...,N$ ensure a weak $O(N)$ symmetry. Furthermore, we include $O(N)$ symmetric two body pump and loss processes $\hat{L}_3(\mathbf{x}) = \sum_i \hat{\phi}_i(\mathbf{x})\hat{a}_i(\mathbf{x})$ and $\hat{L}_4(\mathbf{x}) = \sum_i \hat{\phi}_i(\mathbf{x})\hat{a}_i^\dagger(\mathbf{x})$ with rates $\gamma_3 \equiv \lambda_d$, $\gamma_4 \equiv \lambda_p$

similar to the case of the single mode quantum van der Pol oscillator [110]. We now perform the following steps: pass to the equivalent Keldysh path integral description of the Lindbladian time evolution, introduce the canonical field momentum $\hat{\pi}_j(t,\mathbf{x}) = \frac{1}{\sqrt{2}}(\hat{a}_j(t,\mathbf{x}) + \hat{a}_j^\dagger(t,\mathbf{x}))$ and take the semiclassical limit to obtain an MSRJD action, see [8] for a review. Since the conjugate momentum appears only quadratically, we can perform the Gaussian integration over it, analogously to passing from a Hamiltonian path integral to a Lagrangian in equilibrium (quantum) field theory. Neglecting irrelevant terms that are higher order in field amplitudes or derivatives acting on noise fields, we arrive at the MSRJD action (3.5a) with the couplings $\gamma = \gamma_{out} - \gamma_{in}$, $r = \gamma^2 + r_c^2$, $u = 2\lambda_p$, $u' = 3\lambda_d - \lambda_p$, $\lambda = \lambda_c + (3\lambda_d + \lambda_p)\gamma$, $D = \frac{1}{2}(\gamma_{in} + \gamma_{out})(r_c^2 + 2\gamma^2)$.

The choice of interaction and Lindblad operators, involving ϕ operators, while giving simple expressions for the parameters of Eq. (3.5a), is somewhat artificial. However, the calculation can be done analogously when including squeezing terms $\sim c\hat{a}_i\hat{a}_i + h.c.$ that the bosonic $U(1)$ symmetry to $\mathbb{Z}_2$ on the quadratic level, and again one arrives at our effective model description: By symmetry, we expect the same effective long wavelength model to emerge.

8

Summary and Outlook

8.1 Summary

In this thesis we have analysed time crystalline order as a stable phase of nonequlibrium matter. We focused on determining the universal scaling laws emerging at the critical transitions into time crystalline order and within the phase and gave examples on how these phases may be realised in physical systems. The starting point of the entire analysis is the nonthermal $O(N)$ model introduced in chapter 2. It is a generalization of model A of the Halperin and Hohenberg classification to include irreversible force terms. As such, it is a minimal field theory solely based on symmetries which results in a certain structural simplicity. We have shown, that in these models, for any internal $O(N)$ symmetry group, next to the transition into a statically ordered phase already present in equilibrium, there is a time-crystalline phase, where an order parameter traces out a limit cycle, for suitably strong drives. We employed the tool box of nonequilibrium field theory, to determine the universality classes of the transitions into the time crystal. We have identified a novel, nonthermal universality class for the onset of time-crystalline order from a fully symmetric phase. The nonthermal nature of the critical scaling at this transition is most pronounced, when looking at an effective temperature defined by fluctuation-dissipation relations and observable through probes of the spectral occupation of

fluctuations. Such a 'temperature' (there is of course no true thermodynamic temperature in such a set up), diverges as one tunes to the critical point. Notably, the effective field theory governing the critical point in principle allows for the emergence of an effective equilibrium. The corresponding fixed point is however unstable to any perturbation away from equilibrium and in principle an infinitesimal deviation from an effective equilibrium suffices for the RG flow to carry the system to the nonthermal fixed point upon coarse graining. The transition between the statically ordered phase and the rotating phase is governed by a critical exceptional point, leading to a superthermal occupation of low frequency fluctuations. This is poised to melt down any preexisitng order before reaching the transition into the limit cycle phase. By means of a controlled solution of the Dyson-Schwinger equations at this transition, we have shown, that symmetry restoration is not the ultimate fate of the CEP, but that there is a fluctuation induced first order transition between ordered and rotating phase for sufficiently large order. Within the time-crystalline ordered phase, next to the Goldstone modes of broken internal symmetry generators, there is a Goldstone mode of time translation. We have shown, that this Goldstone mode is generically described by the KPZ universality class impacting the scaling behavior within the phase. On top, in low dimensions, there is vertices destroying quasi long range order at large distances. In the presence of internal Goldstone modes, a one-loop RG analysis shows, that next to KPZ scaling there is novel weak scaling fixed points possible.

The structural simplicity of the nonthermal $O(N)$ model, the fact that it is solely based on symmetry considerations, suggests, that it emerges for any system meeting the symmetry conditions, i.e. a weak $O(N)$ symmetry and breaking of detailed balance, upon coarse graining. The crucial question is, whether one can drive a system reasonably, such that the effective antidamping transition is triggered without simply heating the system up. We have shown four different routes to achieve that. Pumping systems that in equilibrium fall into the universality class of model A by a parametric drive at high frequencies leads to a highly occupied reservoir at half the drives frequency through parametric resonance. This reservoir pumps the slow, long wavelength degrees of freedom and can trigger the instability towards time crystalline order. It however also heats the system up and thus a low equilibrium damping of the slow modes is necessary to realize the time-crystal. In contrast, an arbitrarily weak drive is sufficient to induce the rotating phase in the $O(2)$ ferrimagnet described in chapter 7.2. Extending the basic principle of driven-dissipative exciton-polariton condensation [64, 111] to bosonic spinors that transform under an additional $O(N)$ group also realises the universality classes presented in this thesis.

We also connect to the case of nonreciprocally coupled order parameter fields studied in active matter.
In summary, we have developed a field theoretical framework to determine universal phenomena associated to spontaneous breaking of time translation symmetry. For all identified transitions as well as the time-crystalline phases, we have derived first results for the respective scaling exponents. These scaling behaviors are predict to emerge in nonequilibrium systems meeting the respective symmetry conditions and developing time-crystalline order. Further, we developed new mechanisms to realize time-crystalline order in magnetic systems inspired by the field-theoretic framework.

8.2 Discussion Outlook

At this point we want to collect and comment on open ends and caveats of the presented results and point to future directions. One of the key steps in the study of time-crystalline order is to make it accessible in realistic set-ups. While the parametric pumping scheme put forward here provides a general pathway towards realization in magnetic systems, the mechanism has to be adapted for a concrete system, using accurate, quantitative values for spin wave dispersions, life-times and scattering length to fine tune the equilibrium model A type model to capture a realistic material. A parametric driving may be induced by oscillating electric fields, i.e. laser irradiation, as in [65]. To derive its exact strength therefore requires knowledge of the light-matter coupling in the respective material. An important next step would be the large scale simulation of more microscopic spin models subject to parametric drives. One should however not be discouraged, a similar driving scheme was successfully employed experimentally to induce a 'magnon condensation' in microwave-pumped Yttrium iron garnet (YIG) films [112, 113]. We expect that the universal properties of YIG can be captured by the field theoretic tools at hand, however the spin wave dispersions in YIG have minima at finite wavevectors and the condensation occurs at such a finite wavevector leading to pattern formation. A careful analysis of the consequences of this for the effective field theory is subject of future work.
Measuring the scaling behavior in these systems (most likely in large scale simulations), puts the field theoretic predictions developed in this thesis to the test. A first example are the numerical simulations of one-dimensional Van der Pol arrays presented in 6.2 which indeed display the predicted KPZ scaling. The theory predictions for the novel universal exponents at the transition into the limit cycle are however less quantitatively reliable, as they are derived in a perturbative expansion $\epsilon = 4 - d$. This expansion is obviously not controlled in three dimensions and a quantitative

prediction of the exponents calls for the use of more sophisticated nonperturbative methods, such as the functional RG [98]. The qualitative features such as the breaking of equilibrium conditions leading to violations of fluctuation-dissipation relations are however expected to hold.

The exponents describing the behavior of the Goldstone modes within the time crystalline ordered phase is much more accessible than the critical exponents of the transition, as they do not require fine-tuning to the critical point. Time-crystalline systems without any internal symmetries may prove a viable route to realize KPZ physics in large systems, allowing to access the strong coupling fixed point of the two-dimensional KPZ equation and even the roughening transition in three dimensions experimentally. A task that remained elusive so far. Next to the pumped magnetic systems put forward in this thesis, modern metametarials seem to provide a promising avenue in that direction. The single Van der Pol oscillator was for instance designed to describe stable oscillations in driven electrical circuits and one may realise the Van der Pol lattices by building lattices out of such electrical circuits subject to noise in the spirit of topolectrics [114].

The analysis of the Goldstone modes of the larger $O(N) \times SO(2)$ group indicates that there is fixed points with entirely novel, albeit weak, scaling exponents. This is very promising, but should be taken with a grain of salt. The scaling results presented in this thesis hold in one dimension at strong coupling fixed points. In the case of the KPZ equation its special symmetries render the one-loop exponents exact even on the nonperturbative level. This is not the case for the generalized equations of motion of the Goldstone modes of the $O(N) \times SO(2)$ model. While in principle there may be a hidden or emergent symmetry rendering exponents exact in the cases where the system flows to a KPZ fixed point, the results for the novel fixed points should not be trusted too much, the numerical simulations reported in [61] however support the results for the oscillating phase. On top of that, the effective theory is built on the assumption, that the decay of the correlation functions of the original order parameter field is dominated by gapless phase fluctuations. This clearly breaks down at long scales both in one and two dimensions for the $O(N) \times SO(2)$ such that low dimensional fixed points are only observable up to a length scale which has to be determined. For $d \geq 2$, there may be entirely new nonequilibrium transitions beyond the KPZ transition, motivating a more thorough investigation.

Acknowledgements

At this point I want to express my gratitude to all the people that have played crucial roles in my academic life throughout the four and a bit years that were my time as a PhD student.
First and foremost, I want to thank my advisor Sebastian Diehl for not only giving the possibility to pursue a PhD in his group but also for the productive but also lively and open atmosphere in his group, the many very fruitful and maybe sometimes fruitless but always open, educative and fun discussions and his constant support. It was not an easy decision for me, if and where to go for a PhD and I never regretted my choice. Many thanks to Joachim Krug for acting as a second examinor for this thesis and to Andy Millis for hosting me as a visitor for five months at the Flatiron Institute in New York.
I am deeply grateful to Romain whom I have worked with on all topics covered in this thesis and discussed on an almost daily basis. I have greatly enjoyed our team work.
Thanks to all my friends and colleagues at the institute, the 12noon lunch group, the other Diehl group members and of course my long term office mate Thomas. Special thanks go to Nico and Bernhard. I arrived in Cologne for this PhD in summer 2020 hardly knowing anyone amidst what was still the early phase of the pandemic and its shutdowns and social distancing. Even though not knowing me at all, they have immediately adopted me, mainly through zoom-coffees for which I am very grateful.
Thanks to Johannes, Thomas and Björn for proofreading the introduction of this thesis.

Appendix

8.3 Transition between static order and oscillations

In chapter 5, we have focused on the transition between static order and rotating phase and have swept the transition between static order and the oscillating Van der Pol phase under the rug. The appendix may be the right place to peek under that rug.

For $N = 1$, this is the only available phase, but for $N > 2$, it competes with the rotating phase. The transition from the statically ordered to the oscillating phase does not occur via a CEP. Indeed, the linearized equation of motions in the static phase are given by, see Sec. 5.2,

$$\partial_t^2 \delta\rho + (\delta + 2u'\rho_0 - Z\nabla^2)\partial_t \delta\rho + 2\lambda\rho_0 - v^2\nabla^2)\delta\rho = 0, \tag{8.1}$$

for the amplitude and

$$\partial_t^2 \theta_i + (\delta - Z\nabla^2)\partial_t - v^2\nabla^2)\theta_i = 0, \tag{8.2}$$

for the Goldstone modes. When $u' > 0$, upon tuning δ to zero, the damping of the amplitude mode remains positive, while the Goldstone modes become unstable and start to rotate in order to compensate for the negative damping. However, when $u' < 0$, the first instability occurs for the amplitude mode, which starts to display van der Pol oscillation. At the critical point, $u'\rho_0 + \delta = 0$, the dispersion of the amplitude modes are

$$\omega_{1,2} = \pm\sqrt{2\lambda\rho_0}, \tag{8.3}$$

indicating that this transition occurs through a finite frequency instability as analysed for the direct transition in chapter 4. It is however not N but the single amplitude mode $\delta\rho$ that becomes critical. This leads to the hypothesis that the

transition is described by the finite frequency criticality of the d-dimensional Van der Pol oscillator. From a symmetry point of view, this seems plausible, as in the transition from static order to oscillations only time translation symmetry is spontaneously broken. The unbroken internal group $O(N-1)$ is the same in both phases. But do we expect the $N-1$ additional Goldstone modes that exist on both sides of the transition to change the critial theory? We found in chapter 4, that the critical theory of the Van der Pol oscillator is captured by a complex field $\psi(t,\mathbf{x}) \in \mathbb{C}$ that becomes critical. Couplings this field minimally to the phase fluctuations $\vec{\theta} \in \mathbb{R}^N$ leads to couplings of the form

$$S_{\theta\Psi} = \int_{t,\mathbf{x}} g\tilde{\psi}^*\psi(\nabla\vec{\theta})^2 \tag{8.4}$$

which has canonical dimension $[g] = (d-2)/2$ and is thus irrelevant close to the upper critical dimension and we thus deduce that the transition between static order and oscillating phase is governed by the $N = 1$ Van der Pol universality, which as determined in 4 falls into the universality class of the noisy, complex Gross-Pitaevskii equation. A more thorough field theoretic analysis can substantiate or falsify this expectation in the future.

The careful reader might have noted, that at the transition between symmetric order and limit cycle phase the sign of $u - u'$ determines the competition between oscillating and rotating phase, whereas for the transition between order and limit cycle it is the sign of u'. This can be connected by analytically deriving the dispersions of the fluctuations in the rotating phase and check for instabilities. This is done in 8.3.1 and from (8.8), we can analytically extract the dispersions of the modes involving the amplitude fluctuations. There is indeed a mode that becomes unstable, for values of the parameters which agree with numerical simulations. The exact expression of this dispersion is rather complicated but simplifies in some limits. In particular, deep in the rotating phase, i.e at large E, the threshold is found to be $u' > u$. It confirms that u tends to stabilize the swap phase and u' the rotating phase. On the contrary, for $E \to 0$, the rotating phase is stable for any positive value of u'.

8.3.1 Phase-amplitude representation

In this appendix, we give detailed derivations of the action describing the fluctuations around the static and rotating orders obtained by writing the fields in a phase-

amplitude decomposition

$$\phi = \sqrt{\rho_0 + \delta\rho}\exp(ET_{1,2}t)\exp(\sum_{i=2}^{N}\theta_i T_{1,i})\hat{e}_1, \quad \tilde{\phi} = \sqrt{\rho_0}\exp(ET_{1,2}t)\exp(\sum_{i=2}^{N}\theta_i T_{1,i})\tilde{\chi}, \tag{8.5}$$

where $\tilde{\chi} \in \mathbb{R}^N$ is parametrized as $\tilde{\chi} = (\tilde{\delta\rho}, \tilde{\theta}_2, \ldots, \tilde{\theta}_N)$. The static ordered phase is included as a special case $E = 0$. For simplicity we drop summation indices in the following, and use $\vec{T} = \theta_i T_{1,i}$. The derivative terms like $\tilde{\boldsymbol{\phi}}^T \partial_t \boldsymbol{\phi}$ generate terms $\exp(-\vec{T})\partial_t \exp(\vec{T})$ and higher orders in derivatives, which have to be evaluated using the infinitesimal form of the Baker Campbell Hausdorff formula. Since we are only interested in the quadratic action at this point, one can however truncate to

$$\exp(-\vec{T})\partial_t^n \exp(\vec{T}) = \sum_i (\partial_t^n \theta_i) T_{1,i} + O(\theta^2) \tag{8.6}$$

and equivalently for the gradient terms. In the case of the statically ordered phase we thus arrive at the quadratic action displayed in the main text in Sec 5.2. In the rotating phase, i.e. at finite angular velocity E, we immediately arrive at the quadratic action for the perpendicular phase fluctuations $S_\perp^0$

$$S_\perp^0 = \rho_0 \int_{\mathbf{x},t} \tilde{\theta}_i(\partial_t^2 - Z\nabla^2\partial_t - v^2\nabla^2 + E^2)\theta_i - D\tilde{\theta}_i^2. \tag{8.7}$$

The parallel (θ) and amplitude ($\rho = \frac{\delta\rho}{2\rho_0}$) fluctuations however mix on the quadratic level:

$$\begin{aligned} S_{\rho\theta}^0 = \rho_0 \int_X &\tilde{\rho}(\partial_t^2 + (2u'\rho_0 - Z\nabla^2)\partial_t - v^2\nabla^2)\rho + \tilde{\theta}(\partial_t^2 - Z\nabla^2\partial_t - (v^2 + ZE)\nabla^2)\theta \\ &- 2E\tilde{\rho}\partial_t\theta + \tilde{\theta}(2u\rho_0 E + 2E\partial_t)\rho - 2D(\tilde{\theta}^2 + \tilde{\rho})^2 \end{aligned} \tag{8.8}$$

This action clearly violates the thermal symmetry conditions since the coupling between phase and amplitude are not symmetric. We can access the dynamics of the slow phase fluctuations alone by performing the Gaussian integration over the gapped amplitude field on the level of the path integral. This yields the following effective Gaussian action for the phase field (after proper rescaling of the field)

$$S_\parallel^0 = \rho_0 \int_X \tilde{\theta}(\partial_t^2 + (\bar{\delta} - \bar{Z}\nabla^2)\partial_t - \bar{v}^2\nabla^2)\theta - 2D\tilde{\theta}^2 \tag{8.9}$$

where the shifted couplings close to the transition, i.e. for small angular velocities E are

$$\bar{\delta} = |\delta| + O(E^2), \quad \bar{Z} = Z + O(E), \quad \bar{v}^2 = v^2 + O(E). \tag{8.10}$$

This procedure of integrating out the amplitude mode (i.e passing to a NLσM) can be carried beyond the quadratic level to derive the nonlinearities for the interacting theory. For the case $N = 2$, this can be done without any truncation in θ, while for $N > 2$, a truncation in θ_i leads to terms of the form (5.67) discussed in the main text. The precise coefficients obtained through this procedure do not really matter as they will not remain intact in the RG flow once one starts coarse graining the dynamics. The important point is that with the rescaled fields used in (5.42), there is always a contribution of order one in a ρ_0^{-1} expansion that therefore does not vanish in the large ρ_0 limit.

8.4 Explicit loop calculations

A slightly modified version of this appendix has been published as an appendix in [44].
In this appendix, we compute the integrals arising from loop corrections which are given in the main text. We start by the two-loop sunset diagram because there is no momentum running through the loop which simplifies the analysis and then discuss the one-loop integral with momentum transfer.

8.4.1 Two-loop sunset

Let us prove Eq. (5.50) which gives the correction to δ induced by g_1 and comes from the diagram 5.3c. In the following, all integrals are considered to be suitably regularized in the UV when divergent. It reads

$$I_{2l} = \int_{Q_1,Q_2} \omega_1^2 G^K(Q_1)\omega_2^2 G^K(Q_2) i(\omega_1+\omega_2) G^R(Q_1+Q_2). \tag{8.11}$$

The frequency integrals can be performed, and after rescaling of momenta $q_{1,2} \to q_{1,2}\delta^{1/2}$, we obtain

$$\begin{aligned} I_{2l} =& \frac{\delta^{d-3}}{4} \int_{\mathbf{q_1},\mathbf{q_2}} \frac{f_1(\mathbf{q_1},\mathbf{q_2}) + O(\delta)}{A(\mathbf{q}_1,\mathbf{q}_2)\Delta(\mathbf{q_1}^2)\Delta(\mathbf{q_2}^2)} \\ A(\mathbf{q}_1,\mathbf{q}_2) =& \frac{v^2}{\delta}\left[(\mathbf{q_1}\cdot\mathbf{q_2})^2 - (\mathbf{q_1}\mathbf{q_2})^2\right]^2 \\ &+ f_2(\mathbf{q_1},\mathbf{q}_2)\left[\Delta(\mathbf{q_1}^2) + \Delta(\mathbf{q_2}^2) + \Delta((\mathbf{q_1}+\mathbf{q_2})^2)\right] + O(\delta) \end{aligned} \tag{8.12}$$

In this expression, we defined f_1 and f_2, two functions independent of v whose precise forms are not important for the argument. The only property we will use is that $f_1(\mathbf{q_1},\mathbf{q_2}) = f_2(\mathbf{q_1},\mathbf{q_2})$ when $\mathbf{q_1}$ and $\mathbf{q_2}$ are aligned. We neglected the subleading terms in δ which do not contribute to the leading infrared divergence. However, as discussed in the main text for the one-loop integral (5.46), we keep a higher order term in the denominator because the leading term can in fact become small under certain conditions. This is the case for every momentum if δ/v^2 is large. In this regime, the integral reduces to

$$I_{2l} = \frac{\delta^{d-3}}{2} \int_{\mathbf{q_1},\mathbf{q_2}} \frac{1}{\Delta(\mathbf{q_1}^2) + \Delta(\mathbf{q_2}^2) + \Delta((\mathbf{q_1}+\mathbf{q_2})^2)} \frac{1}{\Delta(\mathbf{q_1}^2)\Delta(\mathbf{q_2}^2)}, \tag{8.13}$$

and behaves as δ^{d-3}, i.e. exactly as the tadpole diagram 5.3b. Now, approaching the CEP where δ/v^2 becomes small, the first term in the denominator of Eq. (8.12) dominates for generic momenta, but still vanishes when $\mathbf{q}_1$ and $\mathbf{q}_2$ are aligned. The integrand thus behaves as δ^{d-3} when the momenta are almost aligned, But only as δ^{d-2} when they are not, giving a subleading contribution to the integral. We thus have a resonance condition to get the highest divergence. This is shown in figure 8.1a. Formally, the denominator of the integrand in (8.15) behaves as a Dirac distribution. To make it apparent, we rewrite the integral over $\mathbf{q}_2$ using hyperspherical coordinates around $\mathbf{q_1}$,

$$I_{2l} \underset{\delta\to 0}{\sim} \frac{\delta^{d-3}}{4} \int_{\mathbf{q_1}} \int q_2^{d-1} \mathrm{d}q_2 \mathrm{d}\Omega_{d-1}^{q_2} \frac{1}{\Delta(q_1^2)\Delta(q_2^2)} I_{\text{sub}}, \tag{8.14}$$

where

$$I_{\text{sub}} = \int \frac{\mathrm{d}\theta \sin(\theta)^{d-2} f_1(q_1,q_2,\cos(\theta))}{\frac{v^2}{\delta}(q_1q_2)^2\left[\cos(\theta)^2-1\right]^2 + f_2(q_1,q_2,\cos(\theta))\left[\Delta(q_1^2)+\Delta(q_2^2)+\Delta((\mathbf{q_1}+\mathbf{q_2})^2)\right]}, \tag{8.15}$$

where θ is the angle between $\mathbf{q}_1$ and $\mathbf{q}_2$.

This last integral (8.15) can be brought to the following form,

$$I_{\text{sub}} = \eta^2 \int \mathrm{d}\theta \sin(\theta)^{d-2} \frac{a(\cos(\theta))}{\left[\cos(\theta)^2 - 1\right]^2 + \eta^2 b(\cos(\theta))^2}, \tag{8.16}$$

with $\eta = \sqrt{\delta/v^2}$ and a, b smooth non-vanishing functions around ± 1. We dropped all the dependencies in momentum for the sake of clarity. Using $x = \cos(\theta)$, the fraction in (8.16) is of the form

$$F(x) = \frac{1}{(x^2-1)^2 + \eta^2 b(x)^2} = \mathrm{Im}\left(\frac{1}{((x^2-1) - i\eta b(x)}\right) \tag{8.17}$$

$$= \frac{1}{2}\mathrm{Im}\left(\frac{1}{x - 1 - \frac{i\eta}{2}b(x)} - \frac{1}{x + 1 + \frac{i\eta}{2}b(x)}\right) \xrightarrow[\eta\to 0]{} \frac{\pi}{2}\left(\delta(x-1) + \delta(x+1)\right). \tag{8.18}$$

It indeed behaves as a Dirac distribution, reflecting the resonance condition. At small but finite η, the Dirac distributions are slightly extended, and while performing the integral in (8.15), we can use that $\eta^2 F(x)$ is essentially equal to one for $|\cos(\theta) \pm 1| < \eta$ and zero otherwise. It means that only small deviations of $\cos(\theta)$ around ± 1 of order η contribute to the integral, i.e. only small deviations of θ of order $\sqrt{\eta}$ around zero and π, and we can only keep the leading terms in a series expansion around these points for the other terms. Integration then yields

$$I_{\text{sub}} \sim \int_0^{\sqrt{\eta}} \mathrm{d}\theta \theta^{d-2} a(1) + \int_{\pi-\sqrt{\eta}}^{\pi} \mathrm{d}\theta (\pi - \theta)^{d-2} a(-1), \tag{8.19}$$

$$\sim C\eta^{\frac{d-1}{2}} = C\left(\frac{\delta}{v^2}\right)^{\frac{d-1}{4}}, \tag{8.20}$$

where C is a multiplicative constant, proving Eq. (5.50), $I_{2l} \sim \delta^{d-3}\left(\frac{\delta}{v^2}\right)^{\frac{d-1}{4}}$ since the remaining integrals are free of any parameters. We emphasise that the additional variable δ/v^2 enters the corrections, reflecting the absence of a full scaling solution at the CEP. This is confirmed by numerical integration over the momenta presented in Fig. 8.1b in two and three dimensions: I_{2l}/δ^{d-3} is indeed a function of δ/v^2 only, and the power law behaviors found at small δ agree quantitatively with the analytical results.

The same structure arises for the other sunset integrals (e.g. with g_2 instead of g_1 as vertices or the sunset obtained from diagram 5.3d), and they can be computed using the same procedure.

It is also instructive to rephrase this discussion using $(\mathbf{q}, t)$ variables in the loops. The corresponding expressions are obtained by Fourier transform with respect to

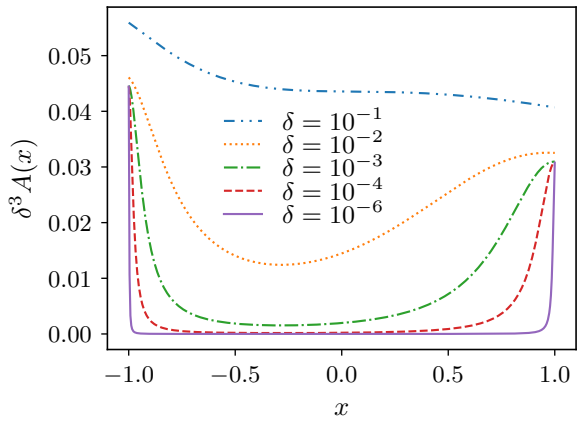

(a)

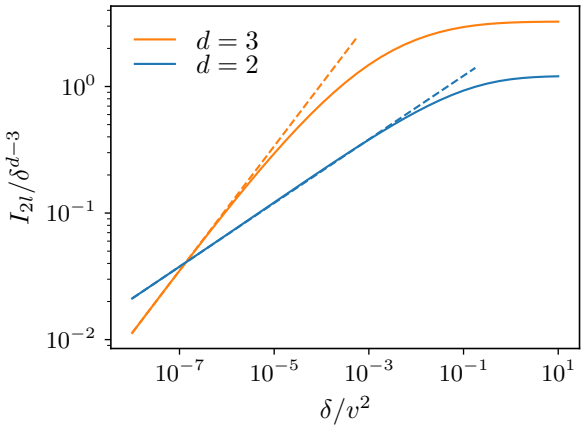

(b)

Figure 8.1: (a) The integrand of (8.12), denoted $A(x)$, is plotted as a function of $x = \cos(\theta)$ where θ is the angle between p_1 and p_2, $\tilde{p}_1 = 1/2$, $\tilde{p}_2 = 1$, $v = 1$ and different values of δ. At small δ, it becomes sharply peaked around $x = \pm 1$, reflecting the resonance condition. (b) I_{2l}/δ^{d-3}, plotted in $d = 2, 3$ is a function of δ/v^2 only. At large $\delta/v^2 \ll 1$ the integral behaves as δ^{d-3} but gets suppressed by an additional power law when the ratio δ/v^2 is small. The power law behaviors (indicated by the dashed lines) agree quantitatively with (8.19).

time to their $(\mathbf{q},\omega)$ counterparts. The integral I_{2l} becomes

$$I_{2l} = \int_t \int_{\mathbf{q_1}} G_D^K(\mathbf{q_1},t) \int_{\mathbf{q_2}} G_D^K(\mathbf{q_2},t) G_D^R(\mathbf{q_1}+\mathbf{q_2},t) \cos(v|\mathbf{q}_1|t)\cos(v|\mathbf{q}_2|t)\cos(v|\mathbf{q}_1+\mathbf{q}_2|t), \tag{8.21}$$

where we denote $G_D^R(\mathbf{q},t) = \Theta(t)\exp(-\Delta(\mathbf{q}^2)t)$ and $G_D^K(\mathbf{q},t) = \exp(-\Delta(\mathbf{q}^2)|t|)/\Delta(\mathbf{q}^2)$, purely dissipative Green's functions which are also those that appear in model A. Absent the oscillating terms associated to v, this integral scales as δ^{d-3} and displays a typical $z=2$ behavior. Now, the oscillating terms (seen as perturbation of this scenario) oscillate faster and faster at finite t in the scaling regime where we choose $t \sim q^{-2}$. In the spirit of a Rotating Wave Approximation (RWA), we can keep only the non-oscillating terms. Since the oscillating terms are of the form $\exp(ivt(\pm|\mathbf{q_1}+\mathbf{q_2}| \pm |\mathbf{q_1}| \pm |\mathbf{q_2}|))$, we recover our resonance condition, $\mathbf{q}_1$ and $\mathbf{q}_2$ have to be aligned to yield a significant contribution.

8.4.2 One-loop integral

We now discuss Eqs. (5.44) and (5.45), involved in the corrections of the quartic interactions coming from the diagrams displayed in Fig. 5.4. The calculation is closely related to the one done for the sunset integral above, and a similar resonance conditions arises. The diagrams read, with ω_p the frequency and $\mathbf{p}$ the momentum entering the loop,

$$\begin{aligned} I_{1l,I}(\mathbf{p},\omega_p) &= \int_{\mathbf{q},\omega} i(\omega+\omega_p)\omega^2 G^R(\mathbf{q}+\mathbf{p},\omega+\omega_p)G^K(\mathbf{q},\omega) \\ &= \int_{\mathbf{q},t} G_D^K(\mathbf{q},t)G_D^R(\mathbf{q}+\mathbf{p},t)\cos(v|\mathbf{q}|t)\cos(v|\mathbf{q}+\mathbf{p}|t)\exp(i\omega_p t), \end{aligned} \tag{8.22}$$

respectively in $\mathbf{q},\omega$ and $\mathbf{q},t$ variables.

Before discussing the finite momentum case, we note that for $\mathbf{p}=0$, after performing the integral over the frequency and rescaling of momentum $q \to q\delta^{1/2}$, the integral reduces to

$$I_{1l,I}(\mathbf{p}=0) \sim \delta^{\frac{d-4}{2}} \int_{\mathbf{q}} \frac{1}{\Delta(\mathbf{q}^2)(-i\tilde{\omega}_e + \Delta(\mathbf{q}^2))}, \tag{8.23}$$

in the scaling regime where $\tilde{\omega}_p = \omega_p/\delta \sim 1$. We also again use $\Delta(y) = y+1$. This is in line with formula (5.44).

Now at finite momentum, there is several resonances that can arise depending on the precise value of the external frequency and momentum. The first resonance

is found for frequencies close to $\omega_p \sim \pm v|\mathbf{p}|$, and exactly corresponds to the one we have in the sunset integral: $\mathbf{p}$ and $\mathbf{q}$ have to be aligned. Intuitively, this can be understood from the RWA argument we developed above: the oscillating terms in (8.22) are, when $\omega_p = \pm v|\mathbf{p}|$, of the form

$$\exp(ivt(\pm|\mathbf{q}+\mathbf{p}| \pm |\mathbf{q}| \pm \omega_e)) = \exp(ivt(\pm|\mathbf{q}+\mathbf{p}| \pm |\mathbf{q}| \pm \pm v|\mathbf{p}|), \tag{8.24}$$

which is the same form we got for the sunset diagram. They are not oscillating again exactly when $\mathbf{p}$ and $\mathbf{q}$ are aligned. This peculiar resonance directly originates from the non-vanishing real part of the relation dispersions at the CEP, and it can be checked explicitly that the highest divergences of the Gaussian Green's functions in $(\mathbf{q}, \omega)$ coming from (5.23) are obtained exactly for $\omega = \pm v|\mathbf{q}|$. In a sense, while the divergence occurs through the imaginary part of the dispersion relations, the real part acts to some extent like a finite frequency scale (because it goes infinitely slower to zero for small momenta) around which the divergences occur. This is technically very reminiscent of the role of a finite momentum scale in the Brazvoskii's scenario [58] where it is also the reason why loops with momentum transfer are negligible.

To make the link with the sunset diagram explicit, the integral with $\omega_e = \pm v|\mathbf{p}|$ can be written as

$$I_{1l,I}(\mathbf{p}, \omega_p = \pm v|\mathbf{p}|) \sim \delta^{\frac{d-4}{2}} \int_{\tilde{\mathbf{q}}} \left[\frac{\pi|\tilde{\mathbf{p}}| \left(\tilde{\mathbf{p}}\cdot\tilde{\mathbf{q}} + \tilde{\mathbf{q}}^2\right) + O(\delta)}{\Delta\left(\tilde{\mathbf{q}}^2\right)} \right.$$
$$\left. \left(i\frac{v}{\sqrt{\delta}} \left[(\tilde{\mathbf{p}}\cdot\tilde{\mathbf{q}})^2 - \tilde{\mathbf{p}}^2\tilde{\mathbf{q}}^2\right] + |\tilde{\mathbf{p}}| \left(\tilde{\mathbf{p}}\cdot\tilde{\mathbf{q}} + \tilde{\mathbf{q}}^2\right) \left[\Delta\left(\tilde{\mathbf{q}}^2\right) + \Delta\left((\tilde{\mathbf{p}}+\tilde{\mathbf{q}})^2\right)\right] + O\left(\delta\right) \right)^{-1} \right]. \tag{8.25}$$

Its real part is exactly the integral over $\mathbf{q}_2$ in Eq. (8.12), with $\mathbf{p}$ playing the role of $\mathbf{q}_1$. This renders the intuition developed around Eq. (5.49) rigorous, and we can thus use the analysis done in the previous section. Again, we have to keep a higher order term in the denominator because its contribution can dominate the integral in some cases. When approaching the CEP, δ is small with respect to v^2. In that case, the second term dominates only when $v^2/\delta[(\tilde{\mathbf{p}}\cdot\tilde{\mathbf{q}})^2 - \tilde{\mathbf{p}}^2\tilde{\mathbf{q}}^2]^2$ is sufficiently small. It is again true for every momenta $\mathbf{q}$ when $\tilde{p}^2v^2/\delta$ is small i.e. for small dimensionless momentum $\tilde{p} \ll \delta^{1/2}/v$ and the integral behaves as $\delta^{(d-4)/2}$, proving Eq. (5.44). But for a finite dimensionless momentum $\tilde{p} \sim 1$, the resonance condition appears, and the integrand in (8.25) behaves again as a Dirac distribution: the highest divergence is found when $\mathbf{q}$ and $\mathbf{p}$ are aligned, as in the sunset integral. This allows us to perform the integral, and using the result of the previous section, it leads to (5.45).

Interestingly, there is another type of resonance. In particular, at zero frequency and finite dimensionless momentum, see Eq. (5.46) where we got a different resonance condition: the highest divergence is found when $v^2\,(\mathbf{p}^2 + 2\mathbf{p}\cdot\mathbf{q})$ is small. This resonance condition also shows up as very sharp and non-analytic behavior which allows us to get the scaling of the integral with δ in a similar fashion. We find, for some $\tilde{p}$ not too large, a slightly different behavior, $I_{1l,I} \sim \delta^{(d-4)/2}(\delta/v^2)^{1/2}$ when δ is small. We can expect the frequency and momentum contributing the most to the loops to sit on the highest divergences and thus to involve the first scaling (5.45). Anyway, this cannot change the conclusions of the main text because both behaviors lead to smaller divergences at finite momentum for any frequency, no matter the precise power law we get.

To conclude, we found that for a finite frequency but at zero momentum, the loop is given by (8.23), and thus assume a usual scaling form with frequency $\tilde{\omega} = \omega/\delta$. Therefore, we do not need to use specific frequency dependencies of the different couplings as we do for the momentum dependencies.

8.5 Dyson-Schwinger equations

A slightly modified version of this appendix has been published as an appendix in [44].

8.5.1 $N = 2$ case

The DSE constitute an exact hierarchy of equations between the 1PI vertices. It emerges as consequence of the shift invariance of the effective action. It is discussed for the usual ϕ^4 case e.g. in [115] but the method can be applied directly within the MSRJD framework. The effective action can be written using the shift invariance with respect to to both fields, see (3.10),

$$\Gamma[\vartheta, \tilde{\vartheta}] = \int \mathcal{D}i\tilde{\theta}\mathcal{D}\theta e^{-S[\vartheta+\theta,\tilde{\vartheta}+\tilde{\theta}]+\frac{\delta\Gamma}{\delta\vartheta}\theta+\frac{\delta\Gamma}{\delta\tilde{\vartheta}}\tilde{\theta}}. \tag{8.26}$$

The DSE can be obtained by taking functional derivatives with respect to the fields of this equation. To simplify notation in the following, we use the Nambu fields $\Theta = (\vartheta, \tilde{\vartheta})$ and introduce

$$\Gamma^{(n)}_{I_1\dots I_n}[\Theta] = \frac{\delta^n\Gamma}{\delta\Theta_{i_n}(X_n)\dots\delta\Theta_{i_1}(X_1)}[\Theta], \tag{8.27}$$

with I_j a super-index including internal and external indices, $I_j = \{i_j, X_j\}$. Functional derivatives with brackets e.g. $\Gamma^{(n)}_{I_1 \dots I_n}[\Theta]$ denote functional derivatives before any evaluation on the equation of motion. The formalism can be readily extended to an N-component field by including the resulting indices within the internal indices.

Since the action does not contain any term independent of $\tilde{\theta}$ which would break conservation of probability, we define the master DSE by taking a derivative with respect to the response field which yields

$$\Gamma^{(10)}[\tilde{\vartheta}, \vartheta; X_1] = \langle S^{(10)}[\tilde{\vartheta} + \tilde{\theta}, \vartheta + \theta; X_1] \rangle. \tag{8.28}$$

This equation tells us that the dressed equation of motion is given by the expectation value of the bare equation of motion. In the following we work with the bare action given by (5.39) and (5.42),

$$S = \int_{\mathbf{x},t} \tilde{\theta}(\partial_t^2 + (-K\nabla^2 + \delta)\partial_t - v^2\nabla^2)\theta - D\tilde{\theta}^2 + \frac{g_1}{6}\tilde{\theta}(\partial_t\theta)^3 + \frac{g_2}{2}\tilde{\theta}\partial_t\theta(\nabla\theta)^2, \tag{8.29}$$

which describes the fluctuations of the Goldstone mode for $N = 2$. It is a fourth order polynomial, so a series expansion in the fluctuating fields θ and $\tilde{\theta}$ stops at finite order and gives

$$\Gamma^{(1)}_{I_1} = S^{(1)}_{I_1} + \frac{1}{2}S^{(3)}_{I_1}G - \frac{1}{6}S^{(4)}_{I_1}GGG\Gamma^{(3)}, \tag{8.30}$$

where sums over indices and Θ dependencies are implicit.

This master DSE gives relations between the full 1PI vertices and involves the renormalized propagator, making it a non-perturbative method. By taking additional functional derivatives with respect to the fields, one can generate equations for higher order vertices. Approaching the transition from the phase where $\langle \partial_t\theta \rangle = 0$ i.e the static ordered phase in our case, we can concentrate on the 1PI vertices evaluated at $\Theta = 0$. If a series expansion around $\tilde{\vartheta} = 0$ and $\vartheta = 0$ is valid, this also describes the broken phase. We expect it to be the case close to the first-order phase transition. Note that this is also the case in Brazovskii scenario where the calculations done around zero and around a finite order parameter agree well [96]. For the retarded inverse Green-function, we get

$$\begin{aligned}
&\Gamma^{(1,1)}(P, \Theta = 0) = S^{(1,1)}(P) + \frac{1}{2}\int_Q S^{(12)}(P, -P, Q)G^R(Q) \\
&- \frac{1}{2}\int_{Q_1,Q_2} S^{(13)}(P, Q_1, Q_2, -(P + Q_1 + Q_2)) \\
&\times G^K(Q_1)G^K(Q_2)G^R(Q_1 + Q_2 + P)\Gamma^{(13)}(-Q_1, -Q_2, (P + Q_1 + Q_2), -P),
\end{aligned} \tag{8.31}$$

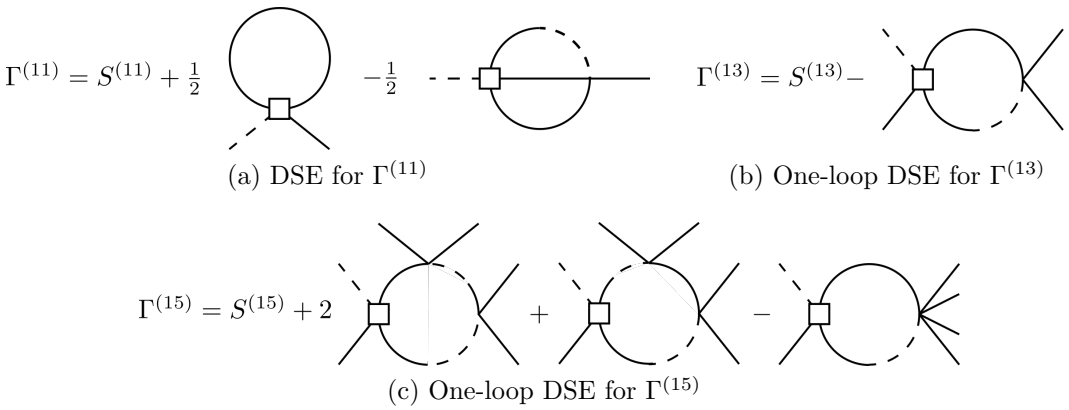

(a) DSE for $\Gamma^{(11)}$

(b) One-loop DSE for $\Gamma^{(13)}$

(c) One-loop DSE for $\Gamma^{(15)}$

Figure 8.2: Diagrammatic representation of the DSE. The solid and solid-to-dashed lines correspond respectively to the *full* Keldysh and retarded Green functions. The vertices correspond also to the *full* vertices $\Gamma^{(13)}$ and $\Gamma^{(15)}$, except for those that are represented with a square box, which correspond to the bare vertices $S^{(13)}$. Diagrams obtained by permutation of external legs attached to θ fields (solid line legs) are not shown.

where we neglected contribution coming from four point vertices that are higher order in $\tilde{\vartheta}$. They are irrelevant at the Gaussian CEP for all dimensions of interest $2 < d < 4$ and only lead to subleading divergences in the following. More generally, all couplings that are irrelevant at the Gaussian CEP fixed point induce smaller loop divergences (it is even the way we define and operator to be irrelevant at the Gaussian fixed-point because of the absence of a full scaling solution). Since the DSE will become one-loop exact in the regime we are interested in, any irrelevant operator brings subleading divergences in the DSE. Diagrammatically, Eq. (8.31) can be represented by Fig. 8.2a.

In the DSE framework, the renormalized effective action is obtained only from dressed tadpole and sunset diagrams. The main difference with the two-loop expression obtained from Fig. 5.3 is that the sunset involves the full fourth-point vertex $\Gamma^{(13)}$ instead of $S^{(13)}$, and we have to specify the form of the vertices used to solve the DSE. As discussed in the main text, the effective action can be parameterize using effective couplings g_1 and g_2 that become momentum dependent upon including interactions because of structure of the loops as discussed in the main text. To be specific, the renormalization depends on the number of pair of momenta that sum to zero, but not on the precise values of these momenta. Based on these considerations,

the four-point vertices can be parameterized as

$$\begin{aligned}
\Gamma^{(13)}(-\mathbf{p_2},\mathbf{p_1},-\mathbf{p_1},\mathbf{p_2},\omega_4,\omega_1,\omega_2,\omega_3) =& i\omega_1\omega_2\omega_3 g_{1,a} - i\omega_3 p_1^2 g_{2,a} - i(\omega_1-\omega_2)p_1\cdot p_2 g_{2,b},\\
\Gamma^{(13)}(-\mathbf{p_2},0,0,\mathbf{p_2},\omega_4,\omega_1,\omega_2,\omega_3) =& i\omega_1\omega_2\omega_3 g_{1,a}\\
\Gamma^{(13)}(-\mathbf{p_1},\mathbf{p_1},-\mathbf{p_1},\mathbf{p_1},\omega_4,\omega_1,\omega_2,\omega_3) =& i\omega_1\omega_2\omega_3 g_{1,b} - i(\omega_1-\omega_2+\omega_3)p_1^2 g_{2,c},\\
\Gamma^{(13)}(0,0,0,0,\omega_4,\omega_1,\omega_2,\omega_3) =& i\omega_1\omega_2\omega_3 g_{1,c},
\end{aligned} \tag{8.32}$$

where $\mathbf{p_1}$ and $\mathbf{p_2}$ are different finite momenta $p_{1,2}\sim\sqrt{\delta}$ and $\omega_4=-(\omega_1+\omega_2+\omega_3)$. All other configurations do not get renormalized.

Anticipating that all couplings will only decrease or stay constant (which can be checked a posteriori), the condition for neglecting the two-loop contributions is therefore given by replacing $\Gamma^{(13)}$ by $S^{(13)}$ in (8.31). The loop diagrams are then computed exactly as in Sec. 5.3.1 and App. 8.4. The condition Eq. (5.64) is thus recovered non-perturbatively, only by considering the sunset topology. When it is fulfilled, the DSE have only one-loop contributions which simplify them considerably, and they can be solved. In particular, from (8.31), the renormalized damping $\bar{\delta}$ satisfies the self-consistent equation (5.51).

The DSE equation for the four-point vertex $\Gamma^{(13)}$ is represented diagrammatically in Fig. 8.2b. We neglected two-loop contributions and the effect of all irrelevant vertices. The corresponding equation is, as in the main text

$$\begin{aligned}
&\Gamma^{(13)}(P_4,P_1,P_2,P_3) = S^{(13)}(P_4,P_1,P_2,P_3)\\
&-\int_Q G^K(Q)G^R(Q+P_1+P_2)\Gamma^{(13)}(-(Q+P_1+P_2),Q,P_1,P_2) + \text{perm.},
\end{aligned} \tag{8.33}$$

where $P_4=-(P_1+P_2+P_3)$ and where the permutations apply on the set P_1,P_2 and P_3. When the condition (5.64) is met, the loop in the right hand side is subleading and negligible whenever there is a running momentum going into the loop. Injecting the forms (8.32) into Eq. (8.33) then allows us to get equations for the different couplings. In particular, we get back Eqs. (5.56a) and (5.56c). The resulting equations form a linear system that can be inverted. The complete solution reads

$$g_{1,a}=\frac{g_1}{1+\alpha_2\bar{\delta}^{\frac{d-4}{2}}},\quad g_{1,b}=g_1\frac{1-\alpha_2\bar{\delta}^{\frac{d-4}{2}}}{1+\alpha_2\bar{\delta}^{\frac{d-4}{2}}},\quad g_{1,c}=g_1\frac{1-2\alpha_2\bar{\delta}^{\frac{d-4}{2}}}{1+\alpha_2\bar{\delta}^{\frac{d-4}{2}}}, \tag{8.34}$$

$$g_{2,a}=\frac{g_2}{1+\alpha_2\bar{\delta}^{\frac{d-4}{2}}},\quad g_{2,b}=\frac{g_2}{1+\alpha_d\bar{\delta}^{\frac{d-4}{2}}},\quad g_{2,c}=\frac{4}{3}\frac{g_2}{1+\alpha_d\bar{\delta}^{\frac{d-4}{2}}}+\frac{2}{3}\frac{g_2}{1+\alpha_2\bar{\delta}^{\frac{d-4}{2}}}-g_2, \tag{8.35}$$

with $\alpha_2 = (g_1 + g_2)K'_d(2-d)/2$ and $\alpha_d = g_2 K'_d(2-d)/d$.

The possibility of a negative quartic coupling (which induces the first-order transition) is cured by taking into account the renormalized six-point vertex $\Gamma^{(15)}$. Being irrelevant, its value is set by the four-point vertex $\Gamma^{(13)}$. Again, its renormalization depends on the configuration of incoming momenta. There are five different configurations which get renormalized differently. We however only need this vertices for vanishing momenta,

$$\Gamma^{(15)}(\mathbf{p}_1 = 0, \dots, \mathbf{p}_5 = 0, -\sum_i \omega_i, \omega_1, \dots, \omega_5) = i\omega_1\omega_2\omega_3\omega_4\omega_5 u_{1,e}, \tag{8.36}$$

with

$$u_{1,e} = 15(g_1+g_2)g_{1,a}^2 \int_q \frac{1}{(q^2+\bar{\delta})^3} - \frac{5}{2}u_{1,e}(g_1+g_2)\int_q \frac{1}{(q^2+\bar{\delta})^2}, \tag{8.37}$$

found using the DSE diagrammatically represented in Fig. 8.2c. It leads immediately to Eq. (5.60).

8.5.2 $N > 2$ case

For $N > 2$, the DSE equations discussed above can be directly used in the N-component case by adding the $O(N)$ indices in the internal indices. As discussed in Sec. 5.3.4, in the regime where the bare condensate is large, the action is simply the generalization of (8.29) to a vector field $\pi \in \mathbb{R}^{N-1}$ with an $O(N-1)$ symmetry. It is given by

$$S_0 = \int_{\mathbf{x},t} \tilde{\boldsymbol{\pi}}\cdot(\partial_t^2 + (-K\Delta+\delta)\partial_t - v^2\Delta)\boldsymbol{\pi} - D\tilde{\boldsymbol{\pi}}\cdot\tilde{\boldsymbol{\pi}} + \frac{g_1}{6}\int_{\mathbf{x},t}\tilde{\boldsymbol{\pi}}\cdot\partial_t\boldsymbol{\pi}(\partial_t\boldsymbol{\pi})^2 + \frac{g_2}{2}\tilde{\boldsymbol{\pi}}\cdot\partial_t\boldsymbol{\pi}(\nabla\boldsymbol{\pi})^2. \tag{8.38}$$

The loops that appear in the perturbative expansion or in the DSE equations (Fig. 8.2) and their scaling properties are therefore the same. The additional $O(N)$ structure only changes the prefactors (sometimes called symmetry factors) of the loops which become N-dependent. The $O(N)$ symmetry factors are the standard $O(N)$ ones and can be found in e.g. [116].

We now show that the quartic coupling controlling the value of the order parameter i.e. the generalization of $g_{1,c}$ also becomes negative and that there is again a first order phase transition. We will therefore concentrate on the renormalization of

g_1, which at the bare level generates the following vertex:

$$\frac{\delta\Gamma^{(4)}}{\delta\tilde{\pi}_a(P_4)\delta\pi_b(P_1)\delta\pi_c(P_2)\delta\pi_d(P_3)} = i\omega_1\omega_2\omega_3\Gamma'^{(13)}_{abcd}(P_4,P_1,P_2,P_3) = i\omega_1\omega_2\omega_3 g_1 T_{abcd}, \tag{8.39}$$

where we define

$$T_{abcd} = \frac{1}{3}(\delta_{ab}\delta_{cd} + \delta_{ac}\delta_{bd} + \delta_{ad}\delta_{bc}), \tag{8.40}$$

and $\Gamma'^{(13)}$ which denotes the part of $\Gamma^{(13)}$ encoding the renormalization of g_1.

We first look at the set of momenta which corresponds to what we called the $g_{1,a}$ coupling above. In perturbation theory, the diagrams 5.4 lead to

$$\begin{aligned}&\Gamma'^{(13)}_{abcd}(-\mathbf{p_1},\mathbf{p_1},-\mathbf{p_2},\mathbf{p_2},\omega_4,\omega_1,\omega_2,\omega_3)\\ &\quad= g_1 T_{abcd} - \alpha_2\bar{\delta}^{\frac{d-4}{2}}\frac{g_1^2}{9}((N'+4)\delta_{ab}\delta_{cd} + 2\delta_{ac}\delta_{bd} + 2\delta_{ad}\delta_{bc}),\end{aligned} \tag{8.41}$$

where $N' = N-1$. However the different Kronecker delta functions get different coefficient because only one diagram among the three of Fig. 5.4 contributes. We thus see that the ansatz done for the vertex using $g_{1,a}$ in (8.32) is not sufficient to self-consistently solve the DSE. We need to parametrize it as

$$\Gamma'^{(13)}_{abcd}(-\mathbf{p_1},\mathbf{p_1},-\mathbf{p_2},\mathbf{p_2},\omega_4,\omega_1,\omega_2,\omega_3) = (g^s_{1,a}\delta_{ab}\delta_{cd} + g^t_{1,a}\delta_{ac}\delta_{bd} + g^u_{1,a}\delta_{ad}\delta_{bc}). \tag{8.42}$$

The DSE equation then gives

$$g^s_{1,a} = g_1\frac{1+\alpha_2\frac{2(N'+2)}{9}\bar{\delta}^{\frac{d-4}{2}}}{(1+\alpha_2\frac{2}{3}\bar{\delta}^{\frac{d-4}{2}})(1+\alpha_2\frac{N'+2}{3}\bar{\delta}^{\frac{d-4}{2}})}, \quad g^t_{1,a} = g^u_{1,a} = \frac{g_1}{1+\alpha_2\frac{2}{3}\bar{\delta}^{\frac{d-4}{2}}}. \tag{8.43}$$

Using again the DSE for the four point function at zero momenta we find

$$\Gamma^{(13)}(0,0,0,0,\omega_4,\omega_1,\omega_2,\omega_3) \equiv g_{1,c}T_{abcd} = \left(g_1 - \alpha_2\bar{\delta}^{\frac{d-4}{2}}\frac{(N+4)g^s_{1,a} + 4g^t_{1,a}}{9}\right)T_{abcd}, \tag{8.44}$$

where we define $g_{1,c}$, underlying the fact that we do not need an extra parameter in that case. This gives, using (8.43),

$$g_{1,c} = g_1\frac{(9-4\alpha_2\bar{\delta}^{\frac{d-4}{2}}(\alpha_2\bar{\delta}^{\frac{d-4}{2}}(N'+2)+3))}{(2\alpha_2+3)(\alpha_2\bar{\delta}^{\frac{d-4}{2}}\ (N'+2)+3)}. \tag{8.45}$$

For $N = 2$, we recover the same result we got for $g_{1,c}$ in (8.34). We indeed see that the couplings $g_{1,c}$ turns negative for sufficiently small damping for all N. By inspecting Eq. (8.37), we see that the sextic coupling $u_{1,e}$ is clearly positive no matter the precise N-factor of the loops, and we therefore find the same first-order scenario.

8.6 Scaling and the breakdown of the gradient expansion

This appendix has been published as an appendix in [44].
We now elaborate in a bit more detail how the scaling of various operators is inferred in the vicinity of the CEP given that canonical power counting does not work due to the breakdown of gradient expansions and the different scaling of coherent period and lifetime of excitations

$$\omega_{\mathrm{CEP}}(\mathbf{q}) = -iK\mathbf{q}^2 \pm v|\mathbf{q}|. \tag{8.46}$$

The scaling is then fixed by finding an ansatz that renders the dimensionfull RG β-functions dimensionless. It is on first sight possible to make a homogeneous scaling ansatz for the effective action of the phase fluctuations by choosing a dynamical critical exponent $z_s = 1$ and thus being forced to have $[K] = -1$, i.e. (dangerously) irrelevant. This however yields Green functions that diverge for all momenta at the Gaussian fixed point.

One therefore has to analyse the divergences of loop contributions to infer the scaling dimensions of various couplings. Due to the breakdown of the derivative expansion it is not possible to infer the scaling of momentum dependent operators by taking momentum derivatives of loops renormalizing for instance the self energy.

We demonstrate this explicitly for the case where one allows a cubic interaction $\sim \lambda\tilde{\theta}(\partial_t\theta)^2$ breaking $O(2)$ to $SO(2)$ as in [66] for comparison. Note, that this coupling is absent at a fixed point with (emergent) $O(2)$ symmetry. This is analogous to the $\mathbb{Z}_2$ symmetric endpoint of the liquid gas transition described by the Ising universality class. Regardless, the loop integral through which such a coupling renormalizes the damping (i.e. the part of the self energy linear in frequencies) is exactly the loop analysed in the main text which renormalizes interactions, cf Fig. 5.4. The following result about the breakdown of the gradient expansion thus also immediately applies to the couplings discussed in the main text. At vanishing momenta, it implies a scaling dimension $6 - d$ for this cubic coupling, like for the ϕ^3 coupling in the Ising case. However, as discussed, the infrared divergence of the loop is lowered at finite

transfer momenta and there is no convergent derivative expansion of this loop close to the fixed point.
If one takes momentum derivatives of this loop, as one would in a derivative expansion of the self energy corrections, one generates spurious singularities as the dependence on dimensionless momenta becomes nonanalytic at $\tilde{p} = 0$, see App. 8.4.2. Now trying to enforce a scaling form for such an expansion of the self energy, as it usually emerges in equilibrium critical phenomena, leads to operators with apparently larger and larger upper critical dimensions. This is an artifact of the break down of the derivative expansion due to the nonanalyticity of the CEP.
Explicitly, such an expansion to fourth order in dimensionless momenta $\tilde{p}$ yields

$$\partial_\omega \Gamma^{(2)} = k^2(Z\tilde{p}^2 + \frac{\delta}{k^2} + \alpha_1' \lambda^2 k^{d-6} + \alpha_2' \lambda^2 k^{d-8} \tilde{p}^2 + \alpha_3' \lambda^2 k^{d-10} \tilde{p}^4 + O(\tilde{p}^4)). \quad (8.47)$$

Cutting this expansion at order $\tilde{p}^2$ would imply that there is an operator $\sqrt{\alpha_2'}\lambda$ with dimension $[\sqrt{\alpha_2'}\lambda] = \frac{8-d}{2}$ inferring an upper critical dimension $d_c = 8$ [66]. Going to order $\tilde{p}^4$ one would then however diagnose $d_c = 10$ from the operator $\sqrt{\alpha_3'}\lambda$. Clearly arbitrarily large upper critical dimensions are generated within such an expansion, demonstrating again that a standard derivative expansion is inapplicable in this case.

8.7 Flow equations within the rotating phase

Here, we give the dimensionfull flow equations for the complex action of the Goldstone modes of the rotating phase analysed in chapter 6.3. They are derived equivalently to the ones of the oscillating phase given in the main text, by evaluating the

Feynman diagrams 6.3,6.4. Using $Z_\theta = Z_D + iZ_c$ and $g = g_d + ig_c$ they read:

$$\Lambda\partial_\Lambda Z_\alpha = \Lambda^{d-2}\frac{(d-2)\left(2\gamma_\alpha Z_d^2\lambda_\alpha^2 + (N-2)\gamma_\theta Z_\alpha^2 g_d\lambda_\theta\right)}{dZ_\alpha^2 Z_d^2} \tag{8.48}$$

$$\Lambda\partial_\Lambda Z_\theta = \Lambda^{d-2}\Big(\frac{g^2\gamma_\alpha(4Z_\alpha - d(Z_\alpha+Z_\theta))}{dZ_\alpha(Z_\alpha+Z_\theta)^2} - \frac{2\gamma g\lambda_\theta(Z_\alpha+Z_\theta^*-4Z_d)}{Z_d(Z_\alpha+Z_\theta^*)^2}\Big) \tag{8.49}$$

$$\Lambda\partial_\Lambda\gamma_\alpha = \Lambda^{d-2}\Big(\frac{\gamma_\alpha^2\lambda_\alpha}{Z_\alpha^3} + 2(N-2)\frac{\gamma_\theta^2\lambda_\theta}{Z_d^3}\Big) \tag{8.50}$$

$$\Lambda\partial_\Lambda\gamma_\theta = \Lambda^{d-2}\frac{|g|^2\gamma_\alpha\gamma_\theta(Z_\alpha+Z_d)}{Z_\alpha Z_d(Z_c^2+(Z_\alpha+Z_d)^2)} \tag{8.51}$$

$$\Lambda\partial_\Lambda\lambda_\alpha = \Lambda^{d-2}\frac{4(N-2)g_c^2\lambda_\theta}{Z_d^3} \tag{8.52}$$

$$\begin{aligned}\Lambda\partial_\Lambda\lambda_\theta =& \frac{\lambda_\theta\Lambda^{d-2}}{Z_\alpha^2 Z_d^2(Z_c^2+(Z_\alpha+Z_d)^2)} \\ &\Big(2\gamma_\alpha Z_d\Big(2\lambda_\alpha Z_d(g_c Z_c + g_d(Z_\alpha+Z_d)) - |g|^2 Z_\alpha(Z_\alpha+Z_d)\Big) \\ &+ 4\gamma_\theta Z_\alpha\lambda_\theta\Big(g_d Z_\alpha(Z_\alpha+Z_d) - g_c Z_\alpha Z_c - 2\lambda_\alpha Z_d(Z_\alpha+Z_d)\Big)\Big)\end{aligned} \tag{8.53}$$

$$\begin{aligned}\Lambda\partial_\Lambda g =& \Lambda^{d-2}g^*\Bigg(\frac{2g^*\gamma_\alpha(2\lambda_\alpha - g)}{Z_\alpha(Z_\alpha+Z_\theta^2)} \\ &- 4\gamma_\theta\lambda_\theta\frac{(Z_\alpha+Z_\theta^*)^2(g_d Z_d + ig_c(Z_\alpha+Z_d+Z_\theta)) + 2Z_d(Z_\alpha+Z_\theta)^2\lambda_\alpha}{Z_d^2(Z_c^2+(Z_d+Z_\alpha)^2)^2}\Bigg)\end{aligned} \tag{8.54}$$

Bibliography

[1] P. C. Hohenberg and B. I. Halperin. Theory of dynamic critical phenomena. *Reviews of Modern Physics*, 49(3):435–479, jul 1977.

[2] M. C. Cross and P. C. Hohenberg. Pattern formation outside of equilibrium. *Reviews of Modern Physics*, 65(3):851–1112, jul 1993.

[3] L. P. Kadanoff. Scaling laws for Ising models near T(c). *Physics*, 2:263–272, 1966.

[4] Kenneth G Wilson and Michael E Fisher. Critical exponents in 3.99 dimensions. *Phys. Rev. Lett.*, 28(4):240, 1972.

[5] N. Goldenfeld. *Lectures on phase transitions and the renormalization group*. Addison-Wesley, 1992.

[6] J. Zinn-Justin. *Quantum Field Theory and Critical Phenomena (4th edition)*, volume 113 of *International Series of Monographs on Physics*. Clarendon Press, Oxford, 2002.

[7] Joachim Krug. Origins of scale invariance in growth processes. *Adv. Phys.*, 46(2):139–282, apr 1997.

[8] L M Sieberer, M Buchhold, and S Diehl. Keldysh field theory for driven open quantum systems. *Reports on Progress in Physics*, 79(9):096001, aug 2016.

[9] Lukas M. Sieberer, Michael Buchhold, Jamir Marino, and Sebastian Diehl. Universality in driven open quantum matter, 2023.

[10] Tamás Vicsek, András Czirók, Eshel Ben-Jacob, Inon Cohen, and Ofer Shochet. Novel type of phase transition in a system of self-driven particles. *Phys. Rev. Lett.*, 75:1226–1229, Aug 1995.

[11] John Toner and Yuhai Tu. Long-range order in a two-dimensional dynamicallong-range order in a two-dimensional dynamical XY model: How birds fly togethermodel: How birds fly together. *Physical Review Letters*, 75(23):4326–4329, dec 1995.

[12] Tamás Vicsek and Anna Zafeiris. Collective motion. *Physics Reports*, 517(3):71–140, 2012. Collective motion.

[13] M. Ballerini, N. Cabibbo, R. Candelier, A. Cavagna, E. Cisbani, I. Giardina, V. Lecomte, A. Orlandi, G. Parisi, A. Procaccini, M. Viale, and V. Zdravkovic. Interaction ruling animal collective behavior depends on topological rather than metric distance: Evidence from a field study. *Proceedings of the National Academy of Sciences*, 105(4):1232–1237, 2008.

[14] Dirk Helbing, Illés Farkas, and Tamás Vicsek. Simulating dynamical features of escape panic. *Nature*, 407(6803):487–490, Sep 2000.

[15] Nicolas Bain and Denis Bartolo. Dynamic response and hydrodynamics of polarized crowds. *Science*, 363(6422):46–49, 2019.

[16] Suraj Shankar, Anton Souslov, Mark J. Bowick, M. Cristina Marchetti, and Vincenzo Vitelli. Topological active matter. *Nature Reviews Physics*, 4(6):380–398, Jun 2022.

[17] Aditi Mitra, So Takei, Yong Baek Kim, and A. J. Millis. Nonequilibrium quantum criticality in open electronic systems. *Phys. Rev. Lett.*, 97:236808, Dec 2006.

[18] Thomas Risler, Jacques Prost, and Frank Jülicher. Universal critical behavior of noisy coupled oscillators. *Phys. Rev. Lett.*, 93:175702, Oct 2004.

[19] M. Foss-Feig, P. Niroula, J. T. Young, M. Hafezi, A. V. Gorshkov, R. M. Wilson, and M. F. Maghrebi. Emergent equilibrium in many-body optical bistability. *Phys. Rev. A*, 95:043826, Apr 2017.

[20] Haye Hinrichsen. Non-equilibrium critical phenomena and phase transitions into absorbing states. *Advances in Physics*, 49(7):815–958, November 2000.

[21] Géza Ódor. Universality classes in nonequilibrium lattice systems. *Rev. Mod. Phys.*, 76:663–724, Aug 2004.

[22] P. Bak, C. Tang, and K. Wiesenfeld. Self-organized criticality: An explanation of the 1/f noise. *Phys. Rev. Lett.*, 59:381–384, Jul 1987.

[23] Gunnar Pruessner. *Self-organised criticality: theory, models and characterisation*. Cambridge University Press, 2012.

[24] Mehran Kardar, Giorgio Parisi, and Yi-Cheng Zhang. Dynamic Scaling of Growing Interfaces. *Phys. Rev. Lett.*, 56(9):889–892, mar 1986.

[25] Kazumasa A. Takeuchi. An appetizer to modern developments on the kardar–parisi–zhang universality class. *Physica A: Statistical Mechanics and its Applications*, 504:77–105, aug 2018.

[26] Patrick Bruno. Impossibility of spontaneously rotating time crystals: A no-go theorem. *Physical Review Letters*, 111(7):070402, aug 2013.

[27] Haruki Watanabe and Masaki Oshikawa. Absence of quantum time crystals. *Physical Review Letters*, 114(25):251603, jun 2015.

[28] Michel Fruchart, Ryo Hanai, Peter B. Littlewood, and Vincenzo Vitelli. Non-reciprocal phase transitions. *Nature*, 592(7854):363–369, apr 2021.

[29] Ryo Hanai, Alexander Edelman, Yoji Ohashi, and Peter B. Littlewood. Non-hermitian phase transition from a polariton bose-einstein condensate to a photon laser. *Physical Review Letters*, 122(18):185301, may 2019.

[30] Ryo Hanai, Daiki Ootsuki, and Rina Tazai. Photoinduced non-reciprocal magnetism. *arXiv preprint arXiv:2406.05957*, 2024.

[31] Thomas Suchanek, Klaus Kroy, and Sarah A. M. Loos. Irreversible mesoscale fluctuations herald the emergence of dynamical phases, 2023.

[32] F. Iemini, A. Russomanno, J. Keeling, M. Schirò, M. Dalmonte, and R. Fazio. Boundary time crystals. *Physical Review Letters*, 121(3):035301, jul 2018.

[33] Berislav Buča and Dieter Jaksch. Dissipation induced nonstationarity in a quantum gas. *Physical Review Letters*, 123(26):260401, December 2019.

[34] Hans Keßler, Jayson G. Cosme, Michal Hemmerling, Ludwig Mathey, and Andreas Hemmerich. Emergent limit cycles and time crystal dynamics in an atom-cavity system. *Physical Review A*, 99(5):053605, may 2019.

[35] Phatthamon Kongkhambut, Jim Skulte, Ludwig Mathey, Jayson G. Cosme, Andreas Hemmerich, and Hans Keßler. Observation of a continuous time crystal. *Science*, 377(6606):670–673, aug 2022.

[36] Uwe C. Täuber. *Critical Dynamics*. Cambridge University Press, mar 2014.

[37] B. van der Pol. A theory of the amplitude of free and forced triode vibrations. *Radio Review*, 1:701–710, 754–762, 1920.

[38] Stefan Walter, Andreas Nunnenkamp, and Christoph Bruder. Quantum synchronization of a driven self-sustained oscillator. *Physical Review Letters*, 112(9):094102, March 2014.

[39] Stefan Walter, Andreas Nunnenkamp, and Christoph Bruder. Quantum synchronization of two van der pol oscillators. *Annalen der Physik*, 527(1–2):131–138, August 2014.

[40] Tony E. Lee and H. R. Sadeghpour. Quantum synchronization of quantum van der pol oscillators with trapped ions. *Physical Review Letters*, 111(23):234101, December 2013.

[41] Shovan Dutta and Nigel R. Cooper. Critical response of a quantum van der pol oscillator. *Physical Review Letters*, 123(25):250401, December 2019.

[42] Lior Ben Arosh, M. C. Cross, and Ron Lifshitz. Quantum limit cycles and the rayleigh and van der pol oscillators. *Physical Review Research*, 3(1):013130, feb 2021.

[43] Romain Daviet, Carl Philipp Zelle, Achim Rosch, and Sebastian Diehl. Nonequilibrium criticality at the onset of time-crystalline order. *Phys. Rev. Lett.*, 132:167102, Apr 2024.

[44] Carl Philipp Zelle, Romain Daviet, Achim Rosch, and Sebastian Diehl. Universal phenomenology at critical exceptional points of nonequilibrium O(n) models. *Phys. Rev. X*, 14:021052, Jun 2024.

[45] Michael Berry. Physics of nonhermitian degeneracies. *Czech. J. Phys.*, 54:1039, 2004.

[46] W D Heiss. Exceptional points of non-hermitian operators. *Journal of Physics A: Mathematical and General*, 37(6):2455–2464, jan 2004.

[47] H. Hodaei, A. U. Hassan, S. Wittek, H. Garcia-Gracia, R. El-Ganainy, D. N. Christodoulides, and M. Khajavikhan. Enhanced sensitivity at higher-order exceptional points. *Nature*, 548:187, 2017.

[48] W. Chen, S. K. Özdemir, G. Zhao, J. Wiersig, and L. Yang. Exceptional points enhance sensing in an optical microcavity. *Nature*, 548:192, 2017.

[49] C. Poli, M. Bellec, U. Kuhl, F. Mortessagne, and H. Schomerus. Selective enhancement of topologically induced interface states in a dielectric resonator chain. *Nat Commun.*, 6:6710, 2015.

[50] Yuto Ashida, Zongping Gong, and Masahito Ueda. Non-hermitian physics. *Advances in Physics*, 69(3):249–435, 2020.

[51] Julia M. Zeuner, Mikael C. Rechtsman, Yonatan Plotnik, Yaakov Lumer, Stefan Nolte, Mark S. Rudner, Mordechai Segev, and Alexander Szameit. Observation of a topological transition in the bulk of a non-hermitian system. *Phys. Rev. Lett.*, 115:040402, Jul 2015.

[52] H. Zhou, C. Peng, C. Yoon, Y. Hsu, K. A. Nelson, L. Fu, J. D. Joannopoulos, M. Soljacic, and B. Zhen. Observation of bulk fermi arc and polarization half charge from paired exceptional points. *Science*, 359:1009–1012, 2018.

[53] S. Weimann, M. Kremer, Y. Plotnik, Y. Lumer, S. Nolte, K. G. Makris, M. Segev, M. C. Rechtsman, and A. Szameit. Topologically protected bound states in photonic parity-time-symmetric crystals. *Nat. Mater.*, 16:433–438, 2017.

[54] Lei Xiao, Tianshu Deng, Kunkun Wang, Gaoyan Zhu, Zhong Wang, Wei Yi, and Peng Xue. Non-hermitian bulk-boundary correspondence in quantum dynamics. *Nature Physics*, 16(7):761–766, mar 2020.

[55] T. Helbig, T. Hofmann, S. Imhof, M. Abdelghany, T. Kiessling, L. W. Molenkamp, C. H. Lee, A. Szameit, M. Greiter, and R. Thomale. Generalized bulk–boundary correspondence in non-hermitian topolectrical circuits. *Nature Physics*, 16(7):747–750, jun 2020.

[56] Alexander Cerjan, Sheng Huang, Mohan Wang, Kevin P. Chen, Yidong Chong, and Mikael C. Rechtsman. Experimental realization of a weyl exceptional ring. *Nature Photonics*, 13(9):623–628, jun 2019.

[57] Emil J. Bergholtz, Jan Carl Budich, and Flore K. Kunst. Exceptional topology of non-hermitian systems. *Rev. Mod. Phys.*, 93:015005, Feb 2021.

[58] S. Brazovskii. Phase transition of an isotropic system to a nonuniform state - jetp 41, 85 (1975). *Soviet Phys JETP.*, 41, 01 1996.

[59] Léonie Canet, Hugues Chaté, Bertrand Delamotte, and Nicolás Wschebor. Nonperturbative renormalization group for the kardar-parisi-zhang equation: General framework and first applications. *Physical Review E*, 84(6):061128, December 2011.

[60] Deniz Ertaş and Mehran Kardar. Dynamic roughening of directed lines. *Physical Review Letters*, 69(6):929–932, August 1992.

[61] Deniz Ertaş and Mehran Kardar. Dynamic relaxation of drifting polymers: A phenomenological approach. *Physical Review E*, 48(2):1228–1245, August 1993.

[62] Iacopo Carusotto and Cristiano Ciuti. Quantum fluids of light. *Rev. Mod. Phys.*, 85(1):299–366, feb 2013.

[63] M. Wouters and I. Carusotto. Absence of long-range coherence in the parametric emission of photonic wires. *Phys. Rev. B*, 74(24):245316, dec 2006.

[64] Michiel Wouters and Iacopo Carusotto. Excitations in a nonequilibrium bose-einstein condensate of exciton polaritons. *Phys. Rev. Lett.*, 99:140402, Oct 2007.

[65] Nicklas Walldorf, Dante M. Kennes, Jens Paaske, and Andrew J. Millis. The antiferromagnetic phase of the floquet-driven hubbard model. *Phys. Rev. B*, 100:121110, Sep 2019.

[66] Ryo Hanai and Peter B. Littlewood. Critical fluctuations at a many-body exceptional point. *Physical Review Research*, 2(3):033018, jul 2020.

[67] Ryo Hanai. Nonreciprocal frustration: Time crystalline order-by-disorder phenomenon and a spin-glass-like state. *Physical Review X*, 14(1):011029, February 2024.

[68] Yael Avni, Michel Fruchart, David Martin, Daniel Seara, and Vincenzo Vitelli. The non-reciprocal ising model. *arXiv preprint arxiv:2311.05471*, 2024.

[69] Thomas Suchanek, Klaus Kroy, and Sarah A. M. Loos. Irreversible mesoscale fluctuations herald the emergence of dynamical phases. *Physical Review Letters*, 131(25):258302, December 2023.

[70] Mark J. Bowick, Nikta Fakhri, M. Cristina Marchetti, and Sriram Ramaswamy. Symmetry, thermodynamics, and topology in active matter. *Phys. Rev. X*, 12:010501, Feb 2022.

[71] Tobias Nadolny, Christoph Bruder, and Matteo Brunelli. Nonreciprocal synchronization of active quantum spins. *arXiv preprint arXiv:2406.03357*, 2024.

[72] Sarah A. M. Loos, Sabine H. L. Klapp, and Thomas Martynec. Long-range order and directional defect propagation in the nonreciprocal XY model with vision cone interactions. *Phys. Rev. Lett.*, 130:198301, May 2023.

[73] Nina del Ser, Lukas Heinen, and Achim Rosch. Archimedean screw in driven chiral magnets. *SciPost Phys.*, 11:009, 2021.

[74] Nina del Ser and Vivek Lohani. Skyrmion jellyfish in driven chiral magnets. *SciPost Phys.*, 15:065, 2023.

[75] Phoebe Tengdin, Benoit Truc, Alexey Sapozhnik, Lingyao Kong, Nina del Ser, Simone Gargiulo, Ivan Madan, Thomas Schönenberger, Priya R. Baral, Ping Che, Arnaud Magrez, Dirk Grundler, Henrik M. Rønnow, Thomas Lagrange, Jiadong Zang, Achim Rosch, and Fabrizio Carbone. Imaging the ultrafast coherent control of a skyrmion crystal. *Phys. Rev. X*, 12:041030, Dec 2022.

[76] C. de Dominicis. Techniques de renormalisation de la theorie des champs et dynamique des phenomenes critiques. *Le Journal de Physique Colloques*, 37(C1):C1–247–C1–253, jan 1976.

[77] P. C. Martin, E. D. Siggia, and H. A. Rose. Statistical dynamics of classical systems. *Physical Review A*, 8(1):423–437, jul 1973.

[78] Hans-Karl Janssen. On a lagrangean for classical field dynamics and renormalization group calculations of dynamical critical properties. *Zeitschrift für Physik B Condensed Matter and Quanta*, 23(4):377–380, dec 1976.

[79] Daniel J Amit and Victor Martin-Mayor. *Field Theory, the Renormalization Group, and Critical Phenomena*. WORLD SCIENTIFIC, jun 2005.

[80] Alex Kamenev. *Field Theory of Non-Equilibrium Systems*. Cambridge University Press, sep 2011.

[81] R. Bausch, H. K. Janssen, and H. Wagner. Renormalized field theory of critical dynamics. *Z. Phys. B*, 24(1):113–127, 1976.

[82] A Andreanov, G Biroli, and A Lefèvre. Dynamical field theory for glass-forming liquids, self-consistent resummations and time-reversal symmetry. *Journal of Statistical Mechanics: Theory and Experiment*, 2006(07):P07008–P07008, jul 2006.

[83] Camille Aron, Giulio Biroli, and Leticia F Cugliandolo. Symmetries of generating functionals of langevin processes with colored multiplicative noise. *Journal of Statistical Mechanics: Theory and Experiment*, 2010(11):P11018, nov 2010.

[84] G Györgyi, I Kondor, L Sasvári, and T Tél. *From Phase Transitions to Chaos*. WORLD SCIENTIFIC, 1992.

[85] Camille Aron, Daniel G Barci, Leticia F Cugliandolo, Zochil González Arenas, and Gustavo S Lozano. Dynamical symmetries of markov processes with multiplicative white noise. *Journal of Statistical Mechanics: Theory and Experiment*, 2016(5):053207, may 2016.

[86] Charles P. Enz, editor. *Dynamical Critical Phenomena and Related Topics*. Springer Berlin Heidelberg, 1979.

[87] Vincent R. Overbeck, Mohammad F. Maghrebi, Alexey V. Gorshkov, and Hendrik Weimer. Multicritical behavior in dissipative ising models. *Phys. Rev. A*, 95:042133, Apr 2017.

[88] Igor Herbut. *A Modern Approach to Critical Phenomena*. Cambridge University Press, 2007.

[89] L. M. Sieberer, S. D. Huber, E. Altman, and S. Diehl. Dynamical Critical Phenomena in Driven-Dissipative Systems. *Phys. Rev. Lett.*, 110(19):195301, 2013.

[90] Ferdinand Verhulst. *Nonlinear Differential Equations and Dynamical Systems*. Springer Berlin Heidelberg, 1996.

[91] Hikaru Kawamura. Universality of phase transitions of frustrated antiferromagnets. *Journal of Physics: Condensed Matter*, 10(22):4707–4754, jun 1998.

[92] L. M. Sieberer, S. D. Huber, E. Altman, and S. Diehl. Nonequilibrium functional renormalization for driven-dissipative Bose-Einstein condensation. *Phys. Rev. B*, 89(13):134310, apr 2014.

[93] Uwe C. Täuber and Sebastian Diehl. Perturbative field-theoretical renormalization group approach to driven-dissipative bose-einstein criticality. *Physical Review X*, 4(2):021010, apr 2014.

[94] Thomas Risler, Jacques Prost, and Frank Jülicher. Universal critical behavior of noisy coupled oscillators: A renormalization group study. *Physical Review E*, 72(1):016130, jul 2005.

[95] Hikaru Kawamura. Renormalization-group analysis of chiral transitions. *Physical Review B*, 38(7):4916–4928, sep 1988.

[96] P. C. Hohenberg and J. B. Swift. Metastability in fluctuation-driven first-order transitions: Nucleation of lamellar phases. *Physical Review E*, 52(2):1828–1845, aug 1995.

[97] Quentin Fontaine, Davide Squizzato, Florent Baboux, Ivan Amelio, Aristide Lemaître, Martina Morassi, Isabelle Sagnes, Luc Le Gratiet, Abdelmounaim Harouri, Michiel Wouters, Iacopo Carusotto, Alberto Amo, Maxime Richard, Anna Minguzzi, Léonie Canet, Sylvain Ravets, and Jacqueline Bloch. Kardar–parisi–zhang universality in a one-dimensional polariton condensate. *Nature*, 608(7924):687–691, aug 2022.

[98] N. Dupuis, L. Canet, A. Eichhorn, W. Metzner, J.M. Pawlowski, M. Tissier, and N. Wschebor. The nonperturbative functional renormalization group and its applications. *Physics Reports*, 910:1–114, may 2021.

[99] M. D. Schwartz. *Quantum Field Theory and the Standard Model*. Cambridge University Press, 2014.

[100] Masaru Hongo, Suro Kim, Toshifumi Noumi, and Atsuhisa Ota. Effective field theory of time-translational symmetry breaking in nonequilibrium open system. *Journal of High Energy Physics*, 2019(2):1–37, 2019.

[101] Andrea Pagnani and Giorgio Parisi. Numerical estimate of the Kardar-Parisi-Zhang universality class in (2+1) dimensions. *Phys. Rev. E*, 92(1):010101, jul 2015.

[102] Ehud Altman, Lukas M. Sieberer, Leiming Chen, Sebastian Diehl, and John Toner. Two-Dimensional Superfluidity of Exciton Polaritons Requires Strong Anisotropy. *Phys. Rev. X*, 5(1):011017, feb 2015.

[103] Liang He, Lukas M. Sieberer, Ehud Altman, and Sebastian Diehl. Scaling properties of one-dimensional driven-dissipative condensates. *Phys. Rev. B*, 92(15):155307, oct 2015.

[104] Konstantinos Deligiannis, Quentin Fontaine, Davide Squizzato, Maxime Richard, Sylvain Ravets, Jacqueline Bloch, Anna Minguzzi, and Léonie Canet. Kardar-parisi-zhang universality in discrete two-dimensional driven-dissipative exciton polariton condensates. *Phys. Rev. Res.*, 4:043207, Dec 2022.

[105] Wolfgang Demtröder. *Experimentalphysik 1 - Mechanik und Wärme*. Springer-Verlag, Berlin Heidelberg New York, 2008.

[106] L. M. Sieberer, A. Chiocchetta, A. Gambassi, U. C. Täuber, and S. Diehl. Thermodynamic equilibrium as a symmetry of the Schwinger-Keldysh action. *Phys. Rev. B*, 92(13):134307, oct 2015.

[107] Christoph Sürgers, Gerda Fischer, Patrick Winkel, and Hilbert v. Löhneysen. Large topological hall effect in the non-collinear phase of an antiferromagnet. *Nature Communications*, 5(1):3400, Mar 2014.

[108] Tsuyoshi Omi, Yoshito Watanabe, Nobuyuki Abe, Hajime Sagayama, Akiko Nakao, Koji Munakata, Yusuke Tokunaga, and Taka-hisa Arima. Antiferromagnetic-to-ferrimagnetic phase transition with large electric-polarization change in a frustrated polar magnet $cabaco_4o_7$. *Phys. Rev. B*, 103:184412, May 2021.

[109] Amber C. McConnell, Joshua D. Bell, and Joel S. Miller. Pressure-induced transition from an antiferromagnet to a ferrimagnet for mnii(tcne)[c4(cn)8]1/2 (tcne = tetracyanoethylene). *Inorganic Chemistry*, 51(18):9978–9982, 2012.

[110] Lior Ben Arosh, M. C. Cross, and Ron Lifshitz. Quantum limit cycles and the rayleigh and van der pol oscillators. *Phys. Rev. Res.*, 3:013130, Feb 2021.

[111] J Kasprzak, M Richard, S Kundermann, A Baas, P Jeambrun, J M J Keeling, F M Marchetti, M. H. Szymańska, R. André, J L Staehli, V Savona, P B Littlewood, B Deveaud, and Le Si Dang. Bose–Einstein condensation of exciton polaritons. *Nature*, 443(7110):409–414, sep 2006.

[112] S. O. Demokritov, V. E. Demidov, O. Dzyapko, G. A. Melkov, A. A. Serga, B. Hillebrands, and A. N. Slavin. Bose–einstein condensation of quasi-equilibrium magnons at room temperature under pumping. *Nature*, 443(7110):430–433, Sep 2006.

[113] P. Nowik-Boltyk, O. Dzyapko, V. E. Demidov, N. G. Berloff, and S. O. Demokritov. Spatially non-uniform ground state and quantized vortices in a two-component bose-einstein condensate of magnons. *Scientific Reports*, 2(1), June 2012.

[114] Ching Hua Lee, Stefan Imhof, Christian Berger, Florian Bayer, Johannes Brehm, Laurens W Molenkamp, Tobias Kiessling, and Ronny Thomale. Topolectrical circuits. *Communications Physics*, 1(1):39, 2018.

[115] Jan Horak, Jan M. Pawlowski, and Nicolas Wink. Spectral functions in the ϕ^4-theory from the spectral dyson-schwinger equations. *Physical Review D*, 102(12):125016, dec 2020.

[116] Hagen Kleinert and Verena Schulte-Frohlinde. *Critical Properties of Phi4-Theories*. World Scientific, jul 2001.